The University Of Sheffield.

Modelling aspects of Alzheimer's disease pathology without the transgenics; understanding the effects of brain disease on neurovascular coupling and neuroimaging signals

By:

Gaia Brezzo

A thesis submitted in partial fulfilment of the requirements for the degree of Doctor of Philosophy

The University of Sheffield

Faculty of Science

Department of Psychology (Neuroscience)

September 2017

For James and your constant belief in me

Abstract

The aim of this research was to develop non-transgenic rodent models relevant to Alzheimer's disease (AD) to investigate the effects of cholinergic, inflammatory and ageing manipulations upon neurovascular function and neurovascular coupling. The use of imaging techniques including functional magnetic resonance imaging (fMRI) have revolutionised the way in which we approach the study of the healthy human brain, helping to shed light onto the processes by which neurodegenerative diseases occur. Non-invasive imaging methods including fMRI are currently limited by their inability to measure neuronal activity directly. Thereby animal models are an invaluable tool in extending our understanding of the underling neurovascular coupling mechanisms, the *connection* between neuronal activity and blood flow, and their relationship to diseased states. *In vivo* neurovascular research is warranted as ample findings implicate altered biological mechanisms including neurovascular coupling in the pathogenesis of AD.

In this thesis neurovascular function and coupling were investigated *in vivo* utilising a multi-modal approach by obtaining measures of haemodynamics and neuronal activity (with laser-speckle-contrast-imaging, two-dimensional optical imaging and multichannel electrodes) and by further informing upon these changes with immunohistochemistry. The major findings of this work are: (1) reduced cholinergic function leads to neurovascular uncoupling; (2) acute systemic inflammation alters *in vivo* haemodynamic function and; (3) is associated with significant underlying changes in the status of the neurovascular unit; and (4) in an early-ageing model inflammation-driven changes in haemodynamic function occur more rapidly after an acute challenge. These findings provide important insights into how disease-related mechanisms impact upon neurovascular coupling which in turn may directly impact upon the brain imaging signals acquired from clinical populations. Additionally, this thesis demonstrates that neurovascular coupling should be assessed across a range of stimulation input parameters in order to confidently determine the effects of experimental manipulations.

Acknowledgments

I firstly would like to thank my supervisor Chris for teaching me everything I know, for all of the guidance on everything thesis but also for his support for my professional development and for always encouraging me to get the most out of my PhD (by doing more than the 'science'). I also what to thank Julie for her incredible positivity in spite of everything not working (for a short while thankfully!) and for giving me the opportunity to learn a new set of skills. And the cups of tea – those were a life saver.

A very warm thank you goes out to Kam for all of your support and for your blind faith in me and my capabilities. I will look back at all of our laughs, jokes and tears we shared over the past two years during the long (sometimes never-ending) hours in SITraN with a smile. And of course the lunch clubs, and no lunch club could be complete without Kendra and Llywelyn – there was never a dull moment with you all around, a breath of fresh air from all of the lab work, teaching, analysis and writing.

And of course a massive thank you has to go to my parents. Alla mia mamma e al mio papà, a tutti i tentativi tramite Skype di spiegarvi (soprattutto alla mamma) cosa faccio dalle 9 alle 5 tutti i giorni. Senza il vostro incoraggiamento e l'opportunità che mi avete dato tutti quegli anni fa non sarei stata sicuramente in grado di raggiungere questi livelli. So che siete entrambi orgogliosi di me e spero lo sarete sempre.

But of course I also have another set of 'parents' to thank – Marion and Steve for your incredible support from the very start of my studies and for attending as many of my graduations as you did for your own son (+1 shortly!). I will never forget your kindness.

And of course the biggest thank you goes out to James. The one person that has been with me through it all. You always believe in me, even when I don't. Your support, encouragement and reassurance have been irreplaceable and I can't express into words how much you have helped me achieve this. I know you will be forever by my side no matter what crazy adventure I decide to embark upon next. I promise not to talk about neurovascular 'stuff' to you ever again (or at least not for a little while).

A special mention also goes to Aneurin for throwing me into the deep end of the public engagement world which I fell in love with, becoming a massive part of my PhD. And to Aisling, lively, full of humour and good tips, an amazing person to learn from.

A lot of other mentions are due to both the Denny and the SITraN gangs – in short, thank you everyone for all the help over the years. In particular Natalie and Lynne for all of your insights and help with the histology and 'occasional' office gossip.

Contents

Lists of Figures

Chapter I

Chapter II

Chapter III

Chapter IV

Chapter V

Chapter VI

Appendixes

List of Tables

Chapter IV

Chapter V

Chapter VI

Abbreviations

Aβ	Amyloid Beta
ABC	Avidin Biotin Complex
ABC-HRP	Horseradish peroxidase-Conjugated Avidin Biotin Complex
ABC-AP	Alkaline Phosphatase-Conjugated Avidin Biotin Complex
ACh	Acetylcholine
AD	Alzheimer's Disease
AJ	Adherens Junction (Protein)
ALS	Amyotrophic Lateral Sclerosis
AP	Alkaline Phosphatase
APP	Amyloid Precursor Protein
AQP4	Aquaporin 4
AUC	Area Under the Curve
BBB	Blood Brain Barrier
BOLD	Blood Oxygen Level Dependence
CAA	Cerebral Amyloid Angiopathy
CBF	Cerebral Blood Flow
CBV	Cerebral Blood Volume
CID	Carrageenan-induced Inflammatory Pain
COLL IV	Collagen IV
COX-1	Cyclooxygenase -1
COX-2	Cyclooxygenase -2
CNS	Central Nervous System
DAB	3,3'-Diaminobenzidine
dH_2O	Distilled water
DPX	Distyrene Plasticizer Xylene
EC	Endothelial Cell
FAB Rat	Samaritan Alzheimer's Rat
FFPE	Formalin-Fixed Paraffin-Embedded
***f*MRI**	Functional Magnetic Resonance Imaging
GABA	Gamma-Amino Butyric Acid
GFAP	Glial Fibrillary Acidic Protein
icv	Intracerebroventricular
IHC	Immunohistochemistry
iv	Intravenous
HD	Huntington's Disease
HIVD	Immunodeficiency Virus Dementia
H&E	Haematoxylin & Eosin
IBA-1	Ionized Calcium Binding Adaptor Molecule 1
ICAM-1	Intercellular Adhesion Molecule 1
IFNγ	Interferon Gamma
IP-10	Interferon Gamma-induced Protein
IL (-10, -1β, -6)	Interleukin
ISF	Interstitial Fluid
LFP	Local Field Potential

LPS	Lipopolysaccharide
LSCI	Laser Speckle Contrast Imaging
MABP	Mean Arterial Blood Pressure
MCT1	Monocarboxylate transporter 1
MCP-1	Monocyte Chemoattractant Protein 1
MCT1	Monocarboxylate transporter 1
MRI	Magnetic Resonance Imaging
MUA	Multiunit Activity
MS	Multiple Sclerosis
NE	Norepinephrine
NF-κB	Nuclear Factor κB
NVC	Neurovascular Coupling
NVU	Neurovascular Unit
NO	Nitric Oxide
OIS	Optical Imaging Spectroscopy
PET	Positon Emission Tomography
PD	Parkinson's Disease
PDGFRβ	Platelet-Derived Growth Factor Receptor Beta
ROI	Region of Interest
ROS	Reactive Oxygen Species
S1FL	Forelimb Region of the Primary Somatosensory Cortex
SOM	Somatostatin
SS	Somatosensory Area
SSp-bfd	Primary Somatosensory Area – Barrel Field
TBI	Traumatic Brain Injury
TBS	Tris Buffered Saline
TJ	Tight Junction (Protein)
TRC	Tri-sodium Citrate
TRT	Total Recording Time
TLR-4	Toll-like-receptor 4
TGF (β1, β)	Transforming Growth Factor
TNFα	Tumour Necrosis Factor Alpha
VIP	Vasoactive intestinal polypeptide
VCAM-1	Vascular Cell Adhesion Molecule 1
B	Bregma

Chapter I

Introduction

1.1 Chapter summary

The neurovascular unit is essential for maintaining brain health and is the substrate of neurovascular coupling, the intimate relationship between brain blood flow and neuronal activity. Strong evidence implicates neurovascular dysfunction and neurovascular uncoupling in the early pathogenesis of neurodegeneration that occurs in Alzheimer's disease (AD). Cholinergic dysfunction and inflammation are also two key disease features of AD. Nevertheless, the characterisation of the effects of acetylcholine and inflammation on neurovascular function and neurovascular coupling remain elusive. Furthermore ageing plays a fundamental role in the development of AD pathology, in inflammation and is also accompanied by changes in neurovascular coupling. Extensive transgenic models have been developed for the study of AD pathophysiology but no model is able to replicate the full complexity of the disease. Thus, the use of non-transgenic rodent models is key in isolating and modelling specific features of pathology enabling the assessment of disease-related processes on neurovascular function and neurovascular coupling with a high degree of control.

High spatiotemporal resolution methods which provide characterisation of neurovascular function and neurovascular coupling changes such as the ones utilised in this thesis (laser speckle contrast imaging [LSCI], two-dimensional optical imaging spectroscopy [2D-OIS], multichannel electrophysiology), due to their invasiveness, require the use of an animal model and in many cases the use of anaesthesia. Careful selection of anaesthetic regime can decrease the impact of anaesthesia upon measured variables but its effects on physiological parameters should still be kept in consideration. The rodent barrel cortex with its topographical representation of each whisker provides the opportunity to map with a high degree of precision the relationship between evoked neuronal activity and subsequent changes in cerebral blood flow (CBF), thereby it is perfectly suited for the assessment of neurovascular coupling relationships.

This thesis aims to utilise a multi-modal approach to investigate neurovascular function, by employing immunohistochemistry (IHC) to characterise changes in the neurovascular unit (NVU) and interrogate how cellular changes impact upon *in vivo* imaging signals. This additional method furthermore increases the translational impact of preclinical studies to human research where tissue from post-mortem repositories is increasingly available for study.

By firstly investigating the neurovascular changes that occur from cholinergic manipulation and inflammation in a healthy non-transgenic animal will secondarily enable

the understanding of how these neurovascular changes impact upon and interact in disease, giving scope to expand such work in transgenic models.

This thesis aims to develop *in vivo* rodent models, relevant to AD, by employing cholinergic, inflammatory and ageing manipulations to investigate the effects of these disease-related processes upon neurovascular function and neurovascular coupling.

1.2 An overview of the neurovascular unit and its role in neurovascular function

The neurovascular unit (NVU) is a complex integrated system of neurons, glia (astrocytes and microglia), endothelial cells (ECs), pericytes and vascular smooth muscle cells (VSMCs) (Moskowitz, Lo, & Iadecola, 2010; Petzold & Murthy, 2011; Zlokovic, 2008; Zlokovic, 2011) that together are able to maintain appropriate brain homeostasis (Stanimirovic & Friedman, 2012). The high metabolic demands of the brain are met by a vast network of arteries, arterioles and capillaries which deliver oxygen and nutrients in a highly regulated manner (Kisler, Nelson, Montagne, & Zlokovic, 2017). The arteries split from the surface pial arteries and dive down into the brain parenchyma narrowing and branching into arterioles and capillaries. The NVU can be found along the length of the vascular tree with differing NVU members at varying vascular depths, which is illustrated in Figure 1.1. The NVU is instrumental for neurovascular function with each cellular member acting upon it. Neurons alongside astrocytes are responsible for initiating signals of vasodilation, whist ECs, pericytes and VSMCs orchestrate these signals to induce changes in cerebral blood flow (CBF) (Girouard & Iadecola, 2006). It has become apparent that in order to understand how the brain functions in health and disease it is imperative to consider both the function of each individual cellular component and the interactions of the entire cell community in regulating CBF.

1.2.1 Neurons in neurovascular function

Neurons are electrically excitable cells with the ability to produce and transmit information though chemical and electrical signals via their synapses. During synaptic activity neurons release a wide range of neurotransmitters such as acetylcholine, gamma-amino butyric acid (GABA), neuropeptides, catecholamines and glutamate. Some neurotransmitters have direct vascular effects, whereas others such as glutamate act via more complex pathways, stimulating the release of other neurotransmitters, such as nitric oxide (NO) (Fergus & Lee, 1997; Iadecola, 1998; Lok et al., 2007). The release of these substances in the brain extracellular space reaches blood vessels through diffusion causing relaxation of VSMCs and thus impacting upon vasodilation (Drake & Iadecola, 2007a). It has been estimated that nearly every neuron in the human brain has an individual capillary thereby re-highlighting the importance of the neuro-vascular relationship (Zlokovic, 2008). Astrocytes are in close proximity to neurons and react to released neuronal neurotransmitters to bring about changes in CBF (Section 1.2.2.1). The role of neurons in mediating CBF and neurovascular coupling is discussed in Section 1.3.2.

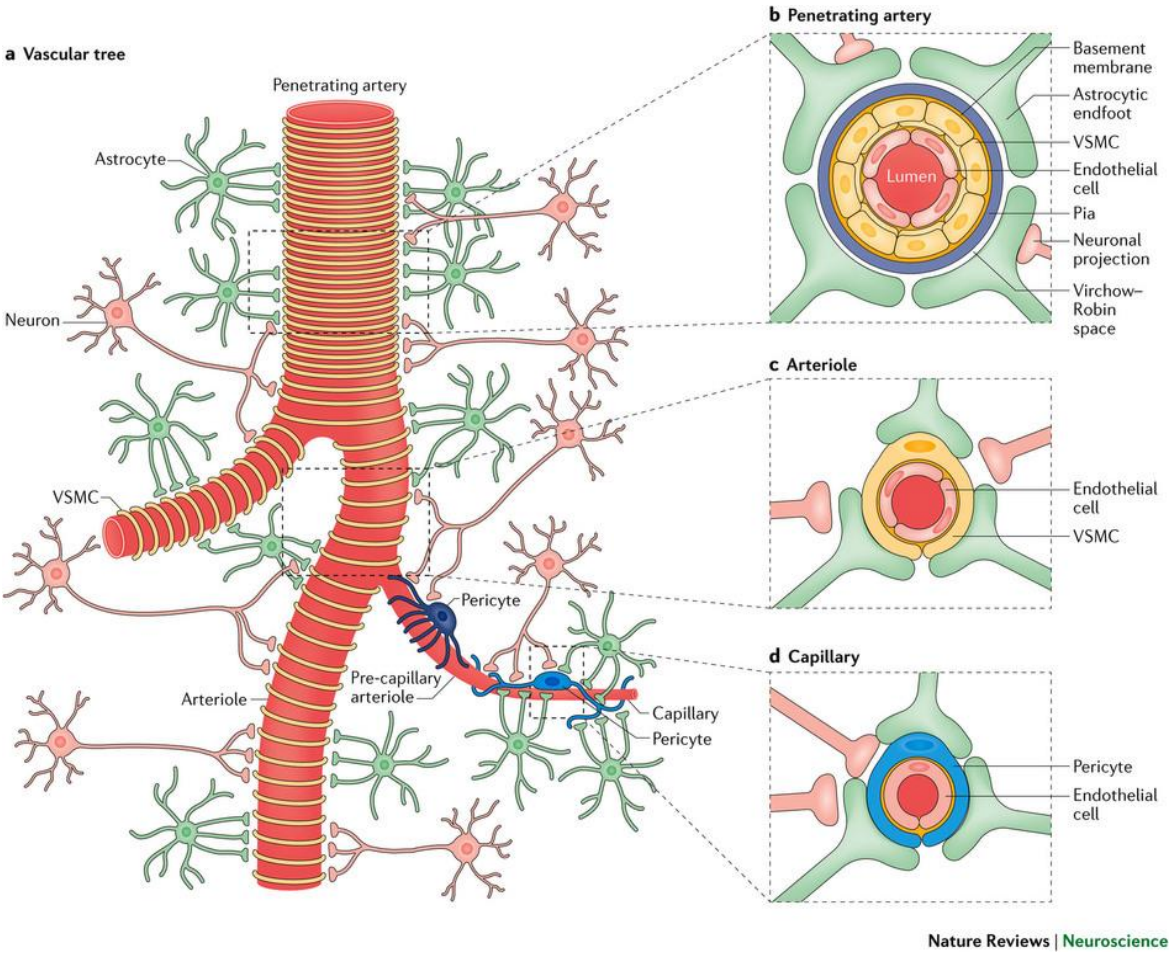

Figure 1.1. Schematic of the neurovascular unit (NVU) along the vascular tree. Neurons, astrocytes, vascular smooth muscle cells (VSMCs), pericytes and endothelial cells (ECs) make up the NVU. The cellular composition of the NVU varies along the vascular tree **(a)** although principal cellular components such as astrocytes and neurons remain present throughout. At the level of penetrating arteries **(b)** ECs line the vessel wall and are ringed by layers (1-3) of VSMCs ensheathed by a layer of pia. Astrocytes endfeet do not directly project onto the pia, they instead project on the Virchow-Robin space, containing CSF. Neuronal projections directly innervate astrocyte endfeet. At the arteriole level **(c)** astrocytes endfeet coverage is in direct contact with the VSMCs (only 1 layer), neuronal projections can be found on astrocyte endfeet. Lastly at the capillary level **(d)** ECs wrap around the lumen which are subsequently enshealded by pericytes making direct contact with ECs (no layer of VSMCs is present). Pericytes and ECs are covered by astrocyte endfeet which are innervated by neurons. At this vascular level pericytes also appear to be directly innervated by neurons. Figure taken from Kisler et al. (2017).

1.2.2. Glia

Glia are a group of cells that include astrocytes and microglia which provide support to other cellular components of NVU by maintaining homeostasis, responding to and resolving injury and regulating blood flow.

1.2.2.1 Astrocytes

Astrocytes cover 99% of cerebral capillaries and play a vital role in cell-to-cell interactions, every day maintenance and development of the NVU and blood brain barrier (BBB) characteristics (Abbott, Rönnbäck, & Hansson, 2006; Erdő, Denes, & de Lange, 2017). Astrocytes play a role in the formation and maintenance of tight junctions (TJ) and upregulation of the distribution of transporters and enzymes (O'Donnell, Ding, & Nedergaard, 2015). These cells might serve as functional intermediates between neurons and blood vessels, in the day to day regulation of cerebral vascular permeability (Ballabh, Braun, & Nedergaard, 2004) as virtually all signalling molecules targeting the vasculature must first act on or pass through astrocytes in order to reach VSMCs (Petzold & Murthy, 2011). Astrocytes are organised in different domains and share a close anatomical and functional relationship with neuronal synapses (Barres, 2008; Haydon, 2001), reinforcing their involvement in conveying changes in neuronal activity levels to the vasculature (Petzold & Murthy, 2011).

Their relationship with neurons include uptake of potassium ions released by neurons into the extracellular space during action potential (Durand, Park, & Jensen, 2010; Mehta et al., 2013). Neuronal signalling activates astrocyte calcium channels, triggering the release of potassium which spreads into the space between astrocytes endfeet and arteriole VSMCs. The arteriole response is modulated by the amount of potassium available, where a higher concentration leads to depolarization and vasoconstriction and a lower concentration leads to hyperpolarization and vasodilation (Filosa et al., 2006; Lok et al., 2007). Astrocytes thus regulate contraction and relaxation of VSMCs thereby modulating CBF (Leybaert, 2005; Takano et al., 2006; Witthoft & Karniadakis, 2012).

Astrocytes also play a role as metabolic partners to neurons by converting glucose into lactate which is then provided to neurons as a source of energy (Magistretti & Pellerin, 1996) and by mediating calcium signalling to modulate the strength of excitatory and inhibitory synapses (Simard & Nedergaard, 2004). Lastly, these cells play a critical role in the water and electrolyte homeostasis of the NVU (Barres 2008). It is estimated that a single astrocyte can regulate and sense the function of over one million synapses in its domain emphasising their role as a key NVU player in coordinating neurovascular

function (Koehler, Roman, & Harder, 2009). The role of astrocytes in neurovascular coupling is further discussed in Section 1.3.3.

1.2.2.2 Microglia

Microglia are regarded as the immune system frontline defence but in recent years these cells have also been recognised as an important cellular component of the NVU (Aguzzi, Barres, & Bennett, 2013; Kettenmann, Hanisch, Noda, & Verkhratsky, 2011; Noda, Ifuku, Mori, & Verkhratsky, 2013). Although not in direct contact with vessels, microglia communicate with other NVU cells, including astrocytes and neurons to maintain brain homeostasis. In the healthy brain microglia are closely associated with the tripartite synapse where the astrocyte presynaptic process joins the neuronal synapse (Kettenmann et al., 2011; 2012; Aguzzi et al., 2013). In this position microglia are able to communicate with both pre and post synaptic neuronal terminals and astrocyte processes. These cells have also been shown to respond to neuronal activity by releasing factors that module neuronal function, including cytokines, NO, adenosine triphosphate (ATP) and glutamate. Finally, these cells have also been shown to have a role in synaptic plasticity and synaptic pruning during development (Kettenmann et al., 2011; Kettenmann, Kirchhoff, & Verkhratsky, 2013). As immune surveyors, microglia scavenge apoptotic cells, tissue debris, extracellular molecules and amyloid-β (Harry, 2013; Kettenmann et al., 2011; Kofler & Wiley, 2011).

1.2.3 Endothelial cells (ECs)

ECs create a membrane around blood vessels which is specialised in limiting the entry of plasma components, metabolites, peptides, proteins, red blood cells and leukocytes into the brain (Zlokovic, 2011); forming an interface between brain and blood (Abbott, 2003; Abbott, Patabendige, Dolman, Yusof & Begley, 2010). In conjunction with glia and VSMCs, ECs promote clearance of toxic substances from the CNS (Zlokovic, 2008). At rest, ECs suppress transcription of other adhesion molecules (ICAM-1, VCAM-1 and E-selectin) and do not interact with leukocytes (Ley & Reutershan, 2006; Pober & Sessa, 2007). ECs have also been shown to play an important role in vascular tone regulation mediated by the release of vasoactive factors including NO, free radicals, prostacyclin and endothelin (Faraci & Heistad, 1998; Girouard & Iadecola, 2006), and directly act to regulate these signals to VSMCs thereby regulating blood flow (Busse & Fleming, 2006; Pober & Sessa, 2007). Chen et al. (2014) recently demonstrated that disruption to ECs signalling halts propagation of vasodilation in pial arteries following stimulation and significantly attenuates the haemodynamic response.

1.2.4 Pericytes

Pericytes ensheath capillary ECs (Armulik, Abramsson, & Betsholtz, 2005; Kisler et al., 2017) and are located between astrocytes and neurons (Zlokovic, 2008). These cells are recognised as having multiple roles within the NVU including microcirculation (Hamilton, Attwell, & Hall, 2010), regulation of BBB permeability (Armulik et al., 2010) and in the formation of new blood vessels (Gerhardt & Betsholtz, 2003). If hypoxia or traumatic brain injury occurs, pericytes have been reported to rapidly migrate away from brain microvessels (Dore-Duffy et al., 2000; Gonul et al., 2002) thereby increasing BBB permeability (Armulik, Genové, & Betsholtz, 2011; Armulik et al., 2010; Daneman, Zhou, Kebede, & Barres, 2010). Pericytes have been shown to have contractile properties thereby suggesting that regulation of capillary blood flow may be a function of these cells (Bandopadhyay et al., 2001). More recently, Hall et al. (2014) demonstrated capillary pericytes to be regulators of CBF as well as initiators of functional imaging signals, by being the first vascular elements to dilate in response to neuronal activity. Their addition to cultured ECs and astrocytes seem to bring about formation of capillary-like structures (Ramsauer, Krause, & Dermietzel, 2002), reinforcing their role in the control and direction of blood flow.

1.2.5 Vascular smooth muscle cells (VSMCs)

VSMCs line the walls of blood vessels and have contractible properties, allowing dynamic changes in luminal volume (Hill-Eubanks, Werner, Heppner, & Nelson, 2011) and blood flow (Amberg & Navedo, 2013). These cells respond to calcium (Ca^{2+}) and potassium (K^{+}) signalling between astrocytes and neurons by changing their vessel diameter accordingly; thereby changes in the contractile state of VSMCs increases or decreases vascular diameter thus leading to increases or decreases in blood flow through the vessel determining the vascularisation of the surrounding tissue (Amberg & Navedo, 2013). As such, events that affect [Ca^{2+}] have clear physiological and pathophysiological consequences on VSMCs contractibility and thus regulation of blood flow. Similarly to [Ca^{2+}], neuronal NO hyperpolarises and relaxes VSMCs thereby directly mediating their dilatory response (Kisler et al., 2017). Furthermore, VSMCs have a role in regulating the contractility of intracerebral arteries (Kuchibhotla, Lattarulo, Hyman, & Bacskai, 2009; Takano, Han, Deane, Zlokovic, & Nedergaard, 2007). As both VSMCs and ECs are connected by homocellular gap junctions these cells are able to extend their vasodilation retrogradely (Sokoya et al., 2006), allowing extension of their vasodilatory response hundreds of micrometres from the original site of activation (Erinjeri & Woolsey, 2002).

1.2.6 The blood brain barrier (BBB)

The blood brain barrier (BBB) is often regarded as a 'physical' barrier to diffusion involved in regulating the movement of molecules, cells and ions between the CNS tissue and the blood. The BBB is comprised of ECs that line the cerebral microvessels which work closely with TJ proteins formed by transmembrane proteins that halt diffusion between cells (Abbott, Patabendige, Dolman, Yusof, & Begley, 2010; Abbott et al., 2006; Begley, 2003). Other cells within the NVU are also involved in the maintenance and function of the BBB (Abbott et al., 2006; 2010). Astrocyte endfeet envelop blood vessels and are in direct contact with neuronal axons. Astrocytes help the formation and maintenance of TJ proteins and upregulate the distribution of transporters and enzymes (Dorovini-Zis, 2015), perivascular macrophages help maintain brain homeostasis by providing immune surveillance and pericytes help maintain BBB permeability levels (Armulik et al., 2011) and provide structural stability to the vessel wall (Ballabh et al., 2004). The BBB also acts as a transport barrier ensuring the passage of oxygen, vitamins, proteins and nutrients from the blood to the brain (Bundgaard & Abbott, 2008) and restricting passage of larger molecules such as peptides. The BBB protects the CNS from fluctuations in ionic composition that would disrupt axonal and synaptic signalling and prevents any cross talk between peripheral and CNS neurotransmitters (Abbott et al., 2006). Metabolically, the BBB impedes and limits the passage of toxins and pathogens from entering the brain and plays an important role in effluxing waste and toxic metabolites from the CNS (Abbott et al., 2010).

1.3 Neurovascular coupling: the relationship between CBF and neuronal activity

The close relationship between neuronal activity and blood flow has provided a unique opportunity to investigate and map brain function by utilising changes in flow as a derivative of brain function. Neurovascular coupling refers to a regulated phenomenon aimed at ensuring that an adequate supply of oxygen and glucose is delivered to neurons during task performance (Cauli & Hamel, 2010). This supply is achieved by increases in local CBF, through vasodilation which is mediated by the extensive network of cerebral blood vessels (Petzold & Murthy, 2011). Neurovascular coupling is achieved by neurons and glia initiating vasodilatory signals, which are transduced into vascular changes by ECs, pericytes and VSMCs leading to CBF increases (Girouard & Iadecola, 2006). Thus, neurovascular coupling can be defined as the process by which neuronal activity influences the haemodynamic properties of the surrounding vasculature (D'Esposito,

Deouell, & Gazzaley, 2003). Understanding the role of neurovascular coupling and CBF regulation is becoming more important for the understanding of neurodegenerative diseases mechanisms, including Alzheimer's (AD), Parkinson's (PD), and Huntington's disease (HD) and neurological conditions such as epilepsy, as all of these conditions have increasingly been associated with a degree of neurovascular disruption and neurovascular uncoupling (Attwell et al., 2010; Girouard & Iadecola, 2006; Iadecola, 2004; Kisler et al., 2017).

Driven in part by the wide expansion of fMRI, the mechanisms that are involved in mediating neurovascular coupling have in the last twenty years been subject to intense study (Iadecola, 2004; Girouard & Iadecola, 2006; Shih et al., 2012; Kisler et al., 2017; Sutherland et al., 2017) and to this day its intricate signalling is still under investigation. Several contributors and mediators have been identified to play a role in CBF changes and thus neurovascular coupling. These include vasoactive factors and neurotransmitters, central pathways, interneurons and astrocytes (for a detailed review see Girouard & Iadecola, 2006). What has emerged clearly from this past research is a multimodal view of vasodilation. Multiple mediators originating from multiple NVU cells acting on the cerebral vasculature on different levels to jointly bring about CBF changes (Girouard & Iadecola, 2006). These factors will be reviewed below, and are illustrated in Figure 1.2. Increasing our understanding of the cellular mechanisms and pathways that underpin neurovascular coupling in health and disease will enable more accurate interpretation of blood oxygen level dependent (BOLD) fMRI signal data in non-invasive human imaging.

1.3.1 The roles of vasoactive factors in neurovascular coupling

Lactate and adenosine are both thought to be involved in the neurovascular signalling. Lactate that is produced as a result of brain activation increases hydrogen ion concentration which produces vasodilation (Attwell & Iadecola, 2002). Astrocytes also appear to have a role in the production of lactate by metabolising glucose during gliosis (Pellerin et al., 1998). Neurons would then uptake the produced lactate to facilitate ATP synthesis (Girouard & Iadecola, 2006). Adenosine is instead produced during ATP catabolism and is regarded to be a strong vasodilator involved in the neurovascular coupling signal in both cerebrum and cerebellum (Ko, Ngai, & Winn, 1990; Li & Iadecola, 1994). Vasoactive neurotransmitters, such as dopamine, GABA and acetylcholine have also been implicated in vasodilation whereby neurotransmitters are released from neurovascular projections in close contact to blood vessels thus modulating the CBF response (Girouard & Iadecola, 2006). Vasoactive factors mediated and released by neuronal activity and neurotransmitter receptors have also been shown to have a role in neurovascular coupling.

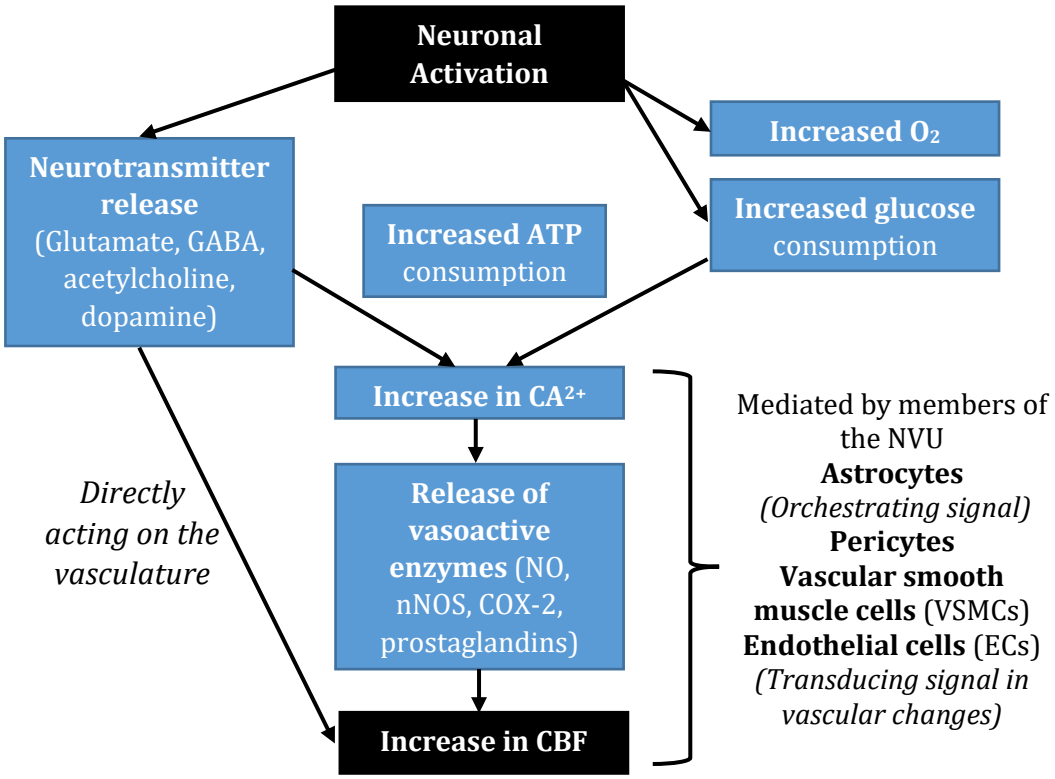

Figure 1.2. Diagram of neurovascular coupling mechanisms. Following neuronal activation which is accompanied by metabolic changes (increased O_2, ATP and glucose consumption) and neurotransmitter release, cells of the NVU (astrocytes, pericytes, VSMCs and ECs) begin orchestrating or transducing the signal into vascular changes (increase in CBF). Released neurotransmitters can also act directly on the vasculature thereby modulating CBF changes.

Glutamate receptor activation produces increases in blood flow mediated by vasodilation, dilating pial arterioles as well as cerebral microvessels. Calcium changes (Ca^{2+}) mediate the production of [Ca^{2+}] enzymes such as the neuronal isoform of NO synthase (nNOS) which leads to the production of NO, a potent vasodilator (Busija, Bari, Domoki, & Louis, 2007). Inhibition of nNOS in the cortex is associated with a reduced increase in CBF as a result of neuronal activity, highlighting a possible role of NO in neurovascular coupling (Attwell et al., 2010). NO has also been implicated in the modulation of the astrocytic pathways responsible for dilation and constriction of blood vessels (Attwell et al., 2010).

Like nNOS and NO, cyclooxygenase (COX) metabolised from arachidonic acid produced by increases in [Ca^{2+}] creates several prostaglandins involved in vasodilation. Of the four COX isoforms, COX-2 appears to be the one involved in neurovascular coupling. CBF increases appear to be mediated by COX-2 inhibitors which most likely release prostaglandins

(Niwa, Araki, Morham, Ross, & Iadecola, 2000). COX-2 location, on axon terminals and dendritic process in close contact to arterioles and glial processes, strengthen its role in vasodilation and neurovascular coupling (Girouard & Iadecola, 2006).

Lastly GABA, acting via the $GABA_A$ receptors also mediates a component of the vasodilatory response in the cortex by stimulation of the basal forebrain; it although remains unclear if this is a direct effect on the vasculature or if this effect is mediated by neurons or astrocytes (Attwell et al., 2010).

1.3.2 Neurons and neurovascular coupling

Neuronal activity requires the consumption of adenosine triphosphate (ATP) by neurons (and astrocytes) which is supplied by oxygen and glucose delivery from the surrounding capillaries (Shulman & Rothman, 2005). Control of vascular energy supply by neuronal activity is mediated by feedforward mechanisms, where neuronal activity is coupled with increases in CBF and energy supply (Attwell et al., 2010). Activated neurons can act directly via their receptors on the local vasculature or indirectly via astrocytes (Cauli & Hamel, 2010). Directly, neurons release vasoactive mediators including glutamate which increase the concentration of $[Ca^{2+}]$ in neurons and glia, triggering the synthesis of nNOS, prostaglandins and epoxyeicosatrienoic acids (Attwell et al., 2010).

In vivo arterioles start to dilate 500 milliseconds after increases in $[Ca^{2+}]$, suggesting that vasodilatory messengers must be released prior to this time. Haemodynamic responses are observed to initiate 600 milliseconds after sensory evoked stimulation (Devor et al., 2003), suggesting that only fast $[Ca^{2+}]$ releasing cells can impact upon the early phase of the haemodynamic response – such as neurons and astrocytes.

1.3.3 Astrocytes and neurovascular coupling

Astrocytes have for some time been viewed as the cellular substrate for mechanisms that relate changing neuronal activity and metabolic demand to precisely controlled changes in local blood supply (Attwell et al., 2010; Howarth, 2014; Lind, Brazhe, Jessen, Tan, & Lauritzen, 2013; Takano et al., 2006). Astrocytes have been reported to elicit both vasoconstriction and vasodilation on brain arterioles (for a review see Howarth, 2014).

The most popular hypothesis of CBF control in response to neuronal demand (activity) by astrocytes is triggered by an increase in $[Ca^{2+}]$ in response to neuronally released glutamate. Calcium elevations in astrocytes are produced by the activation of metabotropic glutamate receptors (mGluRs) and by propagation of calcium waves from adjacent astrocytes via gap junctions (Drake & Iadecola, 2007b). This increase in $[Ca^{2+}]$

would then activate a downstream production and release of vasoactive substances (Takano et al., 2006; Zonta et al., 2003). Zonta et al. (2003) showed that neuronal activity is able to trigger astrocytic calcium waves that correspond temporally with local arteriole vasodilation and that direct stimulation of individual astrocytes produces rapid vasodilation of nearby arterioles.

The role of astrocyte [Ca^{2+}] transients in the control of CBF during neurovascular coupling *in vivo* still remains highly debated. Recent data analysis advances (Lind et al., 2013) increasing the sensitivity of recorded [Ca^{2+}] transients have 'reinstated' the role of astrocytes [Ca^{2+}] transients in mediating neurovascular coupling which were seen by some (Nizar et al., 2013; Wang et al., 2006) as too slow to impact upon it. Furthermore, the role of glutamate in mediating CBF increases has been called into question. Retina based studies argue that neuron-glia signalling may instead be mediated by the release of ATP by neurons (Metea & Newman, 2006) and it has been further shown in cortex that [Ca^{2+}] astrocyte signals can be evoked by ATP (Sun et al., 2013). The role of astrocytes in neurovascular coupling is complex, requiring further investigation, for example in validating other mechanisms of CBF modulation such as glutamate transport and astrocytic control of CBF in pathology (Howarth, 2014).

Astrocytic K^+ signalling is a further mechanism that has been shown to impact upon neurovascular coupling (Filosa et al., 2006). Astrocyte processes at the synapse uptake neuronally released K^+ during activation and release it at their endfeet, which are in direct contact with the local vasculature, thereby acting as a powerful vasodilatory mediator. Although this K^+ signalling by astrocytes has been observed in brain slices, it still requires validation *in vivo* (Attwell, et al., 2010).

1.4 Alterations in neurovascular unit and neurovascular function

1.4.1 Effects of altered brain microcirculation

Changes in brain microcirculation are noticeable during NVU breakdown. Microvascular deficits diminish CBF influx and therefore diminish oxygen, energy substrates and nutrient supplies. This impedes clearance of neurotoxic molecules that accumulate or deposit on neurons, non-neuronal cells and in ISF. Reduction of capillary density, rise in endothelial pinocytosis, a decrease in mitochondrial content and accumulation of collagen during altered brain microcirculation are also observed (Farkas, 2001; Iadecola, 2004). Furthermore, changes to the length of brain capillaries leads to a reduction and diminished transport of energy substrates and nutrients across the BBB, as well as reducing the clearance of potential neurotoxins from the brain (Bailey, Rivara, Rocher, &

Hof, 2004; Wu et al., 2005). More recently, pericyte loss in pericyte-deficient mouse models has been shown to lead to brain vascular damage. There are two parallel pathways in which this damage occurs: a BBB breakdown with accumulation of serum proteins with potential toxic blood derived products and a reduction in brain microcirculation progressing to tissue hypoxia thereby leading to secondary neuronal degeneration (Winkler et al., 2011; Zlokovic, 2011).

1.4.2 Effects of altered global CBF and autoregulation

Tied to brain microcirculation reductions in global CBF have aggravating consequences for the NVU. A 20% reduction of CBF, as seen in normal ageing, is associated with diminished cerebral protein synthesis (Hossmann, 1994). More severe reductions (such as the ones occurring during neurodegenerative processes) lead to shifts of intracerebral pH and water as well as accumulation of glutamate and lactate in brain ISF (Drake & Iadecola, 2007a). CBF reductions of 50% or more impair ATP synthesis and decrease the ability for neurons to fire action potentials. Increased reductions of 80% or more, which are similar to the ones found after ischemic stroke, lead to an imbalance of electrolytes and ischemic neuronal death (Zlokovic, 2008).

1.4.3 BBB changes

In an altered physiological state where one or more NVU cellular components are affected, BBB function is impaired (Dorovini-Zis, 2015). BBB breakdown occurs through several factors; the disruption of TJ and adherens junctions (AJ), increase in bulk-flow fluid transcytosis and/or enzymatic degeneration of the capillary basement membrane. Pericyte deficiency can also lead to reduction in expression of TJ proteins and increase bulk-flow transcytosis across the BBB, leading to BBB breakdown. In mice, an age-dependent progressive loss of pericytes can lead to BBB disruption and microvascular degeneration to then cause neuronal dysfunction, cognitive decline and neurodegenerative changes (Bell et al., 2010). BBB breakdown leads to impeded clearance of various molecules in the brain. This build-up of serum proteins such as immunoglobulins and albumin, can cause brain swelling, oedema and suppression of capillary blood flow (Bell et al., 2010; Zhong et al., 2009). It has also been reported that high concentrations of thrombin lead to neurotoxicity and memory impairments accelerating neurovascular damage and BBB disruption (Chen, Cheng, Yang, & Lyden, 2010; Mhatre et al., 2004). Similarly, accumulation of plasmin leads to neuronal injury and high levels of fibrin speed up the process of neurovascular damage (Paul, Strickland, & Melchor, 2007).

1.4.4 Neurovascular uncoupling

Neurovascular uncoupling is termed as an alteration in the relationship between CBF and neuronal activity, whereby CBF is no longer matched to the metabolic requirements of neuronal tissue. Such disruption has been shown to impair the delivery of substrates to brain cells and impede the removal of by-products arising from cerebral metabolism (Girouard & Iadecola, 2006) thereby damaging the cells of the NVU. Alterations of the brain microenvironment and thus cellular interactions of the NVU are ubiquitous features of several pathologies including AD and have been implicated as causal factors in disease development (De Strooper & Karran, 2016; Sweeney, Sagare, & Zlokovic, 2015; Zlokovic, 2011). The exact process or processes involved in neurovascular dysfunction and the underlying cellular substrates of these effects remains unclear.

1.5 Neurodegenerative diseases

In most neurodegenerative diseases early disease processes remain elusive (Haass, 2010) and early disease biomarkers are yet to be identified (Blennow, 2010). Reductions of CBF and breakdown of BBB are two early and critical changes that have been associated with or have been shown to precede neurodegenerative disease development (Bell et al., 2010; Zhong et al., 2009). In conjunction with neuroimaging, epidemiological and pathological studies have suggested that brain microcirculation and blood flow reductions seem to precede cognitive decline (Bell et al., 2010; Ruitenberg et al., 2005; Vermeer et al., 2003).

The *vascular hypothesis of neurodegeneration* as proposed by Zlokovic (2011) states that increased BBB permeability leads to accumulation of vasculotoxic and neurotoxic molecules which quickly evolves into a reduced influx of CBF leading to hypoxia in turn compromising neuronal and synaptic function (Hawkins & Davis, 2005; Zlokovic, 2005; Zlokovic, 2011). It has been shown that vascular insults may contribute, initiate or play a joint role in neurodegeneration (Zlokovic, 2011) thereby making initial vascular events such as hypoxia and inflammation causes and not consequences of neurodegeneration (Stanimirovic & Friedman, 2012). A modified version of the hypothesis of neurodegeneration is illustrated in Figure 1.3, presenting neurovascular coupling as a key preceding step to neurodegeneration. Furthermore, the roles of cholinergic dysfunction and systemic inflammation upon neurovascular coupling are yet to be fully characterised alongside their roles in promoting and advancing the development of neurodegenerative diseases such as AD.

1.5.1 Alzheimer's Disease (AD)

Alzheimer's disease (AD) is a neurodegenerative disease and the most common type of dementia worldwide. The pathology is characterised by elevated levels of amyloid-β (Aβ) protein developing into amyloid plaques leading to neuronal and vascular toxicity (Hardy & Selkoe, 2002; Tanzi, Moir, & Wagner, 2004) and presentation of neurofibrillary tangles of hyperphosphorylated tau protein (NFTs) (Selkoe & Podlisny, 2002). These features can be observed in brain areas key to memory and cognitive function such as the hippocampus, frontal cortex, amygdala and entorhinal cortex (Hof & Morrison, 2004). AD can be categorised into early-onset (familial) or late-onset (sporadic) and each arises from different mechanisms.

Early onset AD accounts for <1% of all AD cases (Blennow, de Leon, & Zetterberg, 2006; Hardy & Selkoe, 2002) and has a strong genetic component, characterised by mutations of three genes, presenilin-1, presenilin-2 and APP (Campion et al., 1999; Waring & Rosenberg, 2008) or a duplicate of the APP gene (Rovelet-Lecrux et al., 2006), which by altering APP processing greatly increase Aβ deposition (Hardy, 2006). Late-onset cases are sporadic in origin and causes are highly likely to be multifactorial (Chen et al., 2013) and linked to several mechanisms including neuroinflammation, TBI, diabetes, ageing and the presence of the ApoE ε4 allele (Breteler, 2000; Iqbal & Grundke-Iqbal, 2010). The ApoE ε4 allele has been implicated in cholesterol metabolism, the activation and neurotoxic production of microglia to Aβ as well as CNS and systemic infection (Barger & Harmon, 1997; Moretti et al., 2005). Only recently genes with important roles in immunity have been implicated in the development of late-onset AD (Jones et al., 2010), suggesting that individuals who develop AD may have an inability to adequately respond to infections (Licastro, Carbone, Ianni, & Porcellini, 2011).

Amyloid deposition is considered the hallmark of AD (Palop & Mucke, 2010) and the amyloid cascade hypothesis has been central in the research concerning its pathophysiology and development. The hypothesis states that an imbalance between the production and clearance of Aβ is key to the development of AD, which then secondarily triggers neuronal degeneration and leads to overt cognitive symptoms (Hardy & Allsop, 1991; Hardy & Selkoe, 2002; Hardy & Higgins, 1992). Over the years AD has although been recognised to display other features besides Aβ accumulation and NFTs, including cholinergic dysfunction, neuroinflammation, oxidative stress, neurodegeneration, microvascular dysfunction, and BBB breakdown (Stolp & Dziegielewska, 2009; Zlokovic, 2011).

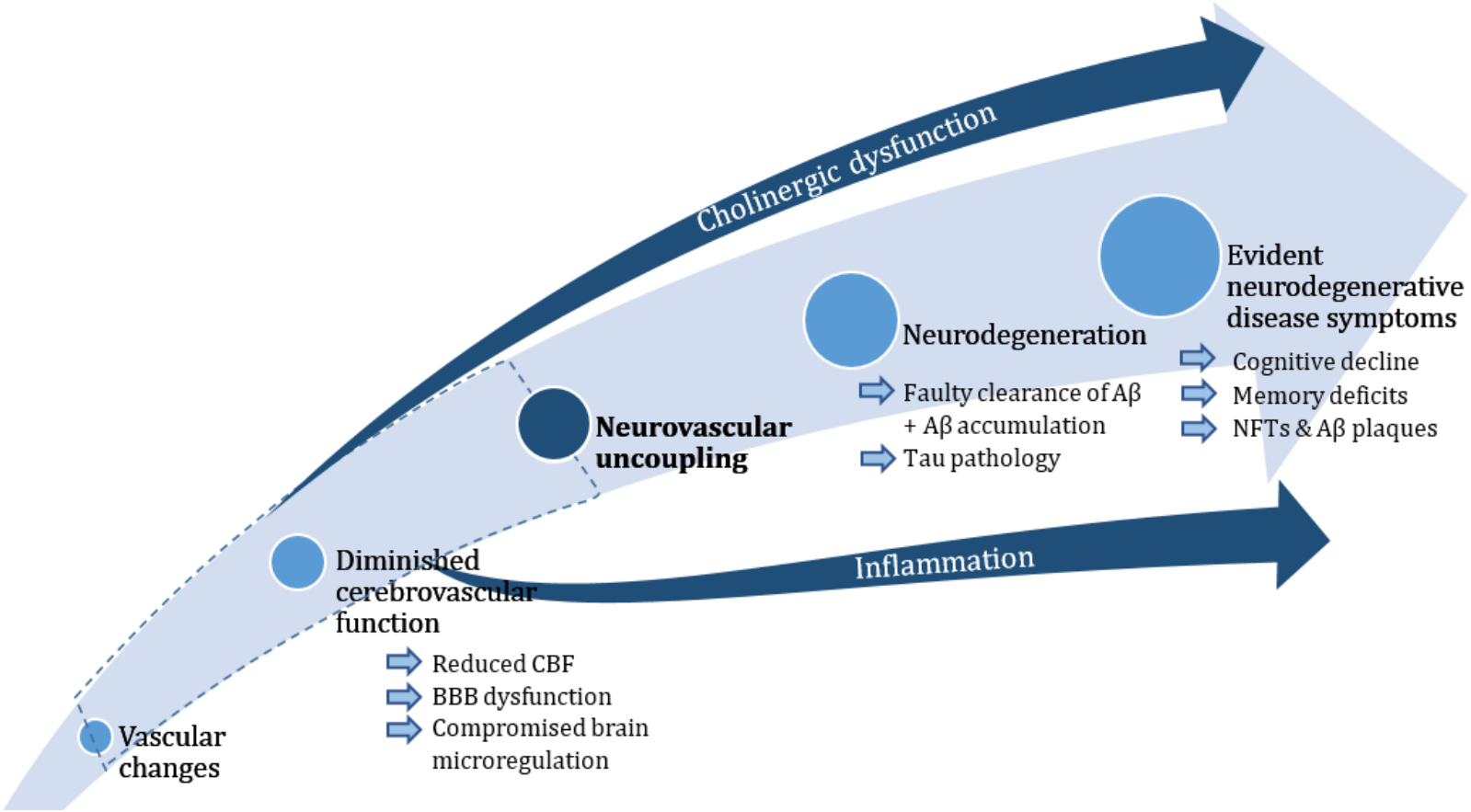

Figure 1.3. Illustration of the vascular hypothesis of neurodegeneration of AD as described by Zlokovic (2011) with thesis additions. Neurodegenerative disease development starts with vascular changes leading to diminished cerebrovascular function causing CBF, microregulation and BBB changes. Before neurodegeneration and development of overt symptoms a further change in neurovascular function occurs: neurovascular uncoupling. As such this thesis aims to investigate, with models relevant to AD, the impact of cholinergic dysfunction and systemic inflammation (associated darker smaller arrows) on vascular function and neurovascular uncoupling (segmented section of the arrow).

Cholinergic dysfunction, neuroinflammation and ageing are key in the pathogenesis of AD. Each factor forms the basis of an experimental chapter of this thesis (Chapter III, Chapter IV and Chapter VI respectively) and are briefly described below. Understanding, the effects of acetylcholine and neuroinflammation on neurovascular function and neurovascular coupling will enable characterisation of early brain changes that underlie AD pathology before the development of NFTs and Aβ plaques. Pathological changes leading to AD development have been shown to occur decades prior to clinical manifestation of symptoms (Bookheimer et al., 2000; Filippini et al., 2009; Sperling, 2011), thus the most effective disease modification or prevention strategies will encompass those that target early neuropathological changes. Furthermore, characterising inflammatory and cholinergic processes leading to neurovascular dysfunction in younger to middle-aged cohorts may provide the best results and timing to implement therapeutic treatments.

1.5.1.1 Cholinergic dysfunction

The cholinergic dysfunction seen in AD arises from the loss of cholinergic neurons in the basal forebrain (Arendt, Bigl, Arendt, & Tennstedt, 1983), which leads to a central cholinergic deficit, thereby decreasing acetylcholine levels, leading to memory and cognitive deficits (Cummings & Back, 1998). It is currently the only treatment target available for AD patients, in the mild to moderate stages of the disease, where cholinesterase inhibitors (ChEI) are used to elevate brain acetylcholine levels to partly counteract cognitive deficits (Klafki, Staufenbiel, Kornhuber, & Wiltfang, 2006). Evidence for cholinergic dysfunction impacting upon the regulation of CBF and neurovascular coupling forms the basis of experimental Chapter III and is reviewed in detail in Section 3.3.

1.5.1.2 Inflammation: Aβ driven and systemic

Inflammation is triggered by an immune response which can be of systemic or central origin (neuroinflammation). Debate in the literature exists between the role of inflammation in AD as a cause or consequence of the underlying pathology. The inflammation observed in AD brains has been related to the accumulation of Aβ, which triggers a pro-inflammatory response augmenting disease state (Eikelenboom et al., 2012; Grammas, 2011; Holmes et al., 2009; Wyss-Coray & Mucke, 2002). Of the cellular components of the NVU microglia and astrocytes appear to have a key role in inflammation. Both glia cells change activity profile when interacting with Aβ and Aβ plaques, becoming reactive and producing cytokines and neurotoxins (El Khoury, Hickman, Thomas, Loike, & Silverstein, 1998) and accumulating in the proximity of Aβ

plaques (Itagaki, McGeer, Akiyama, Zhu, & Selkoe, 1989; McGeer, Itagaki, Tago, & McGeer, 1987; Perlmutter, Barron, & Chui, 1990; Rodriguez, Olabarria, Chvatal, & Verkhratsky, 2009). On the other hand both glia cells have also been found to produce anti-inflammatory cytokines (El Khoury et al., 1998; Sofroniew & Vinters, 2010) (see Section 5.2). Furthermore, microglia express receptors that promote clearance of Aβ thereby restricting senile plaque formation (El Khoury et al., 1998; Simard, Soulet, Gowing, Julien, & Rivest, 2006) and astrocytes have also been implicated in the clearance of Aβ and Aβ oligomers alongside other neurotoxic waste products (Xie et al., 2013). A recent paper (Montacute et al., 2017) has further implicated the susceptibility of AD to inflammation by showing an increased microglial response during infection in both the cortex and hippocampus of 3xTg-AD mice irrespective of the infection being localised to the brain or the periphery; demonstrating that a neuroinflammatory response can be triggered and/or exacerbated by a systemic inflammatory stimulus.

The mechanism or mechanisms by which inflammation impacts upon AD is not fully understood but shows a strong link with ageing (further discussed in Chapter VI). Upregulation of systemic pro-inflammatory markers is a common feature of ageing and these markers are associated with an increased rate of cognitive decline (Holmes et al., 2009; Perry, Cunningham, & Holmes, 2007; Perry, Newman, & Cunningham, 2003). Furthermore, systemic inflammation has been associated with an increased incidence of AD, with risk increasing with repeated infections (Dunn, Mullee, Perry, & Holmes, 2005). The co-morbidity between AD and infection may be partly explained by immunosenescence, the deterioration of the immune system due to age, as this process is characterised by increased susceptibility to infection (Dorshkind, Montecino-Rodriguez, & Signer, 2009) and as the incidence of AD becomes more prominent with age.

1.5.1.3 Ageing

Age remains the number one risk factor for the development of AD (Bartzokis, 2004). With the incidence of AD development doubling every five years after the age of 60 (Qiu, Kivipelto, & von Strauss, 2009) and with the majority of AD diagnosis occurring in people aged over 65. Ageing brain changes including ones of neuroinflammatory origin appear to alter brain health and function leading to the development of neurodegenerative conditions (Eikelenboom et al., 2012; Grammas, 2011; Iadecola, 2010; Lee et al., 2008; Perry et al., 2007; Schmidt et al., 2002). The ageing process leads to an activation of an innate immune response leading to a chronic state of inflammation associated with cognitive decline (Cribbs et al., 2012). NVU cellular changes also occur, where microglia and astrocytes become primed, eliciting a bigger immune response due to their lowered

activation threshold (Frank, Barrientos, Watkins, & Maier, 2010). Ageing is also characterised by a decline in adaptive immunity and T helper 2 response (Franceschi et al., 2007), proposed to arise from factors that increase the imbalance between pro-inflammatory and anti-inflammatory networks (Holmes, 2013) resulting in a chronic low-grade pro-inflammatory state (Cevenini, Monti, & Franceschi, 2013).

1.5.1.4 Structural and neurovascular components of AD pathology

Neuroimaging methods including MRI, fMRI and positron emission tomography (PET) have been instrumental in gathering data regarding anatomical and functional changes in the AD brain. With MRI it became possible to quantify the progressive cerebral and hippocampal atrophy associated with AD pathology (Ferreira & Busatto, 2011), predict future sites of amyloid formation (Badea, Johnson, & Jankowsky, 2010) and in a recent study (van de Haar et al., 2016) show impairment of the NVU leading to CBF reduction and BBB impairment. Furthermore as atrophy of the hippocampus and entorhinal cortex are early structural changes and are also well correlated with NFT pathology, they have emerged as a valuable biomarker to track disease progression (Adlard et al., 2014). Diffusion weighted imaging (DWI) and diffusion tensor imaging (DTI) have instead been used to investigate white matter changes and detect microstructural and connective changes in hippocampus and limbic system tracts due to axonal degeneration and neuronal loss (Adlard et al., 2014).

In order to gain insight into the neurovascular dysfunction that precedes the neuronal loss observed with MRI, other neuroimaging technologies such as fMRI have been used to assess changes in CBF, cerebral blood volume (CBV) and BOLD. Studies have revealed severely altered cerebrovascular function, presenting with decreases in resting CBF and attenuation of increases in CBF by activation (Iadecola, 2004). Furthermore there is growing evidence that cerebrovascular reactivity or cerebrovascular reserve, the capacity of brain vasculature to enhance flow above basal levels in response to a challenge (measured with carbon dioxide, CVR-CO_2), is impaired in AD (Glodzik, Randall, Rusinek, & de Leon, 2013) and in young adults carrying the APOE ε4 allele (the best-established genetic risk factor for developing late-onset AD) (Suri et al., 2015). AD patients also show decreased coordinated activity in the default mode network (DMN) (Bokde, Ewers, & Hampel, 2009; Dickerson & Sperling, 2009). Changes in brain metabolism are also present: studies using fludeoxyglucose (FDG)-PET and single-photon emission computer tomography (SPECT), which measure synaptic activity and brain metabolism by tracking glucose, have revealed hypometabolism and hypoperfusion in AD brains (Johnson, Fox, Sperling, & Klunk, 2012). Taken together these findings highlight AD pathology as a

neurovascular disease which may be underpinned by neurovascular uncoupling. By understanding changes in neurovascular function which have been shown to precede both amyloid pathology and cognitive symptoms (Iadecola, 2004) it may be possible to develop interventions that could provide a degree of neuroprotection (Hamel, Royea, Ongali, & Tong, 2016) and modify vascular reserve (Glodzik et al., 2013).

1.6 Methods of studying neurodegeneration and neurovascular function

1.6.1 Imaging

The use of fMRI has proven an invaluable tool to image the haemodynamic response in a clinical setting. fMRI to this day is a non-surpassed method in non-invasive imaging studies (Belliveau et al., 1991). However, it poses controversy in its interpretation. The measured haemodynamic response, BOLD signal originates from the changing concentration of deoxyhaemoglobin in the microvasculature that surrounds an activated region (Mandeville et al., 1999; Turner, 2002), as such the BOLD signal reflects the ratio between paramagnetic deoxygenated haemoglobin and non-paramagnetic oxygenated haemoglobin (D'Esposito et al., 2003). Neuronal activity has the ability to alter this ratio via its influence on factors such as CBF, CBV and the cerebral metabolic rate of oxygen consumption ($CMRO_2$), as such the BOLD signal is an indirect measure of neuronal activity. Furthermore, as fMRI tracks changes in blood flow and oxygenation changes as surrogates of neuronal activity, disruption of neurovascular coupling in brain disease can confound interpretation of functional imaging data especially when imaging individuals with altered cerebrovascular dynamics (as they occur in ageing and in neurodegenerative disease).

Imaging techniques used in animal research overcome fMRI limitations in both spatial and temporal resolution (Boorman et al., 2010; Tian et al., 2010b) and allow for concurrent measurement of blood flow and neuronal activity (Martin, Martindale, Berwick, & Mayhew, 2006; Martin, Zheng, Sibson, Mayhew, & Berwick, 2013). In addition, from these measurements other significant parameters such as $CMRO_2$ (Jones, Berwick, Johnston, & Mayhew, 2001) and predictions of BOLD fMRI signal, to aid translation to human research, can be extrapolated (Kennerley, Mayhew, Boorman, Zheng, & Berwick, 2012). Thus, mapping relevant pathological changes to *in vivo* measurements in the context of disease will be key in utilising non-invasive imaging biomarkers to predict, diagnose and study neurodegenerative disease.

In the context of this thesis, two invasive-imaging methodologies will be employed for *in vivo* experiments: laser speckle contrast imaging (LSCI) and two-dimensional optical imaging spectroscopy (2D-OIS) as these methods offer superior temporal and spatial

resolution compared to preclinical fMRI. These methods are described in detail in Chapter II (Section 2.3.1).

1.6.2 Electrophysiology

The insertion of electrodes into the brain enables recording of neuronal activity across different spatial and temporal scales. Multi-unit activity (MUA) and local field potentials (LFP) are extracellular recorded signals that give a measure of local neuronal output and dynamics. The LFP signals refer to low frequency content (<500Hz) and it is believed to arise from the membrane currents of the neurons in close proximity to the electrode. The signal is characterised by large depolarisations due to stimulation, with the strongest response occurring during the first stimulation and gradually decreasing in size. The MUA signal instead represents high frequency content (<1000Hz) and local neuronal spiking (output of neuronal population). LFP have been shown to correlate most closely with BOLD responses and the haemodynamic response whereas MUA tends to return to baseline, adapting to repeated stimulations (Goense & Logothetis, 2008; Logothetis, Pauls, Augath, Trinath, & Oeltermann, 2001). These results suggest that the haemodynamic signal appears to reflect intracortical processing and input as opposed to overall spiking output (Logothetis et al., 2001). Electrophysiology is often combined with imaging methodologies to concurrently characterise the neurovascular response (Berwick et al., 2008; Boorman et al., 2015; Boorman et al., 2010; Martin et al., 2006; Martin et al., 2013).

Electrophysiological methods utilised in this thesis are described in Chapter II (Section 2.3.2)

1.6.3 Immunohistochemistry (IHC)

Immunohistochemistry (IHC) is a technique widely utilised in the fields of disease diagnosis, drug development and biological research. It is a precise histological method of characterising morphology, distribution and location of specific cellular components within their original tissue by forming an interaction with a target antigen and an antibody. This technique is applicable on a range of species (including human post mortem brains) enabling important characterisation of cell morphology in brain health as well as identification of cellular changes in disease. In the context of neurodegenerative disease research, a limitation of this technique is the ability to characterise 'end point' changes alone. The inability to characterise ongoing disease changes may prove identification of early disease features more difficult unlike the 'ongoing' changes that can be obtained with *in vivo* imaging techniques. Nevertheless LSCI and 2D-OIS imaging techniques are not able to provide morphological details on the cellular components of the

NVU and how these may change in the context of disease. Thereby, when possible, imaging and IHC methodologies should be jointly used to characterise the NVU from whole brain to single cell.

This method is further discussed in Chapter V (Section 5.5.2) where it has been used to characterise the cellular components of the NVU in the context of acute systemic inflammation.

1.7 Modelling neurodegenerative disease in preclinical models

Rodents, in particular mice and rats, are the most frequently used animals for experimental research, as their short gestation period, high birth rate, small size and low maintenance requirements make them ideal to breed and manage (Sarasa & Pesini, 2009). The discovery of specific genes (APP, presenilin 1 and 2) involved in the development of early-onset AD offered the opportunity to investigate disease pathogenesis by modelling AD in mice (McGowan, Eriksen, & Hutton, 2006). In the development of transgenic lines, mice have been historically preferred due to technical reasons concerning ease of transgene injection and higher embryo survival (Do Carmo & Cuello, 2013) thus an array of transgenic mouse lines are currently available. Transgenic mouse models have been imperative in modelling the *amyloid hypothesis,* in identifying the impact of Aβ oligomeric forms on cognition and in extrapolating biomarkers of AD during asymptomatic stages of the disease (Do Carmo & Cuello, 2013).

Rat transgenic models are lengthier and more complex to create thereby availability and number has significantly lagged behind that of mice. Prior to transgenics becoming available, much work investigating the cholinergic hypothesis of AD in rats was developed with chemical and lesion-induced naïve animals. Furthermore the discovery of Aβ as central to the development of plaques began the development of cerebral infusion of Aβ models in both physiologically normal (naïve) and non-transgenic rats (Do Carmo & Cuello, 2013). Lastly CBF dysregulation models also exists, whereby occlusion or restriction of the carotid artery recreates a similar microenvironment of memory impairments, neuronal dysfunction, Aβ oligomerisation and synaptic changes as seen in AD (Walsh et al., 2002).

1.7.1 The importance of naïve animal models

Mice and rats have been instrumental in the understanding of APP processing (Sarasa & Pesini, 2009) and rats have further been used to understand the effects of Aβ load on the cholinergic, serotonergic and noradrenergic systems as well as in characterising the

effects of Aβ in the context of age and diet (Gonzalo-Ruiz, Sanz, Arévalo, Geula, & Gonzalo, 2005). It is, however, important to note that no one animal model encapsulates all aspects of AD pathology. The primary structures of the Aβ peptide alongside their profile in mice and rats differ from that of humans (Du et al., 2007; Sarasa & Pesini, 2009). Furthermore, comparisons between transgenic models is difficult as it is highly dependent on animal genetic background and the promoter used to insert the transgene, thereby giving rise to different histological and clinical features in each model (Lecanu & Papadopoulos, 2013). The complexities in genetic and environmental factors (such as diet, physical activity, microbiome) which interact to cause late-onset AD, render late-onset AD models more challenging to create (Onos, Rizzo, Howell, & Sasner, 2016), as such this underlines the importance and relevance of utilising non-transgenic rodent models as part of neurodegenerative disease research.

When simulating and investigating aspects of disease which are most often regarded as risk factors or are co-morbid to disease progression, it is imperative to be able to accurately measure these changes independently of other factors including the underlying disease state. This enables more controlled, accurate modelling and tracking of the progression to early NVU and neurovascular function disruption. Naïve animal models facilitate and allow this level of control, as processes including cholinergic dysfunction and inflammation can be separated from the underlying disease state. It is by firstly identifying and quantifying early neurovascular changes in the brain of a healthy (naïve) animal that will allow clear delineation of disease-facilitating changes that can then be quantified and investigated in animal disease models and ultimately patients. Furthermore, naïve models are able to offer a non-genetic variant to the study of disease, a crucial element in research investigating neurodegenerative diseases such as AD, where the sporadic form of this condition far outnumbers the prevalence of the genetic one. Thereby the work conducted in this thesis has utilised non-transgenic models to recapitulate specific aspects of AD pathology in isolation to understand their independent effects on neurovascular function.

1.8 Choosing an appropriate animal model for *in vivo* research

The methodology used in this thesis to obtain haemodynamic and electrophysiology measurements in an altered state of functioning is invasive and thus cannot be measured without the use of an animal model. The rat physiology, morphology and genetic makeup is closer to humans then that of mice with substantial evidence that rat models provide physiological data that is relevant to human data in both normal and disease states (Do Carmo & Cuello, 2013; Gibbs et al., 2004; Hyder, Rothman, & Bennett, 2013; Jacob & Kwitek, 2002; Lin, 1995). In addition, the rat's larger body and brain size allows better

drug administration and as a whole displays more robust physiology for long duration *in vivo* imaging, electrophysiology, neurosurgery and neuroimaging (Sanganahalli et al., 2013). Lastly, learning and memory physiological systems have been extensively studied in rats (Sanganahalli et al. 2013) and rat behaviour is better characterised compared to mice. Furthermore, rat models have been extensively optimised for *in vivo* research where several techniques are concurrently applied in order to acquire multimodal data (Berwick et al., 2008; Martin et al., 2006; 2013; Boorman et al., 2010; 2015; Spain et al., 2015). As this thesis aims to concurrently acquire imaging and electrophysiological data a reliable and stable set up is required, thus making rats an excellent choice of model.

1.9 The importance of the rodent barrel cortex to neurovascular research

The whisker to barrel cortex pathway is well characterised and is commonly used in neurovascular coupling studies (Lecrux & Hamel, 2011). These whiskers operate to such a high degree of sensitivity which is comparable to primates' fingertips (Carvell & Simons, 1990). Each whisker is topographically mapped within the barrel cortex (Lübke & Feldmeyer, 2007) thereby providing the opportunity to map with a high degree of precision the relationship between evoked neuronal activity and changes in CBF (Lecrux et al., 2011; Staiger et al., 2000). Whisker stimulation in the barrel cortex activates pyramidal cells and a subset of GABA interneurons which co-localise vasoactive intestinal polypeptide (VIP) whilst inhibiting others which co-localise somatostatin (SOM) (Gentet et al., 2012). This translates into the release of mediators including COX-2 metabolites from activated pyramidal cells resulting in the haemodynamic response (Hillman, 2014; Lecrux & Hamel, 2016). Haemodynamic responses originating from stimulation of the barrel cortex have been robustly observed with single point measurements such as laser-Doppler flowmetry and various imaging techniques such as LSCI, optical imaging and BOLD fMRI (Lecrux & Hamel, 2016).

The topographical map of whisker representation in the barrel cortex is represented in Figure 1.4. In rodents the layout of the whiskers is precisely matched to the layout of the barrels in the somatosensory cortex. Whiskers are arranged in rows, where each whisker projects to a single cortical column in the contralateral barrel (somatosensory) cortex via the trigeminal nerve, brainstem and thalamic relays (Figure 1.4, blue arrows). Each cortical column is composed of six layers. Single whisker sensory information from the ventral posterior medial (VPM) thalamus arrives in layer 4, whereas the supragranular layers (2/3) and the infragranular layers (5/6) perform integrative functions (Aronoff & Petersen, 2008).

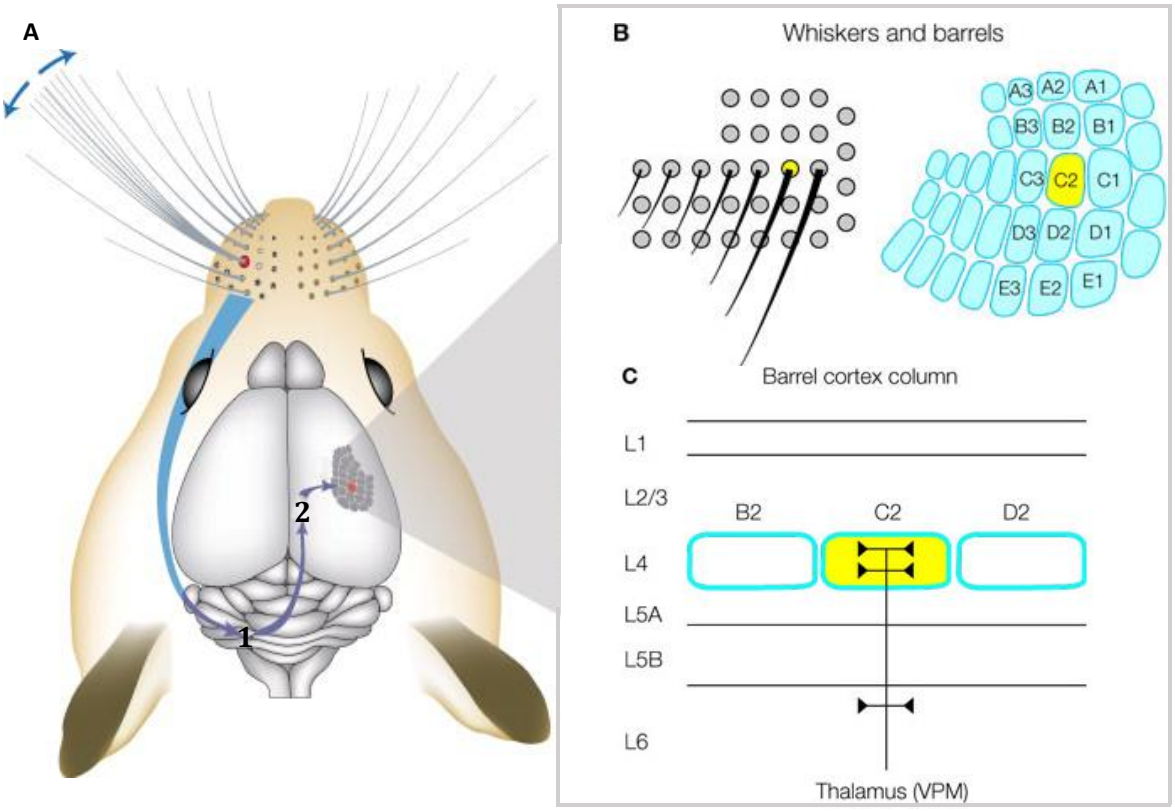

Figure 1.4. Representation of the rodent barrel cortex. Each whisker is topographically mapped to its corresponding barrel in the contralateral somatosensory cortex (A-B). Each barrel column is made up of 6 layers (C). Layer 4 directly receives sensory information from the whiskers relayed via the trigeminal nerve, brainstem (1) and VPM thalamus (2) (blue arrows). Figure adapted from Knott et al. (2002) and Aronoff and Petersen (2008).

1.10 The use of anaesthesia

Despite already developed methods of haemodynamic and neuronal recording in awake animals (Martin et al., 2006; Martin et al., 2013), invasive concurrent measurements of neurovascular function and drug treatments as performed in this thesis still require the use of anaesthesia. The effects of anaesthesia on physiological parameters are well documented and should be kept in consideration. Urethane anaesthetic has been shown to produce a mild cardiovascular depression (Field, White, & Lang, 1993) but remains a suitable choice for invasive surgery. Urethane induces a long lasting surgical anaesthesia suitable for stereotaxic manipulation and neurosurgery for a minimum of 8 hours (long half-life). It also has minimal respiratory and cardiovascular effects (Wildt, Hillen, Rauws, & Sangster, 1983) and has a stable neuronal activity readout (Angel & Gratton, 1982) by not hindering neuronal firing or neurotransmission in various subcortical areas and in the peripheral nervous system (Maggi & Meli, 1986). Lastly, and of importance to Chapter III of this thesis, urethane has no effect on acetylcholine release (Halliday, Little, & Paton, 1979).

1.11 Overall thesis aims and hypotheses

The overall **aim** of this thesis is to model the AD relevant factors of (i) cholinergic changes, (ii) systemic inflammation and (iii) ageing to better understand their effects on blood flow, neurovascular function and neurovascular coupling. This aim will be addressed by:

(1) Utilising non-transgenic rodent models to characterise effects of cholinergic modulation (Chapter III) and acute systemic inflammation (Chapter IV and Chapter VII) upon *in vivo* neurovascular function and neurovascular coupling changes.

(2) Performing a detailed characterisation of neurovascular unit cellular changes in acute systemic inflammation with immunohistological techniques and by relating observed cellular changes to *in-vivo* neurovascular effects (Chapter V).

(3) Comparing inflammation-driven changes in neurovascular function in a young and middle-age model (Chapter VI).

(4) Extrapolating findings to assess how these results can be relevant to the understanding of neurovascular dysfunction in AD.

In relation to the above aims, the following **hypotheses** were formulated for each experimental chapter:

(1) **Chapter III:** Decreases in brain cholinergic function will lead to an alteration in neurovascular coupling relationships, where stimulus evoked changes (increases or decreases) in neuronal demand are not accompanied by concomitant changes in CBF.

(2) **Chapter IV:** An acute systemic inflammatory challenge will alter neurovascular function, by changing how stimuli inputs are converted to haemodynamic response functions, thereby mediating neurovascular uncoupling.

(3) **Chapter V:** An acute systemic inflammatory challenge will result in acute changes in glia cell morphology (gliosis) and increased uptake of inflammatory markers such as ICAM-1 by ECs.

(4) **Chapter VI:** An acute systemic inflammatory challenge in middle aged animals will result in exacerbated neurovascular changes, whereby alterations in how stimuli inputs are converted to haemodynamic response functions will occur at an earlier time point..

Chapter II

Materials and Methods

2.1 Chapter summary

This chapter describes in detail the methods employed in this thesis including animal preparation, surgery, physiological monitoring, experimental design and procedures for data collection and statistical analysis. When possible these explanations are accompanied with a figure. Details of perfusion and histological processing are also described for the relevant experimental Chapters (V, VI).

Two imaging methodologies were used in this thesis, laser speckle contrast imaging (LSCI) for experimental Chapters III, IV, VI and two-dimensional optical imaging spectroscopy (2D-OIS) for experimental Chapters IV and VI to measure with high spatiotemporal resolution haemodynamic response changes in the rat's barrel cortex. Description of both experimental techniques follows a brief overview of the theoretical background and application of this methodology in the experimental design. Electrophysiology for neuronal recording was also employed in Chapter III (multichannel electrode) and in Chapter IV (surface electrode), a brief overview of the technique and its application in this thesis is given. Haemodynamic (and neuronal) changes were measured with (insertion of electrodes in the whisker pad) and without sensory stimulation (hypercapnia).

All studies conducted in this thesis were approved by the UK Home Office under the Animals (Scientific Procedures) Act 1986 and the University of Sheffield Animal Welfare and Ethical Review Body (AWERB, local ethics committee). All procedures were conducted under a U.K. Home Office licence.

2.2 Animal preparation

All studies conducted in this thesis were approved by the UK Home Office under the Animals (Scientific Procedures) Act 1986 and the University of Sheffield Animal Welfare and Ethical Review Body (AWERB, local ethics committee). All procedures were conducted under a U.K. Home Office licence.

2.2.1 Animals

Female Hooded Lister rats were bred or purchased from Charles River Ltd (Kent, UK). Animals were kept at a 12-hour light/dark cycle environment at a temperature of 22 ^{0}C with access to food and water *ad libitum* and housed in polycarbonate cages (*n*=3 per cage) under pathogen free barrier conditions in the Biological Services Unit at the University of Sheffield. Animals were fed conventional laboratory rat food. All animals except in Chapter VI were aged 3-5 months and weighed between 220-330g. Females were chosen as their lower and more constant body weight facilitates experimental monitoring and allows stable surgical anaesthetic depth to be achieved quicker. At three months of age rats have reached adulthood in neurodevelopmental terms with adult levels of synaptic density, neurotransmitters, myelination and behavioural phenotype (Semple, Blomgren, Gimlin, Ferriero, & Noble-Haeusslein, 2013). Data acquired from three-month old animals can thus be compared to a healthy human adult and used to quantify baseline measures of neurovascular variables and related changes due to cholinergic or inflammatory challenges.

2.2.2 Surgical procedures

2.2.2.1 Anaesthesia

Lister rats were anaesthetised with an intraperitoneal injection of urethane (1.25mg/kg in 25% solution), with additional doses of anaesthetic (0.1ml) administered if necessary. Route of injection was selected as i.p injection which achieves a deep state of anaesthesia in a short duration (Maggi & Meli, 1986). Anaesthetic depth was determined by means of hindpaw pinch-reflex testing.

2.2.2.2 Tracheotomy

Animals were tracheotomised to allow artificial ventilation. The procedure was performed by laying the animal on its back. With the use of a scalpel blade a 10mm incision was made directly below the animal's trachea. Blunt dissection of the skin, tissue membrane and muscle was performed until the trachea was exposed. The trachea was then separated from the below tissue membrane by passing forceps underneath it. Following this a thread

of suturing string is passed beneath it, in order to tie the tracheotomy tube in place once inserted. A small incision is then made in between two cartilage rings of the trachea with the use of spring-micro scissors. The incision is then enlarged with the insertion of a pre bevelled cannula used as the tracheotomy tube (Portex, 3 mm outer diameter, 50-55mm in length). It was crucial to establish that when inserting the tracheotomy tube the animal continued breathing and that this operation was not causing any breathing distress. It was important to ensure that the tracheotomy tube was level with the mouth and that it did not extend beyond it as this would cause the animal to re-breath some exhaled air. The posterior end of the tube stopped before the bifurcation of the trachea into bronchi, to maintain a physiological breathing circuit. The tracheotomy tube was then secured into place with the previously placed thread and the incision was sutured following monitoring of breathing rhythm. Superglue was further used to provide further hold of the tracheotomy tube.

2.2.2.3 Vessel cannulations

A left femoral artery cannulation was performed for mean arterial blood pressure (MABP) monitoring and blood gas analysis. A left femoral vein cannulation was also performed to allow for continuous administration of phenylephrine. Vessel cannulations were performed by keeping the animal in the same supine position as for the tracheotomy, where a 20mm incision was made from the top of the thigh and peritoneal cavity margin at a 45^0 angle in a rostro-medial direction. Blunt dissection of the skin and membrane tissue was performed to expose the vessels. These were then carefully separated from each other and from the adjacent nerve. Cannulation for both vein and artery are identical. Upon separation both vessels are threaded with suture string and tied off towards the leg of the animal. A further thread is placed further ahead of the vessel towards the peritoneal cavity, this is subsequently used to tie the cannulas in place. A sprung micro-clamp is then used to clamp the end of the vessel closest to the peritoneal cavity to stop blood flow before the vessel is incised. By utilising spring-micro scissors the vessel is incised towards the leg of the animal. A pre-bevelled cannula (Portex, 0.80mm outer diameter, 400mm in length) is then inserted up the vessel (towards the stomach). Attached to the cannula is a 1mL plastic syringe, filled with heparinised saline (50 units of heparin per mL). The micro clamp is then removed whilst the cannula is held into place and inserted into the vessel for a further 20mm. If the cannula is safely inserted (it does not push back) and blood flow flows back into the cannula it can be tied with the previously placed suture threads. Once both vessels are cannulated the opening is sutured shut and glued.

2.2.2.4 Thin cranial window

Animals were then placed in a stereotaxic frame (World Precision Instruments Inc., USA) for the remaining of the surgical procedure. To enable LSCI and OIS recording, the skull was exposed via a midline incision of 20-25 mm wide. Skin was retracted by blunt dissection. Bregma was localised and the muscle overlaying the lateral aspect of the skull (temporalis muscle) was also retracted to allow more lateral exposure. Subsequently a section overlaying the left somatosensory cortex (barrel cortex) was thinned to translucency with a dental drill (Figure 2.1). This section was approximately located 1-4mm posterior and 4-8mm lateral to Bregma (Chapin & Lin, 1984). A thinned skull was typically between 100 and 200 μm thick and the local vasculature could be clearly observed whilst ensuring the skull was not damaged. Care was taken to ensure that the skull remained cool by frequently bathing the area with saline. This technique ensures integrity of the skull and brain whilst allowing for laser speckle and optical imaging recordings.

2.2.3 Physiological measurements

Temperature was maintained at 37 ^{0}C (± 0.5 ^{0}C) throughout surgical and experimental procedures with the use of a homoeothermic blanket (Harvard Apparatus, USA). Animals were artificially ventilated with room air using a small animal ventilator (SAR 830, CWE Inc, USA): the breathing rate of each animal was assessed and modified according to each individual animal's blood gas measurements. Respiration rates of the animals ranged from 58 to 75 breaths per minute.

Blood pressure was monitored during the experiment with a pressure transducer attached to a 5mL plastic syringe containing heparinised saline (Wockhardt, UK, 50 units of heparin per mL). The artery cannula was then attached to the transducer. This system recording real time data used a previously written Spike2 software. It was important to ensure that no air bubbles were present in the transducer as this would produce an inaccurate reading. Flushing of heparinised saline was always performed before attaching the cannula.

Periodically arterial blood from the femoral artery was allowed to flow back from the cannula into a cartridge (iSTAT CG4+, Abbott Point of Care Inc., USA) and analysed for blood gas to ensure normoxia and normocapnia (values should be within defined range: PO_2 =75-85mmHg, PCO_2 =26-40mmHg, SO_2 =95-100%) using a blood gas analyser (VetScan, iSTAT-1, Abaxis, USA). Total volume of arterial blood extracted at one time did not surpass 95μL. If the animal was found to be outside of normal levels the experimental

run would be stopped and ventilation parameters were readjusted until the animal returned to normoxia. This is especially important as changes in blood level concentrations of O_2 alters both the synthesis of the glial and neuronal messengers and the levels of lactate and adenosine which modulate the pathways by which these messengers regulate vascular tone (Attwell et al., 2010) and thus impact upon neurovascular coupling.

With the cannulated left femoral vein infusion of phenylephrine (Sigma, Aldrich, 0.2-0.4mg/hr) was administered to stabilise blood pressure under the effect of anaesthesia. Phenylephrine is an alpha-adrenergic agonist which constricts blood vessels thus increasing MABP. It is impermeable to the BBB. Administration of phenylephrine is crucial as urethane has been shown to cause mild hypotension (Maggi & Meli, 1986b) and if left unmanaged this would cause an alteration in the imaging signals recorded as a large 0.1Hz vasomotor oscillation in the vasculature (Hudetz, Roman, & Harder, 1992; Mayhew et al., 1996). MABP was kept between recognised physiological limits of 100-110mmHg (Golanov, Yamamoto, & Reis, 1994). Phenylephrine was administered through the use of a syringe pump (Sp200i, World Precision Instruments Inc., USA).

2.3 *In vivo* data acquisition

All imaging and electrophysiology data were acquired within a ferromagnetic cage upon a pneumatic suspension bench system to create a vibration isolated workstation (Vision Isostation, Newport Corporation, USA). This set up is used to minimise any electromagnetic interference that can influence electrophysiology measurements, as well as any vibrations that influences instruments such as microscopes, to ensure improved resolution, repeatability and clearer signal. Earth leads were used to ground electrical items within the ferromagnetic cage to further reduce noise.

2.3.1 Imaging

2.3.1.1 Laser speckle contrast imaging (LSCI)

This technique firstly described by Fercher and Briers (1981) has since been widely used to monitor the spatial-temporal characteristics of CBF in both normal and pathophysiological conditions of brain metabolism. LSCI provides full-field imaging of CBF with the ability to track the temporal evolution of CBF changes (Boas & Dunn, 2010; Dunn, Bolay, Moskowitz, & Boas, 2001) on the cortical surface providing excellent spatial resolution to individual vessels. This overcomes the limitations of laser-Doppler flowmetry that can only provide CBF related information from a limited number of points in the brain (Dirnagl, Kaplan, Jacewicz, & Pulsinelli, 1989) and by not being constrained by

mechanically moving a beam or scope across the field of interest as is required with laser-Doppler. LSCI further provides better spatial and temporal resolution which are constrained by non-invasive imaging technologies such as fMRI and PET (Calamante, Thomas, Pell, Wiersma, & Turner, 1999; Heiss et al., 1994).

LSCI provides arbitrary perfusion units by illuminating an area of tissue with laser light to produce a random interference effect (speckle pattern). When an area or object is illuminated by laser light, the backscattered light forms a random interference pattern which consists of light and dark areas. If the movement in the area is limited or static, the speckle pattern will remain stationary giving high contrast, conversely if the area has high movement, such as flowing blood cells, the speckle pattern will change over time, appearing more blurred thereby leading to a reduction in local contrast. Thus the level of blurring is quantified by the speckle contrast, where high flow rates have low contrast and low flow rates are defined by high contrast. LSCI contrast level has been found to correlate with blood flow and by analysing the fluctuations in the speckle pattern, speckle contrast values which provide a measure of blood flow can be calculated. The speckle contrast factor (K) is defined as the ratio between the standard deviation, σ_s of the intensity and mean of the intensity, $\langle I \rangle$ (Briers & Webster, 1996).

$$speckle\ contrast, K = \frac{\sigma_s}{\langle I \rangle} \quad (1)$$

K is constrained by values between 0 and 1, where K values near 1 indicates no movement (no blurring, lower blood flow) and values near 0 indicated high movement (high blurring, higher blood flow). LSCI is constrained by region size and should be within the region of 5x5 or 7x7 pixels to ensure accurate determination of σ_s and $\langle I \rangle$ and to avoid loss of spatial resolution which comes from utilising larger regions with more pixels (Dunn et al., 2001). By using the spatial characteristics of the intensity fluctuations (Fercher & Briers, 1981), high spatial and temporal resolution two-dimensional maps of CBF can be obtained by imaging the speckle pattern onto a charge coupled device (CCD) camera and quantifying the spatial blurring of the speckle pattern that results from the imaged area, building a picture or a pattern of change of blood flow over time (Dunn et al., 2001).

LSCI is highly susceptible to movement artifacts which can arise within repeated imaging sessions between and within animals (Ayata et al., 2004; Winship, 2014). Care was taken to ensure camera positioning was consistent across imaging session between animals, which was in itself constrained by the positioning of the 16-channel electrode (Chapter III) and OIS (Chapter IV and VI) and thus should have a high degree of consistency between groups. Furthermore blood flow data obtained with LSCI in this thesis is used to describe

relative changes in CBF and not used to calculate blood flow velocity, where the exact relationship between speckle contrast and flow velocity remains elusive (Winship, 2014). In a study conducted by Ayata et al (2004) the authors demonstrated that correlation time values for speckle fluctuations are highly reproducible and can thus be used to compare CBF measures across animals. Lastly the preparation utilised for LSCI in this thesis (thinned cranial window, as detailed in Section 2.1.2.4) minimises brain pulsations reflecting arterial or intrathoracic pressure fluctuations which create motion artifacts in an open cranial window preparation (Ayata et al., 2004).

CBF data were acquired via a LSCI camera (Full field Laser Perfusion Imager (FLPI-2), Moor Instruments, UK) in Chapters III, IV and VI of this thesis. The LSCI camera was positioned above the thinned cranial window to enable CBF recording (Figure 2.1). This allowed for capture of real time high resolution blood flow images. Images were acquired at 25Hz at a spatial resolution of approximately 10μm/pixel. At the start of each recording a 60s data acquisition period was acquired to obtain a measure of baseline CBF.

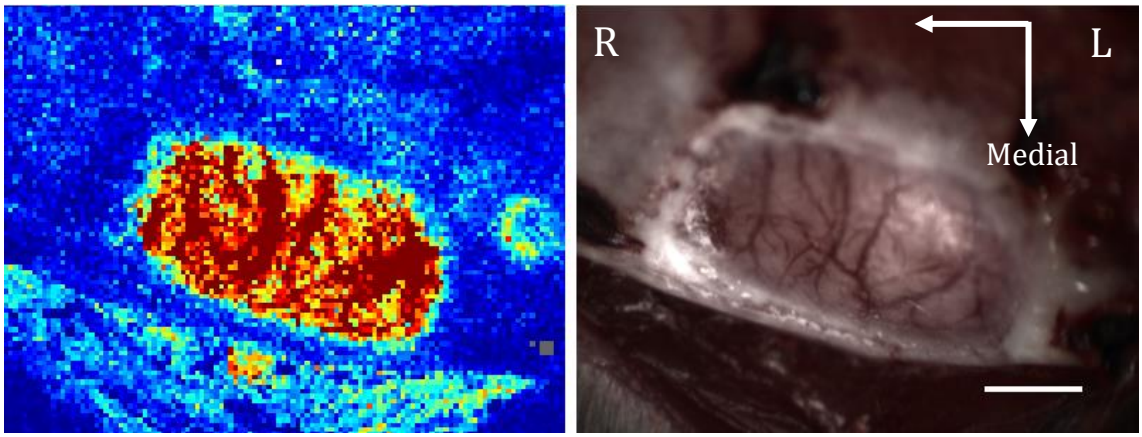

Figure 2.1. Thinned cranial window in preparation for LSCI. Speckle pattern resulting from LCSI camera recording of blood flow under a thinned window overlaying the left barrel cortex, alongside a photo of the cranial window. Mapping of the speckle pattern to the underlying vasculature can be clearly seen. Scale bar represents 2mm.

2.3.1.2 Two-Dimensional Optical imaging spectroscopy (2D-OIS)

OIS is a well-established technique in the field of animal research for investigating underlying mechanisms of the haemodynamic response to increased neuronal activity (Boorman et al., 2015; Boorman et al., 2010; Jones et al., 2001; Martin et al., 2002; Mayhew et al., 2001). This technique monitors changes in blood volume and oxygen saturation (SO_2) calculating the total (HbT) and relative concentrations of deoxy-haemoglobin (HbR) and oxy-haemoglobin (HbO_2) present in the brain tissue. This is characterised by the difference in absorption spectra of deoxy-haemoglobin and oxy-haemoglobin during neuronal activation (Cohen, 1973), where deoxy-haemoglobin and oxy-haemoglobin present with different absorption coefficients as a function of wavelength (Figure 2.2). The 2D-OIS technique utilised in this thesis has been described in detail previously (Berwick et al., 2005) and will only be briefly outlined here. To generate spatial maps of haemodynamic response, the cortex was illuminated with four wavelengths of light (495 ± 31 nm, 559 ± 16 nm, 575 ± 14 nm, and 587 ± 9 nm) using a Lambda DG-4 high-speed galvanometer (Sutter Instrument Company, USA). The remitted light passes through a focal lens (100mm, Leica Ltd) and a microscope at 0.65-6x magnification to finally reach a Dalsa 1M60 CCD camera. Each camera pixel represented 75x75μm of cortex with a temporal resolution of 125ms with a frame rate of 32Hz synchronised to the filter switching, thereby giving a frame rate of 8Hz (8 frames per second for each wavelength). The spectral analysis was based on the path length scaling algorithm (PLSA), which uses a modified Beer-Lambert Law with a path length correction factor. This technique has been previously described by Berwick et al. (2005). Haemoglobin concentration in the tissue was estimated to be 104μm based on previous measurements (Kennerley et al., 2005) and saturation estimated to be 50% when breathing room air. Finally, where haematocrit (number of red blood cells per unit-volume of blood) is assumed to be constant, fractional changes in HbT are equivalent to fractional changes in CBV. During whisker stimulation a rapid increase of oxygen (HbO_2) and blood volume (HbT) are observed paired with a concomitant decrease in deoxygenated blood (HbR). These measures are correlated with an increase in CBF, which can be measured via methods including LSCI.

OIS was used in Chapters IV and VI of this thesis, where a 10s baseline period was acquired at the start of each paradigm before whisker stimulation commenced.

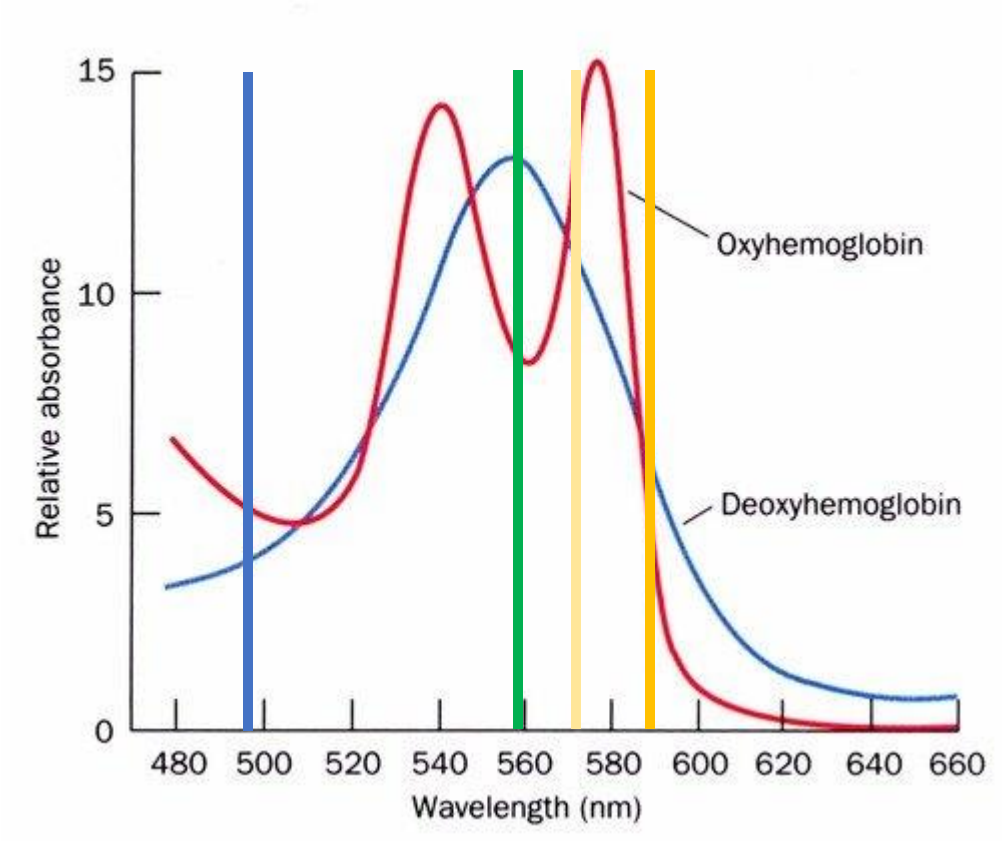

Figure 2.2. Absorption spectra for OIS imaging. Spectra for specific absorption for oxygenated (HbO_2) and deoxygenated (HbR) haemoglobin as a function of wavelength. The four coloured lines approximately represent the wavelengths (495 ± 31 nm, 559 ± 16 nm, 575 ± 14 nm, and 587 ± 9 nm) used to illuminate the cortex utilising a Lambda DG-4 high-speed galvanometer (Sutter Instrument Company, USA). The absorbance coefficient gives a measure of change in concentration of HbO_2 and HbR (SO_2). Total volume (HbT) is the summation of both.

2.3.2 Electrophysiology

To reduce electrophysiology data noise the stereotactic frame was grounded with crocodile clips and a grounding wire was passed through the animal's nape of the neck (scruff) directly attached to the electrode holder before the start of data collection. Both electrophysiological set ups and recordings are shown in Figure 2.3.

2.3.2.1 16 channel electrode acute preparation

Local field potentials (LFPs) were measured, concurrently, by inserting a 16-channel electrode (16 linearly arranged recording sites; 100µm spacing; 177µm^2 area, NeuroNexus Technologies) through the previously thinned cranial window. A small burr hole was drilled in the upper right quadrant of the window to penetrate the skull and the dura was carefully resected with a fine needle. The electrode attached to connector pins was inserted perpendicular to the cortical surface under stereotaxic control until the tip reached a depth of 1,500µm. Data were acquired at 10 kHz using a preamplifier unit that was optically coupled to a data acquisition device (Medusa, Tucker-Davis Technologies). Experimental control was implemented using custom-written Spike2 code running on a PC attached to a Micro1401 controller unit (Cambridge Electronic Design, UK). This software also controlled stimulus delivery which was directly synchronised to the LSCI camera. Location of the barrel cortex was guided by stereotactic co-ordinates and by the consistent regular pattern of the vasculature in this region (Cox, Woolsey, & Rovainen, 1993). Data recording did not commence until 60 minutes after electrode insertion to ensure no effects of cortical spreading depression were present (Ba et al., 2002). LFP signals recorded from this 16-channel electrode are assumed to derive from integrated sub-threshold dendrite and synaptic processing.

As OIS and LSCI have limited depth of field (DOF), these methods are constrained in measuring surface haemodynamic responses, whereas 16-channel electrophysiology is able to measure neuronal activity at multiple infragranular layers. Thereby these imaging and neuronal signals are derived from differing cortical layers and could thus be separate of each other (Huo, Smith, & Drew, 2014). Research has shown that both MUA and LFP responses have concomitant activity changes across all cortical layers and this was found robustly in somatosensory (Einevoll et al., 2007), motor (Chakrabarti, Zhang, & Alloway, 2008), visual (Xing, Yeh, Burns, & Shapley, 2012) and auditory (Szymanski, Rabinowitz, Magri, Panzeri, & Schnupp, 2011) cortices. This suggests a strong degree of response uniformity throughout the varying cortical layers whereby deep layer neuronal activity would still be adequately accompanied to surface layer neuronal activity and thus

comparable to surface haemodynamic responses. In addition, MRI measures which are not constrained by the same DOF limitations as OIS and LSCI have consistently found CBV changes to be parallel when comparing between deep layer and surface vessels (Herman, Sanganahalli, Blumenfeld, Rothman, & Hyder, 2013; Huber et al., 2014) and arterial dilation has been shown to rapidly propagate from deep layers to surface ones (Tian et al., 2010a).

2.3.2.2 Carbon fibre surface electrode

This non acute preparation was developed for non-invasive electrophysiology recording utilised in Chapter IV and Chapter VI in order to not incur an additional inflammatory response by disrupting intracranial pressure. The thin cranial window was prepared as described previously (Section 2.2.2.4) and an adjacent concave hole was drilled in order to position the electrode tip as close as possible to the thin window without covering any of the window itself to ensure optimal OIS and LSCI recording. The electrode, built in house was made of carbon fibres and soldered to an amplifier. Carbon fibres were selected as their small diameter could provide optimal recording in a small space and provide good conduction of electrophysiological signals. A small amount of electroencephalography (EEG) gel was used to cover the concave hole to 'shield' the electrode from electrical noise and further improve conduction.

2.3.3 Stimulations

2.3.3.1 Electrical stimulation of the whisker pad

The barrel cortex was activated by electrical stimulation of the contralateral whisker pad to the cranial window (right). Stimulation was delivered via two subdermal stainless steel needle electrodes (12mmx0.3mm, Natus Neurology Incorporated, USA) directly inserted into the whisker pad in a caudal direction which transmitted an electrical current of 1.0mA with a pulse width of 0.3ms. The electrical current is generated by an independent amplifier (Isolated Stimulator DS3, Digitimer Ltd., UK) which directly attaches to the electrodes. This intensity has been shown to evoke a large haemodynamic response without altering physiological factors such as blood pressure and heart rate. Multiple stimulation paradigms were employed in each Chapter, for *multifrequency stimulation*, the whiskers were stimulated at each of six frequencies (1, 2, 5, 10, 20 & 40Hz), for 2s with a stimulus pulse width of 0.3ms. The order of stimulation frequencies was pseudorandomised with 10 trials at each frequency (60 trails in total) and an inter-trial interval (ISI) of 25s. For *long duration stimulation* a 16s stimulus, at 10Hz; 10 trials; 60s ISI was used. These paradigms are illustrated in Figure 2.4.

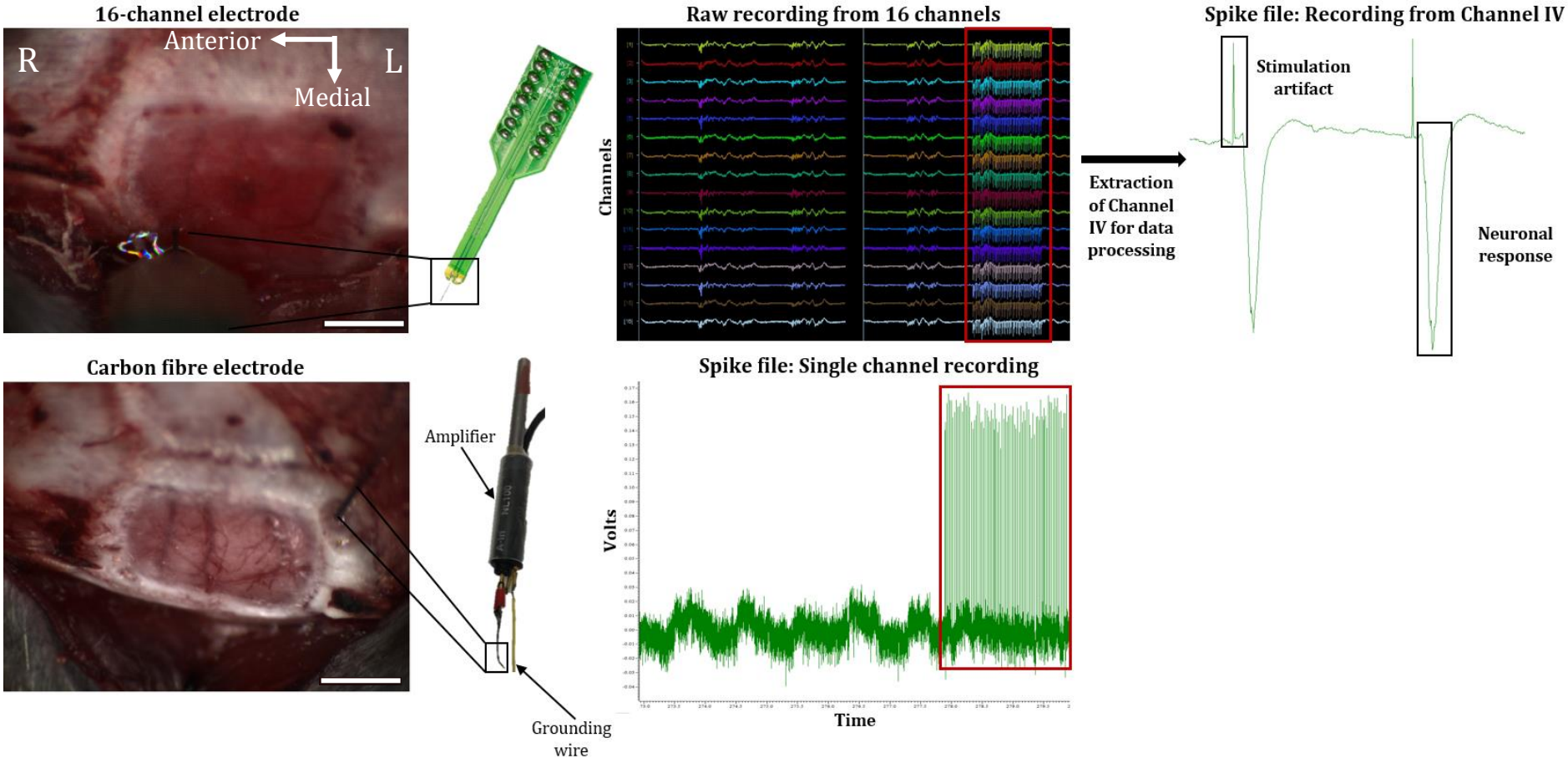

Figure 2.3 Electrophysiological experimental set up for 16-channel and carbon fibre electrodes, showing positioning of respective electrodes to the thinned cranial window. The 16-channel electrode is perpendicularly inserted in the upper right quadrant of the thinned window; the carbon fibre electrode is placed into a secondary thinned section adjacent to the thinned window. Raw 16-channel or single channel recording are then shown followed by single channel section (for 16-channel electrode only, stimulation artifact and neuronal response are further indicated).
Legend: ☐ Whisker stimulation. Scale bar represents 2mm.

Multifrequency paradigm *(2s, 1-40Hz, ISI 25s, 60 trials)*

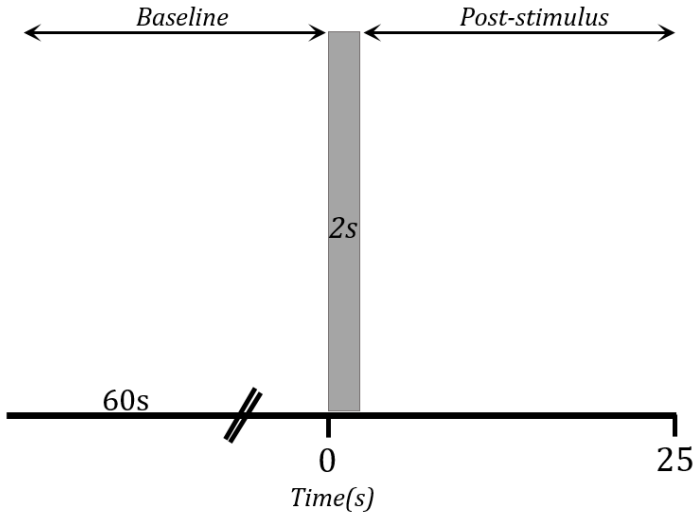

Long stimulation paradigm *(16s, 10Hz, ISI 60s, 10 trials)*

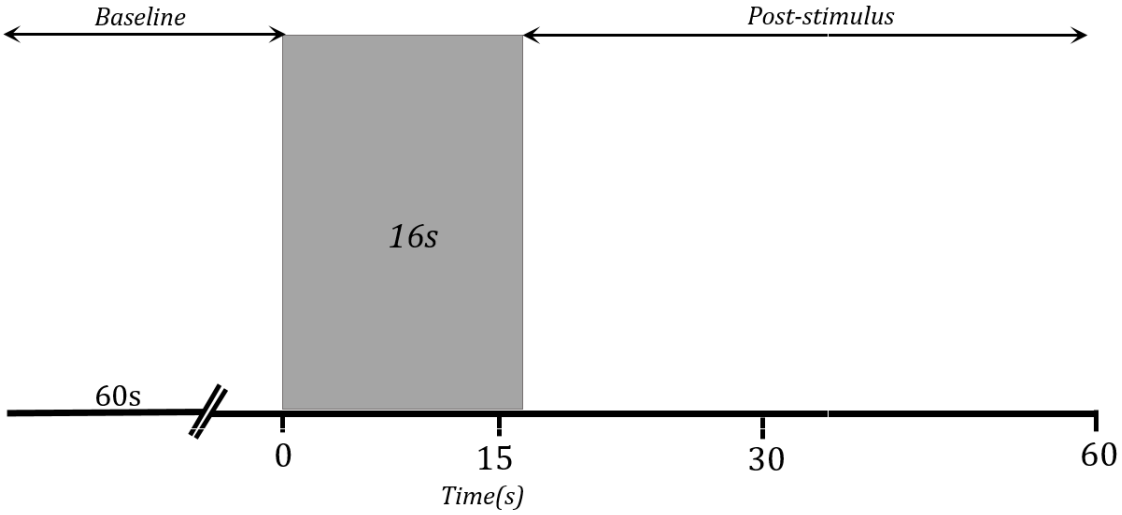

Figure 2.4. Illustration of a single trial from short multifrequency stimulation (top) and long stimulation (bottom) paradigms. For multifrequency paradigms 60 trials (10 trails per frequency) were presented at 1, 2, 5, 10, 20, 40Hz for 2s with a 25s interstimulus interval (ISI). The paradigm lasted 25 minutes in total. For long stimulation paradigms 10 trials were presented at 10Hz for a duration of 16s with an ISI of 60s. The paradigm lasted 11 minutes. Each paradigm had a 70s baseline acquisition period.

2.3.3.2 Hypercapnia challenge

A hypercapnia challenge is used as a measure of vascular reactivity which is independent of neuronal activity changes. Hypercapnia elicits changes in cerebral haemodynamics (blood flow and blood volume) producing a vasodilatory response (Haining, Turner & Pantall, 1970; Grubb, Raichle, Eichling & Ter Pogosian, 1974) without altering the metabolic rate of oxygen consumption ($CMRO_2$) (Lu et al., 2008). This technique is particularly useful in determining vascular tone and vascular reactivity of administered drugs.

Animals were ventilated using room air at a respired rate that matched their own spontaneous breathing (~58-75 breaths per minute). During a hypercapnia challenge a 10% concentration of carbon dioxide in medical air (9L medical air, 1L CO_2) was administered to the air supply tube of the ventilator. Thirty-second long challenges were repeated four times at intervals of 210 seconds in the absence of whisker stimulation. An interval of 210 seconds ensured that the animal's physiological parameters returned to baseline levels before delivering the next challenge. These challenges were performed at the end of each stimulation paradigm set (multifrequency and long stimulation).

2.4 Perfusion

Animals selected for immunohistochemical analysis were transcardially perfused with a pump (Masterflex L/S, Cole-Parmer Instrument Company, UK) at a rate of 34ml/hr following imaging and electrophysiology recording (Chapter IV and VI). By holding the sternum and cutting through and around the rib cage, the thoracic cavity was opened to expose the diaphragm, the rib cage was then retracted with a pair of forceps. The heart was subsequently exposed by carefully cutting through the diaphragm and by gently removing the connective tissue surrounding the heart. By gently gripping the heart, a needle was inserted into the lower-left quadrant of left atrium and held in place for the duration of the perfusion with a clamp. As the pump was switched on the right atrium was cut in order to relieve pressure and allow the cleared blood to flow out of the animal. Animals were perfused with saline (0.9% warmed to 37 ^{0}C) with the addition of heparin (0.1ml/300ml) via the inserted needle. To extract the brain, the animal was decapitated, the remaining scalp skin and tissue resected to expose the back of the skull. The skull and surrounding cartilage was carefully removed with a pair of rongers to expose the brain. The brain was finally extracted by cutting through the olfactory bulbs and optic tracts.

2.4.1 Fixation

Following perfusion with saline, the pump was momentarily stopped, and clamped to prevent the formation of any bubbles and the saline replaced with 4% PFA 0.1M (pH 7.4) to achieve fixation. The brain was extracted (as described above) and cut into four regions (incisions made through the junction of cerebellum and brain stem to cortex (1), posterior to middle cortex (2) middle cortex to frontal cortex (3) and frontal cortex to pre-frontal cortex (4)) in the coronal plane, thereby enabling observation of cell changes across the cortex and deeper brain structures on one slide (Appendix A). This approach allowed good visualisation of somatosensory (barrel) cortex in the first two regions and visualisation of deeper brain structures (hippocampus). Cut brains were embedded in paraffin wax as detailed below (Section 2.5).

2.4.2 Freezing

Gene expression analysis requires the preservation of RNA material which is destroyed during the fixation process. To ensure preservation of RNA animals were transcardially perfused and the brain was quickly removed from the skull as described above (Section 2.4). The brain was then quickly sectioned in half to separate the two hemispheres with a scalpel. The right hemisphere was immediately placed in 10% neutral buffered formalin (CellPath Ltd, UK) for immunohistochemistry protocols whilst the left hemisphere was further sectioned in four as detailed above (Section 2.4.1). Following sectioning the left hemisphere was slowly lowered in a transducer and snap frozen in liquid nitrogen, the brain was submerged for a total of 30 seconds to ensure deep and homogenous freezing. Frozen brains were stored at -80 C° until OCT embedding for cryostat sectioning. The right hemisphere was cut post fixation in the same four sections and embedded in paraffin wax as described below.

2.5 Histological preparation

The extracted brains were fixed for 24-48 hours (in 4% PFA or 10% neutral buffered formalin) and placed in an automatic carousel tissue processor (Leica, USA) for tissue preparation by dehydration in increasing concentrations of alcohol (70%, for 6 hours, 95% for 4 hours, absolute for 4 hours). This initial protocol is utilised to ensure removal of any water and remaining fixative from the tissue. The tissue is then cleared in xylene (by removing dehydrating solutions for 4 hours). The tissue is then finally embedded in paraffin wax for 4 hours. The resulting formalin/PFA-fixed paraffin-embedded (FFPE) blocks can be cut and stored long term without experiencing any tissue degradation.

Subsequently, serial sections of the FFPE tissue were cut on a rotary microtome (Leica, USA) to a thickness of 5μm and collected onto silane coated charged slides.

2.6 Data processing

2.6.1 Imaging data (LSCI and OIS)

LSCI and OIS data were processed in Matlab using a custom written code. Imaging data were analysed using SPM (The FIL Methods Group, 2016) implemented in a custom Matlab interface. Regions of interest (ROIs) were determined using a thresholded activation map and expected to include contributions from arterial, venous and parenchymal (capillary bed) compartments. Selection of ROI is illustrated in a flow chart in Figure 2.5. To determine if selected ROI size differed between groups statistical analysis were conducted for each data set in each chapter. LSCI and OIS time series of haemodynamic changes for each stimulation trials were then extracted from the ROI. LSCI time series were down-sampled to 5Hz (from 25Hz). Data from each stimulation trial were extracted and divided by the pre-stimulus baseline period (10s), to yield a measure of percentage change (fractional changes) in CBF, HbO_2, HbR and HbT. Time series were averaged across trials according to stimulation condition. Area under the curve (AUC) and maxima for each response were calculated.

2.6.2 Electrophysiology data (16-channel and surface electrode)

Neuronal recordings for computing local field potentials were extracted from a surface electrode or from a single channel of the multichannel electrode that corresponded to a cortical depth of ~500-600μm (layer IV). Responses were averaged across trials. AUC measurements were calculated from the response to each pulse in the stimulation train (0-50ms period, with respect to the stimulus pulse) and summed to quantify neuronal response magnitudes.

2.6.3 Cerebral metabolic rate of oxygen ($CMRO_2$) estimation

The cerebral metabolic rate of oxygen consumption ($CMRO_2$) in the brain is considered to be an index of brain health and energy homeostasis (Liu et al., 2014) as well as being directly linked to cell energy and neuronal activity (Ge et al., 2012). Estimation of $CMRO_2$ can thus provide a measure to assess the neurovascular coupling relationship by assessing possible changes in oxygen delivery or oxidative metabolism. Lastly $CMRO_2$ together with CBF and CBV forms the basis of the fMRI signal, where changes in $CMRO_2$ causes changes in blood oxygenation levels (D'Esposito et al., 2003). $CMRO_2$ can be estimated utilising HbR, HbT and CBF values (obtained here with OIS and LSCI). The method utilised in this

thesis has been previously described in detail (Mayhew et al., 2000; Mayhew et al., 2001) and has been used to estimate $CMRO_2$ in humans (Boas et al., 2003) and in the anaesthetised rat (Jones et al., 2001).

The ratio method (Jones et al., 2001) can be used to relate the changes in the venous compartment haemoglobin concentrations to the haemoglobin concentration changes across all vascular compartments. The ratio method may be written as:

$$\left(\frac{\Delta CMRO_2 + CMRO_{2,0}}{CMRO_{2,0}}\right) = \left(\frac{\Delta CBF + CBF_0}{CBF_0}\right)\left(1 + \gamma R\frac{\Delta[HbR]}{[HbR_0]}\right)\left(1 + \gamma T\frac{\Delta[HbT]}{[HbT_0]}\right)^{-1} \quad (2)$$

Where the subscript 0 denotes baseline value, the γR and γT denote the ratio of haemoglobin changes observed in the venous compartment with respect to those across all vascular compartments (Jones et al., 2001; Boas et al., 2003) and Δ denotes change.

2.7 Statistical analysis

Statistical analyses vary between experimental Chapters III, IV, V and VI as animal groups and design differ. Furthermore the use of varying methods of imaging and immunohistochemistry require different statistical tests. Thereby individual statistical analyses are reported for each chapter. All statistical analyses were conducted using SPSS 23. A *p* value below 0.05 was considered to be a significant effect. P*ost hoc* t-tests were conducted to further probe differences between and within experimental conditions and corrected for multiple comparisons. Data were checked for both homogeneity and normality assumptions.

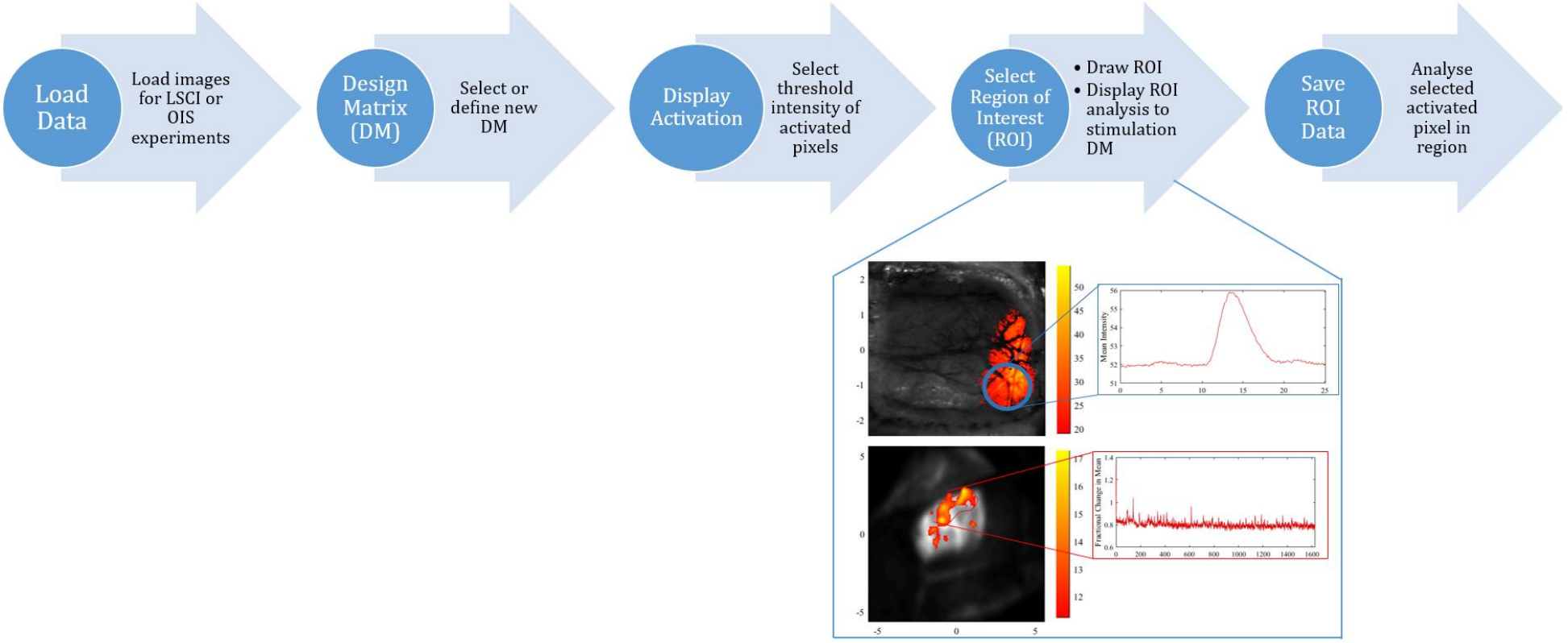

Figure 2.5. Flow chart illustrating the processing steps for both LSCI and OIS data. LSCI and OIS data region of interest (ROI) is extracted based on thresholded activation maps with contributions from arterial, venous and parenchymal (capillary bed) compartments. A design matrix matching the stimulation paradigm is initially applied to the data which allows for visualisation of activated pixel during stimulation which can then be thresholded to select an ROI.

Chapter III

Cholinergic Modulation of Neurovascular Coupling and Neuroimaging Signals

3.1 Chapter summary

The aim of this chapter is to evaluate the effects of pharmacologically manipulating levels of acetylcholine on haemodynamic, neuronal and neurovascular coupling measures and to identify neurovascular coupling effects of donepezil (current pharmacological treatment for AD) as its effects on neurovascular function are currently unknown.

Acetylcholine (ACh) and degeneration of discrete populations of cholinergic neurons have long been implicated in the pathophysiology of Alzheimer's disease (AD). ACh is furthermore a potent vasodilatory neurotransmitter and given the known vascular and neurovascular changes observed in AD, an important question is how alterations in cholinergic function affect cerebral blood flow (CBF) regulation and neurovascular coupling (Lecrux & Hamel, 2016). Despite the known association between changes in CBF and cholinergic dysfunction little is currently known on how altered acetylcholine neurotransmission affects neurovascular coupling.

This chapter provides evidence that modulation of brain acetylcholine alters the relationship between neuronal and haemodynamic responses, with a neurovascular uncoupling effect associated with reduced cholinergic function. This finding has implications for the interpretation of BOLD fMRI and BOLD phMRI data in both animal and human imaging studies where cholinergic function may be different between experimental or patient groups. These findings support the notion that cholinergic modulation of neurovascular function may be an important component of the increasingly recognised neurovascular changes associated with AD, highlighting a role for cholinergic drugs in normalising neurovascular function. Lastly, the results obtained in this study demonstrate modulation of acetylcholine upon a range of stimulations, suggesting an alteration in how stimulus inputs convert to haemodynamic response functions, thereby resulting in an altered neurovascular response.

3.2 The roles of the neurotransmitter acetylcholine

Acetylcholine (ACh) is a vasodilatory neurotransmitter in the central nervous system (CNS) and the peripheral nervous system (PNS). Acting through muscarinic and nicotinic receptors, ACh has been shown to have roles in attention (Himmelheber, Sarter, & Bruno, 2000), arousal and memory processes (Micheau & Marighetto, 2011) whereby in these brain 'on' states ACh-releasing basal forebrain (BF) neurons activate (Lecrux et al., 2017). Furthermore ACh is involved in sleep regulation (Jones, 2005) where reductions in ACh levels can be observed in slow-wave sleep (Hasselmo & Sarter, 2011). Lastly, ACh has been tied to decision making, in improving neuron-to-neuron transmission, enhancing cognitive functioning (Bartus, Dean, Beer, & Lippa, 1982; Cummings, 2000; Lawrence & Sahakian, 1995) and in determining the local handling of CBF (Iadecola, 2004).

3.2.1 Acetylcholine and AD

ACh is of particular interest in AD because of its degeneration in the nucleus basalis of Meynert, leading to cholinergic dysfunction (Whitehouse, Price, Clark, Coyle, & DeLong, 1981). Several studies (Arendt et al., 1983; Salehi, Dubelaar, Mulder, & Swaab, 1998; Whitehouse et al., 1981) also report neuronal and cell loss, atrophy and decreases in neuronal activity. Degeneration of this discrete population of cholinergic neurons has been found to be directly linked to the progressive deterioration of cognitive and memory functions that are observed in AD patients (Arendt et al., 1983; Cummings & Back, 1998).

3.2.2 The development of cholinergic drugs for the treatment of AD

Several CNS penetrating cholinergic drugs such as donepezil have been developed in an attempt to counteract the effects of cholinergic neuronal loss for the treatment of AD and have been shown to reduce disease symptoms by improving both memory and cognitive functions (Massoud & Gauthier, 2010; Takada et al., 2003). Rosengarten et al. (2009) showed that after acetylcholinesterase inhibitor (AChEI) treatment (administration of rivastigmine) vasoregulative function improved in patients with vascular dementia. Furthermore Meyer et al. (2002) suggested that the use of donepezil on mild cognitive impairment (MCI) patients may be effective in delaying the onset of AD. Despite the cognitive, behaviour and function improvements observed with cholinesterase inhibitors, these treatments are only effective in treating cognitive impairments in the mild to moderate stages of AD (Klafki et al., 2006; Massoud & Gauthier, 2010) and only target symptoms of the disease, failing to halt disease progression (Massoud & Gauthier, 2010).

3.3 Blood flow alterations and neurovascular dysfunction in AD

AD has also become associated with pathological changes in blood flow regulation and in the neurovascular apparatus that supports it, causing neurovascular uncoupling (Iadecola, 2004; Zlokovic, 2008). In human studies reductions in CBF correlate with cognitive impairment (Farkas, 2001) as well as being a risk factor in the development of AD later in life (Hirao et al., 2005; Matsuda, 2007). An fMRI study (Rombouts, Goekoop, Stam, Barkhof, & Scheltens, 2005) has shown that task associated increases in CBF are delayed in MCI patients and that these deficits become more prominent in AD patients. Furthermore, multimodal MRI techniques have recently revealed impairment of NVU function in early AD (van de Haar et al., 2016). These findings implicate altered CBF regulation as an early event in the development of AD pathology and research is thus beginning to investigate how interventions to improve neurovascular function could provide a degree of neuroprotection from neurodegenerative diseases.

3.4 The link between cholinergic dysfunction and neurovascular uncoupling; the need for *in vivo* multimodal measurements

CBF reductions are closely linked to dysfunction and loss of cholinergic innervation in the BF and medial septum as well as loss of projection fibres to the neocortex and the hippocampus from the nucleus basalis and medial septum respectively (Bell et al., 2006). These cholinergic neurons directly project to the microvasculature of the frontoparietal cortex to regulate ACh mediated vessel dilation, with a consequent pathophysiological impact on CBF when altered, impaired or lost (Farkas, 2001). Given the known vascular and neurovascular changes observed in AD, an important question is how alterations in cholinergic function affect CBF regulation and neurovascular coupling (Lecrux & Hamel, 2016). Disruption of the cholinergic system may lead to alterations in neurovascular coupling because of the known vasoactive properties of ACh (Bell et al., 2006; Farkas, 2001). Similarly, pharmacological treatment of AD symptoms using cholinergic drugs may alter neurovascular coupling, impacting upon both preclinical and human clinical fMRI and PET research studies that use haemodynamics as proxy imaging measures of neuronal activity. Despite the known association between changes in CBF and cholinergic dysfunction little is currently known on how altered ACh neurotransmission affects neurovascular coupling.

This question has been partly addressed by two recent studies utilising rodent models. A preclinical pharmacological MRI (phMRI) study (Kocsis et al., 2014) suggested that cognitive enhancement effects of cholinergic drugs were mediated by their vascular and

not neuronal actions, as a peripherally acting cholinesterase inhibitor (neostigmine) was shown to reverse the memory disturbing effects of the muscarinic (cholinergic) antagonist scopolamine in rats despite its inability to cross the BBB. Secondly, a recent study (Lecrux et al., 2017) was the first to investigate how sensory evoked neurovascular coupling is altered by ACh neurotransmission *in vivo* utilising concurrent measures of electrophysiology and CBF imaging. These results suggested that ACh tone modifies both the magnitude of neuronal and hemodynamic responses to sensory stimulation as well as the strength of the correlation between these measures.

Nevertheless, several important questions remain. Firstly, the haemodynamic and neurovascular effects of the most widely prescribed treatment for AD, the cholinergic agonist donepezil, have not been evaluated in this context. Secondly, the assessment of neurovascular function by Lecrux et al. (2017) relies on long-duration stimuli to elicit a 'steady-state' neuronal/vascular response, whereas in assessing dynamic neurovascular coupling it is advantageous to utilise brief stimuli so as to inform on the initial neurovascular impulse-response function independent of longer-latency non-linearities in coupling (Martin et al., 2013; Martindale et al., 2003). This is especially important for the analysis and interpretation of BOLD fMRI studies where the short-latency impulse response function serves as the basis for the canonical model of the hemodynamic response (Logothetis, 2008). Thirdly, because it has previously been shown that anaesthesia used in preclinical studies can affect stimulus-response and neurovascular coupling parameters (Martin et al., 2006; Masamoto & Kanno, 2012). Thus it is important to establish the neurovascular coupling relationship using a wider range of stimulation 'inputs', rather than a unitary stimulus type so as to provide improved assurance that findings are robust beyond specific stimulation parameters and experimental (anaesthetic) conditions (Martin, 2014).

3.5 Study overview and hypothesis

The present study was designed to identify *in-vivo* the effects of pharmacological manipulations of brain ACh on neuronal, haemodynamic and neurovascular coupling measurements by directly comparing effects of donepezil and scopolamine treatments. Scopolamine, blocks the activity of the muscarinic acetylcholine receptor (mACh) (Bajo et al., 2015), inducing a decrease in cholinergic function, leading to transient cognitive amnesia and electrophysiological changes which resemble those observed in AD (Ramos Reis, Eckhardt, Denise, Bodem, & Lochmann, 2013; Sannita, Maggi, & Rosadini, 1987). As such, scopolamine administration is an adequate pharmacological treatment to approximate the changes in brain activity which underlie AD (Ebert & Kirch, 1998). Effects of neurovascular coupling and neurovascular function will be investigated with a complementary set of measurements of LSCI to measure CBF and electrophysiology for the recording of neuronal activity using a range of sensory stimuli. Finally correlations between CBF and neuronal activity were used to assess the neurovascular coupling relationship during cholinergic modulation.

The main **hypothesis** for this chapter is that decreases in brain cholinergic function will lead to an alteration in neurovascular coupling relationships, where stimulus evoked changes (increases or decreases) in neuronal demand are not accompanied by concomitant changes in CBF.

3.6 Chapter aims

This study aimed to address

(1) The effects of pharmacologically manipulating levels of acetylcholine on
    a) Neuronal,
    b) Haemodynamic and
    c) Neurovascular coupling measurements in the rat brain

(2) Identify any neurovascular coupling effects of cholinergic manipulation to inform upon interpretation of imaging signals acquired from studies utilising haemodynamics as proxy measures of neuronal activity.

3.7 Method

3.7.1 Animals and pharmacological treatment

Eighteen hooded Lister rats (4-5 month old, 220g-320g) were randomly assigned to one of three groups (control, scopolamine or donepezil, *n* = 6 per group). Haemodynamic and electrophysiological data were concurrently acquired in all treatment groups in a repeated measures design. Each animal received an intravenous injection based on drug condition: scopolamine animals received 2mg/1ml of scopolamine (Tocris, UK) dissolved in saline; the donepezil animals received a dose of 2mg/kg of donepezil (Tocris, UK) dissolved in saline; control animals were administered a saline vehicle (1ml).

3.7.2 Surgical procedures

Animals were anaesthetised with an intraperitoneal injection of urethane (1.25mg/kg), and anaesthetic depth was monitored by means of hindpaw pinch-reflex. Once anaesthetic depth was achieved animals were tracheotomised to allow artificial ventilation, their left femoral artery and vein cannulated to measure MABP and allow phenylephrine infusion. A thin cranial window was then prepared once the animal was placed in a stereotactic frame over the left somatosensory cortex. All procedures were as described in Chapter II (Section 2.2.2). In addition the right vein was cannulated to allow drug administration without needing to interrupt phenylephrine infusion.

3.7.3 Physiological measurements

During surgical and experimental procedures animals were kept under strict physiological monitoring, as described in Chapter II (Section 2.2.3). Temperature was maintained at 37 ^{0}C (± 0.5 ^{0}C), animals were ventilated and blood pressure measurements monitored. To ensure normoxia and normocapnia, blood gases were analysed using a blood gas analyser. Physiological parameters were within normal ranges throughout experimental duration (mean values: PO_2 =78mmHg(±6.66) PCO_2 =36mmHg(±2.41) SO_2 =96%(±1.07)). MABP was within recognised physiological limits (101±8.4).

3.7.4 Imaging and electrophysiology

CBF data were acquired through a LSCI camera positioned above the thinned cranial window. Images were acquired at 25Hz at a spatial resolution of approximately 10μm/pixel. Total recording time varied depending on stimulation paradigm but a 60s baseline data acquisition period was acquired in each paradigm to obtain a measure of baseline blood flow.

LFPs were measured using a 16-channel electrode inserted through a small burr hole made in the previously thinned cranial window as detailed in Chapter II (Section 2.3.2.1). Data were acquired at 10 kHz using a preamplifier unit that was optically coupled to a data acquisition device (Medusa, Tucker-Davis Technologies). Experimental control was implemented using custom-written Spike2 code running on a PC attached to a Micro1401 controller unit (Cambridge Electronic Design, UK). This software also controlled stimulus delivery which was directly synchronised to the LSCI camera.

3.7.5 Experimental design

One hour after electrode placing and once physiological parameters (blood pressure, blood gases) were within the normal range, data acquisition commenced. Experimental runs began with a 60s acquisition of baseline CBF and electrophysiological data. Data were acquired at prior to (*pre*) and after (*post*) administration of cholinergic drugs (or saline control). Electrical whisker stimulation (1.0 mA) was delivered via two subdermal electrodes inserted into the contralateral whisker pad (right). Two stimulation paradigms were used, *multifrequency* (2s duration) and *long stimulation* (16s duration) as detailed in Chapter II (Section 2.3.3.1).

3.7.6 Data processing and statistical analysis

All (n = 18) animals' data were processed and included in final statistical analysis. Data were processed in Matlab (2016a) using a custom written code as detailed in Chapter II (Section 2.6). ROI size was consistent across animals, with no significant difference between groups ($F(2,17,) = 1.926$, p=.180). Area under the curve (AUC) and maxima for each response were calculated for both CBF and electrophysiology data.

All statistical analyses were conducted using SPSS 23. Statistical comparisons within groups using response magnitude values (AUC) or maxima (depending on stimulation design) were performed using repeated measures analysis of variance (ANOVA) or paired t-tests. For multifrequency data, after initial repeated measures ANOVA analysis, subsequent repeated measures *post hoc* t-tests were performed to determine any frequency specific differences pre/post drug administration. 16s data were analysed with repeated measures t-tests. A p value below 0.05 was considered to be a significant effect.

3.8 Results

3.8.1 Baseline blood flow and baseline neuronal activity

To assess any effects of drug administration upon baseline CBF the average perfusion value across a 30s period prior to the onset of stimulation in both multifrequency stimulation experimental paradigms (at the start of data collection and after drug administration) was calculated. A one-way ANOVA on CBF baseline differences (across the saline, scopolamine and donepezil treated animals) found no difference between groups, $F(2,17)=2.62$, $p=.106$. To assess any effects of drug administration upon baseline cortical neuronal activity EEG power over a 30s period of electrophysiological data acquired at the same two time points as the CBF baseline measures was computed. Differences in EEG power were calculated for all five frequency bands and analysed in a one-way multivariate ANOVA. There was no significant main effect of drug group (saline, scopolamine or donepezil) on EEG band power across the 5 bands, $F(10, 22) = 1.56$, $p = .185$; Wilks' $\Lambda = .343$.

3.8.2 CBF responses to somatosensory stimulation

3.8.2.1 Multifrequency 2s stimulations (1-40Hz)

Repeated measures analysis of variance (ANOVA) was applied to CBF response maxima values in order to determine significant effects of drug administration within each drug group. All cases ($n = 18$) were included in the analysis. All drug conditions had a significant effect of stimulation frequency (saline: $F(5,25)=7.75$, $p<.001$; scopolamine: $F(5,25)=10.19$, $p<.001$; donepezil: $F(5,25)=21.17$, $p<.001$) (Figure 3.1 A). Administration of saline did not have a significant effect on the CBF response ($F(1,5)=5.65$, $p=.063$) and there was no significant interaction between drug administration and stimulation frequency ($F(5,25)=2.07$, $p=.103$). Scopolamine or donepezil administration did not itself result in a significant change in the magnitude of CBF responses (scopolamine: $F(1,5)=0.89$, $p=.390$; donepezil: $F(1,5)=1.75$, $p=.244$), however there was a significant interaction effect of drug administration and stimulation frequency upon CBF responses magnitudes for both drugs (scopolamine: $F(5,25)=4.08$, $p=.008$; donepezil: $F(5,25)=5.15$, $p=.002$). Post-hoc analysis of individual stimulation frequencies using paired t-tests indicate significant increases in CBF response magnitudes at 20Hz ($p=.026$) and 40Hz ($p=.020$) for donepezil treated animals (Figure 3.1 B). Scopolamine treated animals showed a marginally non-significant decrease in CBF response magnitude at 40Hz ($p=.071$).

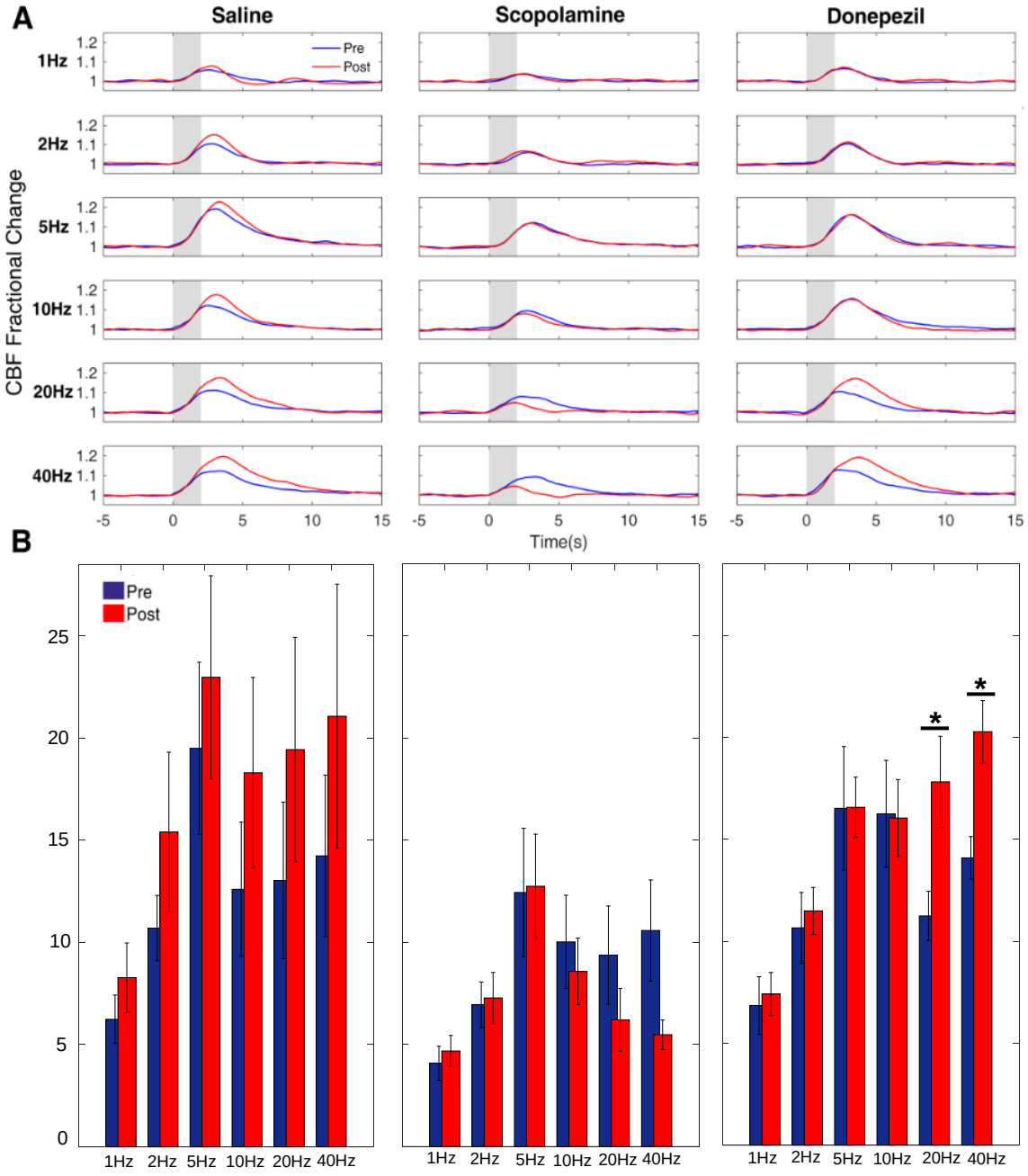

Figure 3.1. Cerebral blood flow (CBF) responses to 2s whisker stimulation at six frequencies, before (pre, blue) **and after** (post, red) **administration of saline, scopolamine or donepezil. (A)** Time series show mean fractional changes in CBF. Grey rectangle indicates stimulation onset/offset and error bars indicate standard error of the mean. **(B)** Bar charts show change in CBF percentage change at maxima. *Represents a significant difference at $p<0.05$ between pre- and post-drug treatment for specific stimulation frequencies.

3.8.2.2 16s long stimulations (10Hz)

Repeated measures t-tests were used to determine significant effects of drug administration on the magnitude of the CBF response to 16s whisker stimulation. Two animals from the saline group were excluded from data analysis as inspection of EEG showed cortical desynchronization. An AUC measure was used to quantify responses to 16s stimulation as the maxima is less representative of the longer response profile than that for the short (2s) multifrequency stimulation. Donepezil administration was associated with a significant increase in CBF response magnitude ($t(5)= -2.64$, $p=.046$) (Figure 3.2 insert), whereas there was no significant effect for saline ($p=.897$) or scopolamine ($p=.734$) administration.

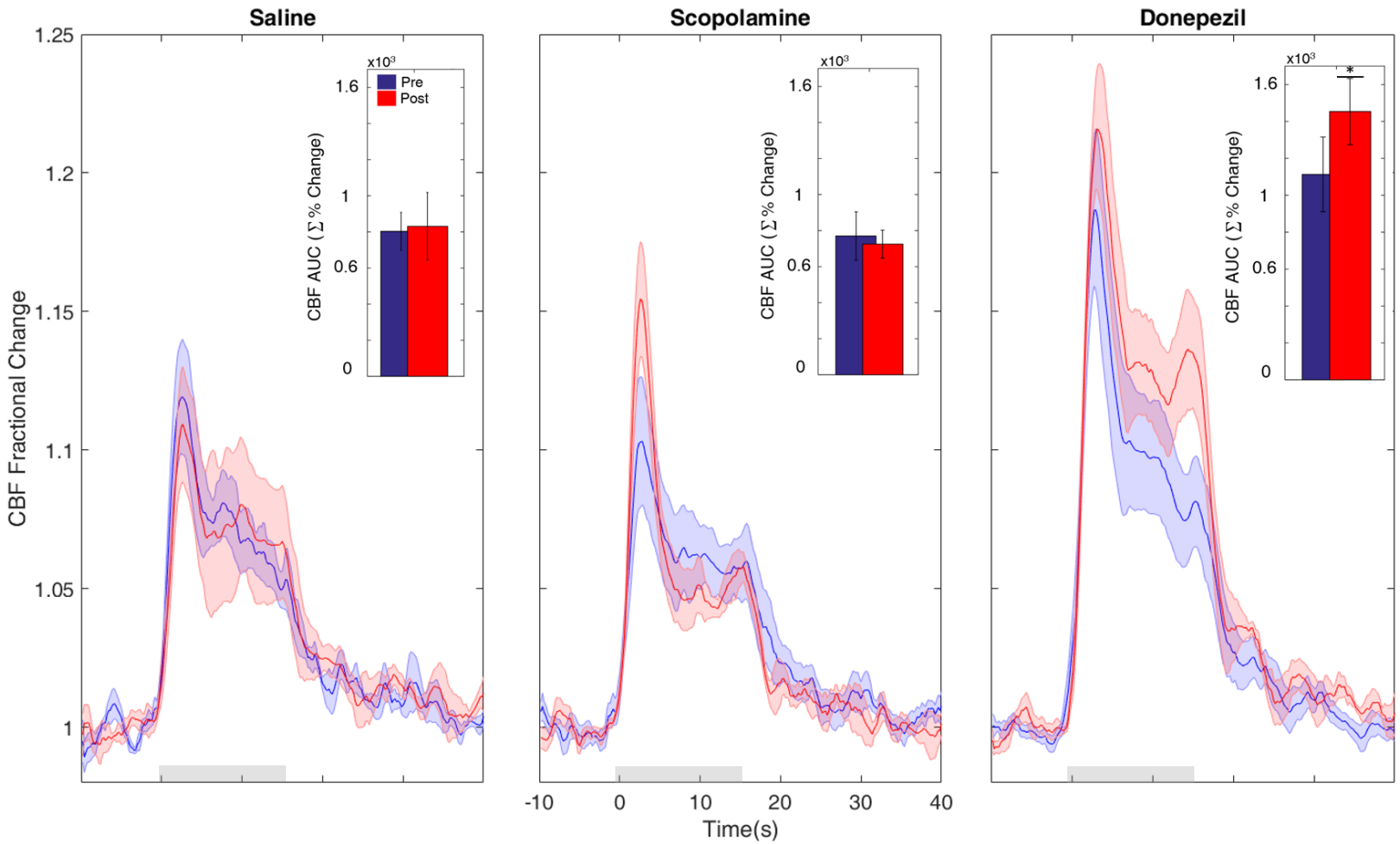

Figure 3.2. Cerebral blood flow (CBF) responses to 16s whisker stimulation, at 10Hz, before (pre, blue) **and after** (post, red) **administration of saline, scopolamine or donepezil.** Time series show mean fractional changes in CBF and bar charts (inset) show change in area under the curve (AUC, units are summed percentage change). Grey rectangle indicates stimulation onset/offset and shaded area represents standard error of the mean. *Represents a significant difference at $p<0.05$ between pre- and post-drug treatment.

3.8.3 Neuronal responses to somatosensory stimulation

3.8.3.1 Multifrequency 2s stimulations (1-40Hz)

Repeated measures analysis of variance (ANOVA) was applied to the calculated AUC values for the LFP responses in order to determine significant effects of drug administration upon neuronal responses to stimulation within each drug group. All cases (n = 18) were included in the analysis. There was a significant effect of stimulation frequency upon LFP response magnitude for all three drugs (saline: $F(5,25)=11.05$, $p<.001$; scopolamine: $F(5,25)=4.55$, $p=.004$; donepezil: $F(5,25)=29.28$, $p<.001$) (Figure 3.3 A). Administration of saline and donepezil (but not scopolamine) had a significant effect upon LFP response magnitude (saline: $F(1,5)=8.85$, $p=.031$; donepezil: ($F(1,5)=10.31$, $p=.024$; scopolamine: $F(1,5)=1.34$, $p=.299$). There was a significant interaction effect of drug administration and stimulation frequency upon LFP response magnitudes for all three drugs (saline: $F(2,25)=5.9$, $p=.001$; scopolamine: $F(2,25)=5.76$, $p=.001$; donepezil: $F(2,25)=9.32$, $p<.001$). Post-hoc analysis of individual stimulation frequencies using paired t-tests indicate significant increase in LFP response magnitude at 20Hz ($p=.009$) and 40Hz ($p=.026$) for donepezil treated animals (as for CBF responses). Scopolamine treatment was associated with an increase in LFP response magnitude at low stimulation frequencies of 1Hz ($p=.009$) and 2Hz ($p=.007$) with a marginally non- significant effect at 40Hz ($p=.085$). Saline treatment produced a marginally significant increase in LFP response magnitude at 40Hz ($p=.048$) (Figure 3.3 B).

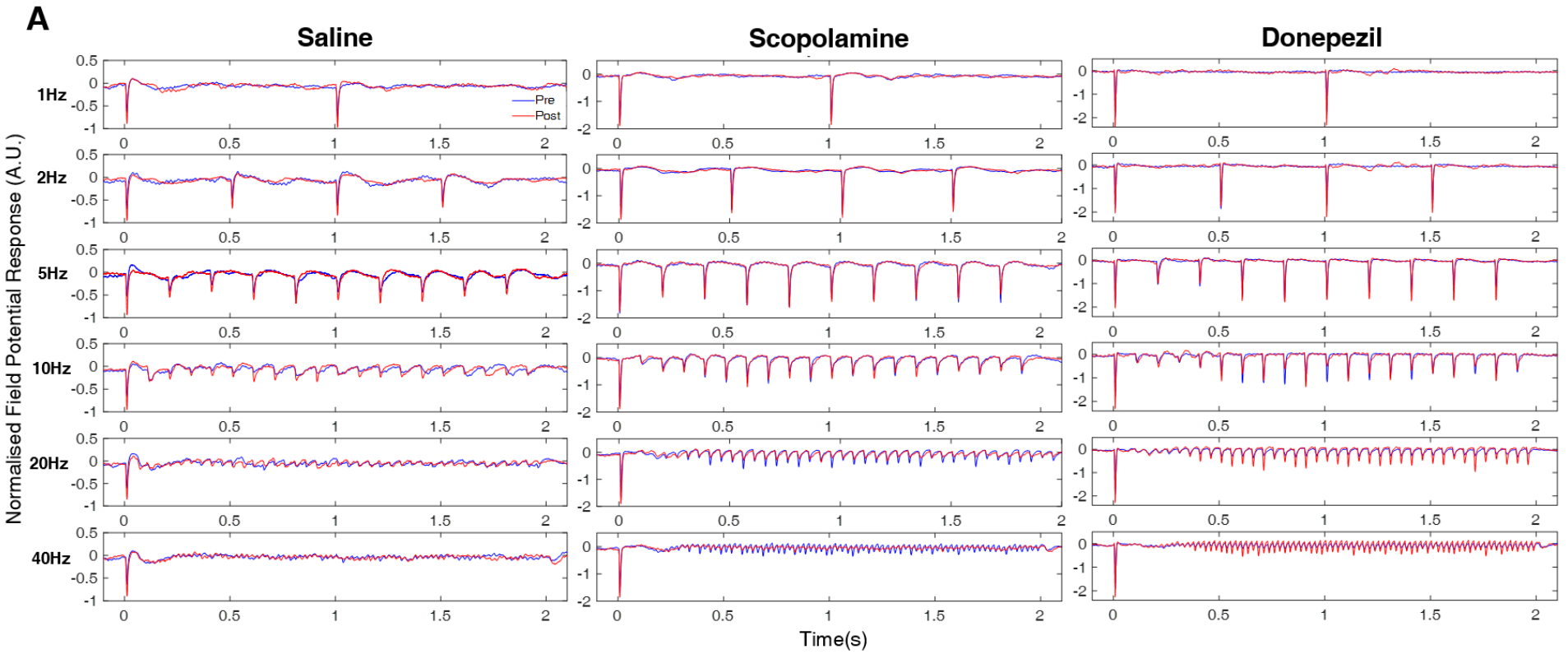

Figure 3.3 A. Time series showing the mean local field potential (LFP) responses to 2s whisker stimulation at six frequencies, before (pre, blue) **and after** (post, red) **administration of saline, scopolamine or donepezil.**

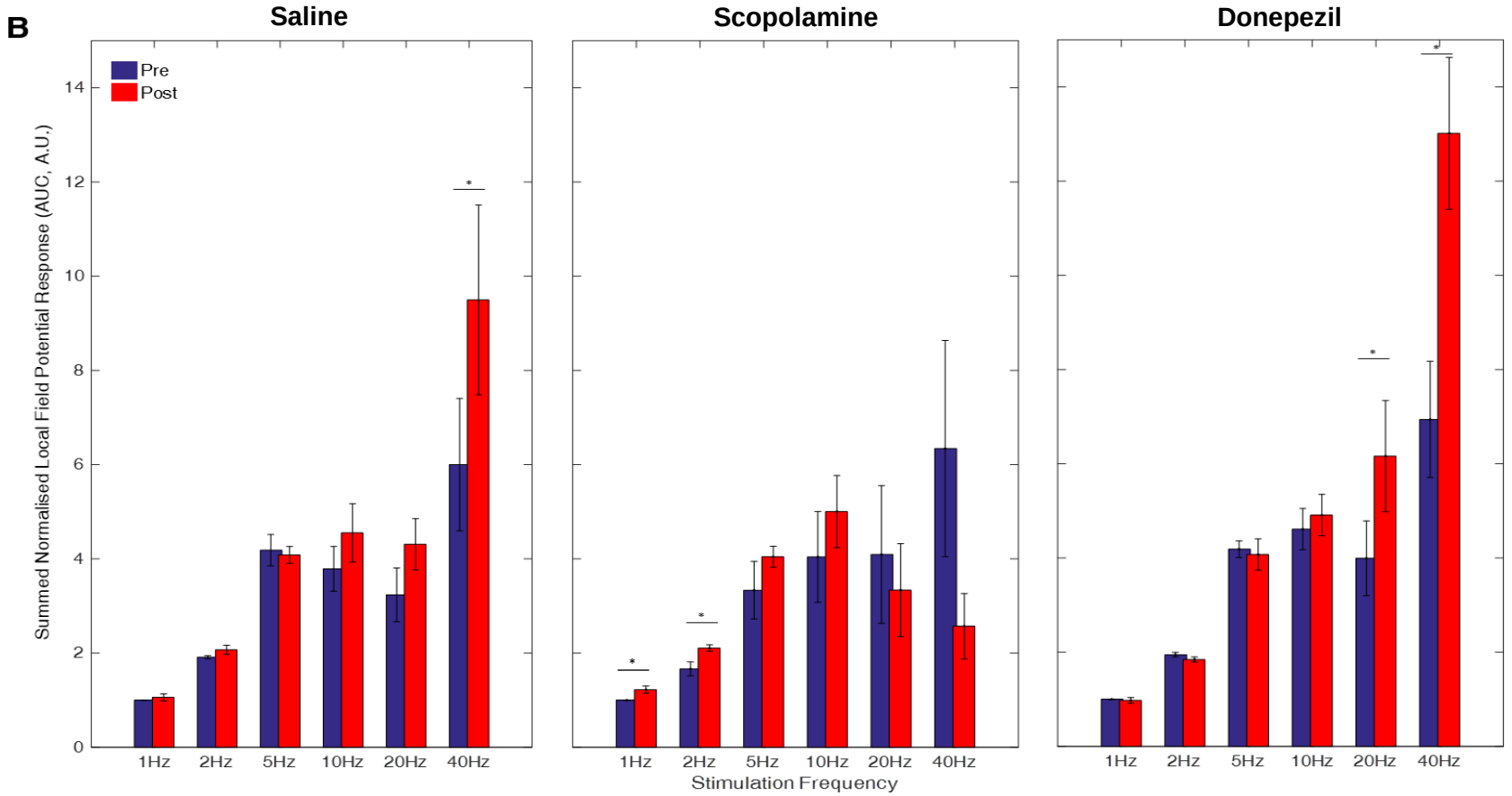

Figure 3.3 B. Bar charts showing summed and normalised local field potential (LFP) responses to 2s whisker stimulation at six frequencies, before (pre, blue) **and after** (post, red) **administration of saline, scopolamine or donepezil**. Data were normalised to the pre-drug average magnitude of the response to the first stimulus pulse for 1Hz stimulation. Area under the curve (AUC) was calculated for each stimulation pulse and then summed across stimulation pulses for each frequency condition. Error bars indicate standard error of the mean. *Represents a significant difference at $p<0.05$ between pre- and post-drug treatment for specific stimulation frequencies.

3.8.3.2 16s long stimulations (10Hz)

Repeated measures t-tests were used to determine significant effects of drug administration on the magnitude of LFP responses to 16s whisker stimulation. In line with results from the CBF data, donepezil administration was associated with a significant increase in LPF response magnitude ($t(5)= -5.43$, $p=.003$) (Figure 3.4), whereas there was no significant effect for saline ($p=.855$) or scopolamine ($p=.112$) administration.

3.8.4 Neurovascular coupling

To assess neurovascular coupling, data were further analysed on a trial by trial basis by plotting haemodynamic and neuronal response magnitudes against one another (Figure 3.5). To reduce inter-animal variability each animals' response values were first divided by their respective mean so as to normalise the datasets. Data from all trials were plotted (a total of 720 data points for each drug group). A linear regression was calculated (by least squares) for each data set in order to characterise the neurovascular coupling relationship from the concurrently measured neuronal and haemodynamic responses. The regression line was significantly different from zero in all datasets except in the scopolamine condition after drug administration (Figure 3.5). T-tests of the difference in the slope of the regression lines revealed a highly significant difference in the scopolamine condition before versus after drug administration ($t(716) = 3.88$, $p<0.001$), suggesting an alteration in neurovascular coupling.

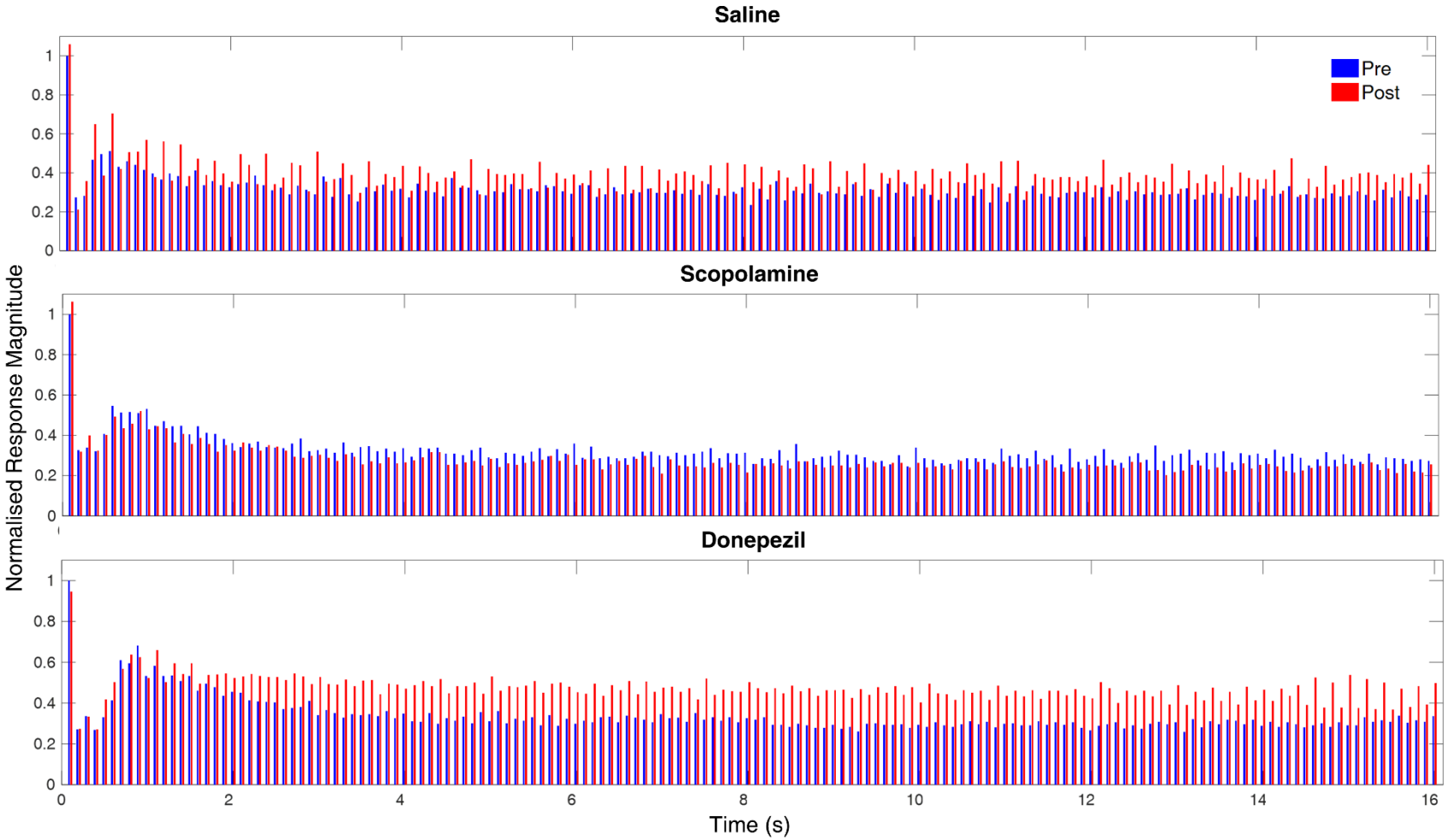

Figure 3.4 Normalised local field potential (LFP) responses to 16s whisker stimulation at 10Hz, before (pre, blue) **and after** (post, red) **administration of saline, scopolamine or donepezil.** Data were normalised to the pre-drug average magnitude of the response to the first stimulus pulse. Figure shows bars representing area under the curve (AUC) calculated for each stimulation pulse over the entire 16s stimulation train (160 pulses).

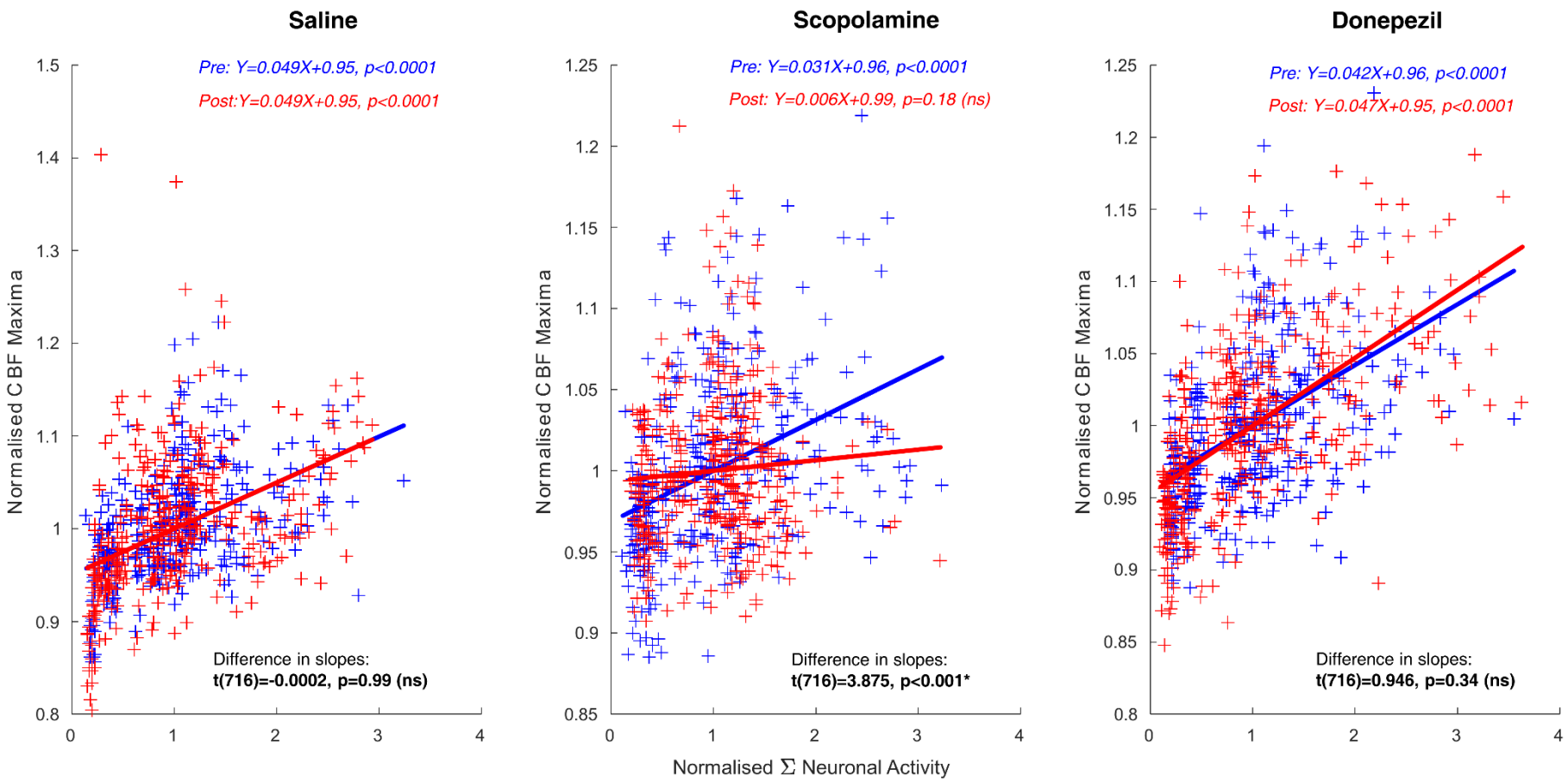

Figure 3.5. Scatterplots to indicate the relationship between magnitude of neuronal and haemodynamic (CBF) responses. Each data point is from a single trial, for a single animal from the multifrequency stimulation experiments (60 trials, 10 at each frequency 1, 2, 5, 10, 20 and 40Hz), before (pre, blue) and after (post, red) administration of saline, scopolamine or donepezil. A linear regression model was applied to characterise neurovascular coupling (blue and red lines). The equation of the regression lines are stated as are the results of a t-test of the significant difference of the slope from zero (red & blue text). A further t-test to determine significant differences in the regression models before and after drug administration was conducted (text in black).

3.9 Discussion

The main finding of this study was an alteration of neurovascular responses, including a change in the neurovascular coupling relationship, by pharmacological manipulation of cholinergic function. The results demonstrate haemodynamic and neuronal signal changes in response to scopolamine and donepezil administration. Scopolamine treatment to block cholinergic signalling was associated with an apparent loss of the monotonic neurovascular coupling relationship with no significant dependence of the magnitude of the CBF response on the magnitude of the neuronal response. These findings have implications for neuroimaging data acquired from clinical cohorts that have reduced cholinergic function such as AD patients (Li et al., 2015), as well as for the use of neuroimaging to study brain effects of cholinergic manipulations on cognitive function (Bajo et al., 2015). Caution should be exercised when interpreting human fMRI data from these groups as these data rely on an assumed monotonic neurovascular coupling function (Spain et al., 2015) where haemodynamic and neuronal response magnitude change in tandem with one another. These findings furthermore highlight that inferences about drug effects on neuronal activity cannot necessarily be extrapolated from haemodynamic neuroimaging signals. Moreover, there is a need for improved understanding of neurovascular consequences of pharmacological manipulations of neurotransmitter systems, which may require further studies that concurrently measure both haemodynamics and neuronal activity.

3.9.1 Acetylcholine manipulations result in specific stimulation frequency effects

Scopolamine and donepezil administration led to a stimulation frequency dependent decrease or increase in CBF and neuronal response magnitude respectively. An altered response pattern is qualitatively indicated by inspecting the bar charts plotting response magnitudes at each stimulation frequency (Figure 3.1). Similar effects are apparent for the neuronal response data (Figure 3.3). The results obtained in this chapter are not able to explain why CBF and neuronal response effects of scopolamine and donepezil treatment appear to only manifest at higher frequencies of sensory stimulation, although similar effects have been observed for serotonergic manipulation (Spain et al., 2015). In addition, comparisons of responses in awake and anaesthetised animals (Martin et al., 2006) to whisker stimulation, reported response magnitude differences between anaesthetic conditions, which again were stimulation-frequency dependent, with more pronounced differences in response magnitudes evident at higher stimulation frequencies. Since acetylcholine is a potent neuromodulator playing an important role in arousal and attention, it is possible that the pharmacological cholinergic challenges used in this study

led to a potentiation of the cortical response to higher sensory stimulation frequencies, as found in awake animals (Castro-Alamancos, 2002), although no evidence for an alteration in baseline cortical neuronal activity was found (Section 3.8.1).

When considering the long (16s) stimulation data, donepezil appears to increase the magnitude of both neuronal and haemodynamic responses (Figure 3.2 and Figure 3.4). Differences for this 10Hz stimulus were not apparent in the data from the short (2s) stimulation paradigm, suggesting that donepezil may impact upon long-latency changes in neurovascular coupling. This modulation of responses during a more sustained stimulus enhances the relevance of these findings for human fMRI research studies, where stimulation paradigms are typically of such longer durations. Scopolamine appears to have a more complex response profile during a long stimulation paradigm, with no significant effects apparent in either the neuronal (Figure 3.4) or haemodynamic data (Figure 3.3), in contrast to the effects observed at shorter stimulation frequencies (although it is noted that these effects were at higher stimulation frequencies than the one used for the long stimulation paradigm).

3.9.2 Scopolamine administration leads to neurovascular uncoupling: effects of trial averaging upon neurovascular data

By plotting trial by trial pre and post cholinergic challenge haemodynamic and neuronal data together to assess neurovascular coupling more directly, a clear pattern of neurovascular uncoupling was evident for the cholinergic antagonist drug scopolamine (Figure 3.5). This was not apparent when analysing haemodynamic and neuronal activity data separately due to the effect of trial averaging in the methods to visualise these data. The difference in the linear regression model before and after administration of scopolamine demonstrates an alteration of neurovascular coupling following pharmacological antagonism of brain acetylcholine by scopolamine, where stimulus evoked changes (increases or decreases) in neuronal demand are not accompanied by concomitant changes in CBF. These results suggest that potentially important effects of experimental manipulations upon relationships *between* neurophysiological parameters may be masked by trial averaging, where such features are discarded as noise.

3.9.3 Donepezil does not appear to affect neurovascular function

No previous study has investigated the effects of donepezil, a widely prescribed drug used in the palliative treatment of AD, upon neurovascular function using concurrent neuronal and haemodynamic measures. Data acquired in this chapter shows increases in both CBF and neuronal response magnitudes following treatment with donepezil. It has been

hypothesised that the increased CBF observed with donepezil treatment may be related to increases in neuronal activity (Tateno, Kobayashi, Utsumi, Morii, & Fujii, 2008), maintenance of adequate CBF supply (Chen, Magnotta, Duff, Ponto, & Schultz, 2006; Nakano, Asada, Matsuda, Uno, & Takasaki, 2001) or normalising flow regulation. As a result, improved blood supply to active neurons in the AD brain (Rosengarten, Paulsen, Molnar, Kaschel, & Gallhofer, 2006) may underlie some of the restoration of cognitive performance afforded by such pharmacological interventions (Li et al., 2012). Although results do not indicate an effect of drug treatment upon baseline CBF, the neurovascular measurements employed in this study appear to support this hypothesis with evidence that acute pharmacological decreases in brain acetylcholine may diminish the capacity of CBF to match changing stimulus-evoked neuronal demands. It can be hypothesised that such an effect will emerge if the prerequisite cholinergic tone for normal vascular responses (Lecrux et al., 2017) is not present, such as under disease conditions.

As donepezil does not, at the dosage used here, affect the relationship between concurrently measured neuronal activity and CBF changes; it is possible that changes in the magnitude of haemodynamic (including fMRI) signals in human or preclinical studies in response to cholinergic agonists do reflect changes in underlying neuronal activity, rather than effects on vascular reactivity. Coupled with the finding of Kocsis et al. (2014) which suggests the effects of cholinergic agonists on cognitive function are due to vascular drug actions (as drug BBB penetration was shown not to be necessary), this raises the possibility that modulation of cortical vascular function can impact directly on neuronal function (Moore & Cao, 2008). Thus, an important extension of this work would be to determine if donepezil treatment is protective of neurovascular function under conditions of cholinergic loss or blockade as it occurs with a cholinergic antagonist pre-treatment or in an AD murine model.

3.9.4 The importance of saline controls in long experimental protocols

Significant findings in control group data, (administration of saline) emphasise the importance of vehicle controls to account for changes over time in preclinical experiments conducted under anaesthesia. These changes were most likely caused by drift in anaesthetic state in the acute experimental protocol used here. The relationship between firing patterns of neurons and anaesthesia has been previously investigated. Erchova et al. (2002) measured the spatial and temporal firing patterns of neurons in the rat barrel cortex under three states of anaesthesia (light surgical state, intermediate and deep) and reported changes in haemodynamic responses across the three stages; thus concluding that haemodynamic changes in all three states were reflected in the differences in

neuronal activity due to anaesthesia. Furthermore such drift has been previously reported in CBV and CBF response measurements (Kennerley et al., 2005), suggesting a degree of caution when comparing BOLD and CBV measurements in an anaesthetised state. Although animals were maintained within a narrow physiological range (using artificial ventilation, monitoring of cardiovascular and blood gas parameters throughout data collection), it is difficult to completely avoid smaller changes which may occur over the course of the experiment. Thus, a vehicle control group is critical to enable these changes to be measured and controlled for in analysis of effects across groups. Despite already developed methods of haemodynamic and neuronal recording in awake animals (Martin et al., 2006; Martin et al., 2013) invasive concurrent measurements of neurovascular function and drug treatments as performed in this study still require the use of anaesthesia and this should be appropriately accounted for.

3.9.5 Limitations

Route of drug administration. A possible limitation of this work, and true of other studies utilising pharmacological manipulations is choice of drug administration route. By performing an i.v injection the drugs chosen in this study (BBB penetrant) have the capacity to reach both the CNS and the PNS. ACh in the PNS is located at the neuromuscular junction, between the motor nerve and skeletal muscle and thereby has an important role in neuromuscular connections, skeletal, smooth muscles and cardiac contractions. During drug administration changes in blood pressure and twitching (only observed with donepezil treatment) were noted as well as concomitant changes in CBF. To account for these effects imaging and electrophysiology recording were only recommenced once physiological parameters returned to pre-injection levels. Furthermore there was no change in overall baseline blood flow following drug administration for any of the treatment groups.

Additional physiological measures such as heart rate to account for any changes in cardiac output could be recorded to obtain a measure of any possible PNS changes due to cholinergic modulation which may affect neurovascular measurements and subsequent results. Direct intracerebroventricular (icv) administration is a possible alternative method of delivering pharmacological treatment although may not be easily employed in the imaging and electrophysiology set up utilised here and ultimately drug diffusion across the BBB would still occur. Icv administration may be useful for the study of non-BBB crossing ACh agonist and antagonist effects on brain neurovascular measures, although the therapeutic applications for human studies utilising this approach may be limited. Finally a drug administration which targets both CNS and PNS has strong

relevance and translation to human pharmacological treatments, as drug therapies such as donepezil are orally administered and thus will interact in both the CNS and PNS.

3.9.6 Future work

The development of a chronic model. The models utilised in this study are acute and thus are less able to mimic the chronic loss of ACh and ACh innervation observed in AD patients. Nevertheless our results have shown neurovascular uncoupling as a result of cholinergic reduction by scopolamine administration and are in agreement with previous research (Lecrux et al., 2017) which has implemented a model of chronic ACh decrease (noradrenergic lesioning with icv injection of saporin). This highlights that both acute and chronic models of ACh decrease can inform upon neurovascular coupling changes, which can be translated, to an extent, in diseases such as AD. Thereby an interesting extension of this work, alongside its application in an AD model, would be to implement it chronically to quantify if similar neurovascular changes are present.

Immunohistochemistry. A further extension for this work and any study looking at ACh innervation is the implementation of immunohistological methods to assess neuronal innervation. A marker for neuronal activation such as c-Fos (Staiger, 2006) would enable interrogation of neuronal network changes as a result of depleted or potentiated ACh levels as employed by Lecrux et al. (2017; 2011). This is of particular importance in neurovascular research as loss of ACh BF neurons has been shown to reduce firing rates in the rat barrel cortex during whisker-evoked sensory stimulation (Herron & Schweitzer, 2000). Furthermore IHC methods would enable quantification of the extent of neuronal loss which could directly be compared to AD patients' post-mortem brains or AD animal models. This would strengthen the translational aspects of preclinical research to human disease.

Assessment of vascular tone. Lecrux et al. (2017) report alteration of the neurovascular coupling relationship due to increases or decreases in ACh tone, thereby altering the fidelity by which haemodynamic signals assess changes in stimulus evoked neuronal activity. Hypercapnia (as discussed in Section 2.3.3.2) is a useful method to assess vascular reactivity and thus could be employed in this study design to assess whether baseline vascular tone is modulated by administration of scopolamine or donepezil. Baseline blood flow and neuronal data acquired in this study do not reveal any changes in baseline blood flow or neuronal activity which should manifest if vascular tone or reactivity was altered. Furthermore, the pharmacological manipulation utilised by Lecrux et al (2017) specifically targeted ACh tone, unlike our pharmacological blockade of ACh receptors (scopolamine)

or inhibition of ACh breakdown (donepezil). Nevertheless assessment of possible tone changes by donepezil would be interesting to assess as AD pathology is characterised by vascular tone dysregulation which is further aggravated by the developing cholinergic deficit (Di Marco, Farkas, Martin, Venneri, & Frangi, 2015). Thereby the development of new drugs that target both vascular tone dysregulation and cholinergic dysfunction could be key in further alleviating and slowing AD progression.

Lastly, and linked to the above point, future research should aim to determine if similar neurovascular effects can be observed with non CNS penetrating drug analogues to scopolamine and donepezil such as butylscopolamine and neostigmine to accurately determine if vascular actions alone, as argued by Kocsis et al. (2014) mediate the neurovascular effects observed in this study.

3.9.7 Conclusion

In conclusion these results provide evidence that modulation of brain ACh alters the relationship between neuronal and haemodynamic responses, with a neurovascular uncoupling effect associated with reduced cholinergic function. This finding has implications for the interpretation of BOLD fMRI and BOLD phMRI data in both animal and human imaging studies where cholinergic function may be different between experimental or patient groups. These findings furthermore support the notion that reduced cholinergic modulation of neurovascular function may be an important component of neurodegenerative diseases such as AD, highlighting a role for cholinergic drugs in normalising neurovascular function.

Chapter IV

Acute Effects of Systemic Inflammation upon *In-Vivo* Neurovascular Function

4.1 Chapter summary

The main aim of this chapter is to investigate the impact of an acute systemic inflammatory challenge on haemodynamic and neuronal signals to assess neurovascular function and neurovascular coupling.

Systemic inflammation has been implicated as a major player in the cascade of multiple neurodegenerative diseases including AD and furthermore systemic inflammation is a strong risk factor in the development of AD (Dunn et al., 2005). Nonetheless, there is a current lack of *in vivo* studies investigating how systemic inflammation and the subsequent neuroinflammatory changes, impact upon neurovascular function and neurovascular coupling. Lipopolysaccharide (LPS) treatment is a standard technique for inducing systemic inflammation *in vivo* and *in vitro* and has been used extensively to investigate the role of inflammation in neurodegenerative disease. As such it represents an ideal starting point to begin the investigation of the effects of systemic (and neuro)inflammation upon neurovascular function.

Following characterisation of *in vivo* changes in neurovascular function, results from this chapter indicate an alteration in haemodynamic signals following LPS administration. Increases in CBF, cerebral blood volume (HbT) and oxyhaemoglobin concentration (HbO_2) were reported in LPS-treated animals. Furthermore, LPS treatment significantly altered how stimulus inputs convert to haemodynamic response functions, thereby suggesting altered neurovascular function. Interestingly, upon estimation of $CMRO_2$ LPS animals show a substantial decrease below baseline suggesting alterations in how oxygen delivery is matched to metabolic demand. LPS animals also show a trend in reduced vascular reactivity (assessed via hypercapnic challenge). This study has implications for the understanding of how neurovascular function changes under an acute inflammatory response. This is of particular importance as the NVU is simultaneously the site of action of neurovascular coupling and in the transition between systemic to neuroinflammatory processes, where an inflammatory insult may cause a shift in the NVU focus, prioritising neuroimmune over neurovascular actions. Lastly these results are relevant to the application of fMRI in subjects or patients with a systemic inflammatory response, as they show that measures underlying fMRI signals ($CMRO_2$ and CBV) are altered in a systemic inflammatory state.

4.2 Systemic inflammation in AD pathology

Mounting evidence (Cunningham, 2013; Frank-Cannon, Alto, McAlpine, & Tansey, 2009; Gao et al., 2011; Heppner, Ransohoff, & Becher, 2015) has emerged indicating inflammation as a major player in the cascade of multiple neurodegenerative diseases. Furthermore human and animal studies strongly suggest systemic inflammation to be a risk factor for the development of AD. In patients with AD, systemic inflammation is associated with increased cognitive decline and elevated levels of TNFα (Holmes et al., 2009). In humans, repeated infections over a five-year period increased the risk of developing AD and there is an increased risk of dementia diagnosis in patients with two or more infections (Dunn et al., 2005). Moreover, chronic infections lead to cerebrovascular dysfunction which also promotes AD development (Li et al., 2011; Strandberg, Pitkala, Linnavuori, & Tilvis, 2003). Lastly, diseases that do not have an infectious component such as atherosclerosis, obesity and diabetes, all risk factors associated with AD, show inflammatory components, reemphasising the key role of inflammation in AD development (Balakrishnan et al., 2005; Casserly & Topol, 2004; Donath & Shoelson, 2011; Recasens, Ricart, & Fernández-Real, 2003).

4.3 Lipopolysaccharide (LPS) as a model of inflammation

Lipopolysaccharide treatment is a current standard technique of inducing inflammation both *in vivo* (Hauss-Wegrzyniak, Dobrzanski, Stoehr, & Wenk, 1998; Pintado et al., 2012) and *in vitro* (Lehnardt et al., 2003). LPS is a component of the outer membrane of gram-negative bacteria which triggers an immune response in the absence of a pathogen. The successful binding to the cell surface receptor CD14 creates a LPS-CD14 complex which interacts with the toll-like-receptor-4 (TLR-4) initiating the release of pro-inflammatory cytokines and chemokines in particular IL-1 and TNF-alpha on monocytes and macrophages (Coin et al., 1996; Nazem, Sankowski, Bacher, & Al-Abed, 2015). LPS produces a complex combination of downstream effects and whilst this can complicate the delineation of the pathways or mechanisms responsible, it remains a valuable model for studying the effect of a complete systemic inflammatory response, *as it occurs in life*, upon a set of specific physiological measurements. Depending on dosage, LPS treated animals display behavioural changes as well as a number of brain NVU cellular changes, including microglia and astrocyte activation (Nazem et al., 2015).

4.4 LPS as a model to investigate the contribution of inflammation to AD

Studies utilising transgenic mice including 3xTg-AD and APPswe report elevated level of Aβ in the hippocampus followed by memory and cognitive impairments (Kahn et al., 2012), tau hyperphosphorylation (Kitazawa, Oddo, Yamasaki, Green, & LaFerla, 2005) and microglial activation during late stage plaque formation (Sheng et al., 2003) following peripheral LPS treatment. Similarly, chronic LPS treatment (4 weeks) has been shown to reproduce components of AD neurobiology in naïve (healthy) rats, including increased astrogliosis and microglial activation, increased levels of IL-1 and TNFα, elevated β-amyloid precursor protein (β-APP) production and behavioural deficits in working memory (Hauss-Wegrzyniak et al., 1998). A single dose (acute) administration of LPS (5mg/kg) in mice (Qin et al., 2007) and in rats (Bossù et al., 2012) also sees increased levels of brain TNFα that remained elevated 10 months' post treatment. Studies focused on blocking LPS-triggered inflammation, such as Lee et al. (2012) report attenuation of memory impairments, neuroinflammation and amyloidogenesis in transgenic mice. Evidence of disease propagation and instigation due to inflammation in both animal (Akiyama et al., 2000; Rosi, Ramirez-Amaya, Hauss-Wegrzyniak, & Wenk, 2004) and human studies (Li et al., 2011; Strandberg et al., 2003) strengthen the role of inflammation in the neuropathogenesis of AD.

4.5 Study overview and hypothesis

There is a current lack of i*n vivo* studies investigating how systemic inflammation impacts upon neurovascular function and which furthermore seek to determine the cellular drivers of these *in vivo* effects by using tissue from the same animals (Chapter V). This is of particular importance as the NVU is simultaneously the site of action of neurovascular coupling, neuroinflammatory responses and in the transition between systemic to neuroinflammatory processes. The LPS model has been used extensively to investigate the role of inflammation in neurodegenerative diseases, thus it represents an ideal starting point to explore the neurovascular effects of systemic inflammation. Investigating the complex downstream effects of a systemic inflammatory response in an AD model is challenging, as a complete and accurate delineation of the pathways and mechanisms responsible may be difficult to separate from that caused by disease alone. Thereby this chapter aims to interrogate the effects of an acute systemic inflammatory challenge upon neurovascular function in a healthy animal. These results can then be used to understand how the changes in neurovascular function caused by underlying systemic (and derived neuroinflammatory) processes may impact upon brain health.

The main **hypothesis** for this chapter is that an acute systemic inflammatory challenge will alter neurovascular function, by changing how stimuli inputs are converted to haemodynamic response functions, thereby mediating neurovascular uncoupling.

4.6 Chapter aims

This study aimed to investigate the impact of inflammation on neurovascular function by measuring *in vivo* brain neurovascular signals under an acute systemic inflammatory challenge in a rodent model by obtaining measures of the haemodynamic response function and neuronal activity in the context of physiological stimuli.

4.7 Method

Anaesthesia, surgical procedures, physiological monitoring and imaging protocols (LSCI, OIS) were carried out as described in Chapter II. Briefly, animals were anaesthetised with an i.p injection of urethane (1.25mg/kg in 25% solution), tracheotomised and the left vein and artery cannulated. A thin cranial window was then prepared. Animal temperature was maintained at 37 ^{0}C (± 0.5 ^{0}C) and sampled blood gases remained within physiological parameters throughout experimental duration (mean values: PO_2 =80%(±9.1) PCO_2 =30.4(±3.7) SO_2 =96%(±1.2)). MABP was also within recognised physiological limits (104±6).

4.7.1 Animals and pharmacological treatment

Female Hooded Lister rats (3-4 month old, *n* = 16, 220g-320g) were assigned to one of two groups (control or LPS, *n* = 8 per group). Haemodynamic and electrophysiological data were concurrently acquired in all treatment groups over time (from 4 hours post injection until 6 hours post injection). Each animal received an intraperitoneal injection based on condition just after loss of movement due to anaesthesia at 9am. Control animals were administered a saline vehicle (1ml/kg), LPS animals received a dose of 2mg/kg LPS-EB (lipopolysaccharide from E.coli, InvivoGen, Europe) dissolved in endotoxin-free water.

4.7.2 Imaging and electrophysiology

OIS and LSCI were performed as described in Chapter II (Section 2.3.1). OIS was performed by illuminating the cortex with four wavelengths of light (495 ± 31 nm, 559 ± 16 nm, 575 ± 14 nm, and 587 ± 9 nm) to generate spatial maps of the haemodynamic response. At the start of each paradigm a 10 second baseline data acquisition period preceded the start of the stimulation train. For LSCI, the camera was positioned over the thinned window and a 70 second baseline data acquisition period was acquired in each paradigm to obtain a measure of baseline blood flow. Data were acquired at a frame rate of 25Hz.

Electrophysiology data were acquired via a carbon fibre surface electrode positioned adjacent to the thinned window, as described in Chapter II (Section 2.3.2.2).

4.7.3 Experimental design

All data were acquired within a ferromagnetic cage as outlined in Chapter II (Section 2.3) to minimise electrical interference. In order to measure the effects of inflammation over time recording of data had to take place at specific time intervals. Initial data acquisition occurred four hours after saline/LPS injection to allow for surgical and imaging

procedures to be set up. To compare LPS changes over time the same stimulation paradigms were repeated a second time to correspond to six hours after LPS/saline injection. Two whisker stimulation paradigms were applied, multifrequency and long stimulation as described in Chapter II (Section 2.3.3.1). The order of stimulation frequency for multifrequency condition was pseudorandomised. A 1.0mA whisker stimulation (0.3ms pulse-width) was delivered via two subdermal electrodes directly inserted in the whisker pad, as detailed in Chapter II (Section 2.3.3). A hypercapnia challenge as described in Chapter II (Section 2.3.3.2) was also included in the experimental design.

4.7.4 Data analysis

4.7.4.1 Data processing

Data acquired from LSCI, OIS and electrophysiological recording was extracted, processed and analysed as described in Chapter II (Section 2.6). A one-way ANOVA on ROI for LSCI ($F(1,13)=0.06$ $p=.811$) and OIS ($F(1,13)=1.54$ $p=.239$) did not reveal a significant difference between groups. Data from each stimulation trial were extracted and divided by the average perfusion value (arbitrary units) over a pre-stimulus baseline period (10s), to yield a measure of percentage (fractional) change in CBF. Time series were averaged across trials according to stimulation condition. Area under the curve (AUC) and maxima for each response were calculated. Two cases (one from each group) were excluded from further statistical analysis due to poor response specificity, thereby a total of $n=14$ ($n=7$ for each group) animals were included in the final statistical analysis.

4.7.4.2 Statistical analysis

Extracted maxima and AUC measurements were analysed in SPSS 23 with appropriate statistical tests dependent on experimental design. Normality and homogeneity of data were assessed prior to analysis. A p value of less than .05 was deemed significant. Additional t-tests (where applicable) were conducted to further probe differences between experimental conditions with correction for multiple comparisons (p value was divided by number of tests).

4.8 Results

4.8.1 Baseline cerebral blood flow

To assess any effects of treatment upon baseline CBF the average perfusion value across a 30s period prior to the onset of stimulation at the start and end of the experimental protocol was calculated. A one-way ANOVA on CBF baselines at +4 hours ($F(1,13)=0.10$ p=.754) and +6 hours ($F(1,13)=0.59$, $p=.458$) post treatment found no difference between groups.

4.8.2 Haemodynamic responses to a short (2s) multifrequency stimulation paradigm

Multivariate analyses of variance (MANOVAs) were applied to HbO_2, HbR, HbT and CBF response maxima or minima (HbR) values in order to determine significant effects of LPS administration at 4 hours and at 6 hours post treatment. All cases ($n=14$) were included in the analysis. At 4 hours post injection, there was a significant effect of stimulation frequency on haemodynamic response magnitude: $F(20, 190) = 7.042$, $p < .001$; Wilks' $\Lambda = .159$, (Figure 4.1 A), with significant effects for each haemodynamic response measure (Table 4.2). However there was no significant interaction between stimulation frequency and treatment ($F(20, 190) = 1.34$, $p = .156$; Wilks' $\Lambda = .645$). LPS administration itself did not result in a significant change in the magnitude of the haemodynamic response $F(4, 9) = 0.33$, $p = .852$; Wilks' $\Lambda = .872$.

At 6 hours post injection, there was a significant effect of stimulation frequency on haemodynamic response magnitude: ($F(20, 190) = 6.41$, $p < .001$; Wilks' $\Lambda = .181$) with significant effects for each haemodynamic response measure (Table 4.2) and a significant interaction effect between stimulation frequency and treatment ($F(20, 190) = 2.31$, $p = .002$; Wilks' $\Lambda = .486$). Individual significant interaction effects for each haemodynamic measure are further reported in Table 4.2. LPS administration itself did not result in a significant change in the magnitude of the haemodynamic response $F(4, 9) = 1.25$, $p = .357$; Wilks' $\Lambda = .643$.

Post hoc analysis of individual stimulation frequencies using independent t-tests (Figure 4.1 A) indicate a significant increase in HbO_2 response magnitude at 5Hz ($p=.049$) and a significant decrease in HbR response magnitude at 5Hz ($p=.022$) at 6 hours post treatment. A representative haemodynamic response profile at a 5Hz stimulation frequency is plotted in Figure 4.1 B for each measure.

Table 4.1. Summary of univariate statistical analyses of haemodynamic responses to a mixed frequency 2s stimulation paradigm for saline/LPS treated animals. * Denotes a significant effect.

Time	Factor		*df*	*F*	*p*
+4 hours after injection	**Frequency**	HbO_2	5,60	15.19	<.001*
		HbR	5,60	18.68	<.001*
		HbT	5,60	11.80	<.001*
		CBF	5,60	17.98	<.001*
	Frequency x Treatment	HbO_2	5,60	0.76	=.581
		HbR	5,60	1.45	=.219
		HbT	5,60	0.54	=.743
		CBF	5,60	0.23	=.949
	Treatment	HbO_2	1,12	0.10	=.758
		HbR	1,12	0.24	=.635
		HbT	1,12	0.02	=.892
		CBF	1,12	0.15	=.703
+6 hours after injection	**Frequency**	HbO_2	5,60	21.45	<.001*
		HbR	5,60	23.86	<.001*
		HbT	5,60	15.25	<.001*
		CBF	5,60	19.13	<.001*
	Frequency x Treatment	HbO	5,60	6.48	<.001*
		HbR	5,60	7.92	<.001*
		HbT	5,60	4.75	=.001*
		CBF	5,60	2.64	=.032*
	Treatment	HbO	1,12	1.21	=.294
		HbR	1,12	2.36	=.151
		HbT	1,12	0.43	=.524
		CBF	1,12	0.07	=.798

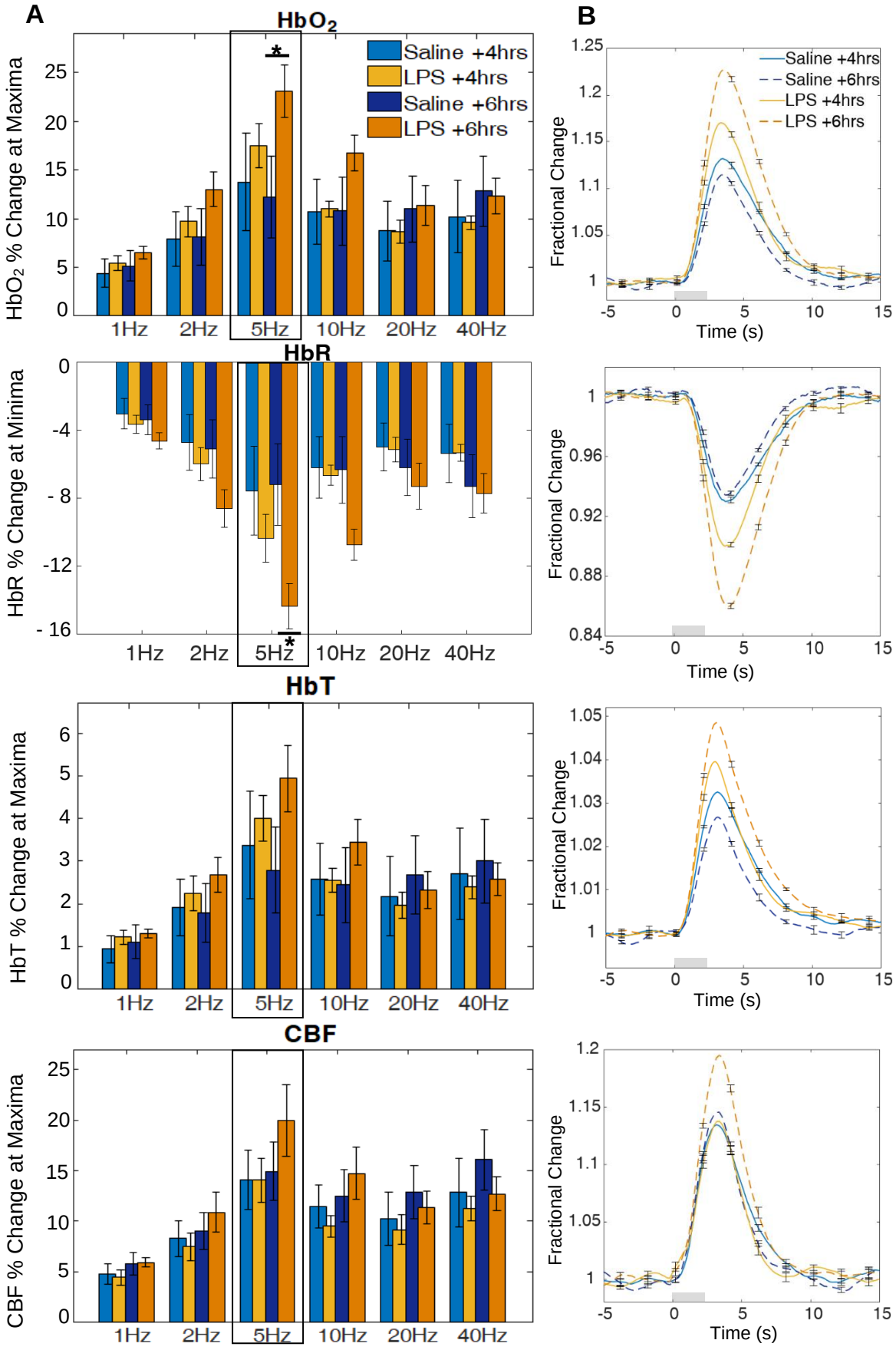

Figure 4.1. Haemodynamic response to 2s whisker stimulation at six frequencies at +4 and +6 hours after LPS/saline administration. (A) Bar charts show % change at maxima or minima (HbR). Post hoc analysis on stimulation frequencies reveal significant effects at 5Hz for HbO_2 and HbR (*denotes significant differences at $p<0.05$) between groups **(B)** Representative 5Hz time series showing mean fractional changes. Grey rectangle indicates stimulation onset/offset and error bars indicate standard error of the mean.

4.8.3 Haemodynamic responses to a long (16s) stimulation paradigm

MANOVAs on AUC measures were used to determine significant effects of treatment on the magnitude of the haemodynamic response (for HbO_2, HbR, HbT and CBF variables) to 16s whisker stimulation at +4 hours and at +6 hours post treatment. Treatment had no significant effect on response magnitude at 4 hours ($F(4, 9) = .316$, $p = .860$; Wilks' $\Lambda = .877$) or at 6 hours ($F(4, 9) = .925$, $p = .490$; Wilks' $\Lambda = .709$) (Figure 4.2 A). Treatment effects for each measure were also not significant (HbO_2 [+4hrs: p=.984; +6hrs: p=.289], HbR [+4hrs: p=.916; +6hrs: p=.456], HbT [+4hrs: p=.906; +6hrs: p=.305], CBF [+4hrs: p=.479; +6hrs: p=.895]) (Figure 4.2 B).

4.8.4 Haemodynamic responses to hypercapnia

Analysis of variance (MANOVA) were used to determine significant effects of treatment on haemodynamic response magnitude (for HbO_2, HbR, HbT and CBF variables) to a 30s hypercapnia challenge at +4 hours and at +6hrs post treatment. Maxima (or minima) values were used to quantify the response. Treatment had no significant effect on response magnitude at 4 hours ($F(4,9)=1.42$, p=.304; Wilks' $\Lambda = .613$) or at 6 hours ($F(4,9)=1.33$, p=.331; Wilks' $\Lambda = .629$) (Figure 4.3 A). Treatment effects for each measure were also not significant (HbO_2 [+4hrs: p=.827; +6hrs: p=.397], HbR [+4hrs: p=.588; +6hrs: p=.861], HbT [+4hrs: p=.618; +6hrs: p=.105], CBF [+4hrs: p=.351; +6hrs: p=.389]) (Figure 4.3 B). A shift in response profile based on treatment can be observed in the HbT measure, where LPS treatment leads to a bigger increase in CBV compared to saline at +6 hours post treatment (LPS: M=1.06, SD=0.022; Saline: M=1.04, SD=0.024). The CBF response to a hypercapnic challenge instead appears to decrease under LPS treatment, this effect is most pronounced at +4 hours post administration (LPS: M=1.35, SD=.15; Saline: M=1.44, SD=.17) but remains non-significant.

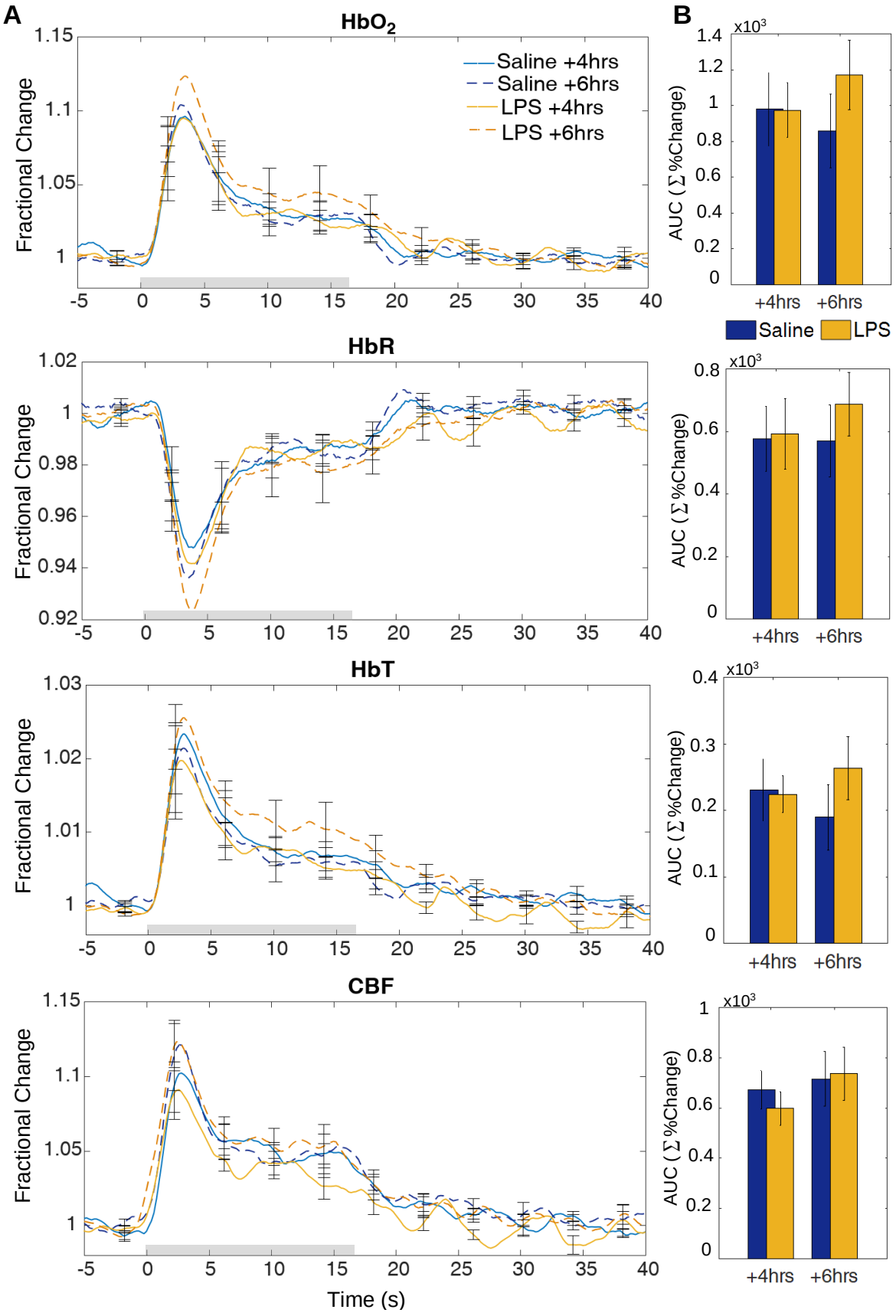

Figure 4.2. HbO_2, HbR, HbT and CBF responses to 16s whisker stimulation, at 10Hz, at +4hrs and +6hrs of LPS/saline administration. (A) Time series show mean fractional changes and **(B)** Bar charts show change in area under the curve (AUC, units are summed percentage change). Grey rectangle indicates stimulation onset/offset. Error bars represents standard error of the mean.

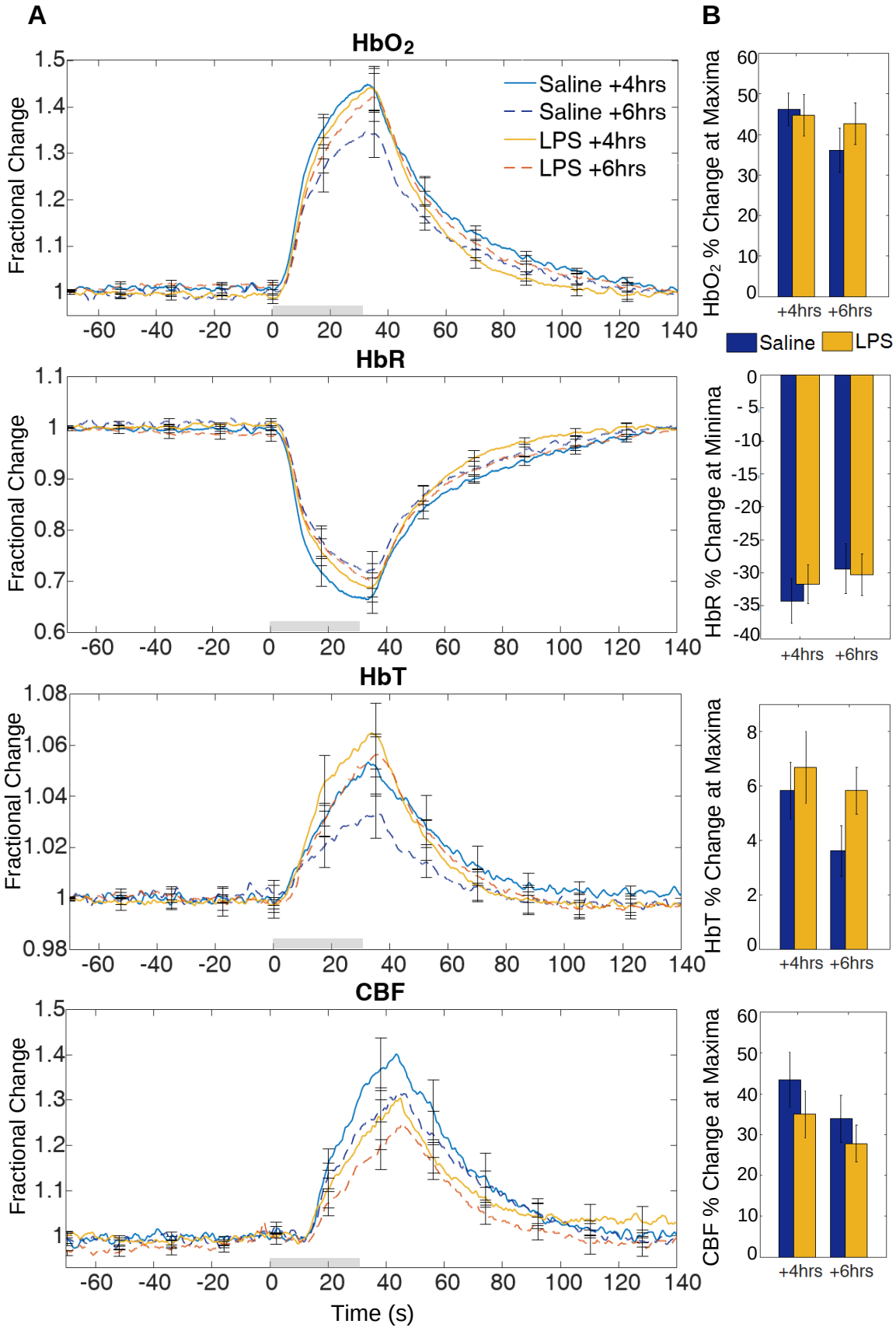

Figure 4.3. HbO_2, HbR, HbT and CBF responses to hypercapnia at +4hrs and +6hrs of LPS/saline administration. (A) Time series show mean fractional changes and **(B)** Bar charts show percentage change at maxima or minima. Grey rectangle indicates the 30s CO_2 challenge onset/offset. Error bars represents standard error of the mean.

4.8.5 $CMRO_2$ estimation

$CMRO_2$ changes were estimated (as described in Section 2.6.3) at both time points (+4 and +6 hours post injection) and for both saline and LPS treated animals (Figure 4.4). Response maxima and AUC were calculated and analysed with one-way ANOVA. Maxima result reveal a marginal non-significant effect between groups at +4hrs after LPS/saline treatment ($F(1,13)=3.5$, $p=.087$). No significant difference between groups was observed at +6 hours after treatment ($F(1,13)=2.5$, $p=.138$). One-way ANOVA AUC results reveal a significant difference at +6 hours ($F(1,13)=6.16$, $p=.029$) between treatment groups. No significant difference was found at +4 hours ($F(1,13)=2.05$, $p=.178$).

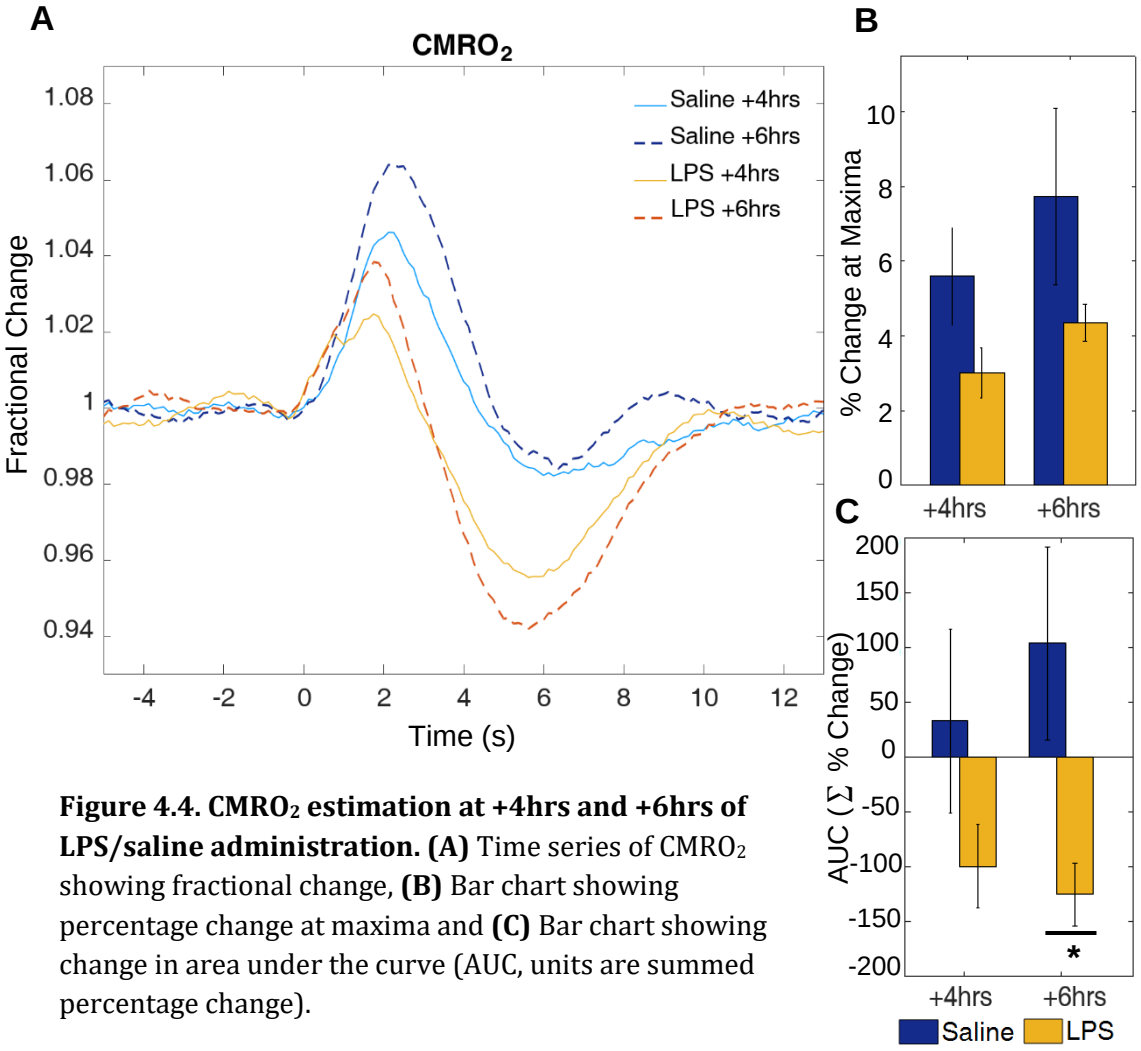

Figure 4.4. $CMRO_2$ estimation at +4hrs and +6hrs of LPS/saline administration. (A) Time series of $CMRO_2$ showing fractional change, **(B)** Bar chart showing percentage change at maxima and **(C)** Bar chart showing change in area under the curve (AUC, units are summed percentage change).

4.8.6 Neuronal Activity

A surface electrode recording was developed for this study so as to obtain neuronal response measures without brain penetration. However technical difficulties meant that the data obtained from this electrode was of a very poor quality and could not be improved without impacting upon the quality of the OIS/LSCI measures. For this reason the electrophysiology data are not reported for this thesis chapter.

4.9 Discussion

The main finding of this study was an alteration in neurovascular function in acutely LPS treated animals demonstrated by assessing how a range of stimuli inputs are converted to haemodynamic response functions. An alteration in this relationship was observed at 6 hours following LPS treatment. Increases in haemodynamic measures were also observed in LPS-treated animals compared to controls with stimulation-frequency specific effects. This underlines the importance of choosing a dynamic stimulus paradigm as disease-related manipulation effects may be dependent on the properties of the stimulus protocol utilised (i.e the level of input to the neuronal-vascular system). Estimation of $CMRO_2$ reveals a possible alteration in how oxygen delivery is matched to metabolic demand following an acute LPS inflammatory challenge. Lastly, LPS-treated animals show a trend in reduced vascular reactivity to a hypercapnic challenge. These findings have implications for the understanding of neuroimaging data acquired from clinical and healthy cohorts which may present with systemic inflammation where the physiological processes which underlie neuroimaging signals acquired in humans (CBF, CBV and $CMRO_2$) may be altered.

4.9.1 Acute and systemic inflammatory effects alter neurovascular responses

LPS administration significantly alters haemodynamic response function. This altered response pattern is qualitatively indicated by inspecting the bar charts plotting response magnitudes at each stimulation frequency (Figure 4.1). This significant difference only emerged at 6 hours following LPS administration, indicating that the developing haemodynamic changes associated with an acute inflammatory challenge only begin to significantly impact upon neurovascular function from a specific time point (≥6 hours). This may be explained by a shift in the NVU focus, prioritising neuroimmune over neurovascular actions as a direct result of an inflammatory insult.

Although a consistent trend in increases in HbO_2, HbT and CBF and a decrease in HbR is observed in LPS-treated animals, stimulation frequency is key in driving significant differences between groups. From this data significant differences between groups were evoked by a 5Hz stimulation for HbO_2 and HbR measures, although the same trend is also observed for HbT and CBF. As previously discussed (Section 3.9.1) stimulation dependent effects have already been reported in the literature (Spain et al., 2015; Martin et al., 2006) and have also been found under cholinergic manipulation (in the previous experimental Chapter, Section 3.8.2.1). It is difficult to assess why significant effects are primarily driven by a specific stimulation frequency, although in this data a trend is evident across all frequencies. These results underline the complexity of the neurovascular coupling

relationships and the importance of including a dynamic range of sensory stimulations in neurovascular research to better assess how the neurovascular system responds to different levels of input in health and under disease-related manipulations.

Altered neurovascular responses are not evident in long stimulation data (16s) (Figure 4.2) although a trend suggesting a similar response profile for LPS treated animals (i.e an increase) is present. This is somewhat surprising as the early 'peak' phase of the response is expected to indicate the same neurovascular changes as in the short 2s stimulation paradigm. This finding further reinforces the need of utilising a range of sensory stimulations as 16s data evoked haemodynamic changes were only assessed with a 10Hz stimulation frequency. It would thus be interesting to investigate if a significant difference between groups was present in a 16s stimulation paradigm utilising a 5Hz stimulation frequency.

Assessing neurovascular coupling across different stimulation lengths enables a detailed assessment on the initial neurovascular impulse-response function (Martin et al., 2013; Martindale et al., 2003) and the assessment of longer-latency changes in coupling. This is of particular importance as human fMRI research studies utilise stimulation paradigms that are typically of longer durations, and rely on short-latency impulse response functions to estimate the haemodynamic response (Logothetis, 2008). It is thus important to assess haemodynamic responses during a short and more sustained stimulus in preclinical research to better relate preclinical research to human fMRI studies and analysis. Furthermore these findings have implications for neuroimaging data acquired in clinical or healthy populations that may present with an underlying systemic infection as these data have shown changes in CBF, CBV and $CMRO_2$ measures resulting from an acute systemic challenge.

4.9.2 Acute systemic inflammation may mediate alterations in how oxygen delivery is matched to metabolic demand

A $CMRO_2$ estimate was calculated to assess possible changes in oxygen delivery or oxidative metabolism. LPS-treated animals showed a trend in reduced $CMRO_2$ maxima at both time points (Figure 4.4), with a more pronounced effect at 4 hours following treatment (statistics marginally not significant). Furthermore by qualitatively assessing the change in the shape of the $CMRO_2$ curve and AUC measures, this data suggests an alteration in how oxygen delivery is matched to metabolic demand; where the increase or decrease of CBF relative to oxygen consumption is altered by LPS treatment. Specifically, whilst $CMRO_2$ is estimated to initially increase in all conditions, in both LPS conditions

(+4hrs and +6hrs) there is a substantial latter decrease below baseline. Computing the AUC reveals a significant difference between LPS and saline conditions at 6 hours. This alteration may in turn reflect a change in neurovascular coupling but this claim requires validation with a direct measure of neuronal activity. Nevertheless altered $CMRO_2$ estimates indicate a change in the relationship between the HbR, HbT and CBF components of the haemodynamic response under LPS treatment. This would in turn predict that BOLD signals, which are also calculated from HbR, HbT and CBF changes will be different under LPS treatment, therefore caution should be taken in interpreting neuroimaging signals acquired from LPS-treated subjects.

4.9.3 Assessment of neuronal activity to inform upon neurovascular coupling

Without a direct measure of neuronal activity it is difficult to fully assess alterations in neuronal activity as a result of an acute inflammatory challenge and to analyse if increases or decreases in neuronal activity are subsequently matched to changes in CBF – the neurovascular coupling relationship. The lack of a concurrent measure of neuronal activity during the acute systemic inflammatory challenge is a limitation of this study. The development of non-invasive electrophysiology methods are thus warranted for experimental setups where invasive electrophysiological recording will impact upon measured variables (see Section 4.9.4). Lastly, the development of such techniques will furthermore enable neurovascular coupling assessment in awake preparations and may thus begin to reduce the use of anaesthesia in neurovascular research.

4.9.4 Can an acute systemic LPS challenge reduce cerebrovascular reactivity?

Animals treated with LPS showed a trend in reduced CBF responses to hypercapnic challenges (Figure 4.3). This reduction was particularly evident at four hours post LPS administration. This altered response could be an indication of changes in vascular tone or reactivity by LPS on the vasculature. This may therefore reflect an alteration in astrocyte function on vascular tone, as these cells have been implicated in mediating hypercapnic vasodilation in health (Howarth et al., 2017). A reduced response to a hypercapnic challenge has been previously observed in an MRI study testing young adults carrying the APOE ε4 allele (Suri et al., 2015), suggesting reduced cerebrovascular reactivity in APOE ε4 carriers. It would thus be interesting to characterise if the reduced cerebrovascular reactivity observed under LPS treatment and in APOE ε4 carriers is mediated by similar effects, as APOE ε4 has been shown to play a key role in inflammation by promoting the expression of inflammatory markers (Fan et al., 2017). Assessment of changes in vascular density may also indicate changes in vascular reactivity, as such immunohistochemical

assessment via a vessel marker label, such as COLL IV, could compare any differences in vascular density and vessel width between saline and LPS treated groups.

4.9.5 Future work

The addition of a measure to assess neuronal activity to investigate neurovascular coupling directly. Suitable non-invasive methods of recording neuronal activity are warranted in *in vivo* preparations where acute electrophysiological measures such as the insertion of a 16-channel electrode may impact upon measured variables. By concurrently measuring haemodynamic and neuronal changes a complete assessment, which does not rely upon estimates of metabolic activity ($CMRO_2$) of the neurovascular coupling relationship would be possible. It would thus be interesting to examine if neuronal demand (increase or decrease) is subsequently met by changes in CBF under an acute inflammatory state and if and how an *oversupply* of oxygen, as measured in LPS-treated animals, may lead to a disruption in neurovascular coupling. Alternatively as 2-photon microscopy enables the measurement of blood flow responses and neuronal and astrocytic calcium firing (Svoboda & Yasuda, 2006) this technique can offer concurrent investigation of the three driving components in the neurovascular coupling relationship. 2-photon microscopy could thus be used to investigate any inflammation-derived changes in neurovascular coupling.

Investigating COX-1. COX-1 has been shown to play a critical role in hypercapnia-evoked CBF increases *in vivo* (Niwa et al., 2001; Howarth et al., 2017). The trend in reduced CO_2-evoked CBF responses in LPS treated animals compared to controls (Figure 4.3) observed in this study may be mediated by an alteration in COX-1. To quantify this, changes in COX-1 expression between saline and LPS treated animals could be assessed via IHC methods. Furthermore dual labelling of COX-1 and an astrocyte marker (such as GFAP) could reveal changes in the CO_2-evoked CBF response, as these cells have been recently implicated in mediating hypercapnic vasodilation in health by increasing calcium signalling, stimulating COX-1 activity and in turn triggering downstream PgE_2 production (Howarth et al., 2017). It would thus be interesting to characterise if an acute systemic inflammatory response alters the role of astrocytes (and derived COX-1 production) thereby impacting upon CBF response during hypercapnia.

Extending the study to include aged animals. Systemic inflammation is intimately tied to ageing and has been show to either dramatically increase the risk of developing AD or to exacerbate cognitive decline in AD patients (Elahy et al., 2015; Fong et al., 2009). As such this study could be further extended to include aged animals to assess how ageing impacts

upon neurovascular function and compare how ageing impacts upon the measured haemodynamic changes following an acute systemic inflammatory challenge. The final experimental chapter of this thesis (Chapter VI) will begin to address this by investigating how age of LPS treatment impacts upon neurovascular function, haemodynamic responses and $CMRO_2$.

4.9.6 Conclusion

In conclusion these results provide evidence that an acute systemic inflammatory challenge alters neurovascular responses, by altering how stimulus inputs convert to haemodynamic response functions. This finding has implications for the understanding of neuroimaging data acquired from clinical and patient cohorts which may present with systemic inflammation where the physiological processes which underlie neuroimaging signals acquired in humans (CBF, CBV and $CMRO_2$) may be altered.

Chapter V

Histological Characterisation of Acute Effects of Systemic Inflammation on the Neurovascular Unit

5.1 Chapter summary

This chapter aim is to investigate the impact of acute systemic inflammation on the cellular pathology of the neurovascular unit (NVU) by utilising tissue from the same LPS challenged animals in the previous *in vivo* study (Chapter IV). It will provide a detailed characterisation of the immunoreactive profile of a panel of NVU cells and quantitatively assess changes in expression. Furthermore it aims to relate NVU cellular changes to the altered neurovascular function observed in Chapter IV.

Inflammatory insults of both systemic and neuroinflammatory origin evoke changes in NVU cells morphology and function, impacting upon neurovascular health. Furthermore changes in expression of adhesion molecules such as ICAM-1 and changes in aquaporin 4 (AQP4) in astrocyte endfeet occur in inflammation, thereby altering neurovascular function.

Following characterisation of NVU glia cells by immunohistochemistry this chapter results reveal changes in astrocytes and microglia morphology with increased expression of GFAP and IBA-1 respectively. These morphological and expression changes may reflect a change in cell phenotype, although this requires validation via gene expression studies. Lastly the observed increases in ICAM-1 expression by ECs support previous literature demonstrating the extensive involvement of ECs in inflammation (Pober & Sessa 2007). This generated the hypothesis of ECs as being initial inflammation responders, whereby changes in activation profile and gene expression propagate to trigger other NVU cells (glia) inflammatory responses. Further characterisation of ECs gene expression would provide additional insights into the phenotype of ECs in systemic inflammation and potentially delineate the propagation of the inflammatory response among the cellular constituents of the NVU. ECs involvement in mediating increases in blood flow during systemic inflammation, in hypercapnia regulation and overall cerebral circulation (via the EP1 receptor) may furthermore help to explain the CBF increases and reduced response to hypercapnia observed in LPS treated animals.

Lastly an increased expression of AQP4 around vessels, as observed in this study may suggest a change in the relationship between AQP4 (astrocyte endfeet) and blood vessels. Characterisation of this relationship via fluorescent labelling may reveal additional changes in AQP4 signalling as well as redistribution of AQP4 following systemic inflammation. This is of particular relevance as it may impact upon neuron-astrocyte interactions and neurovascular coupling due to the regulatory effects of AQP4 on both synapses and blood vessels (Jukkola & Gu, 2015).

5.2 Key neurovascular mediators of inflammation

Any inflammatory insult to the brain must be quickly and precisely regulated to avoid long term damage to neurons which are known to retain high sensitivity to inflammatory stimuli, such as pro-inflammatory cytokines (Graeber, Li, & Rodriguez, 2011; Northrup & Yamamoto, 2010). Current literature indicates both a beneficial and detrimental role from cells directly involved in neuroinflammation, in particular microglia and astrocytes. From recent evidence pericytes have emerged as possible mediators of brain inflammation (Jansson et al., 2014). Dysfunction of the BBB has also been observed during neuroinflammatory events, including upregulation in the expression of intercellular adhesion molecule (ICAM-1). Furthermore, changes in expression of the aquaporin 4 (AQP4) channel, which is directly involved in astrocyte signalling, has also been reported (Auguste et al., 2007). The roles of microglia, astrocytes, pericytes, ICAM-1 and AQP4 in inflammation will be reviewed below as each mediator will be immunohistochemically assessed to characterise the effects of an acute systemic inflammatory challenge on NVU cells.

5.2.1 Microglia

In adult brains microglia are primarily responsible for immune surveillance. Under normal conditions these cells exhibit a ramified morphology termed as 'resting' which dramatically changes into a spherical shape with no ramifications (Kreutzberg, 1996) termed as 'activated' as a result of brain injury or immunological stimuli (including inflammation). In an 'activated' state microglia increase their phagocytic activity and have been shown to release a wide range of pro-inflammatory factors including NO and proinflammatory cytokines such as tumour necrosis factor alpha (TNFα) (Colton & Gilbert, 1987; Liu & Hong, 2003; Moss & Bates, 2001; Sawada, Kondo, Suzumura, & Marunouchi, 1989) which are cytotoxic to neurons. However, microglia have also been shown to release neurotrophic and anti-inflammatory factors (Morgan, Taylor, & Pocock, 2004; Polazzi, Gianni, & Contestabile, 2001) to increase neuronal survival. These findings strengthen the hypothesis that microglia have both neuroprotective and neurotoxic properties, with their phenotype being strongly linked to insult type, disease type and disease progression. Microglia present two major activation profiles: M1 (classical activation) and M2 (alternative activation) (Boche, Perry, & Nicoll, 2013). M1 microglia are associated with tissue damage resulting from activation in response to injury or insult and are pro-inflammatory, whilst M2 microglia are anti-inflammatory and play a major role in tissue repair. Research on chronic neurodegeneration in animal models have reported an M2 profile lacking release of pro-inflammatory factors and expressing transforming

growth factor (TGF)-β1. Cases of inflammation in AD brains have instead reported M1 activation in proximity of Aβ plaques (Griffin, Sheng, Roberts, & Mrak, 1995). These M1 and M2 phenotypes represent extremes of microglial activation and it is highly likely that a full spectrum of intermediate profiles exists within the CNS. Notwithstanding this, unregulated microglial response or over-activation of microglia is known to cause severe neurotoxicity (Block & Hong, 2005).

5.2.2 Astrocytes

Astrocytes play a major role in maintaining homeostasis within the CNS and are also key players in the neuroinflammatory response. Similar to microglia, astrocytes display either a beneficial or detrimental role depending on the activated molecular signalling pathways (Sofroniew, 2009). Astrocytes have been shown to exist in two distinct reactive states, A1 (pro-inflammatory) and A2 (anti-inflammatory) but it is not yet clear if these phenotypes exist as a continuum, with a heterogeneous mixed population of both phenotypes or in multiple distinct activation states (Liddelow & Barres, 2017). During injury astrocytes undergo astrogliosis (a graded continuum of cellular and gene expression changes that increase with insult severity) and secrete pro-inflammatory chemokines and cytokines. However, in contrast to this neurotoxic role, activated astrocytes have also been shown to play a beneficial role, including the up-take of excitotoxic glutamate (Bush et al., 1999; Rothstein et al., 1996), offering protection from oxidative stress (Chen et al., 2001b), releasing adenosine for neuronal protection (Lin et al., 2008), facilitating BBB repair (Bush et al., 1999), and limiting the spread of inflammation to other healthy parts of the CNS (Faulkner et al., 2004; Voskuhl et al., 2009). It has been proposed that reactive astrocytes release pro-inflammatory products at early stages of disease but then switch to a more anti-inflammatory phenotype at later stages of insult and between borders of injury and healthy tissue (Sofroniew & Vinters, 2010).

5.2.3 Pericytes

The position of pericytes, surrounding ECs, and their interactions with astrocytes and microglia enable these cells to respond to signals from the periphery, promoting proinflammatory cytokines production (Fabry et al., 1993). Pericytes actively recruit peripheral immune cells to the brain (Stark et al., 2013; Wang et al., 2012) thus mediating interactions between systemic and brain inflammation (Winkler, Bell & Zlokovic, 2011). Cultured pericytes have been reported to be immunoreactive, secreting cytokines (including TNFα and interleukins (IL) such as LI-1α, IL-3, IL-9, IL-12 and IL-13), NO and chemokines following an immune system challenge (Kovac, Erickson, & Banks, 2011).

Expression of IL-12 suggests an early stage pericyte role in the inflammatory response caused by infection and early pericyte involvement in the inflammatory cascade (Kovac et al., 2011). Interestingly, pericytes express IL-13, an anti-inflammatory cytokine usually produced by microglia alone, following LPS injection in the cortex. *In vivo,* IL-13 expression has been shown to enhance neuronal survival and lead to activated microglia death (Shin et al., 2004). Expression of both pro and anti-inflammatory cytokines may suggest neuroprotective and neurotoxic roles of pericytes as found in other NVU members (microglia and astrocytes).

5.2.4 Intracellular adhesion molecule 1 (ICAM-1)

ICAM-1 plays an important role in immune-mediated cell to cell interactions and intracellular signal transduction (Huber, Campos, Mark, & Davis, 2006). During a normal state of functioning expression of ICAM-1 is low and restricted to cerebral microvessels (Burke-Gaffney & Hellewell, 1996). Although, it can be markedly upregulated on the luminal surface of ECs in the presence of pro-inflammatory mediators such as interferon gamma (IFNγ), TNFα, interleukin 1 beta (IL-1β), and LPS (Huber et al., 2006). Once ECs are activated morphological changes including increased surface expression of adhesion molecules and activation of signalling pathways takes place. Furthermore, upregulation of ICAM-1 has implications for BBB function permeability and structure and is associated with loss of TJs proteins (Huber et al., 2006). ICAM-1 expression and its role in BBB breakdown appears to change as a function of inflammation stage possibly due to the different pathophysiological process that occur in early and prolonged inflammatory states.

Microglia also respond to ICAM-1 upregulation, specifically through central-mediated cerebral inflammation such as ischemia and stroke (Danton & Dietrich, 2003). Microglia are widely distributed across the brain and their ramified processes, many in the proximity of blood vessels and thus in contact with the basal lamina have shown a robust activation response to ICAM-1 (Huber et al., 2006; Lassmann, Zimprich, Vass, & Hickey, 1991).

5.2.5 Aquaporin 4 (AQP4)

AQP4 is the predominant water channel in the CNS which is primarily expressed in astrocytes and found in higher concentrations on astrocyte endfeet contacting capillaries, neuronal synapses and the subarachnoid space (Badaut, Fukuda, Jullienne, & Petry, 2014; Badaut et al., 2000; Jukkola & Gu, 2015). Astrocytes mediate a redistribution of water molecules through neocortical layers (Holthoff & Witte, 1996; Holthoff & Witte, 2000) thus

directly impacting upon neuronal activity. Neuronal activity is associated with a shrinkage of the extracellular space around the active synapses resulting in cellular uptake of water (Agre et al., 2002).

AQP4 has also been implicated in the clearance of harmful substances from the CNS (Badaut et al., 2014; Iliff et al., 2012) whereby AQP4 dysfunction would lead to impaired water and solute handling thus contributing to a build-up of water (oedema) and proteins (including Aβ) (Iliff et al., 2012). Increased expression of AQP4 has been implicated in a number of pathological conditions, including epilepsy and immunodeficiency virus dementia (HIVD) and often presents with astrocyte activation and BBB disruption (Das et al., 2012; St Hillaire et al., 2005). The presence of AQP4 has also been reported in reactive microglia following an intracranial LPS injection in rats (Fukuda & Badaut, 2012; Tomás-Camardiel et al., 2004) but the significance of this AQP4-microglial expression is still not known. TBI studies comparing WT with AQP4 $^{-/-}$ mice report a beneficial role of AQP4 at a later stage of injury by inhibiting microglial activation and promoting oedema resolution, suggesting that AQP4 may play a detrimental role acutely to later switch to a beneficial one (Fukuda & Badaut, 2012). In inflammation the AQP4 protein has been shown to extend its localisation from the cellular endfeet (present in a normal state of function) to all cellular processes (Fukuda & Badaut, 2012). Furthermore a trend in displacement of AQP4 from blood vessels to the parenchyma has been observed following astrogliosis in a model of hypoperfusion (Holland et al., 2015). The impact of this AQP4 extension is not clear but could potentially alter [Ca^{2+}] signalling in astrocytes (Thrane et al., 2011) and thus directly impact upon neurovascular coupling.

5.3 Study overview and hypothesis

Systemic inflammation evokes changes in numerous cell types within the NVU impacting upon its function. It is therefore imperative to characterise the detailed pathology of the NVU in response to acute systemic inflammation and to relate these cellular changes to alterations in neurovascular function.

The main **hypotheses** for this chapter are:

As ECs are in intimate contact with blood vessels ICAM-1 will be significantly upregulated in LPS treated animals, and this will be accompanied by glial activation (upregulation of IBA-1 and GFAP) as the inflammatory response propagates across NVU cells.

As only models of sepsis have shown pericytes detachment from the basal lamina, pericyte detachment will not be a feature of the response to an acute systemic challenge thereby not impact upon BBB integrity.

Lastly, as upregulation of AQP4 is associated with astrocyte activation an increased expression of AQP4 and a redistribution of AQP4 from cellular endfeet to all cellular processes will occur in LPS treated animals.

5.4 Chapter aims

This study aimed to investigate the impact of acute systemic inflammation on the cellular pathology of the NVU by utilising tissue from *in vivo* LPS challenged animals to:

(1) Provide a detailed descriptive characterisation of the immunoreactive profile of astrocytes (GFAP), microglia (IBA-1), ECs (ICAM-1), astrocyte endfeet (AQP4) and pericytes (PDGFRβ) in control compared to LPS cases.

(2) Quantitatively assess the immunoreactive profile of each marker and determine LPS-induced changes in their expression.

Furthermore, there are currently no studies that seek to determine the cellular drivers of *in vivo* neurovascular changes using tissue from the same animals. As such this Chapter also aims to:

(1) Relate cellular changes to the NVU to the measured *in vivo* neurovascular changes observed in Chapter IV.

5.5 Method

5.5.1 Perfusion

Following *in vivo* data acquisition animals were transcardially perfused with saline as detailed in Section 2.4. Following saline perfusion *n*=11 brains were transcardially fixed with 4% PFA in 0.1 PBS (as described in Section 2.4.1). *N*=5 brains were sectioned in half, with the left hemisphere further subdissected in four parts and snapped frozen in liquid nitrogen and the right hemisphere fixed in 10% neutral buffered formalin (as described in Section 2.4.2). Fixed brains and right hemispheres were later subdissected in four regions (as for snapped frozen brains) and embedded in paraffin wax as described in Chapter II. Frozen hemispheres were stored at -80 C° for future gene expression analyses. For IHC protocols only PFA fixed brains were used.

5.5.2 Immunohistochemistry (IHC)

Antibodies allow for detection and visualisation of proteins, present in the tissue of interest. Proteins have antigens (expressers used for identification) and IHC allows for the detection of these antigens by utilising antigen-specific antibodies to characterise and label antigens of interest on the selected protein. The single labelling IHC protocol outlined here (Figure 5.1) utilises the well characterised horseradish peroxidase-conjugated avidin-biotin complex (ABC-HRP [Vector Laboratories, UK]) method with 3,3'-diaminobenzidine (DAB [Vector Laboratories, UK]) as chromogenic substrate. Prior to antibody application tissue was fixed, permeabilised and blocked as described below.

5.5.2.1 Tissue preparation

The fixation process allows the tissue to retain its cellular structures and preserves antigens however the process creates cross links which result from the fixation process and may mask the specific antigen of interest. Thus, antigen retrieval prior to IHC is required to unmask these epitopes.

Tissue preparation for FFPE prior to IHC involved dewaxing sections twice in xylene (5 minutes [Fisher Scientific, UK]), rehydrating to water through a graded series of ethanol for 5 minutes in each concentration (absolute, 95%, 70% [Fisher Scientific, UK]), blocking endogenous peroxidase activity in 3% hydrogen peroxide (H_2O_2) in methanol, (20 minutes [Fisher Scientific, UK]). Sections were then rinsed under running tap water for 5 minutes. Blocking endogenous peroxidase is an essential step to avoid non-specific staining due to the presence of endogenous peroxidase in the tissue which would react during the application of DAB substrate producing non-specific staining.

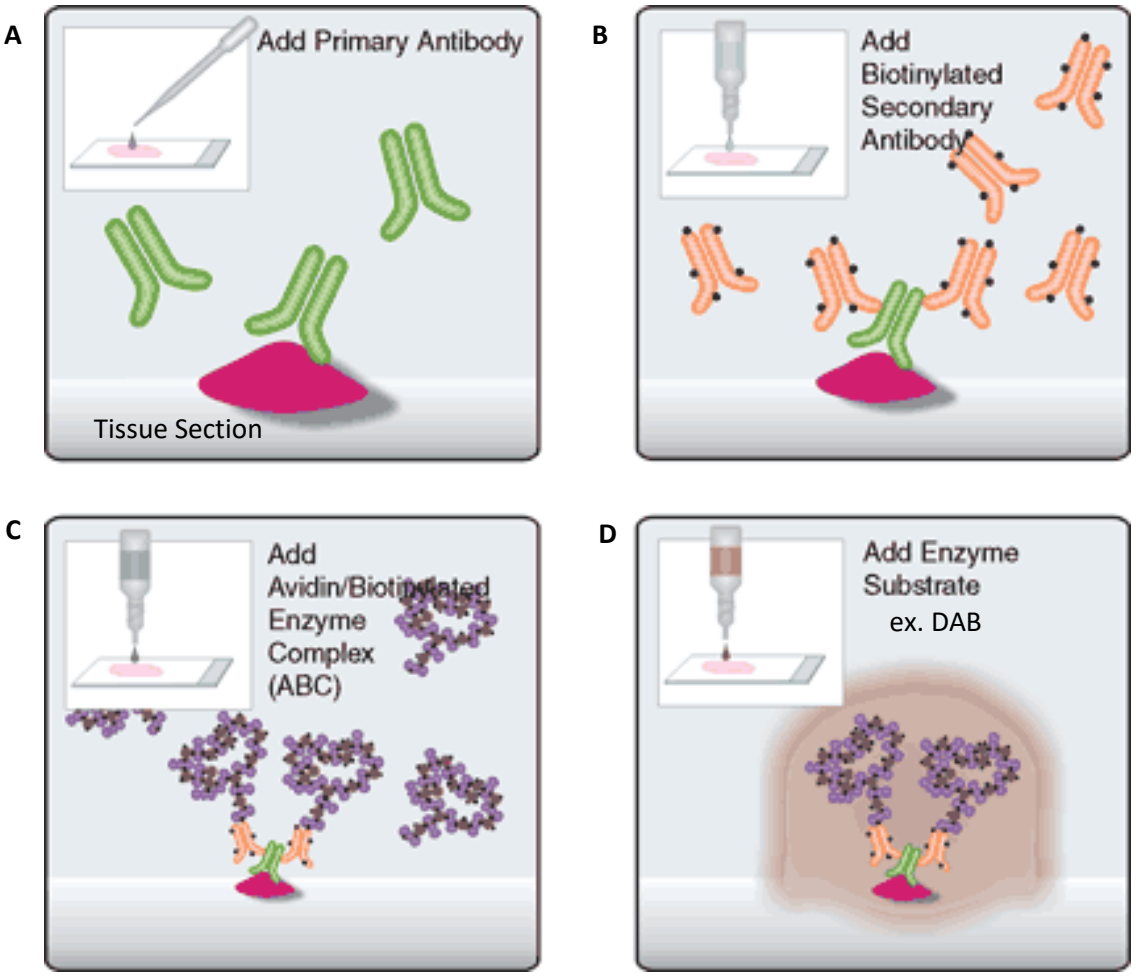

Figure 5.1. Diagram overview of an avidin-biotin complex (ABC) IHC method. After tissue preparation an unlabelled, antigen-specific primary antibody is added and incubated on the tissue section to detect the antigen of interest **(A)**. The primary antibody binds with high affinity to the antigen of interest. **(B)** Then a species-specific biotinylated secondary antibody (specificity against the primary antibody) is added and binds with the primary antibody to amplify the signal. **(C)** An avidin-biotin enzyme complex (ABC) is then added which binds irreversibly to the biotinylated secondary antibody. **(D)** This reaction is then visualised with the use of an enzyme substrate (most commonly DAB) which produces an insoluble precipitate to visualise the antigen of interest. Diagram adapted from Vector Laboratories©.

5.5.2.2 Heat mediated antigen retrieval

To expose the antigen of interest, both high temperature (microwave) and high temperature/high pressure (pressure cooker) antigen retrieval steps were performed at two different pHs (pH 6.5 and pH 9) for all antibodies during the initial antibody optimisation experiments.

For a microwave based antigen retrieval, slides were placed in a slide rack and into a microwavable container filled with tri-sodium citrate (TSC) or Access Super Solution (Menarini Diagnostics, UK) depending on pH (TSC- pH 6.5, Access Super - pH 9). The container was microwaved on full power (800W) for ten minutes. Slides were subsequently washed in running tap water until cool.

For a pressure cooker based antigen retrieval, slides were placed in separate plastic racks and depending on pH condition filled with either Access Super Solution (pH 9, Menarini Diagnostics, UK) or Access Revelation Solution (pH 6, Menarini Diagnostics, UK) solution. Additional containers were filled with tap water to maintain identical conditions across runs (a total of 4 containers used in each pressure cooker run). 500mL of dH_2O was added to the pressure cooker before being sealed. The conditions for the run were as follows: 30s at 125 ºC and 23 PSI. Once the cycle finished the slides were removed from the pressure cooker and rinsed in running tap water until cool.

5.5.3 Controls

All immunohistochemistry protocols included a series of control measures to validate the specificity of the pattern of staining obtained. These included:

- *A negative control* – primary antibody was omitted to ensure absence of non-specific binding of the relevant secondary antibody.
- *An IgG isotype control* – primary antibody was replaced with an IgG isotype control from the same species as the primary antibody. IgG isotype controls were included in all optimisation experiments at identical concentrations as the primary antibody. Specifically, rabbit IgG (Vector Laboratories, UK), goat IgG (Vector Laboratories, UK) and mouse IgG (Vector Laboratories, UK).
- *A positive (internal) control* – tissue sections that previously showed specific staining were included in each run to act as both an internal and an inter-run control.

In the dual labelling protocol each run had a further control for both primary antibodies where one of the two utilised primary antibodies was omitted to confirm genuine staining.

5.5.4 Selected brain regions for IHC analysis

Selected brain regions for IHC analysis were the somatosensory cortex (SS) to include the barrel field and the hippocampus, specifically the dentate gyrus, CA1 and CA3 subfields. The SS is a predominant region encompassing the first layer of cortex extending to the corpus callosum caudally. Moving anteriorly to posteriorly in the brain the SS can be found posteriorly to the lateral ventricle to then extend rostrally directly above the lateral ventricle as the hippocampal CA3 area starts to appear. The SS can be seen starting approximately at +0.10 mm from bregma until approximately -4.20. Dentate gyrus, CA1 and CA3 subfields of the hippocampus appear from -2.10 mm from bregma extending until -6.04 mm (Paxinos & Watson, 1998). Location of the SS and specified hippocampal regions can be seen in Figure 5.2.

5.5.5 Haematoxylin and Eosin (H&E) stain

Selected brain regions were confirmed by haematoxylin and eosin staining prior to IHC protocols and are indicated in Figure 5.3. H&E is a well-established technique to assess architecture of tissue histologically (Bancroft & Gamble, 2008). Haematoxylin, a basic and positively charged dye, stains basophilic structures such as RNA and DNA by reacting with the acidic negatively charged components present in cell nuclei and ribosomes. The dye can then be turned to a purple/blue colour by immersion in Scott's tap water.

In contrast, eosin (acidic negatively charged) reacts with acidophilic (positively charged) cytoplasmic components of cells such as collagen, connective tissue and cytoplasm, staining them pink/red (Bancroft & Gamble, 2008). FFPE sections (5µm) were dewaxed twice in xylene (5 minutes each [Fisher Scientific, UK]), rehydrated to water in a graded series of ethanol for 5 minutes in each concentration (absolute, 95%, 70% [Fisher Scientific, UK]). All sections were rinsed in tap water and placed in Harris's haematoxylin (Cell Path, UK) for 2 minutes at RT. Sections were then rinsed in tap water and differentiated in acid/alcohol for 20-30 seconds and immersed in Scott's tap water for a further 20 seconds before being rinsed in tap water and immersed in eosin for 5 minutes (Leica, UK) at RT. Slides were then quickly washed in tap water and dehydrated through a graded series of alcohols (70%, 95%, absolute) for 20 seconds each before being cleared in xylene prior to mounting. Sections were mounted with Distyrene Plasticizer Xylene mounting media (DPX [Leica, UK]) and glass cover slips (Fisher Scientific, UK). As eosin is water soluble it was important to quickly dehydrate the sections before mounting but at the same time adequate dehydration had to be achieved for appropriate mounting.

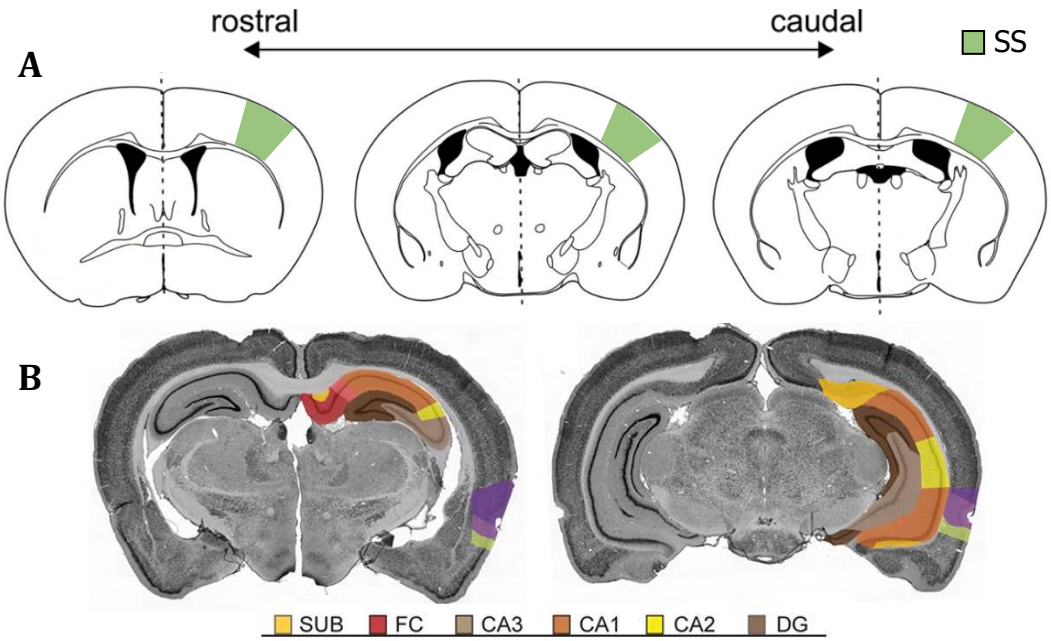

Figure 5.2. Location of somatosensory cortex (A) and hippocampus (B) in the rat brain. The hippocampus is further demarcated in specific subfields and represented at different cortical depths moving caudally due to its changing morphology and prominence of subfields. Legend: **(A)** SS: Somatosensory cortex **(B)** SUB: subiculum FC: fasciola cinereum, DG: Dentate gyrus. Figures adapted from Sakurai, 2013 and Kjonigsen et al., 2011.

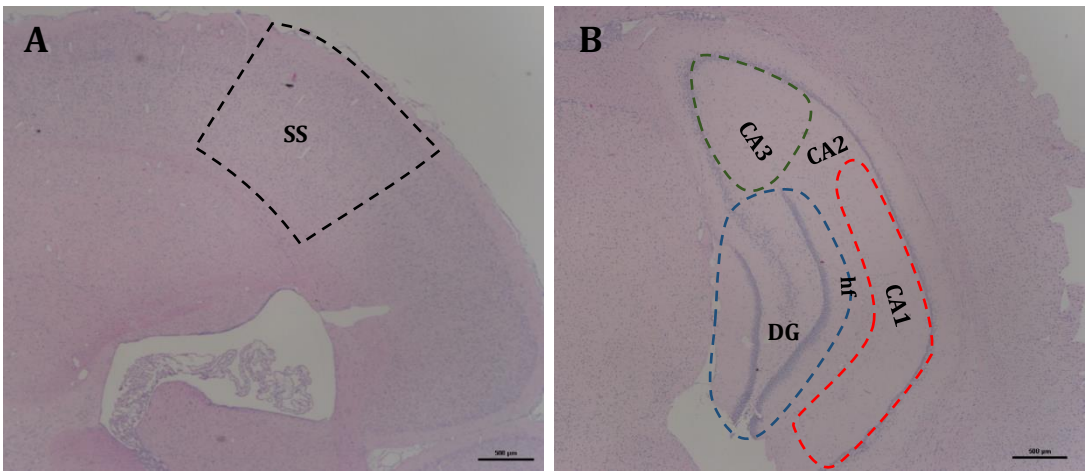

Figure 5.3. Localisation of selected brain regions in FFPE tissue with H&E
Sections stained with H&E as an example of identification of the two selected brain regions: somatosensory cortex (SS) inclusive of barrel field (A) and hippocampus (B) with denoted subfields (Dentate Gyrus- DG, CA1, CA2, CA3) in black, green, blue and red segmented lines. Images for analysis were taken following the above demarcations, excluding the hippocampal fissure (hf) due to high immunoreactivity present in this region. Scale bar represents 500µm.

5.5.6 Antibody selection

A number of antibodies were employed to characterise cellular changes in the NVU, including cell phenotype antibodies to detect microglia (Anti-IBA-1 Polyclonal, Abcam – ab108539), astrocytes (Anti-Glial Fibrillary Acidic Protein – GFAP, Dako – Z0334) and pericytes (biotinylated mouse-PDGFRβ, R&D – BAF1042). Additional staining of inflammation driven changes was investigated with ICAM-1/CD54 (R&D – AF583). Lastly, collagen (Anti-COLL IV, Polyclonal, Abcam – ab6586) was used as a vessel marker for dual labelling. Initial studies were performed to optimise all antibodies at varying concentrations (3 concentrations in total were tested for each antibody) as antibodies against IBA-1, GFAP, AQP4 and PDGFRβ were not previously optimised in rat tissue. For an example of this antibody optimisation experiment please refer to Appendix B. The range of dilutions was based on manufacturer's recommendations. The optimal antibody dilutions, and the accompanying antigen retrieval method are indicated in Table 5.1.

5.5.7 Immunohistochemistry protocol for all single label antibodies

FFPE sections (5μm) were dewaxed, rehydrated to water, blocked for endogenous peroxidase activity as described (Section 5.4.2.1) and underwent antigen retrieval (Table 5.1). Slides were then cooled in running tap water ready for ABC-HRP IHC protocol.

All incubations were carried out at RT unless otherwise stated. ABC-HRP Vectastain Elite Kits (Vector Laboratories, UK) specific to each antibody host species were used. Sections were incubated in 1.5% blocking solution for 30 minutes to prevent non-specific binding of the secondary antibody, as shown in Table 5.1, except the PDGFRβ staining protocol which employed a double strength 3% blocking solution to reduce the high background staining observed with the standard protocol. Subsequently sections were drained to remove excess solution. The slides were then incubated with primary antibody (~200 μL per slide) made up in blocking solution for 60 minutes. Sections were washed in TBS for 5 minutes and then incubated in 0.5% species specific biotinylated secondary antibody for 30 minutes (~200 μL per slide). As the PDGFRβ antibody was directly biotinylated this step was omitted. Sections were again washed with TBS for a further 5 minutes and incubated in 3% ABC-HRP reagent for 30 minutes (ABC reagent was always made up at least 30 minutes prior to use, ~200 μL per slide). Sections were washed in TBS for a further 5 minutes.

Direct visualisation of antibody binding was obtained using the peroxidase substrate DAB (Vector Laboratories, UK [2% buffer, 2% hydrogen peroxide and 4% of DAB in dH_2O). This substrate oxidizes in the presence of peroxidase (introduced to the section in the previous

Table 5.1. Source of antibodies, conditions of use and target antigen for IHC protocols.

Antibody & Supplier	Species & Isotype	Clonality	Dilution	Antigen Retrieval Method	Target Antigen
anti-IBA1 **(Abcam, ab108539)**	Rabbit IgG	Polyclonal	**1:400**	pH9 microwave	*Microglia* (increased expression in reactive microglia)
anti-GFAP **(Dako, Z0334)**	Rabbit IgG	Polyclonal	**1:1000**	pH9 microwave	*Astrocytes* (intermediate filament in reactive astrocytes)
b-PDGFRβ **(R&D, BAF1042)**	Goat IgG	Biotinylated Polyclonal	**1:50**	pH9 pressure cooker	*Pericytes*
ICAM-1/CD54 **(R&D, AF583)**	Goat IgG	Polyclonal	**1:400**	TSC pH6.5 microwave	*ICAM-1 expression* (upregulated in activated ECs)
anti-AQP4 **(Abcam, ab9512)**	Mouse IgG3	Monoclonal	**1:800**	pH9 microwave	*AQP4 expression* (astrocytes endfeet)
anti-COLL IV **(Abcam ab6586)**	Rabbit IgG	Polyclonal	**1:500**	pH6 pressure cooker	*Blood vessels* (Basement membrane)
Rabbit IgG (Vector, UK)	Rabbit IgG	-	GFAP: **1:1000** IBA-1**: 1:400**	pH9 microwave	Isotype Control
Goat IgG (Vector, UK)	Goat IgG	-	PDGFRβ: **1:50** ICAM-1: **1:400**	pH9 microwave	Isotype Control
Mouse IgG (Vector, UK)	Mouse IgG	-	AQP4 **1:800**	pH9 microwave	Isotype Control

Key: TSC – try-sodium citrate.

ABC-HRP step) and hydrogen peroxide (present in the DAB kit) resulting in a deposition of a water-insoluble brown precipitate. Sections were incubated in DAB for 5 minutes then rinsed with dH_2O to quench the enzyme and followed a 5-minute tap wash before counterstaining.

Sections were counterstained with haematoxylin (Cell Path, UK) (30 sec), washed in tap water (1 min), blued in Scott's tap water (30 sec), a blueing reagent to haematoxylin, washed in tap water (1 min), dehydrated through graded series of alcohols for one minute in each concentration (70%, 95%, absolute) and cleared in xylene before being permanently mounted in DPX [Leica, UK] and glass cover slips (Fisher Scientific, UK).

5.5.8 Immunohistochemistry protocol for Periodic Acid Schiff (PAS) staining with PDGFRβ

Periodic Acid Schiff (PAS) is commonly used to localise carbohydrates macromolecules in tissue sections which are most prominent along the basement membrane. Staining results in a magenta/red colour labelling glycogen (glucose) and glycoproteins (sugars).

Following PDGFRB single labelling immunohistochemistry (Section 5.5.7) sections were oxidised with 1% periodic acid solution (5 min), rinsed in tap water, stained with Schiff reagent (VWR Chemicals, ProLabo, Belgium) for 25 minutes and washed in running tap water for 10 minutes. Sections were counterstained with haematoxylin, dehydrated and mounted in DPX as for single labelling protocol.

5.5.9 Immunohistochemistry fluorescent protocol for dual labelling AQP4 and COLL IV

After dewaxing, rehydrating, endogenous peroxidase block and antigen retrieval (microwave pH9) slides were blocked in 1.5% goat serum (Vector Laboratories, UK) in TBS for 60 minutes (~200 µL per slide) at RT. Excess was tapped off and sections were incubated with AQP4 and COLL IV primary antibodies for 1 hour at RT. As antibodies were raised in different species they were incubated simultaneously. Slides were washed thoroughly with TBS (3 washes of 5 minutes each). Sections were then incubated in the dark with species specific conjugated secondary antibodies: donkey anti-mouse Alexa-Fluor 488 (A21202, Life Technologies, Thermo Fisher Scientific, USA) and goat anti-rabbit Alexa-Fluor 568 (A11011, Life Technologies, Thermo Fisher Scientific, USA) at a dilution of 1:500 for 1 hour at RT. Again both secondary antibodies were jointly incubated. Sections were once again washed thoroughly with TBS (3 washes of 5 minutes). Sections were then mounted in mounting medium with DAPI (Vector Laboratories, UK).

A negative control (omission of the primary antibody) was included in every run. A positive control was included for each individual primary antibody to confirm the specificity of each primary antibody.

5.6 Data processing

All slides were imaged, counted and analysed blind in a randomised order. A qualitative description of staining pattern for each antibody was noted in control and LPS treated animals preceding a quantitative analysis.

5.6.1 Image analysis

All images were taken from the hemisphere contralateral to the thinned cranial window (right side), to ensure inflammatory effects were not as a result of the surgery. For the somatosensory cortex (SS), three adjacent belt transects from the outer cortex through to the white matter border were taken for each animal (*n*=11) at x20 magnification (Nikon microscope). Each belt transect contained up to six individual images extending from cortical layer one to layer six (just before the corpus callosum). SS area coordinates for captured imaged were taken between -.40 to -1.80 from Bregma (B) (Paxinos & Watson, 1998). For the hippocampus, random field images were taken per animal (*n*=11) in the subfields of dentate gyrus (DG), CA1 and CA3. Hippocampal area coordinates for captured images were between -3.30 to -5.30 from B (Paxinos & Watson, 1998).

5.6.2 Quantitative analysis

To provide quantitative data obtained from the captured images of both brain regions the analysis software analySIS^{D} was used. Within the analySIS^{D} software custom written macros were developed to determine total immunoreactivity percentage area for GFAP, IBA-1 and ICAM-1/CD54. The average percentage area of immunopositive staining was used for statistical analysis for each of the three makers in both control and LPS cases. To assess AQP4 immunoreactivity a qualitative assessment of staining pattern was used. All slides were analysed blind in a randomised order. An example of an analysed image with developed macro can be found in Appendix C.

5.6.3 Statistical analysis

One control animal exhibited abnormally high immunoreactivity for all cell phenotype markers compared to other control and LPS cases, thus this case was excluded from further analysis due to a suspected infection. The final analysed cohort consisted of *n*=10. Statistical analysis between control and LPS cases was performed on SPSS 23 via

independent sample t-tests to identify a significant difference in immunoreactivity percentage area between groups. A *p* value of less than .05 was deemed significant.

5.7 Results

5.7.1 Immunohistochemistry for optimisation experiments

In total six antibodies were optimised prior to performing IHC in experimental cases as these antibodies had not been previously optimised in rat FFPE tissue. The optimal condition, with high specific antibody signal and minimal background staining, was obtained by testing a range of antibody concentrations and different heat mediated antigen retrieval methods. The optimal condition of use of each antibody is indicated in Table 5.1.

5.7.1.1 Negative and IgG Controls

To determine the specificity of antibody staining and the degree of non-specific staining, negative and IgG controls were included in every IHC run. No specific immunoreactivity was observed in either the omission of primary antibody (negative) controls or IgG controls, as demonstrated in Figure 5.4 and Figure 5.5.

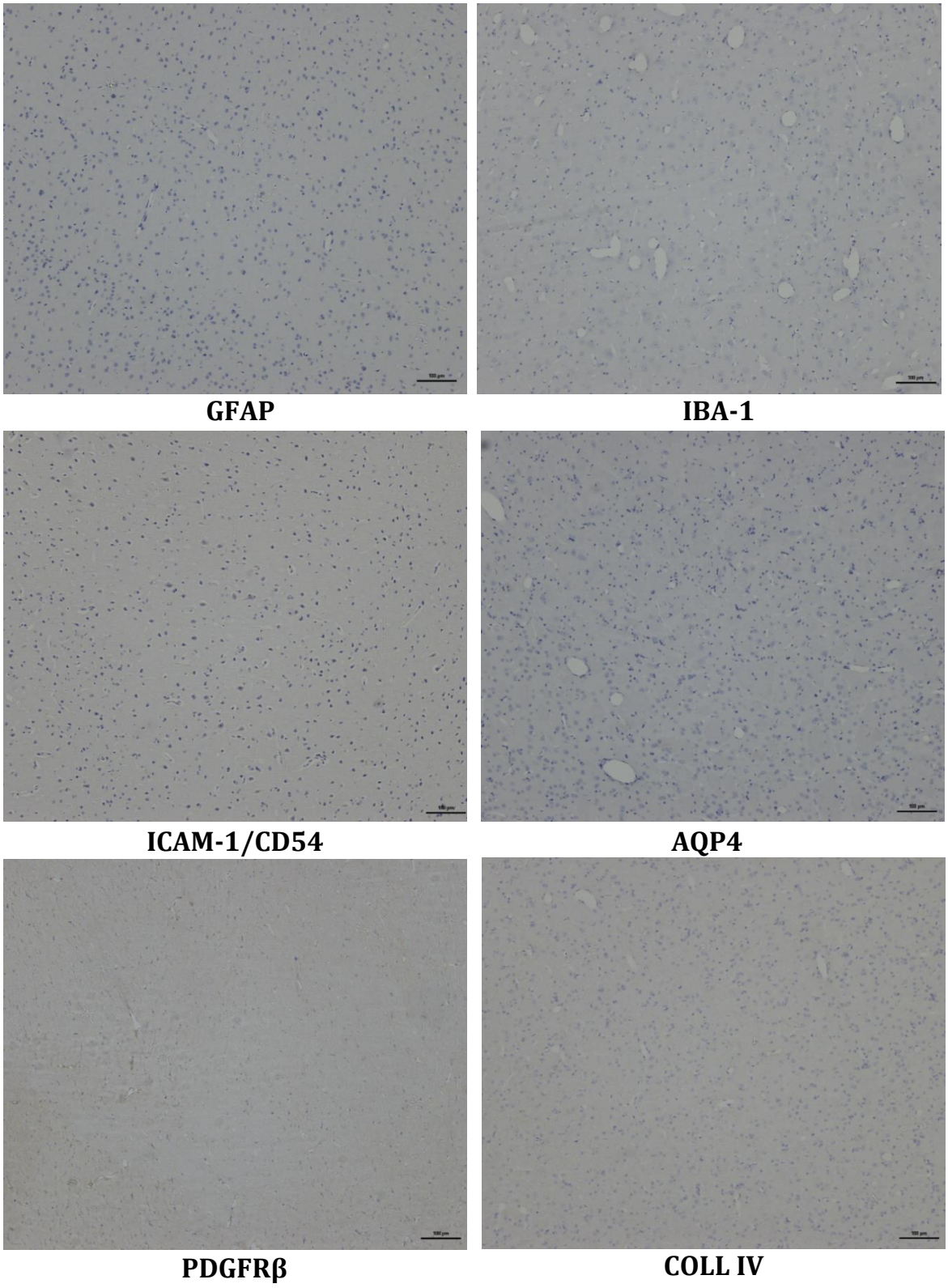

Figure 5.4. Omission of primary antibody (negative) controls. No immunoreactivity was detected following omission of primary antibodies for astrocytes (GFAP), microglia (IBA1), ICAM-1/CD54, AQP4, pericytes (PDGFRβ) and basement membrane (COLL IV). Nuclei counterstained with haematoxylin. Scale bar represents 100μm.

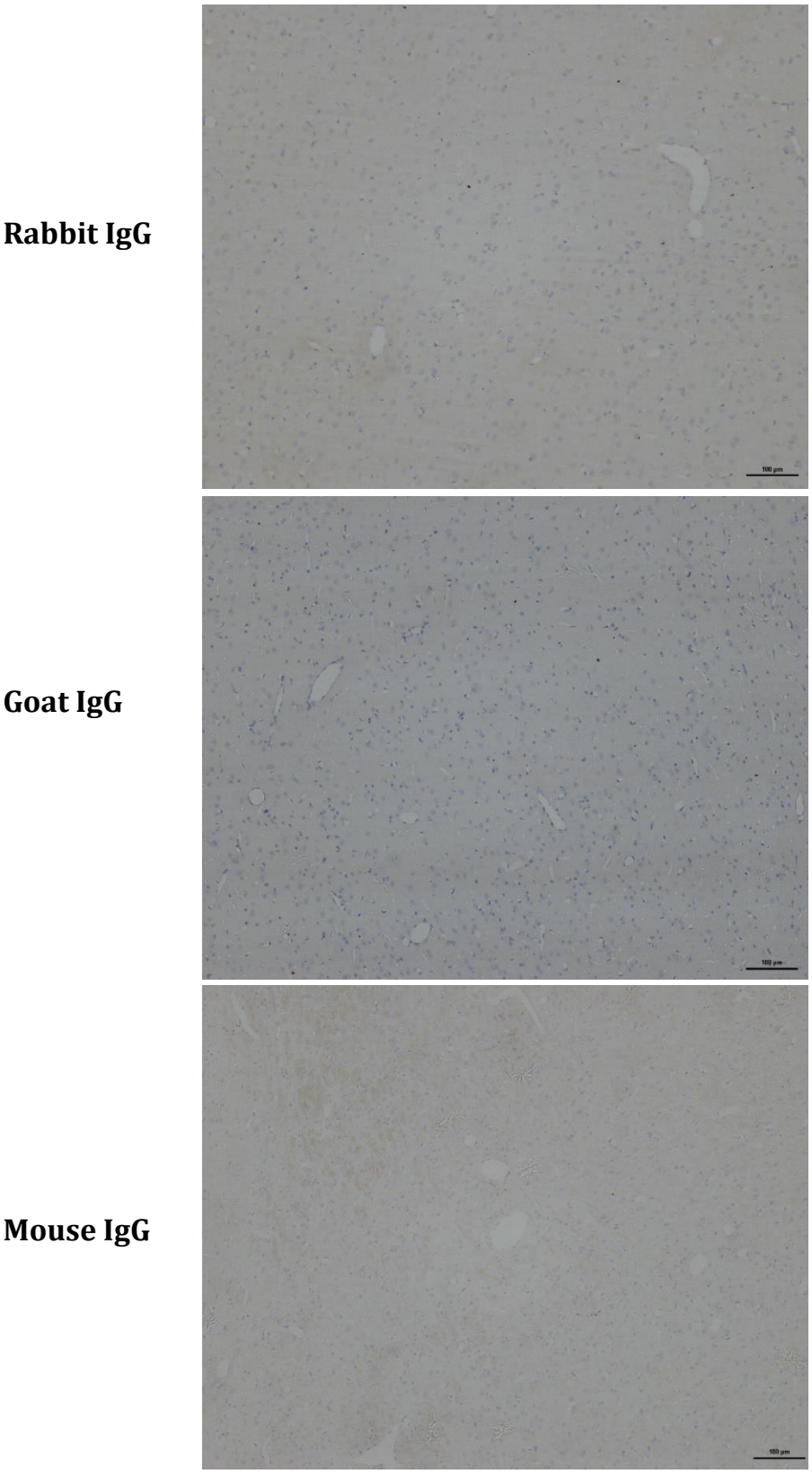

Figure 5.5. IgG isotype controls. No non-specific immunoreactivity was observed in cases incubated with species specific IgG isotype controls. Specifically, rabbit (IBA-1, GFAP, COLL IV), goat (PDGFRβ, ICAM-1/CD54) and mouse (AQP4). Nuclei counterstained with haematoxylin. Scale bar represents 100μm.

5.7.1.2 Qualitative assessment of optimised immunostaining

A representative example of the immunoreactive profile for each optimised antibody is demonstrated in Figure 5.6.

GFAP immunolabelled the cell body and extending ramified processes of astrocytes with a classic stellate morphology (Figure 5.6a red arrow). A regular distribution of $GFAP^+$ cells was observed throughout the tissue. This phenotype is typical of non-reactive astrocytes involved in their role of CNS surveillance and homeostasis.

IBA-1 immunolabelled the cell body and ramified processes of microglia throughout the tissue. $IBA\text{-}1^+$ cells were uniform and bipolar in shape, and were regularly distributed (Figure 4.7b red arrow), indicative of resting microglia, involved in surveying and regulating the CNS.

ICAM-1/CD54 immunoreactivity in optimisation experiments showed labelling of two distinct cell types. From Figure 5.6c ICAM-1 immunoreactivity was moderately associated with the endothelium surrounding the vessel wall (red arrows) and weakly associated with microglial processes (green arrow).

AQP4 immunoreactivity was associated with astrocyte end feet in direct contact with micro vessels (Figure 5.6d blue arrows) as well as deposition around larger vessels (red arrows).

PDGFRβ plays an essential role in blood vessel development by promoting proliferation, migration and recruitment of pericytes and smooth muscle cells to endothelial cells (Nakamura et al., 2016). Although PDGFRβ is also expressed in endothelial cells it is regarded as a viable brain pericyte marker (Arimura et al., 2012; Armulik et al., 2011) and has been previously used to successfully label pericytes (Winkler, Bell, & Zlokovic, 2010). Other pericyte markers like CD13 exist but due to its expression in inflamed endothelium (Armulik et al., 2011) it was regarded as not suitable for this study. In disease states pericytes have been observed to migrate away from vessel walls. In optimisation experiments $PDGFR\beta^+$ pericytes shows a good distribution demarcating vessel walls (Figure 5.6e red arrows) with no detectible migration.

Lastly, **COLL IV**, a component of the basement membrane, immunolabelled capillaries and larger vessels throughout the tissue (Figure 5.6f red arrows).

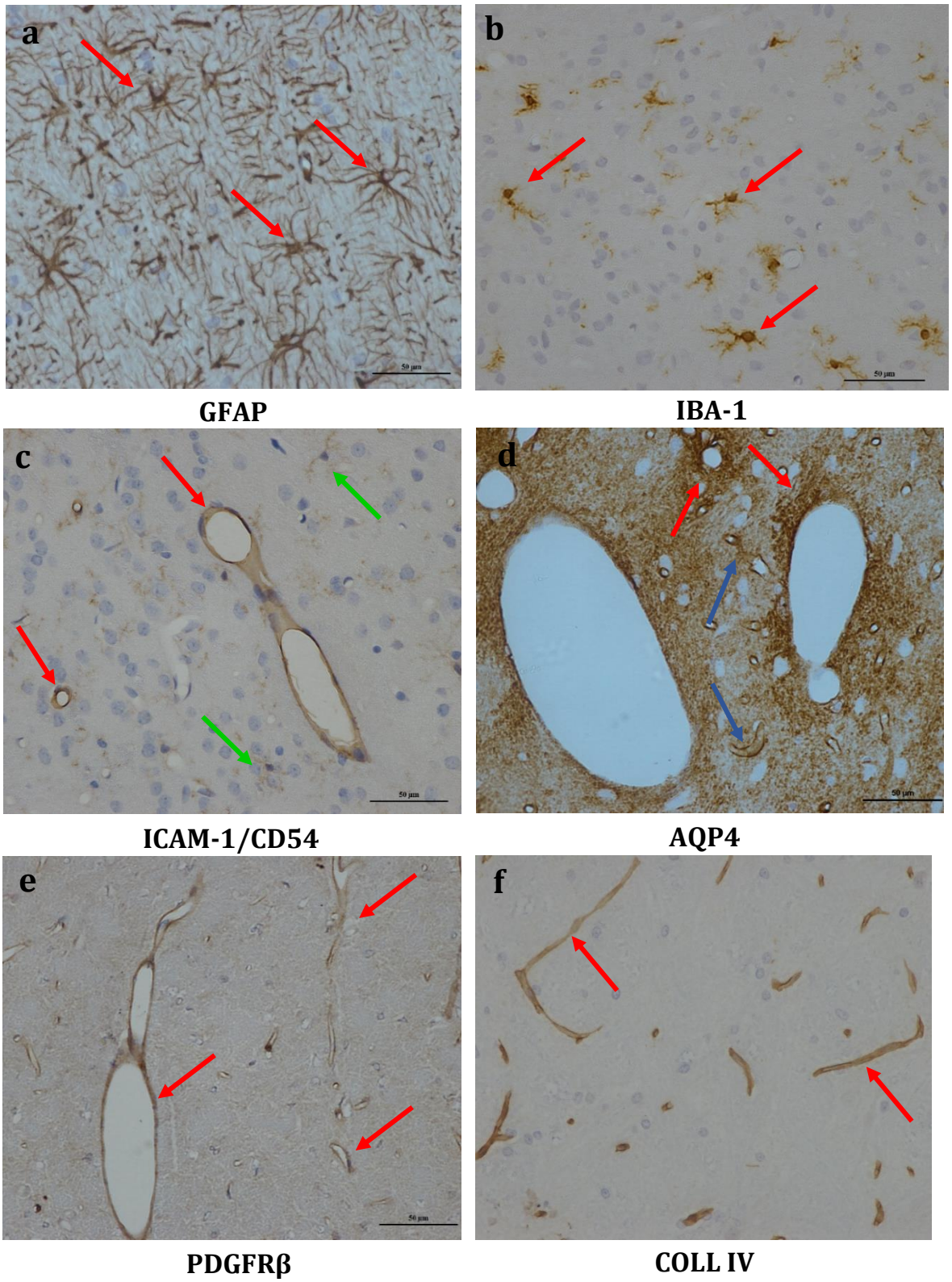

Figure 5.6. Patterns of immunoreactivity of optimised antibodies. IBA-1 immunolabelled microglia with a resting morphology, GFAP immunolabelled astrocyte cell bodies and proximal processes. ICAM-1/CD54 labelled ECs (red arrow) and microglial processes (green arrow). PDGFRβ labelled pericytes and AQP4 labelled perivascular astrocyte processes. All sections were counterstained with haematoxylin. Scale bar represents 50µm.

5.7.2 Immunohistochemistry for control and LPS cohorts

No specific immunoreactivity was observed for either negative or IgG controls, and all inter-run positive controls showed consistent immunoreactivity across all staining runs. A tabulated summary of IHC results (Table 5.2) can be found at the end of this section.

5.7.2.1 SS GFAP immunoreactivity is increased in LPS cases

The control cohort displayed a punctate diffuse pattern of $GFAP^+$ astrocytes throughout the SS cortex (Figure 5.7a). $GFAP^+$ astrocytes appeared to vary in prominence depending on cortical layer depth (more intense immunoreactivity in deeper layers) and location within the SS cortex. GFAP immunolabeled the cell body and proximal processes of astrocytes with a stellate morphology (Figure 5.7b, red arrow). As for the optimisation experiments, each astrocyte non-overlapping surveillance domain could be easily identified around each cell (Figure 5.7b, green arrows). In the hippocampus intense $GFAP^+$ astrocytes were prominent across subfields (Figure 5.7d & Figure 5.8a&b, red arrows). A distinct layer of intense $GFAP^+$ astrocytes was evident at the junction between the DG and CA1 subfields (hippocampal fissure [hf]) (Figure 5.7c). The subfield of CA1 (Figure 5.8a) contained less intensely stained $GFAP^+$ astrocytes, compared to DG and CA3 (Figure 5.7d & Figure 5.8b). The morphology of $GFAP^+$ astrocytes throughout all areas of the control cases is indicative of an inactive astrocyte phenotype.

LPS cases displayed a significant 74 % area increase in GFAP immunoreactivity in SS compared to controls ($t(8)= -4.15$, $p=.003$, Figure 5.8e), with strong labelling of astrocyte cell body and proximal processes (Figure 5.7e). Immunoreactivity was more prominent around vessels suggesting stronger GFAP expression by astrocyte endfeet across the SS cortex (Figure 5.7f, green arrow). $GFAP^+$ astrocytes showed some hypertrophy (Figure 5.7f, red arrow) and individual surveillance domains were less distinguishable; a phenotype indicative of a mild to moderate astrogliosis (Sofroniew & Vinters, 2010) consistent with low level neuroinflammation. Within the DG region of the hippocampus (Figure 5.7h) $GFAP^+$ immunolabelled the astrocyte cell body and proximal extending processes (Figure 5.7h, red arrows). As for control cases, a distinct layer of $GFAP^+$ astrocytes was observed at the hf junction (Figure 5.7g). Distribution of $GFAP^+$ astrocytes was consistent across all hippocampal subfields (Figure 5.8c&d; Figure 5.7h). Intense immunolabelling of astrocyte endfeet along the vessel wall was observed, predominantly in the CA3 subfield (Figure 5.8d, green arrows). GFAP expression in hippocampal subfields for LPS cases was not significantly different from controls (DG: $t(8)= -1.4$, $p=.200$; CA1: $t(8)= -1.94$, $p=.089$; CA3: $t(8)= -.34$, $p=.744$, Figure 5.8e). GFAP expression in LPS treated animals compared to controls showed 12 (DG), 38 (CA1) and 6 (CA3) % area increases.

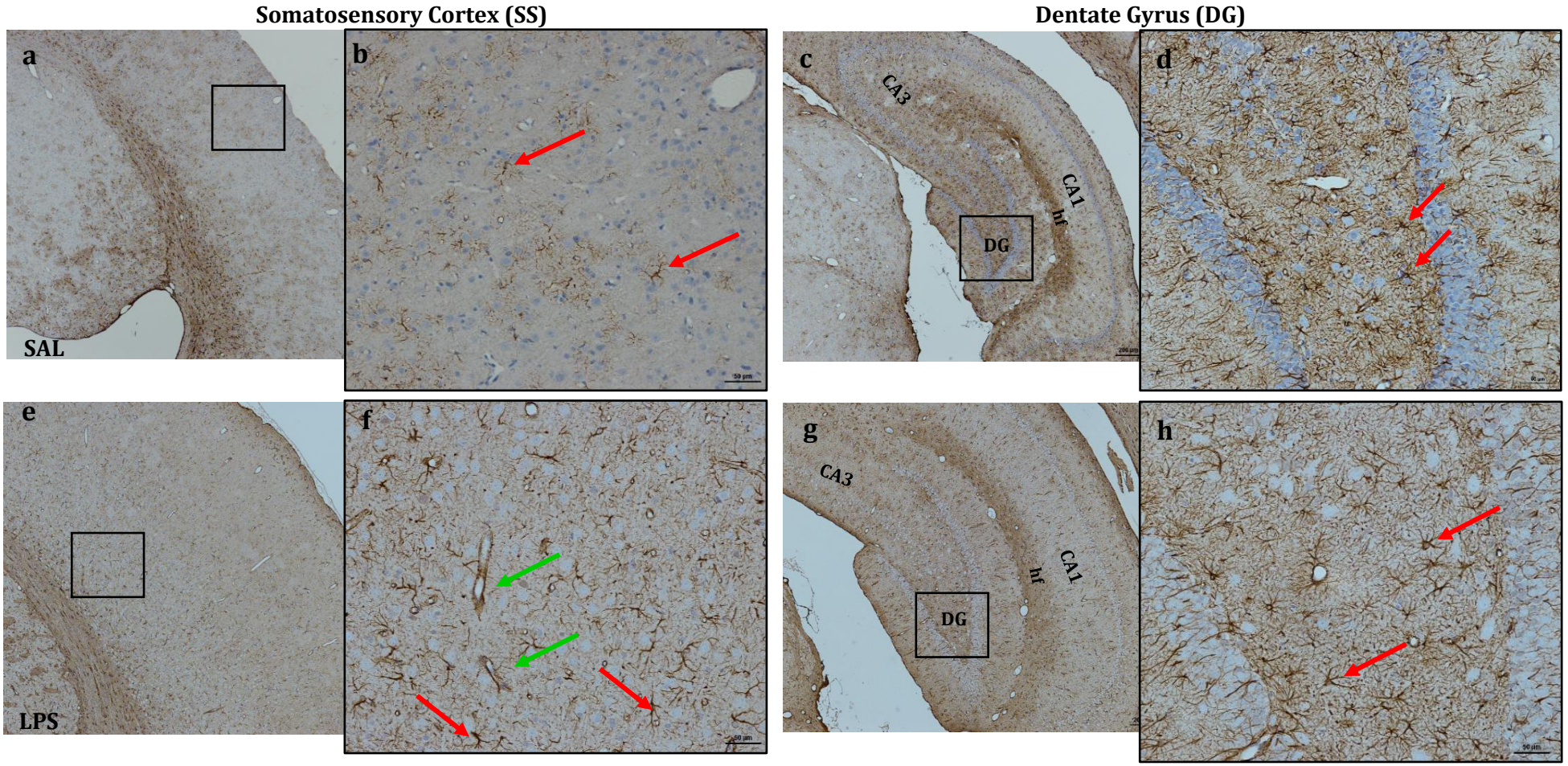

Figure 5.7. GFAP expression in SS and DG. Expression of GFAP by DAB (brown) in SS and DG in saline (SAL)/LPS treated animals. Astrocytes for SAL treated animals were well distinguishable (b&d, red arrows) displaying a stellate non-reactive morphology. In LPS cases, SS astrocytes appeared hypertrophic (f, red arrows) and showed strong immunoreactivity on endfeet in contact with vessels (f, green arrows). Sections were counterstained with haematoxylin. Scale bar represent 200µm and 50µm (insert). Legend: DG = dentate gyrus, hf = hippocampal fissure.

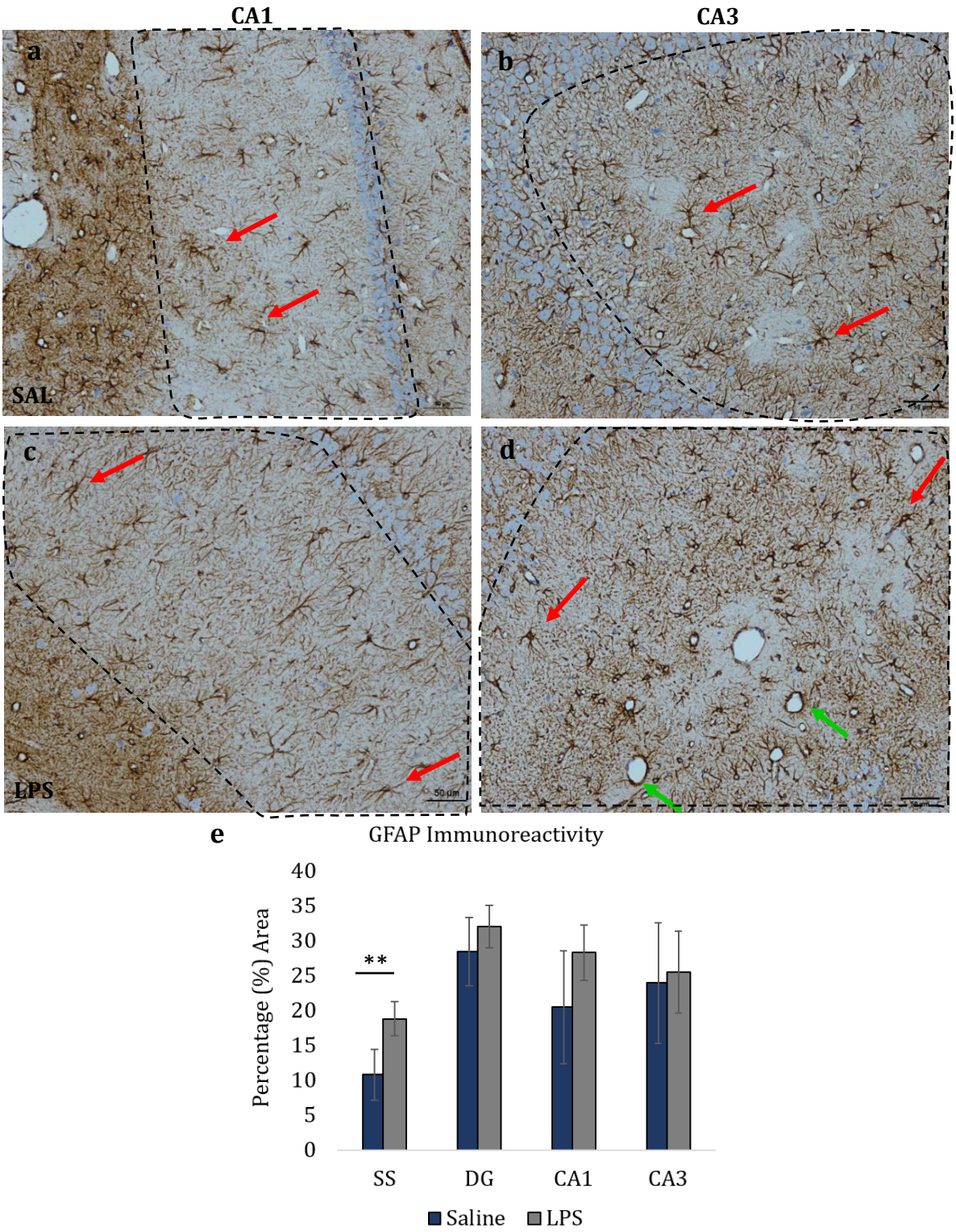

Figure 5.8. GFAP expression in hippocampal subfields CA1 and CA3 and percentage area increases. Expression of GFAP by DAB (brown) in the hippocampal subfields of CA1 and CA3 in SAL/LPS treated animals. Astrocytes for both groups were well distinguishable displaying a stellate morphology (red arrows). In LPS cases CA3 subfield astrocytes showed stronger immunoreactivity on endfeet in contact with vessels (Figure 5.8d, green arrows). Sections were counterstained with haematoxylin. Segmented lines represent area analysed in Analysis[D] corresponding to hippocampal region. Scale bar represent 50µm. Figure 5.8e shows percentage area increases of GFAP immunoreactivity in SS and hippocampal subfields. Significance found only for SS cortex $p<.005$.

5.7.2.2 IBA-1 immunoreactivity increases with LPS treatment

In control cases IBA1 immunolabelled microglia with a punctate diffuse pattern of staining across the SS cortex and cortical layers (Figure 5.9a), consistent with a resting profile: small uniform bipolar body and extending delicate ramified processes (Figure 5.9b, red arrows). In the hippocampal region a similar pattern was observed (Figure 5.9c). IBA1$^+$ microglia were uniform and bipolar in shape with defined processes (Figure 5.9d, red arrows). IBA1$^+$ microglia were prominent in the CA1 subfield and along the junction of the hf (Figure 5.9c). In the DG, IBA1$^+$ microglial cell bodies were less prominent compared to their processes (Figure 5.9d, red arrows). A diffuse spread of IBA1$^+$ microglia was also observed in CA3 (Figure 5.11b, red arrows), again with microglial processes more prominently labelled than cell bodies.

LPS cases displayed a significant 109 % area increase in IBA1 expression compared to controls across SS cortical layers ($t(8)= -3.84$, $p=.005$, Figure 5.11e), with more intense immunolabelling of both microglia cell body and extending processes (Figure 5.9f). IBA1$^+$ microglia displayed a hypertrophic profile, with a larger and rounder cell body and, in some cases, retracted processes (Figure 5.9f, red arrows). Overall more pronounced immunolabelling of microglial processes was observed (Figure 5.9f, green arrows). Microglia appeared hyperramified, with processes more prominently immunolabelled than controls. Microglial hypertrophy and amoeboid appearance are features of reactive microglia activated during inflammation (Boche et al., 2013), suggesting that systemic administration of LPS may be associated with a reactive microglial phenotype. Some microglial clustering was observed along vessels (Figure 5.10a) as well as faint neuronal staining across cortical layers. In the hippocampus IBA1$^+$ microglia immunoreactivity was very prominent (Figure 5.9g) and distribution was consistent across all hippocampal subfields. A concentrated band of IBA1$^+$ microglia was observed at the hf junction. As in the SS cortex, IBA1$^+$ microglia appeared swollen and hypertrophic (Figure 5.9h, red arrows) and displayed retracted and elongated processes (Figure 5.9h red & green arrows). IBA1$^+$ microglial clusters (Figure 5.10b&c) were also a prominent feature of the hippocampal subfields of DG and CA1. As in the SS cortex intense IBA1 immunolabelling of microglia processes was observed in LPS compared to control cases. Weak immunolabelling of pyramidal cells was observed in some LPS cases but was restricted to the DG subfield (Figure 5.9h). IBA1 expression was significantly different between cohort groups in all hippocampal subfields (DG: $t(8)= -2.52$, $p=.036$; CA1: $t(8)= -4.09$, $p=.003$; CA3: $t(8)= -4.3$, $p=.003$, Figure 5.11e). IBA1 expression in LPS treated animals compared to controls showed 72 (DG), 119 (CA1) and 153 (CA3) % area increases.

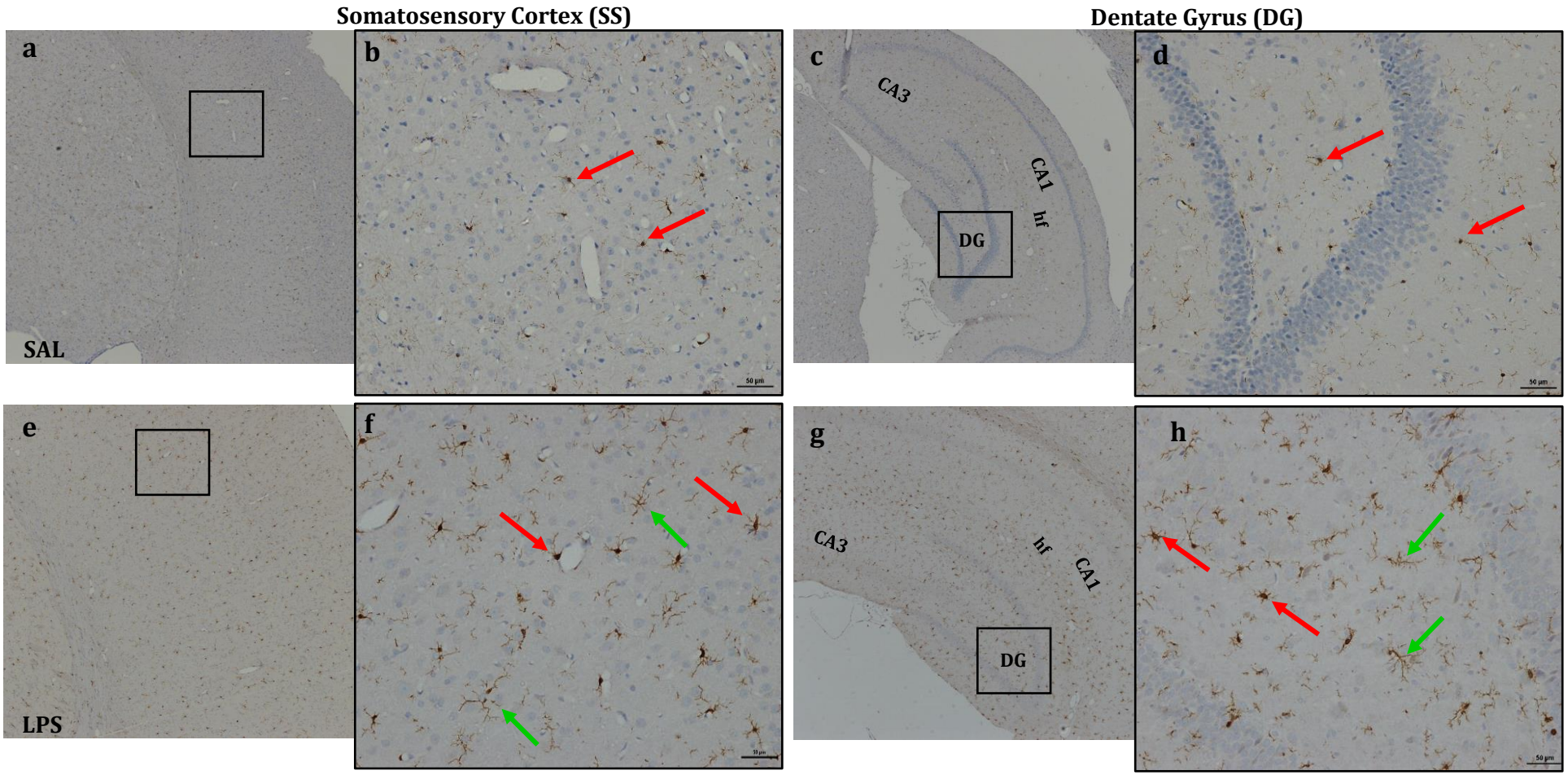

Figure 5.9. IBA-1 expression in SS and DG. Expression of IBA-1 by DAB (brown) in SS and DG in saline (SAL)/LPS treated animals. Microglia for SAL treated animals were well distinguishable (b&d, red arrows) displaying a resting bipolar morphology. In LPS cases IBA-1^{+} microglia appeared swollen and hypertrophic (f&h, red arrows) with a mixture of retracted and extended processes (f&h, green arrows). Sections were counterstained with haematoxylin. Scale bar represent 200µm and 50µm (insert). Legend: DG = dentate gyrus, hf = hippocampal fissure.

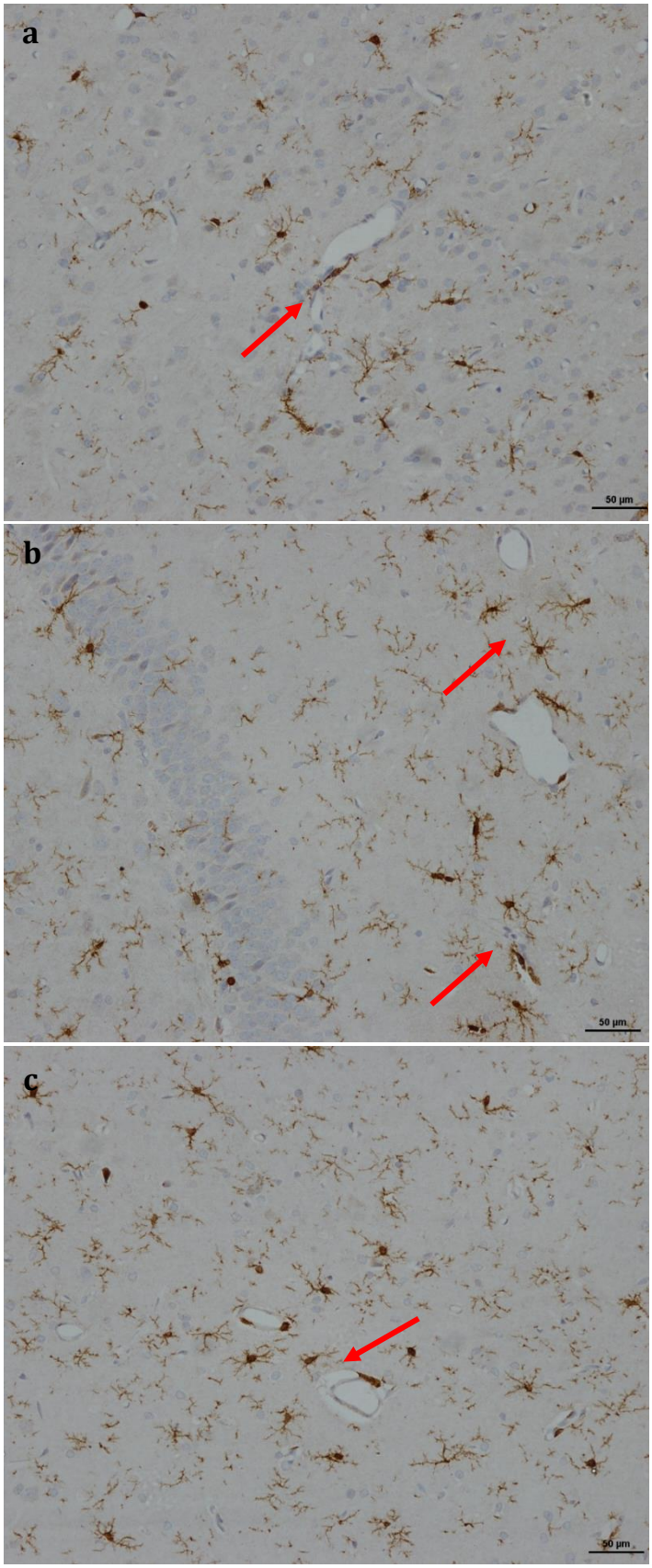

Figure 5.10. IBA-1$^+$ microglial clusters in SS and hippocampus. Clusters of IBA-1$^+$ microglia expressed by DAB (brown) in SS (a) and hippocampal subfields of DG (b) and CA1 (c). Clusters (red arrows) appear to localise around vessels. Sections were counterstained with haematoxylin. Scale bar represents 50µm.

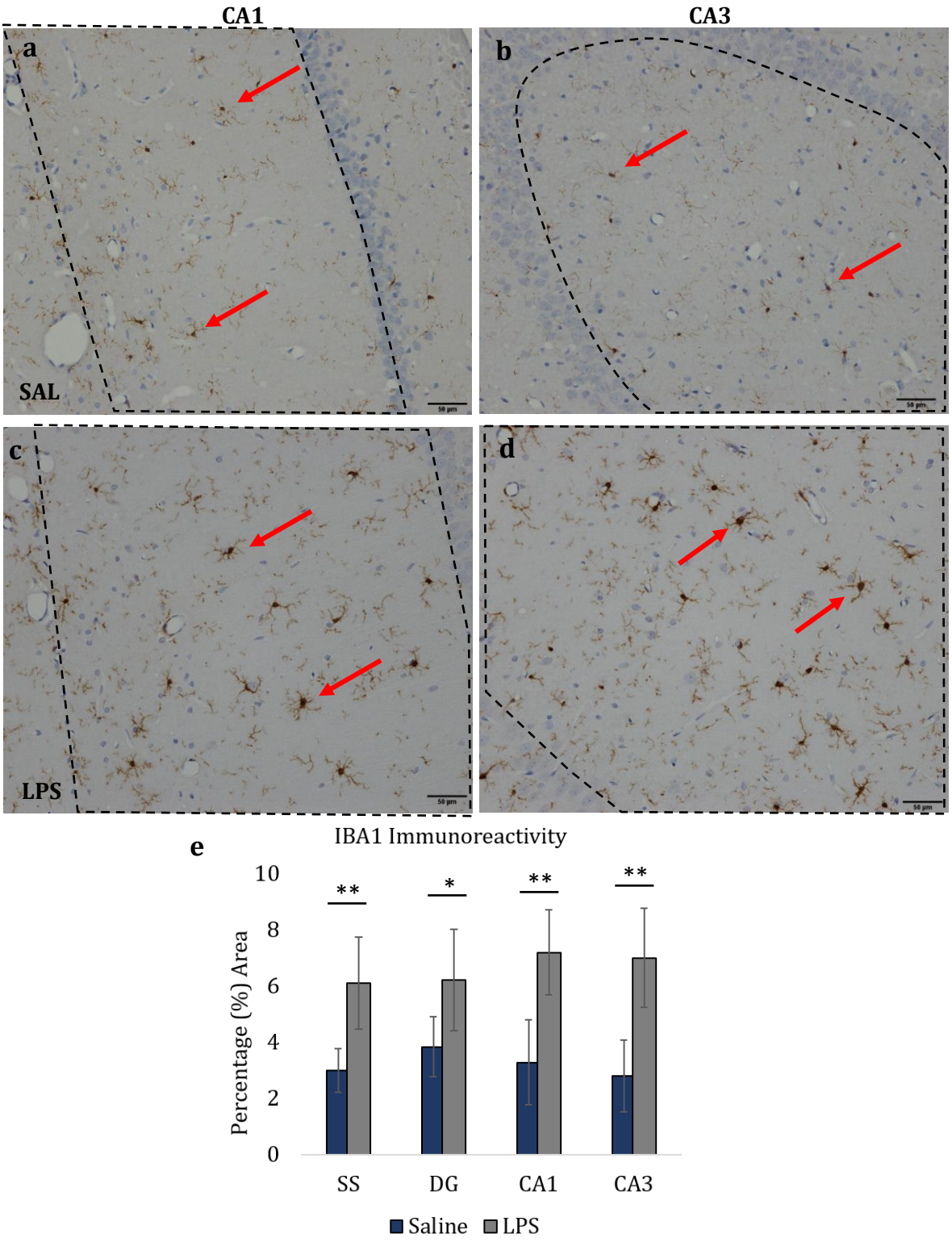

Figure 5.11. IBA-1 expression in hippocampal subfields CA1 and CA3 and percentage area increases. Expression of IBA1 by DAB (brown) in the hippocampal subfields of CA1 and CA3 in SAL/LPS treated animals. Microglia for both groups were well distinguishable with well labelled processes and cell body (red arrows). Across hippocampal subfields microglia morphology and diffusivity was consistent within cases and displayed the same morphology as found in SS and DG. Sections were counterstained with haematoxylin. Segmented lines represent area analysed in Analysis[D] corresponding to hippocampal region. Scale bar represent 50µm. Figure 5.11e shows percentage area increases of IBA-1 immunoreactivity in SS and hippocampal subfields. Significance found for all selected brain regions $^{**}p<.005$ $^{*}p<.05$

5.7.2.3 Increased ICAM-1 immunoreactivity on endothelium and microglial process in LPS treated animals

In control cases ICAM-1$^+$ immunostaining in both SS and hippocampus was very faint, punctate and primarily restricted to vessels (Figure 5.12b&d, red arrows). Very faint immunolabelling of microglial processes was detected in two out of five cases. The vessel staining observed in the hippocampus was primarily restricted to the hf (Figure 5.12c). Isolated ICAM-1$^+$ vessels were observed in the DG subfield (Figure 5.12d, red arrows) as well as CA1 and CA3 (Figure 5.13a&b, red arrows).

In LPS cases intense ICAM-1$^+$ immunostaining was observed in both SS and hippocampus and was significantly different to controls (SS: $t(8)= -6.5$, $p<.001$ DG: $t(8)= -5.47$, $p=.001$, CA1: $t(8)= -4.73$, $p=.001$, CA3: $t(8)= -4.69$, $p=.002$, Figure 5.13e). Percentage area increases for ICAM-1 expression in LPS treated animals compared to controls were 299% in the SS, 236% in DG, 108% in CA1 and 186% in CA3. In the SS cortex vessels were strongly labelled by ICAM-1 uniformly across cortical layers (Figure 5.12e, red arrows). Immunolabelling of microglial processes (Figure 5.12f&h, red arrows) was a feature of all five cases and showed more intense immunoreactivity compared to controls, but was less intense than vessel labelling. Microglial staining was uniform in the cortex extending through all cortical layers. As for control cases, a prominent layer of ICAM-1 immunoreactivity of vessels was observed at hf increasing posteriorly (Figure 5.12g). Delicate ICAM-1$^+$ immunolabelling of microglia processes was observed within all hippocampal subfields (Figure 5.12h & Figure 5.13c&d, green arrows) as was ICAM-1$^+$ vessel staining (Figure 5.12h red arrows & Figure 5.13c&d red arrows).

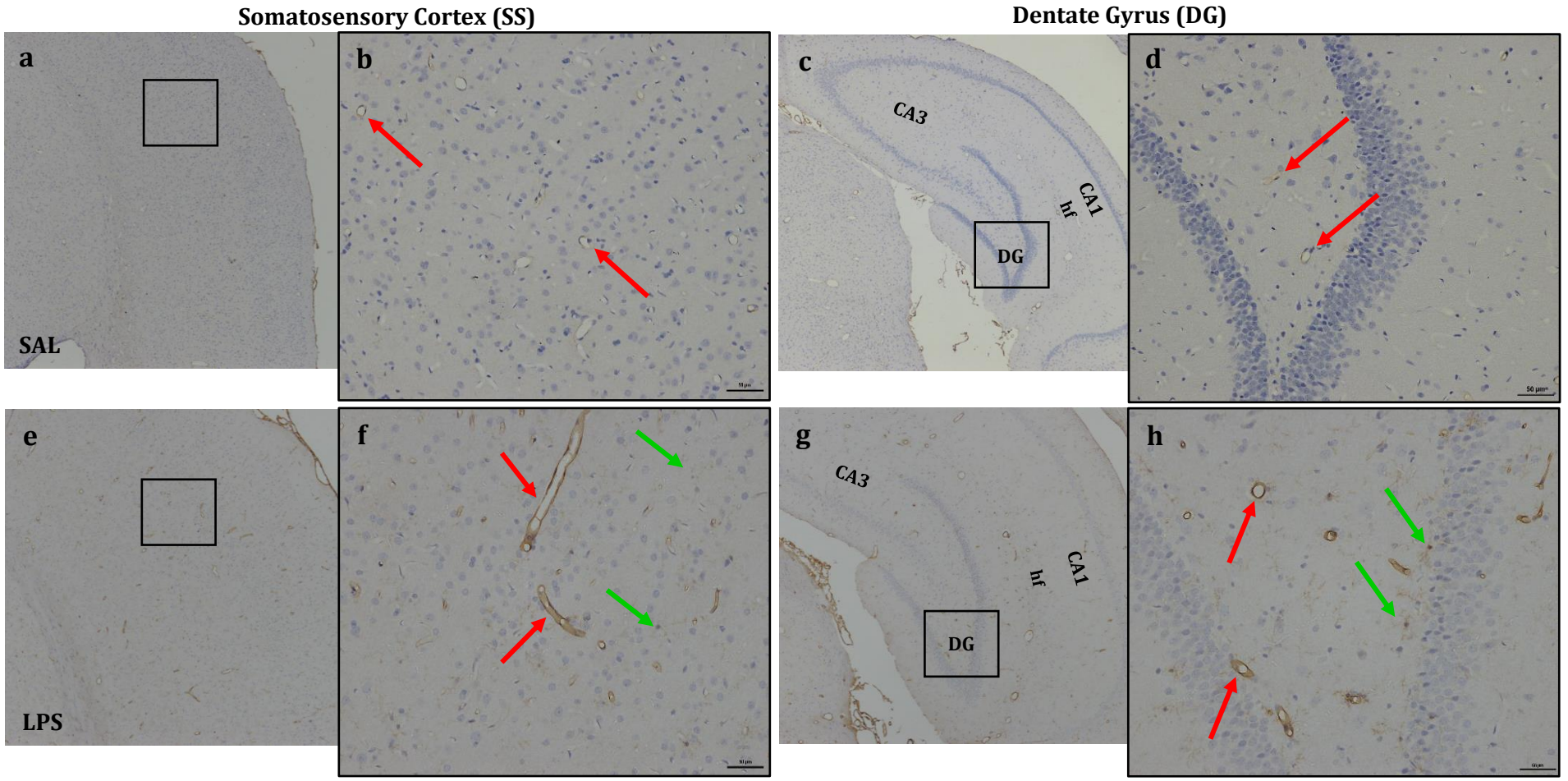

Figure 5.12. ICAM-1 expression in SS and DG. Expression of ICAM-1 by DAB (brown) in SS and dentate gyrus (DG) in saline (SAL)/LPS treated animals. ICAM-1 expression for SAL treated animals was very faint and restricted to few vessels in both SS and hippocampus (b&d, red arrows). In LPS cases vessel immunoreactivity was much more prominent (f&h, red arrows). Microglial process staining was also evident (f&h, green arrows). Sections were counterstained with haematoxylin. Scale bar represent 200µm and 50µm (insert). DG = dentate gyrus, hf = hippocampal fissure.

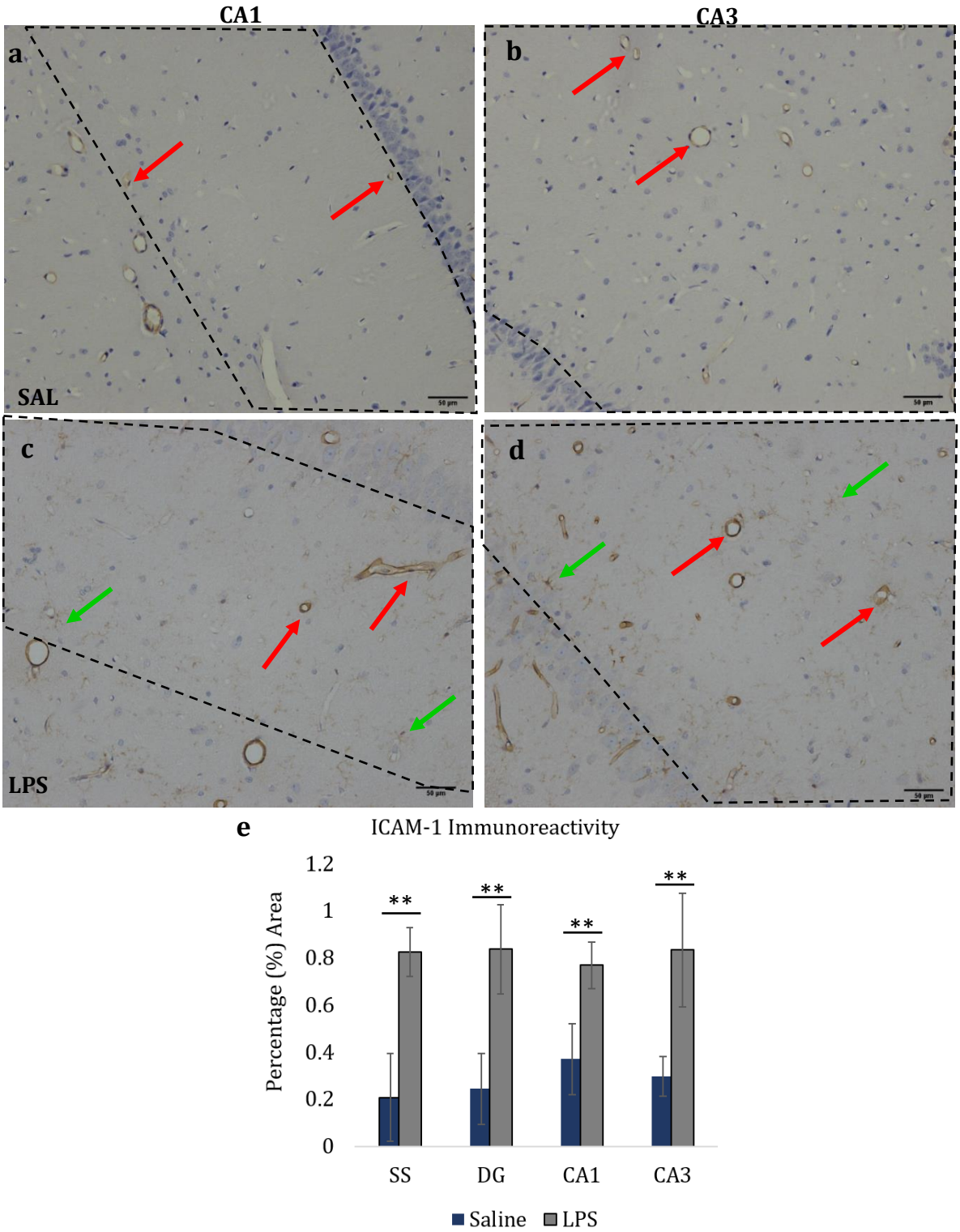

Figure 5.13. ICAM-1 expression in hippocampal subfields CA1 and CA3 and percentage area increases. Expression of ICAM-1 by DAB (brown) in the hippocampal subfields of CA1 and CA3 in SAL/LPS treated animals. ICAM-1 expression was more prevalent in LPS cases in both hippocampal subfields labelling ICAM-1+ vessels (c&d red arrows) and microglial processes (c&d green arrows). Diffusivity and pattern of staining was consistent within cases across SS and hippocampal subfields. Sections were counterstained with haematoxylin. Segmented lines represent area analysed in Analysis[D] corresponding to hippocampal region. Scale bar represent 50µm. Figure 5.13e shows percentage area increases of ICAM-1 immunoreactivity in SS and hippocampal subfields. Significance found for all selected brain regions $^{**}p<.005$.

5.7.2.4 AQP4 immunoreactivity – single labelling

In control cases, faint AQP4 immunoreactivity was observed in SS (Figure 5.14a) but was a prominent feature of the hippocampus (Figure 5.14c). In the SS cortex AQP4 immunolabelling was punctate and focused on astrocyte end feet enveloping the vessels (Figure 5.14b, red arrows). Faint immunoreactivity around larger vessels was also observed (Figure 5.14b, green arrows). Staining intensity correlated with cortical layer depth, where intensity increased as cortical layers deepened. In the hippocampus intense AQP4 immunoreactivity was observed in the hf, mainly associated with astrocyte endfeet in direct contact with vessels (Figure 5.14c). Immunoreactivity within the DG was characterised by diffuse $AQP4^{+}$ depositions of varying intensity (Figure 5.14d, green arrows) and $AQP4^{+}$ vessel staining (Figure 5.14d, red arrows). The CA1 subfield displayed less intense $APQ4^{+}$ immunoreactivity (Figure 5.15a, green arrows) and was restricted to astrocyte endfeet in contact with vessels (Figure 5.15a, red arrows). Staining in the CA3 subfield was more intense than in CA1 and associated with diffuse staining around vessels (Figure 5.15b, green arrows) in addition to discrete vessel staining (Figure 5.15b, red arrows).

In the SS cortex of the LPS cohort AQP4 immunolabelled astrocyte endfeet enveloping the vessels (Figure 5.14b red arrows) as well as immulabelling diffuse depositions around vessels (Figure 5.14b, green arrows). AQP4 expression was also seen extending adjacent to the vessels (Figure 5.14b). Immunolabelling of AQP4 was consistent across cortical layers. In the hippocampal region, intense AQP4 staining was observed at the hf extending further in the CA1 subfield (Figure 5.14g). Immunoreactivity within the DG appeared more diffuse and was mainly restricted to astrocyte endfeet in direct contact with the vessels (Figure 5.14h, red arrows). Within the DG intense immunoreactivity was observed, with labelling of astrocyte endfeet intimately associated with vessels (Figure 5.14h, red arrows) and depositions around visible vessels (Figure 5.14h, green arrows). CA1 and CA3 immunoreactivity (Figure 5.15) was patchier and showed both intense astrocyte endfeet deposition (Figure 5.15c&d, green arrows) as well as vessel staining (Figure 5.15c&d, red arrows).

5.7.2.5 AQP4 immunoreactivity – fluorescent dual labelling

Despite successful optimisation of AQP4 antibody, due to antibody degradation and to multiple issues encountered in switching from a chromogen to a fluorescent tag, fluorescent AQP4 and COLL IV dual labelling could not be included in this chapter results.

5.7.2.6 PDGFRβ immunoreactivity

Due to difficulties experienced in the optimisation of dual labelling protocols of PDGFRβ and COLL IV (as a vessel marker), which resulted in COLL IV masking PDGFRβ signal, a basic PAS histology stain was employed to characterise pericyte loss or detachment from the vasculature. No difference in the pattern of pericyte staining was observed between the control and LPS treated animals, with no evidence of pericyte loss in LPS treated cases (Figure 5.16). Observed immunoreactivity was localised congruently across cohort groups, and was localised to vessels. Interestingly, it was observed that the expression of PDGFRβ appeared to be more intense in LPS treated animals compared to controls (Figure 5.16 red arrows). For control animals the PAS staining on present vessels was the principle feature, whereas LPS animals showed stronger PDGFRβ immunoreactivity with almost no visible PAS staining. This pattern was consistent across SS and hippocampus. Due to the level of tissue degradation experienced during the antigen retrieval protocol, PDGFRβ immunoreactivity was only qualitatively assessed to ensure immunoreactivity was genuine (Analysis[D] could not confidently distinguish between DAB and PAS stain on current background levels). A representative staining pattern across somatosensory and hippocampal areas is displayed in Figure 5.16.

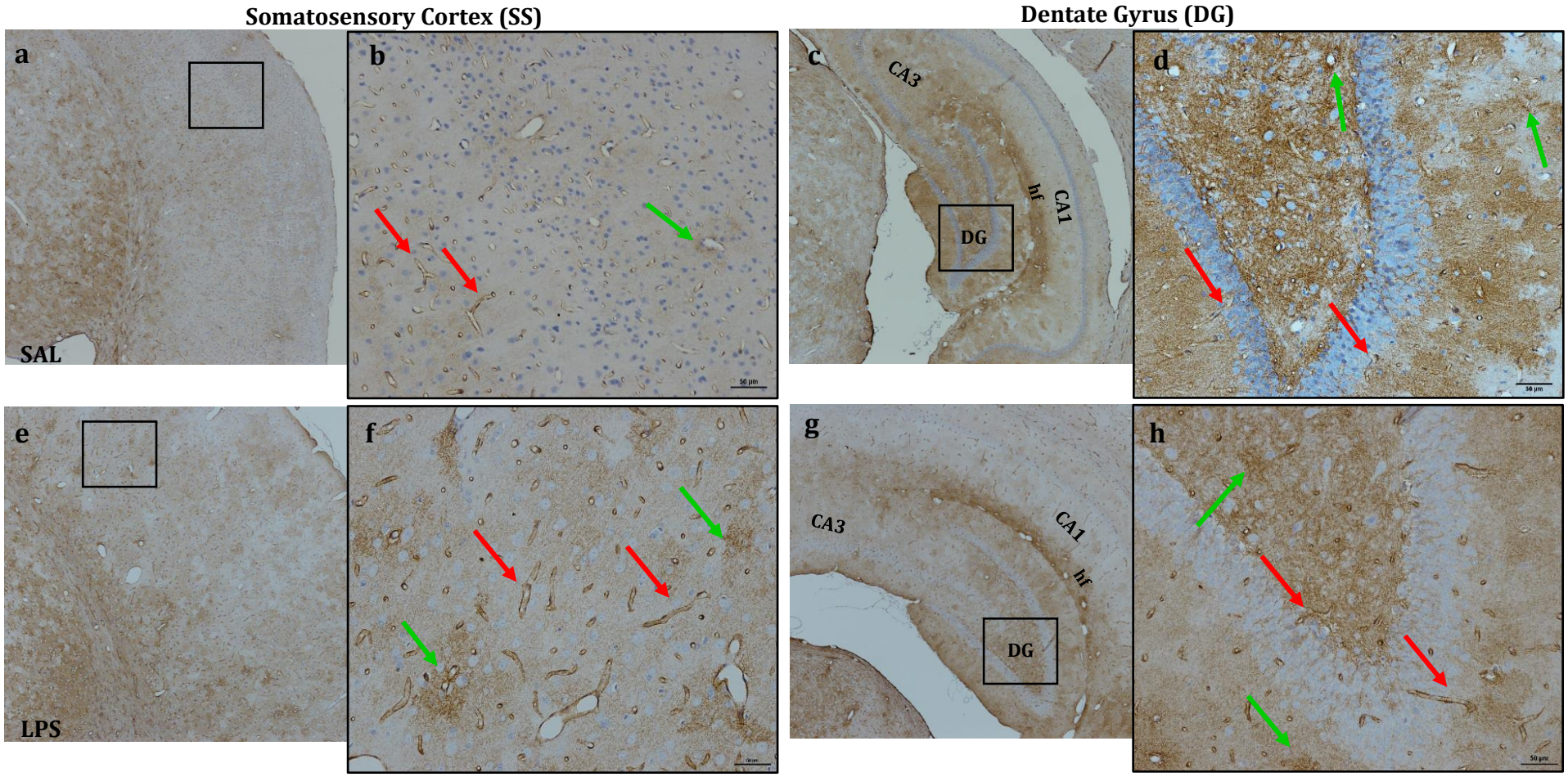

Figure 5.14. AQP4 expression in SS and DG. Expression of AQP4 by DAB (brown) in SS and dentate gyrus (DG) in saline (SAL)/LPS treated animals. AQP4 expression for SAL treated animals was weaker in the SS, showing both astrocyte endfeet staining of vessels and depositions around vessels (red & green arrows). In LPS cases vessel immunoreactivity was much more prominent in both SS and hippocampus (f&h, red arrows). Depositions around vessels also showed stronger immunoreactivity. Sections were counterstained with haematoxylin. Scale bar represent 200µm and 50µm (insert). DG = dentate gyrus, hf = hippocampal fissure.

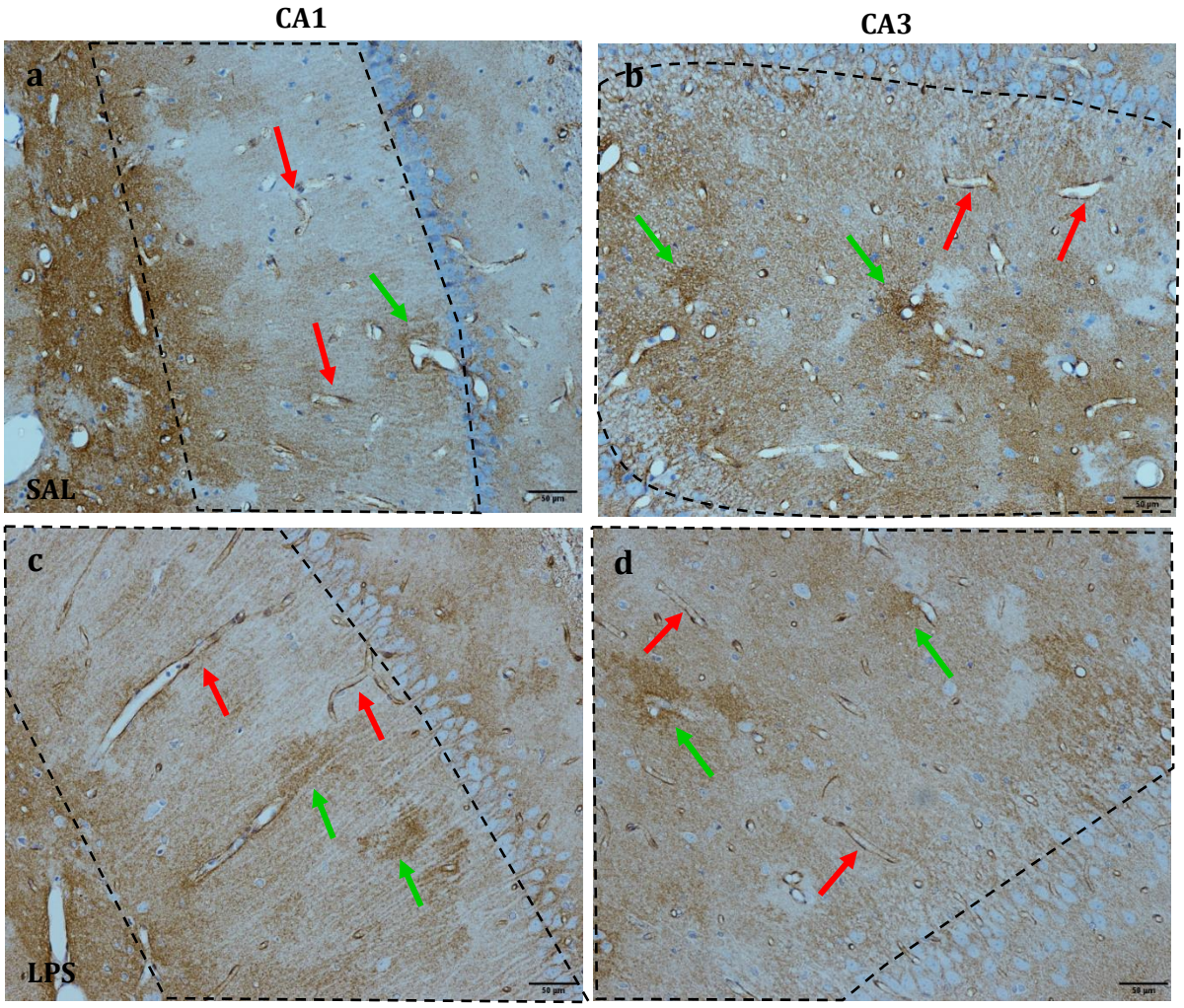

Figure 5.15. AQP4 expression in hippocampal subfields CA1 and CA3. Expression of AQP4 by DAB (brown) in the hippocampal subfields of CA1 and CA3 in SAL/LPS treated animals. AQP4 expression appears on vessels in contact with astrocyte endfeet (red arrows) and appears to be more strongly labelled in LPS cases. Diffuse AQP4⁺ depositions can be observed in both cohorts (green arrows). Diffusivity and pattern of staining was consistent within cases across SS and hippocampal subfields. Sections were counterstained with haematoxylin. Segmented lines demarcate hippocampal subfields examines during qualitative analysis. Scale bar represent 50µm.

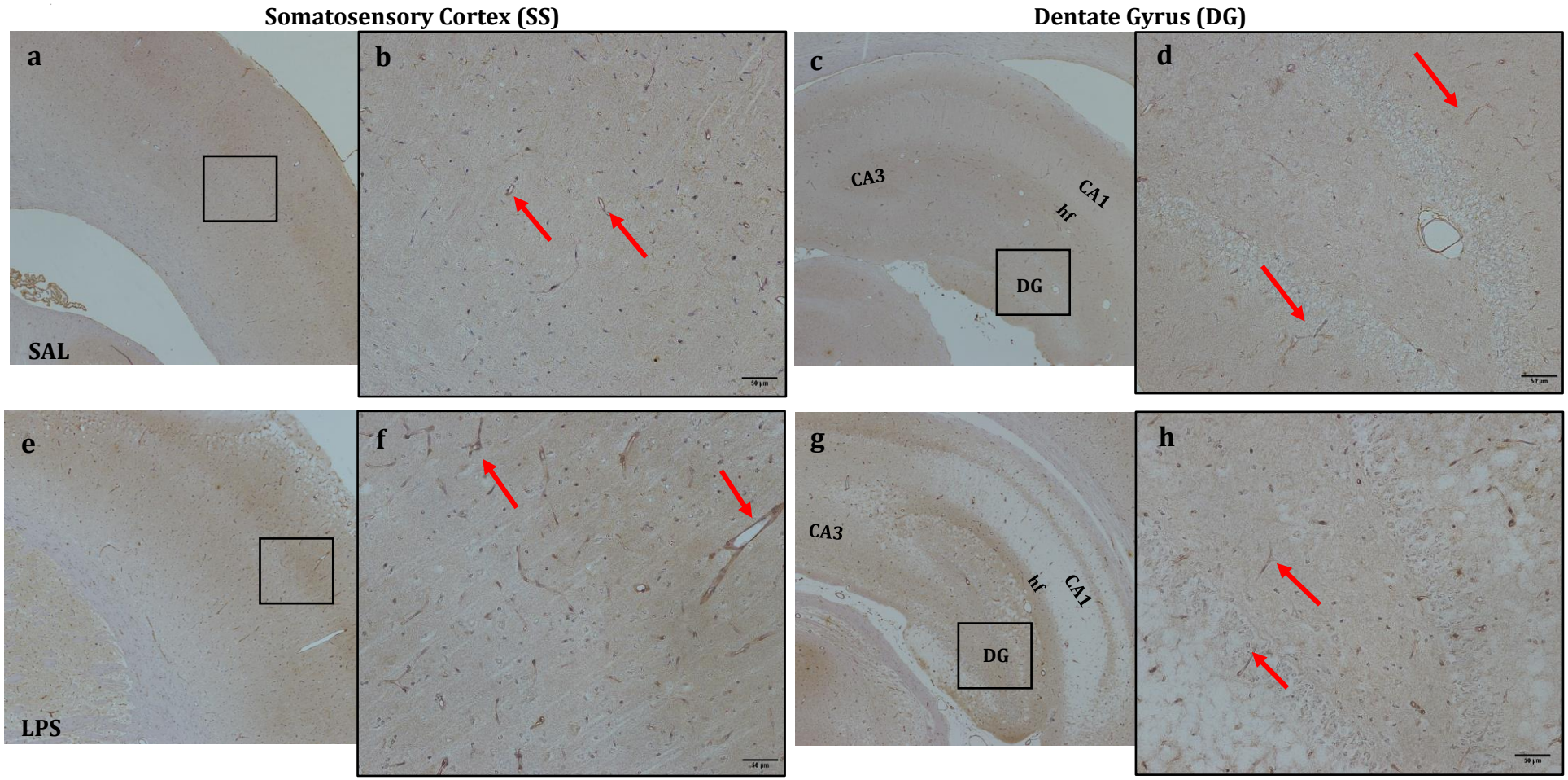

Figure 5.16. PDGFRβ expression in SS and DG. Expression of PDGFRβ by DAB (brown) in SS and dentate gyrus (DG) in saline (SAL)/LPS treated animals. PDGFRβ expression for SAL treated animals was weaker in the SS and DG, showing stronger PAS staining around vessels (b&d, red). In LPS cases PDGFRβ immunoreactivity was more prominent in both SS and hippocampus (f&h, red arrows). Sections were counterstained with haematoxylin. Scale bar represent 200μm and 50μm (insert). DG = dentate gyrus, hf = hippocampal fissure.

Table 5.2 Summary of key findings for IHC results qualitatively and quantitatively comparing LPS treated animals to control cases.

Antibody (Target)	Qualitative Analysis	Statistical Analysis
GFAP (Astrocytes)	**Somatosensory Cortex (SS)** Change in morphology, hypertrophic profile. **Hippocampus** No significant change in morphology or GFAP expression.	LPS cases shows a significant 74 percentage (%) area increase in GFAP immunoreactivity ($t(8)= -4.15$, $p=.003$). No significant differences were found for any hippocampal subfield (DG: $t(8)= -1.4$, $p=.200$; CA1: $t(8)= -1.94$, $p=.089$; CA3: $t(8)= -.34$, $p=.744$).
IBA-1 (Microglia)	Hypertrophic profile (larger cell body with elongated and retracted processes) with increased expression of IBA-1 present in **SS cortex** and **hippocampus**. Clustering localised to vessels.	LPS cases displayed a significant 109 % area increase in IBA1 expression compared to controls across the SS cortex ($t(8)= -3.84$, $p=.005$) and hippocampal subfields (DG: 72 % area increase, $t(8)= -2.52$, $p=.036$; CA1: 119 % area increase, $t(8)= -4.09$, $p=.003$; CA3: 153 % area increase $t(8)= -4.3$, $p=.003$).
ICAM-1 (ECs activation)	Increased expression of ICAM-1 on vessels and microglia (fainter) present in **SS cortex** and **hippocampus.**	Percentage area increases for ICAM-1 expression in LPS treated animals compared to controls were 299% in the SS ($t(8)= -6.5$, $p<.001$), 236% in DG ($t(8)= -5.47$, $p=.001$), 108% in CA1 ($t(8)= -4.73$, $p=.001$) and 186% in CA3 ($t(8)= -4.69$, $p=.002$).
AQP4 (Astrocyte endfeet)	Strong AQP4 labelling around vessels with diffuse depositions across the **SS cortex**. No clear difference in AQP4 expression in **hippocampus.**	
PDGFRβ (Pericytes)	No detectable pericyte loss. Stronger overall PDGFRβ immunoreactivity in **SS cortex** and **hippocampus**.	

5.8 Discussion

This study revealed an increased expression of GFAP and IBA-1 by astrocytes and microglia respectively in LPS treated cases, with both cell types displaying a hypertrophic profile. LPS treated animals also displayed an increase in ICAM-1 expression on both ECs and microglia compared to control (saline treated) cases. Increases in EC ICAM-1 expression is strongly indicative of ECs activation, which has been shown to impact upon blood flow regulation in systemic inflammation and may thus help to explain the observed *in vivo* increases in haemodynamic response in LPS-treated animals. Furthermore ECs regulate hypercapnic response and overall cerebral regulation, thereby potentially mediating the observed changes in hypercapnia and vascular reactivity in LPS-treated animals. Qualitative data on AQP4 and PDGFRβ suggests increased expression of both markers on vessels by astrocyte endfeet and pericytes, respectively. Both changes require further investigation. The role of pericyte-mediated changes in blood flow and their relationship with ECs (at the capillary level) during systemic inflammation is currently unknown. Furthermore studies investigating changes in AQP4 which could indicate an altered relationship between astrocyte endfeet and blood vessels are warranted, as a change in this relationship will impact upon neurovascular function and neurovascular coupling. Assessment of neurovascular health and function utilising a multi-modal approach of *in vivo* and immunohistochemical measures in the same animals is a strength of this study. This approach enables a joint assessment of cellular and haemodynamic changes which together can be used to provide a more complete picture of the altered neurovascular function which occurs during an acute systemic inflammatory response and in the understanding of how NVU cellular changes impact upon haemodynamic signals.

5.8.1 Acute systemic injection of LPS induces activation of somatosensory astrocytes

In the current chapter, LPS-induced changes in astrocyte pathology were investigated by immunostaining for GFAP. GFAP, a filament protein expressed in mature astrocytes is often used as a marker of astrogliosis, as in response to injury astrocytes undergo cellular hypertrophy increasing their GFAP expression (Middeldorp & Hol, 2011). Severity of astrogliosis is dependent on several factors including location (local or distant), type (infection, inflammation or neurodegenerative) and occurrence (acute or prolonged) of trauma (Sofroniew & Vinters, 2010). Upregulation of GFAP was observed in LPS treated animals with a change in morphology and distribution. $GFAP^+$ astrocytes were more prominent, displaying greater immunoreactivity of processes and cell body. Furthermore immunoreactivity was also localised around vessels, suggesting stronger GFAP expression

by astrocyte endfeet. This phenotype is suggestive of mild to moderate astrogliosis (Sofroniew & Viters, 2010) but was only clearly observed in the SS cortex.

5.8.1.1 Further characterisation of astrocytes function with alternative markers to GFAP

The hippocampus is very densely populated by astrocytes, with abundant GFAP expression (Gomi et al., 1995; Shibuki et al., 1996) compared to other cortical areas. As a result of this, detection of acute and short inflammatory astrogliosis may be harder to quantify. IHC results showed a trend of increased GFAP immunoreactivity, particularly in the CA1 subfield, in LPS treated animals, suggesting a possible mild to moderate astrogliosis as the one found in the SS cortex. Observing longer (>7 hours) changes in GFAP expression resulting from an acute inflammatory challenge may help clarify this trend. Furthermore, different subpopulations of astrocytes exist in the brain each with distinctive roles in pathology and health, features and appearance and thus varying in expression of intermediate filaments (IF) including GFAP isoforms (Middeldorp & Hol, 2011). It is possible that acutely and peripherally activated astrocytes, at least in the hippocampus, express other GFAP isoforms and IFs than the one directly utilised in this study. Further quantification utilising other GFAP isoforms alongside additional astrocyte markers (such as ALDH1L1, nestin and vimentin) may help fully elucidate the astrocyte response triggered by an acute LPS challenge. Furthermore hippocampal astrocytes, co-express GFAP and vimentin (Lazarides, 1982) and $GFAP^{-/-}$ transgenic mice have been shown to undergo astrogliosis due to the presence of vimentin (Middeldorp & Hol, 2011; Pekny et al., 1995). Thus characterisation of $vimentin^{+}$ astrocytes in the hippocampus may help delineate any possible differences between cohort groups.

GFAP immunoreactivity has been shown to localise perinuclearly, in thick astrocyte processes (Suzuki et al., 2003) and to approximately label 15% of the astrocyte volume (Bushong, Martone, Jones, & Ellisman, 2002), thereby GFAP immunoreactivity only reveals a small part of the volume of the cell. It may be that changes produced by an acute systemic inflammatory challenge on hippocampal astrocytes may occur in the more extended and fine processes of the cell and thus may not be adequately characterised by GFAP.

Astrocytes play a key role in regulating levels of neurotransmitters in the brain including glutamate, by expressing a number of glutamate transporters and receptors. Glutamate is essential for neuronal function and neurotramission however a build-up of extracellular glutamate can result in excitotoxicity and damage both neurons (Wang & Michaelis, 2010) and glia (Mcdonald, Althomsons, Hyrc, Choi, & Goldberg, 1998). Excitatory amino acid

transporter 1 (EAAT1) and EAAT2 (glutamate aspartate transporter [GLAST] and glutamate transporter-1 [GLT-1] respectively in rodents) have been identified as two key transporters of glutamate (80% of the total uptake) and are located primarily on astrocytes (Maragakis et al., 2004a; Maragakis, Dykes-Hoberg, & Rothstein, 2004b; Rothstein et al., 1996). EAAT1 and EAAT2 are expressed in areas of glutamate release by neurons whereby astrocytes are able to modulate glutamate levels by redistributing their transporters to increase uptake during excessive glutamate levels in the CNS (Shin et al., 2009). EAAT1 and EAAT2 specificity to astrocytes identifies these two transporters as additional functional astrocyte markers and with further characterisation of their expression and/or decreased expression of glutamine synthesis elucidate any possible astrocytic contribution to excitotoxicity and neuronal dysfunction during an acute inflammatory challenge.

5.8.2 LPS mediated acute inflammation increases microglial IBA-1 expression

IBA-1, a microglial marker and protein known to be upregulated by activated microglia (Ito et al., 1998), showed increased immunoreactivity in LPS treated animals. Microglia cells shifted from displaying a ramified 'resting' morphology with low expression of IBA-1 to a hypertrophic profile characterised by a swollen, rounded amoeboid appearance (Boche et al., 2013) and greater staining of processes, appearing hyper-ramified and 'bushy' (Sun, Zheng, Zhao, Lee, & Goldstein, 2008). Morphological changes and increased expression of IBA-1 are suggestive of a phenotype shift from resting to reactive following an acute peripheral injection of LPS. Furthermore IBA-1^{+} microglia in LPS cases were observed to cluster around present vessels, a response possibly driven by the increase in ICAM-1 expression of the inflamed endothelium, as induction of ICAM-1 has been shown to correlate with increased microglial activation in acute inflammation (Huber et al., 2006) (further discussed in Section 5.8.3). Further characterisation of the microglial response in adapting a M1 or M2 phenotype could help elucidate microglial role in an acute inflammatory challenge as promoters of neurovascular alteration or attempting to restore brain homeostasis.

An increased microglial response, characterised by more intense IBA-1 immunoreactivity and increased hyper-ramifications was observed in the hippocampus. CA1 and CA3 subfields displayed respectively a 119 and a 153 % area increases compared to a 109 % area increase in the SS. The hippocampus is known to be most susceptible to damage, showing early degeneration and increased BBB permeability in neurodegenerative diseases such as AD and in ageing (Erdő et al., 2017; Montagne et al., 2015; Sengillo et al., 2013). Microglial activation has been implicated in BBB disruption (Zipser et al., 2007)

and is an early phenomena in the pathogenesis of disease (da Fonseca et al., 2014; Krstic et al., 2012). Sumi et al. (2010) in a study of *in vitro* co-cultured microglia concluded that these cells produce reactive oxygen species (ROS) thereby impairing BBB function and integrity. A rat model of traumatic brain injury (TBI) also observed the production of free radicals and subsequently hydrogen peroxide and NO from activated microglia (Readnower et al., 2010). An increase in oxidative stress leads to an increase in EC permeability (Chodobski, Zink, & Szmydynger-Chodobska, 2011) eventually leading to BBB breakdown. In AD TNF-α and CD200 both expressed by activated microglia modulate inflammation and macrophage function (da Fonseca et al., 2014) leading to increased influx of T cells and macrophages in the CNS due to increased BBB permeability. Assessment of ROS and BBB permeability markers such as fibrinogen, in addition to characterisation of ECs could be employed to further characterise the reactive microglial phenotype reported in this study and establish if this microglial response is similar to the one observed in early BBB breakdown and early AD pathogenesis.

5.8.3 Increased expression of ICAM-1 on the endothelial luminal surface and microglia processes in LPS treated cases

ICAM-1 has an important role in cell-to-cell adhesive interactions and has low expression in cerebral microvessels in normal physiological conditions (Wertheimer, Myers, Wallace, & Parks, 1992). Its upregulation on the luminal surface of ECs is increased in the presence of pro-inflammatory mediators and has been linked to BBB permeability during acute inflammation (Huber et al., 2006; de Fonseca et al., 2014). Previous research (Huber et al., 2005) reports increased ICAM-1 expression and microglia activation after λ-carrageenan-induced inflammatory pain (CIP) as early as 3 hours post CIP induction. IHC analysis showed region specific increases in ICAM-1 and microglia reactivity. Reactivity was limited to the thalamus and parietal cortex with no evidence of ICAM-1 expression and/or microglia activation in the hippocampus or striatal regions (quantified up to +72 hours). This study findings indicate that with an acute LPS peripheral administration cortical as well as hippocampal regions showed upregulation of ICAM-1, expressed by ECs and microglia, as early as 7 hours post LPS administration. This discrepancy may be explained by the different models utilised, both λ-carrageenan and LPS are polysaccharides but are normally administered in different ways in *in-vivo* models (topically vs injected). Furthermore, λ-carrageenan is utilised for pain research whereas LPS is used to simulate an inflammatory cascade found in infections and neurodegenerative diseases with an inflammatory component. Nevertheless, the ability of LPS to elicit an early immune

response not limited to the cortex strengthens the validity of using this model to replicate pathology in key areas affected in neurodegeneration.

Huber et al. (2005) further reports no changes in the serum concentrations of pro-inflammatory cytokines (IL-1β, TNF-α and IL-6) in the early phase of CIP (1-6 hours) but report a five-fold increase of IL-10 (an anti-inflammatory cytokine) at 6 hours post treatment. Thereby indicating the release of a protective phenotype in response to λ-carrageenan in the early immune response phase (<48 hours). IL-10 is essential in the crosstalk between glia cells and neurons (Lobo-Silva, Carriche, Castro, Roque, & Saraiva, 2016) and it has been shown to inhibit pro-inflammatory production of cytokines by microglia, thereby protecting astrocytes from excessive inflammation (Balasingam & Yong, 1996; Ledeboer et al., 2002; Lobo-Silva et al., 2016) and potentiate their production of transforming growth factor (TGF)-β (Norden, Fenn, Dugan, & Godbout, 2014). For neurons IL-10 receptor signalling provides direct support to the cells (Zhou, Peng, Insolera, Fink, & Mata, 2009b), increasing their survival (Zhou, Peng, Insolera, Fink, & Mata, 2009a) thereby modulating neurogenesis (Perez-Asensio, Perpiñá, Planas, & Pozas, 2013). Furthermore faulty IL-10 signalling or production has been implicated in a number of neurodegenerative disease including AD (Kiyota et al., 2012). A comprehensive cytokine profile, including IL-10 expression, would help to elucidate glial roles in early and acute inflammatory LPS challenges as neuroprotective or neurotoxic.

5.8.4 AQP4 characterisation in LPS treated cases

APQ4 characterisation was only qualitatively assessed due to limitations of the current analysis software, whereby the developed macro was unable to accurately detect AQP4 expression that was not associated with vessels. Chromogenic substrate characterisation (DAB) revealed increased AQP4 immunoreactivity on present vessels in LPS treated animals, in both SS and selected hippocampal subfields compared to controls. This increase is in agreement with previous literature which reports an increase in AQP4 in human post-mortem studies of inflammatory diseases (Aoki-Yoshino et al., 2005) and an LPS-mediated increase in the expression level of AQP4 in both glia and myoblast cultured cells (Sugimoto et al., 2017). AQP4 has also been implicated as a major player in neurovascular coupling due to its regulatory effects on both synapses and blood vessels (Jukkola & Gu, 2015). Nevertheless the effects of increased expression and possibly altered AQP4 signalling in neurovascular coupling still remains poorly understood and may be an important contributing factor to the neurovascular dysfunction seen in neurodegenerative conditions such as AD.

5.8.5 Increased expression of PDGFRβ in pericytes of LPS treated animals

Due to the challenges and current unreliability of commercially available pericyte marker PDGFRβ, the quality of staining obtained made quantification unreliable, thereby data were only qualitatively assessed. During sepsis pericytes have been observed to retract from the basal lamina thus increasing BBB permeability (Kovac et al., 2011; Nishioku et al., 2009). Nishioku et al. (2009) observed microvascular structure changes between pericytes and ECs at 6 hours post LPS treatment which resulted in a broken section of the basal lamina alongside pericyte detachment at 24 hours post LPS administration. These changes were coupled with increased IBA-1 and fibrinogen immunoreactivity in LPS treated cases, suggesting BBB leakage, most likely mediated by pericyte detachment. As previously mentioned (Section 4.3), LPS is up-regulated through TLR-4 and pericytes have been shown to express and produce pro-inflammatory cytokines via TLR-4 (Edelman, Jiang, Tyburski, Wilson, & Steffes, 2006) resulting in acute capillary permeability in sepsis models (Edelman, Jiang, Tyburski, Wilson, & Steffes, 2007a; Edelman, Jiang, Tyburski, Wilson, & Steffes, 2007b). No pericyte detachment or loss was observed in this study; it appears likely that detachment of pericytes from the basal lamina via an LPS challenge occurs later (>7 hours) into the inflammatory response and is most evident at high doses (20mg/kg) of LPS administration, during septic shock.

Nevertheless, more intense PDGFRβ immunoreactivity appeared to be present in LPS treated animals. *In-vitro* studies showed an increase in PDGFRα following an LPS challenge (Coin et al., 1996) and externally to the brain, PDGFRβ expression increased following LPS treatment in bile duct epithelial cells (Kassel, Sullivan, & Luyendyk, 2012). The current study suggests that acute exposure to LPS may increase PDGFRβ expression in brain pericytes but further quantitative investigation is required. Lingard-receptor systems such as PDGFRβ and TGF-β have been implicated in regulating vascular stability via endothelial-pericyte cell interactions (von Tell, Armulik, & Betsholtz, 2006), thereby activation of PDGFRβ may bring about changes in vascular stability and thus compromise NVU and BBB function. On the other hand increased PDGFRβ immunoreactivity could signify a pericyte response to maintain vascular stability during an inflammatory challenge, as TGF-β production by pericytes has been linked to up-regulatory mechanisms for BBB function (Dohgu et al., 2005). Future work should aim to characterise with quantitative assessment the role of brain pericytes in systemic inflammation.

5.8.5.1 Current limitations of pericyte markers

Pericyte markers are currently limited, known to be less specific and reliable compared to the well characterised, robust cell phenotype antibodies utilised to label other cellular components of the NVU. Much of the work characterising pericyte biology derives from the study of pericyte deficient transgenic mice models which display disrupted PDGFRβ signalling (Leveen et al., 1994; Lindblom et al., 2003). As such, PDGFRβ remains the most viable pericyte marker available (Arimura et al., 2012; Armulik et al., 2011) and has been shown to be pericyte specific (Winkler et al., 2010). As previously mentioned (Section 5.7.1.2) alternative pericyte markers like CD13 were regarded as unsuitable for this study as CD13 is also expressed in the inflamed endothelium (Armulik et al., 2011).

Characterisation of pericytes with PDGFRβ was challenging in this study. Several trialled PDGFRβ antibodies were associated with high levels of non-specific immunostaining, and were highly unstable when stored and degraded rapidly. The biotinylated PDGFRβ utilised here was the only pericyte antibody that produced an adequate pericyte-specific signal but required the harshest antigen retrieval method resulting in damage to the tissue architecture compared to any other IHC protocol utilised. Hence, qualitative assessment and quantification was challenging and only tentative results can be extrapolated. An extension to this component could involve quantitative assessment of levels of PDGFRβ via Western blots, to determine if an acute peripheral LPS challenge can provoke a change in PDGFRβ expression in brain pericytes. However, it should be noted that Western blots are only able to provide an overall quantitative assessment of changes in protein expression and are unable to ascertain where in the tissue these cellular changes may be occurring. Hopefully with the refinement of antibody specificity further robust characterisation of pericytes by IHC will be possible.

Better characterisation of pericytes by IHC may in turn help to investigate and relate cellular changes to *in vivo* altered haemodynamics, as these cells have been implicated in mediating interactions between systemic and brain inflammation (Winkler, Bell & Zlokovic, 2011) and in the regulation of CBF by being the first vascular elements to dilate in response to neuronal activity (Hall et al., 2014). Investigation of pericyte interactions at the level of the capillary by utilising 2-photon microscopy, where these cells ensheath ECs could furthermore reveal changes in ECs-pericyte relationships as a result of systemic inflammation (and ECs activation) which could thereby impact upon haemodynamics measures (altered neurovascular function) and neurovascular coupling.

5.8.6 Mediators of the LPS induced inflammatory response

CNS cells including microglia (Marzolo, Von Bernhardi, Bu, & Inestrosa, 2000), astrocytes (Chakravarty & Herkenham, 2005) and ECs (Verma, Nakaoke, Dohgu, & Banks, 2006) possess TLR-4 and thus should be directly activated by and respond to an LPS challenge. However, lipopolysaccharides and pro-inflammatory molecules are large and thus should have limited BBB permeability (Holmes, 2013). Evidence from research radioactively labelling LPS (Banks et al., 2015; Banks & Robinson, 2010) has shown little LPS crossing or penetration at the BBB (0.025% of the administered dose) and this penetration was only present at doses of 3mg/kg or higher. Furthermore, 75% of an administered LPS dose binds exclusively to the luminal surface (Banks & Robinson, 2010). Thus, this physical limitation suggests that the observable brain inflammatory response produced by a peripheral administration of LPS is most likely mediated by alternative routes of communication between the brain and the periphery and not by brain receptors (for a comprehensive review see Holmes, 2013). This could explain why studies comparing brain and peripheral inflammatory challenges such as the one by Montacute et al. (2017) report similar levels of brain inflammation.

Hypotheses of potential periphery-to-brain routes include the stimulation of peripheral nerves by cytokines and prostaglandin, where LPS has been shown to induce IL-1β and prostaglandin E2 (PHE2) production in liver cells and relay them to the vagus nerve (Goehler et al., 1999; Goehler et al., 1997); the infiltration of pro-inflammatory cytokines triggered by LPS at sites lacking a BBB, progressing the inflammatory response across the brain (Nadeau & Rivest, 2000); the release of substances from the periphery that are then able to cross the BBB (Qin et al., 2007); the enhanced interactions between immune cells and the BBB (Strosznajder, Chalimoniuk, Strosznajder, Albanese, & Alberghina, 1996); the alteration of BBB permeability directly (Xaio, Banks, Niehoff, & Morley, 2001) which although does not seem to appear for doses lower than 3mg/kg (Banks et al., 2015) or by triggering the cells of the BBB to release pro-inflammatory substances (Quan, He, & Lai, 2003; Verma et al., 2006).

5.8.6.1 ECs appear to be the first NVU cells to mediate an acute LPS inflammatory challenge response

Increases in ICAM-1 and VCAM-1 expression in activated ECs promote the adherence of inflammatory cell monocytes, lymphocytes and macrophages as well as the recruitment of cytokines, growth factors and matrix metalloproteinases (MMPs) (Sprague & Khalil, 2009). In this study, ICAM-1 was used to characterise transmembrane protein upregulation on

ECs and found significant increases in ICAM-1 immunoreactivity in LPS treated animals compared to controls, this increase is strongly indicative of ECs activation. Furthermore their location, at the interface between brain and blood, could pinpoint ECs as initiators of the inflammatory response, undergoing alteration in function and gene expression, which then propagates to the rest of the NVU members (pericytes, endfeet, astrocytes and microglia).

ECs have already been characterised to change their phenotypes in support of various phases of the inflammatory process (Pober & Sessa, 2007). In acute inflammation ECs activation can be characterised into Type I activation, a rapid response which is independent of new gene expression or a slower response which is dependent on new gene expression (Type II activation) (Pober & Cotran, 1990). Type I activation receptor signals (heterotrimeric GPCRs) last no longer than 20 minutes, after which the receptors become desensitised thereby limiting their response. A more sustained inflammatory response is mediated by Type II activation, characterised as a longer-lasting form of EC activation which develops over hours and persists until activated cytokines are no longer present (inflammatory insult has been resolved). Type II activation is mediated by TNF-α and IL-1, deriving from activated leukocytes (Pober & Cortan, 1990). Both activation types lead to increased blood flow, due to an increase of [Ca^{2+}], increased leukocyte recruitment and increased vascular leakage of plasma proteins. As such increases in *in vivo* haemodynamic response as observed in Chapter IV may be explained by activation of ECs, which has been demonstrated in this chapter (significant increase in ICAM-1 expression).

Finally, Type I and Type II ECs activation are characterised by increases in COX-1 and COX-2 respectively (Pober & Sessa, 2007). It would thus be interesting to characterise with IHC, levels of COX-1 and COX-2 expression to determine the type of ECs activation present in this acute LPS model, which may help explain the underlying *in vivo* haemodynamic changes (see below).

5.8.6.2 ECs are key modulators of CBF regulation

The results obtained in Chapter IV indicate LPS-mediated increases in CBF response magnitude during whisker stimulation, but decreases in the magnitude of responses to a hypercapnic challenge. This apparent mismatch may be explained by a difference in the underlying mechanisms and pathway activation resulting from neuronally driven versus non-neuronally driven changes in CBF. A possible mechanism for this effect could be LPS-mediated differences in the involvement of ECs in blood flow regulation in stimulation or hypercapnia conditions. The involvement of COX-1 and COX-2 in response to non-

neuronally and neuronally driven CBF changes has been subject to great study (Iadecola, Pelligrino, Moskowitz, & Lassen, 1994; Kontos, Raper, & Patterson, 1977; Niwa et al., 2000; Niwa, Haensel, Ross, & Iadecola, 2001) and could be a candidate for such an effect. As such research has distinguished COX-2 involvement in neurovascular coupling (Girouard & Iadecola, 2006; Niwa et al., 2000) from COX-1 and COX-1 derived prostaglandin E_2 (PgE_2) and PgE_2 receptors mediating cerebral circulation in the context of hypercapnia (Howarth et al., 2017; Niwa et al., 2001). More recently Uekawa et al. (2016) highlighted the role of EP1 receptors in hypercapnic regulation and overall cerebral circulation and as these receptors are located primarily on ECs, it highlights a key involvement of ECs in the modulation of cerebral regulation in the absence of neuronal input.

Furthermore ECs have been shown to be critical players in mediating neurovascular coupling in health (Chen et al., 2014). Retrograde dilation of pial vessels following sensory stimulation is blocked if EC signalling is interrupted and disruption of ECs at the pial surface leads to a significant attenuation of the haemodynamic response (Chen et al., 2014). These findings could help explain the increases in haemodynamic measures observed in Chapter IV, where such changes could be mediated by increased activity of ECs at the pial surface. This hypothesis should thus be investigated to elucidate a possible role of ECs in mediating haemodynamic responses during an acute systemic inflammatory challenge. Lastly, as ECs are exposed to the bloodstream, both BBB penetrating and non-penetrating substances (such as LPS) could act upon these cells to mediate changes in neurovascular coupling (D'Esposito et al., 2003). Intravenous administration of an anti-inflammatory substance (rofecoxib) was shown to attenuate cortical haemodynamic responses to sensory stimulation (Bakalova, Matsuura, & Kanno, 2002), as such it is possible that administration of LPS could be exerting its inflammatory effects through ECs increasing haemodynamic responses to sensory stimulation.

5.8.7 The crosstalk between NVU cellular components during inflammation

The NVU is regarded as a complex integrated system of vascular and glial cells alongside pericytes and neurons which together are able to maintain brain homeostasis (Stanimirovic & Friedman, 2012). It is thus important to acknowledge individual cellular changes due to inflammation but it is also imperative to address the interactions between NVU components, as no cell operates in isolation. Neurons and astrocytes are known to play an integral part in the regulation of microglia and their phenotype via both soluble and membrane-bound mediators (Perry & Teeling, 2013). Neurons are able to down-regulate microglia and thus suppress inflammation within the CNS by releasing neurotropic factors (Perry & Teeling, 2013). Norepinephrine (NE) and GABA have both

been implicated in suppressing pro-inflammatory cytokine production in microglia, as these cells show to express a variety of receptors for neurotransmitters (Pocock & Kettenmann, 2007). Furthermore, microglia, as well as astrocytes which are in intimate contact with microglia, express GABA(A) and GABA(B) receptors which have been shown to suppress LPS mediated inflammation by inhibition of NF-κB, a key pathway in the instigation of chronic inflammation (Lee, Schwab, & Mcgeer, 2011). Neurons and microglia form ligand-receptor interactions, including receptor TREM-2, which upon linking inhibit down-stream immune signalling and thus down-regulate microglial phenotype (Billadeau & Leibson, 2002; Perry & Teeling, 2013) or are equally able to activate microglia (Daëron, 1997). This is of particular importance in conditions with neuronal degeneration or in acute or chronic neurodegenerative disease as degenerating neurons will be unable to regulate microglial response (Perry & Teeling, 2013). Evidence of the importance of CNS immune suppression for homeostatic maintenance has come from research on TREM-2 mutations which have been associated with an increased risk of developing AD (Guerreiro et al., 2013; Jonsson et al., 2013) and compromised inflammation regulation (Ford & McVicar, 2009).

5.8.8 Strengths and weaknesses of the current acute LPS model

AD is characterised by a chronic low-grade inflammatory response therefore the results obtained from an acute inflammatory challenge may not be directly applicable in the context of AD. Nevertheless, this chapter results have given insights into the changes in neurovascular response, brain imaging signals, vascular and glial pathology following an acute systemic inflammatory challenge. Furthermore, it is important to recognise that chronic and acute inflammation are not completely separate processes and that both may be observed at the same time in the same tissue (Pober & Sessa, 2007). The overlapping features between chronic and acute inflammatory processes arise from the mediators that are most often associated with ECs responses in acute and chronic inflammation which characterise both processes (for example TNF) (Pober & Sessa, 2007); thus findings from acute inflammatory challenges are relevant in chronic inflammation and vice versa. There is a pressing need to understand the communication pathways between the peripheral and central immune systems in order to understand the role of inflammation in AD and ageing and for the development of effective interventions combating inflammation. Thereby future studies should aim to characterise neurovascular and neurovascular coupling changes in a low dose chronic animal model and interrogate how this response is mediated by age to maximise its relevance to human pathology and human ageing.

5.8.9 Future work

Fluorescent label of AQP4 and COLL IV. Due to AQP4 antibody degradation as addressed in Section 5.7.2.5 a dual label of APQ4 and COLL IV could not be included in this chapter results. This additional characterisation could further assess any change in the relationship between AQP4 and blood vessels as a result of an acute systemic inflammatory challenge, as it has been previously shown that AQP4 extends from cellular endfeet to the cellular processes during inflammation (Fukuda & Badaut, 2012). If changes to AQP4 expression were revealed by immunohistochemistry techniques, further quantification and characterisation of AQP4 signalling and potential impact on neuronal activity and neurovascular coupling could be assessed *in vivo* using 2-photon microscopy (see below).

Two photon microscopy. The development of methods such as 2-photon microscopy have provided opportunities to examine the district roles of cells types of interest in neurovascular coupling by characterising blood flow in subsurface vessels alongside cellular activity. It is possible that inflammation may change the role of and communication between NVU cells. For example the relationship between astrocytes endfeet and the vasculature, which if altered, would ultimately modify the regulation of CBF and the vasodilatory response to neuronal activity, as these cells have been shown to be key mediators of neurovascular coupling (Attwell et al., 2010; Iadecola & Nedergaard, 2007). Inflammation-driven changes in these vasoactive pathways have yet to be investigated and may be key in understanding the neurovascular coupling changes observed in AD.

Assessing BBB dysfunction. To further characterise BBB dysfunction in acute inflammation, characterisation of TJP expression and extravasation of serum proteins may highlight possible disruption of ECs which may lead to serum protein accumulation and associated glial activation. The use of Evans blue dye, currently a widely used technique in animal research to assess blood vessel and cellular membrane permeability (Hamer, McGeachie, Davies, & Grounds, 2002) could provide evidence of any BBB disruption as a result of an acute inflammatory challenge. The dye has an affinity to serum albumin which readily penetrates the CNS during BBB dysfunction and can be identified both macroscopically (blue colour) and with fluorescence microscopy (red auto-fluorescence) (Matsuda, Nishikawa, & Tanaka, 1995). Evans blue can although be found in the blood of brain capillaries, as it does not appear to exclusively bind to brain plasma, this can make assessment of BBB breakdown more difficult (dye detected in the brain could be a mixture of dye bound to plasma proteins, dye bound to tissue and free dye). Furthermore,

perfusion of the animal for immunohistological protocols could remove large quantities of the dye (Saunders, Dziegielewska, Møllgård, & Habgood, 2015) and lastly the toxic properties of Evans blue which make is unsuitable for *in vivo* research are all limitations of this approach. Thus the use of dextrans or immunohistological detection in brain sections of proteins such as albumin, immunoglobulin and fibrinogen (Bridges et al., 2014; O'shea, Urrutia, Green, & Colado, 2014) could instead be employed.

Assessing gene expression changes. Furthermore, laser capture microdissection (LCM) of vessels coupled with large scale gene expression transcriptomic profiling could potentially further identify LPS-induced endothelial specific gene changes (Dachet et al., 2014) and characterise non-disruptive changes (Varatharaj & Galea, 2017) in BBB function, such as changes in signalling and cytokines. Transcriptional clustering has been previously used to identify cellular changes in epilepsy (Dachet et al., 2014). This technique has been shown to overcome limitations of gene expression analysis in relating expressed genes to specific cells by identifying and creating clusters with the ability to predict a change in a specific cell type. LCM isolation of a pure population of ECs is not possible due to their intimate relationship with other cellular constituents of the NVU, however transcriptional clustering could be instrumental in predicting EC-specific transcriptomic changes in the brain triggered by systemic inflammatory challenges.

LCM could furthermore be employed to characterise the expression profile of both microglia and astrocytes to characterise their role under an acute state of inflammation. This approach would enable characterisation of other changes in astrocyte and microglia function (for example, are astrocytes expressing a A1 or A2 phenotype and similarly are microglia expressing a M1 or M2 phenotype) which cannot be detected with a candidate approach (characterisation of gliosis), as employed in this thesis.

Lastly, the proposed LCM and transcriptomic analysis in animal models offers the opportunity to compare gene expression results to previously published human post mortem data thereby enabling complementary analysis and a translational aspect to relevant human neuropathologies.

5.8.10 Conclusion

In conclusion this study was successfully able to characterise changes in morphology and expression in NVU cells, providing evidence that an acute systemic inflammatory challenge leads to alterations in the status of the NVU. Changes in cell morphology and expression in astrocytes, microglia, ECs, endfeet and pericytes indicate possible cell phenotype changes although it is noted that this requires validation with gene expression studies. The results

of this study in conjunction with previous *in vivo* data (Chapter IV) were furthermore able to inform upon how cellular changes to NVU cells translate to the observed *in vivo* haemodynamic effects and suggest future studies to further elucidate the roles of ECs and AQP4 in mediating vasodilatory signals during systemic inflammation.

Chapter VI

Acute Effects of Systemic Inflammation on Neurovascular Function in Early Ageing

6.1 Chapter summary

The main aim of this chapter is to directly compare LPS-induced haemodynamic changes in middle-aged (12-month) and young (3-months) rodents to assess LPS-mediated changes in neurovascular function in early ageing.

Ageing is associated with a range of morphological and functional changes in NVU cells which lead to altered CBF and neurovascular function. Decreases in CBF have been shown to occur in midlife (Schultz et al., 1999) developing into global CBF changes in late-ageing (Balbi et al., 2015). As such middle age may be a critical point in which to implement interventions that aim to maintain neurovascular health. Systemic inflammation has a strong link with ageing in either dramatically increasing the risk of developing AD or in exacerbating the already present neuropathology. There is a current lack of *in vivo* studies which focus on the neurovascular changes associated with early ageing and given the known effect of systemic inflammation upon neurovascular function, understanding how inflammatory challenges modulate midlife CBF changes may prove key in the development of interventions alleviating and/or halting inflammatory driven ageing brain changes.

In this chapter, results are presented comparing haemodynamic measures between LPS-challenged young and LPS-challenged middle-aged animals. This reveals faster LPS-mediated changes in middle-aged animals, as a significant change in how stimulus inputs are converted to haemodynamic responses is evident as quickly as four hours after LPS treatment (compared to 6 hours in younger animals). In addition age at time of treatment had a significant effect on measured HbO_2 and HbR variables during a long (16s) stimulation, suggesting a change in the neurovascular coupling relationship which underlies long-latency responses. These results require validation with the addition of an aged-matched control group to ascertain if measured neurovascular function changes are mediated by ageing alone or by an inflammation-ageing interaction.

6.2 Ageing related changes

Physiological (healthy or normal) ageing is defined as a biological process of time-dependent progressive deterioration (Chung et al., 2009) with profound changes in NVU function, NVU cellular changes and BBB functionality (Erdő et al., 2017). The ageing process is also intimately associated with inflammatory changes in the brain which have been linked to an increased risk of developing dementia (Elahy et al., 2015; Dunn et al., 2005) and with a faster rate of cognitive decline in dementia sufferers (Fong et al., 2009). Modelling *in vivo* ageing related changes due to inflammation will be key in understanding how inflammatory challenges lead to the development of neurodegenerative conditions such as AD.

6.2.1 Morphological and functional changes in NVU cells

Ageing is associated with a wide range of changes in the function of NVU cells. Astrocytes have been observed to undergo morphological changes, increasing in size, number, and GFAP expression (Chisholm & Sohrabji, 2016; Hansen, Armstrong, & Terry, 1987; Middeldorp & Hol, 2011; Mouton et al., 2002; Vaughan & Peters, 1974). These morphological changes may in the event of an injury, exacerbate injury response and even lead to poorer patient outcomes (Harris, Choi, & Brooks, 2015). Furthermore, aged astrocytes have also been observed to reduce glutamate uptake thereby facilitating the development of a toxic brain microenvironment (Sohrabji et al., 2013). Microglia also undergo morphological changes and display diminished capacity to migrate, clear waste products and regulate injury and repair by being less able to shift from a pro-inflammatory to an anti-inflammatory phenotype (Ben-Menachem, Johansson, & Svensson, 1982). This heightened level of activation, possibly attributed to an inability to maintain homeostasis in age, may contribute to the deterioration of synaptic plasticity (Erdő et al., 2017) and may explain the maintenance of the neuroinflammatory response observed in aged brains. Pericytes have been shown to degenerate and migrate thereby losing contact with ECs (Scheibel et al., 1983) and undergo morphological changes (Peinado et al., 1998; Peters, Josephson, & Vincent, 1991; Tigges, Herndon, & Rosene, 1995). EC changes in ageing have been linked to increased permeability of the BBB (Farrall & Wardlaw, 2009) and the development of a chronic inflammatory response due to infiltration of serum proteins in the brain (Sohrabji et al., 2013). In addition, it has been shown that ECs lose their ability to release the vasodilator NO thereby reducing vasodilation and tissue perfusion (Csiszar, Pacher, Kaley, & Ungvari, 2005).

6.2.2 Upregulation of pro-inflammatory cytokines and molecules

A range of pro-inflammatory cytokines and molecules are chronically increased in ageing (Godbout et al., 2005). These include COX-2, iNOS, IL-1β, IL-6 and TNF-α, alongside adhesion molecules (AMs) including ICAM-1, VCAM-1 and E-selectin (Chung et al., 2009; Kim et al., 2002; Zou, Jung, Kim, Yu, & Chung, 2004). A transcription factor, NF-κB, is regarded as the primary regulator of widespread systemic inflammatory processes (Chung et al., 2009; Makarov, 2000), regulating the transcription of the aforementioned pro-inflammatory molecules, AMs, iNOS and COX-2 (Böhrer et al., 1997; Brand et al., 1996). NF-κB activation in the regulation of oxidative stimuli during normal conditions is self-limited, ceasing after insult resolution, however in ageing this self-limiting regulation appears to malfunction leading to the development of chronic pro-inflammatory conditions (Chung et al., 2009). Many NF-κB induced proteins (TNF-α, IL-6, IL-1, COX-2) further mediate the activation of NF-κB creating a reoccurring inflammatory loop (Handel, Mcmorrow, & Gravallese, 1995). NF-κB has also been shown to be upregulated in older rodents (Kim et al., 2002; Korhonen, Helenius, & Salminen, 1997).

6.2.3 Neurovascular and CBF changes

Profound changes in neurovascular coupling and CBF are reported in ageing, which have been linked to an increased risk of developing dementia (Farkas & Luiten, 2001), cerebrovascular disease (Jennings et al., 2013) and stroke (Mitchell et al., 2011). Reductions in CBF with age have been reported across multiple species including rats (Berman, Goldman, & Altman, 1988; Ohata, Sundaram, Fredericks, London, & Rapoport, 1981), monkeys (Noda et al., 2002) and humans (Schultz et al., 1999). Ageing has further been associated with increased stiffness and narrowing of both arterioles and capillaries (Park, Anrather, Girouard, Zhou, & Iadecola, 2007). Lastly, ageing is characterised by an increase in ROS, as a result of insulin-like growth factor-1 (IGF-1) deficiency (Toth et al., 2014) which decreases overall NO levels promoting EC dysfunction and compromising neurovascular coupling (Girouard & Iadecola, 2006; Toth et al., 2015). As a result of these vascular changes and compromised neurovascular function, resting CBF has been shown to decrease in age (Farkas & Luiten, 2001) thereby attenuating stimulus-evoked CBF responses (Iadecola, Park, & Capone, 2009). Most interestingly, in humans, CBF decreases have been observed to occur in midlife (50 years) and are thus not just late-ageing features (Schultz et al., 1999). Furthermore, a recent study (Balbi et al., 2015) comparing mouse cerebral vessel function in aged and young mice has suggested a change in pial microvessels in early ageing, before global CBF changes can be observed. This gradual decline in the regulation of CBF in response to neuronal demand was linked to an

increased risk of developing dementia and stroke later in life. Understanding the underlying causes of CBF changes in midlife may prove key in delineating processes leading to the development of dementia in ageing.

Loss of pericytes is also closely linked to changes in brain blood flow and decreases in cerebral capillary perfusion leading to BBB breakdown (Dalkara & Alarcon-Martinez, 2015; Dalkara, Gursoy-Ozdemir, & Yemisci, 2011). Chronic perfusion problems lead to accumulation of blood proteins and toxic macromolecules, vasculature and brain parenchyma damage, BBB dysfunction and neuronal degeneration (Zlokovic, 2008).

6.3 The link between ageing, inflammation and cognitive decline

Ageing and inflammation are strongly linked in the development of cognitive decline. Ageing processes have been implicated as drivers of inflammatory responses (Elahy et al., 2015) and in dementia, chronic and sustained inflammation leads to a faster rate of cognitive decline (Fong et al., 2009). Glial cells (microglia and astrocytes) are much more easily primed in the aged brain and due to their lowered activation threshold produce an exaggerated inflammatory response when triggered (Frank et al., 2010). Astrocytes, even at a very early stage of pathological progression have been shown to exhibit changes in function associated with loss of brain homeostatic reserve and cognitive decline (Rodrigues-Arellano et al., 2016). Older mice show increases in glial activation and behavioural disturbances (Godbout et al., 2005; Godbout & Johnson, 2009; Sankowski, Mader, & Valdés-Ferrer, 2015), suggesting an age mediated central immune response, which appears to worsen with increasing age. Aged mice also show significant attenuation in the expression of BBB TJ proteins and occludin-1 and elevated levels of TNF-α suggesting heightened peripheral inflammation (Elahy et al., 2015). As previously described (Section 1.5.1.3) ageing is further characterised by an imbalance between pro-inflammatory and anti-inflammatory networks. Thereby, it has been hypothesised that age-dependent vulnerability to acute and/or chronic infections is likely caused by a combination of age-dependent increases in Aβ plaque load (Godbout & Johnson, 2009), glial priming and chronic-low grade inflammation (Holmes, 2013). Evidence from both human and animal studies clearly suggest that age mediated inflammation has a pronounced effect on cognitive function, either dramatically increasing the risk of developing AD or exacerbating the already present neuropathology.

6.4 Models of ageing and inflammation

Animal models investigating the effects of inflammation in the context of ageing have primarily focused on characterising microglial response. Consistently microglia have been

shown to increase their expression of pro-inflammatory cytokines, including TNFα, IL-1β and IL-6 (Chelvarajan et al., 2006; Frank et al., 2010; Holtman et al., 2015; Sawada, Sawada, & Nagatsu, 2008; Sierra, Gottfried-Blackmore, McEwen, & Bulloch, 2007) and undergo morphological changes (Streit, 2004; Streit, 2005; Streit, Sammons, Kuhns, & Sparks, 2004) thereby generating the hypothesis that aged microglia become over-responsive and primed with age (Xie, Morgan, Rozovsky, & Finch, 2003; Ye & Johnson, 1999). *In vivo* LPS inflammatory challenges appear to over-stimulate aged microglia compared to young cells but IL-10 expression in also increased (Sierra et al., 2007); suggesting a degree of counterbalancing of pro-inflammatory and anti-inflammatory cytokines and not complete microglial dysfunction.

6.4.1 The importance of targeting the 'middle age' group

There is currently a lack of studies which target early ageing despite emerging evidence reporting CBF decreases (Schultz et al., 1999; Balbi et al., 2015) in this age group. As such this study aims to utilise 12-month aged rodents which in developmental terms, can be compared to a middle-aged human adult (50 years) (Semple et al., 2013; Sengupta, 2013) to investigate the effects of an acute systemic inflammatory challenge in early ageing. Understanding how inflammatory challenges modulate midlife CBF changes, which are known to increase the risk of developing AD in later life (Eikelenboom et al., 2012; Dunn et al., 2005) may prove key in the development of interventions alleviating and/or halting ageing driven brain inflammatory changes.

6.5 Study overview and hypothesis

The current chapter aims to extend the inflammation model utilised in Chapter IV to investigate the effects of acute systemic inflammation in early ageing, providing further data investigating alterations of neurovascular function during systemic inflammation *in vivo*.

Building on the Chapter IV hypothesis that an acute inflammatory challenge alters neurovascular function, this chapter's main **hypothesis** is that an acute systemic inflammatory challenge in middle aged animals will result in exacerbated neurovascular changes, whereby alterations in how stimuli inputs are converted to haemodynamic response functions will occur at an earlier time point.

Furthermore as CBF changes have been shown to manifest in middle age (early ageing) (Schultz et al., 1999; Balbi et al., 2015) it can be **hypothesised** that middle age animals will show changes in baseline CBF (decreases).

6.6 Chapter aims

This study aimed to investigate the impact of an acute systemic inflammatory challenge on neurovascular function in the context of early ageing by:

(1) Obtaining haemodynamic measurements of the haemodynamic response function in the context of physiological stimuli

(2) Comparing middle aged rodent neurovascular function to young rodent responses (data from Chapter IV).

As this study had access to a limited number of aged animals it was not able to include a control (saline treated) aged group and therefore focusses on differences between the two LPS-treated age groups.

6.7 Method

Anaesthesia, surgical procedures, physiological monitoring and imaging protocols (LSCI, OIS) were carried out as described in Chapter II. Briefly, animals were anaesthetised with an i.p injection of urethane (1.25mg/kg in 25% solution), tracheotomised and the left vein and artery cannulated. A thin cranial window was then prepared. Animal temperature was maintained at 37 ^{0}C (± 0.5 ^{0}C) and sampled blood gases remained within physiological parameters throughout experimental duration (mean values: PO_2=77.3%(±8.1) PCO_2 =26(±3) SO_2 =95%(±1.9)). MABP was also within recognised physiological limits, 110 (±8.1). The extracted brains from this study will be processed for IHC and gene expression analyses but due to funding, training and time constraints these results were unable to be included in this thesis.

6.7.1 Animals and pharmacological treatment

Female Hooded Lister rats (12 month old, *n* = 6, 260g-330g) were treated with an intraperitoneal injection of LPS-EB (2mg/kg, lipopolysaccharide from E.coli, InvivoGen, Europe) dissolved in endotoxin-free water just after loss of movement due to anaesthesia at 9am. Haemodynamic data was acquired over two time points (from 4 hours post injection to 6 hours post injection).

6.7.2 Imaging

OIS and LSCI were performed as described in Chapter II (Section 2.3.1). OIS was performed by illuminating the cortex with four wavelengths of light (495 ± 31 nm, 559 ± 16 nm, 575 ± 14 nm, and 587 ± 9 nm) to generate spatial maps of the haemodynamic response. Data were acquired at a frame rate of 32Hz (8 frames per second for each wavelength). At the start of each paradigm a 10 second baseline data acquisition period preceded the start of the stimulation train. For LSCI, the camera was positioned over the thinned window and a 70 second baseline data acquisition period was acquired in each paradigm to obtain a measure of baseline blood flow. Data were acquired at a frame rate of 25Hz.

6.7.3 Experimental design

All data were acquired within a ferromagnetic cage as outlined in Chapter II (Section 2.3) at two time intervals. Two whisker stimulation paradigms were applied, multifrequency and long stimulation as described in Chapter II (Section 2.3.3.1). The order of stimulation frequency for multifrequency condition was pseudorandomised. A 1.0mA whisker stimulation (0.3 ms pulse-width) was delivered via two subdermal electrodes directly

inserted in the whisker pad, as detailed in Chapter II (Section 2.3.3). A hypercapnia challenge was also employed (as per Chapter II, Section 2.3.2.2).

6.7.4 Perfusion

Following *in vivo* imaging and electrophysiology, all animals (n = 6) were transcardially perfused with saline (0.9% warmed to 37 ^{0}C) with the addition of heparin (0.1ml/500ml) as described in Chapter II (Section 2.4). The brain was then quickly removed from the skull and sectioned in half to separate the two hemispheres. The right hemisphere was immediately placed in 10% neutral buffered formalin whilst the left hemisphere was further sectioned in four and snapped frozen in liquid nitrogen as detailed in Chapter II (Section 2.4.2). Fixed hemispheres were embedded in paraffin wax as described in Chapter II (Section 2.5) and frozen hemispheres were stored at -80 C° until OCT embedding for cryostat sectioning.

6.7.5 Data analysis

6.7.5.1 Data processing

Data acquired from LSCI and OIS was extracted, processed and analysed as described in Chapter II (Section 2.6). A one-way ANOVA on ROI for LSCI (F(1,12)=2.88 p=.118) and OIS (F(1,12)=.972 p=.345) did not revealed any significant difference between groups. Data from each stimulation trial were extracted and divided by the average perfusion value (arbitrary units) over a pre-stimulus baseline period (10s), to yield a measure of percentage (fractional) change in CBF. Time series were averaged across trials according to stimulation condition. Area under the curve (AUC) and maxima for each response were calculated. All cases (n=6) were included in the final analysis.

6.7.4.2 Statistical analysis

Extracted maxima and AUC data were analysed in SPSS 23 with appropriate statistical tests dependent on experimental design. Normality and homogeneity of data were assessed prior to analysis. A p value of less than .05 was deemed significant. Additional t-tests (where applicable) were conducted to further probe differences between experimental conditions with correction for multiple comparisons (p value was divided by number of tests).

6.8 Results

6.8.1 Baseline cerebral blood flow

To assess any variation in baseline CBF between young and old LPS treated groups the average perfusion value was calculated across a 30s period prior to the onset of stimulation at the start and end of the experimental protocol. A one-way ANOVA on CBF baselines found a significant difference between groups at +4 hours ($F(1,12)=12.97$ p=.004) and +6 hours ($F(1,12)=11.40$, $p=.006$) post LPS treatment.

6.8.2 Haemodynamic responses to a short (2s) multifrequency stimulation paradigm

Multivariate analyses of variance (MANOVAs) were applied to HbO_2, HbR, HbT and CBF response maxima or minima (HbR) values in order to determine the effect of the animals' age at time of LPS treatment at 4 hours and at 6 hours following LPS administration. All cases (n=13) were included in the analysis. At 4 hours post injection, there was a significant effect of stimulation frequency on haemodynamic response magnitude: $F(20, 173.4) = 8.56$, $p <.001$; Wilks' $\Lambda = .103$ with significant effects for each haemodynamic response measure (Table 6.1). There was also a significant interaction effect of stimulation frequency and age at time of treatment ($F(20, 173.4) = 2.07$, $p =.007$; Wilks' $\Lambda = . 492$). Age at time of treatment itself did not result in a significant change in the magnitude of the haemodynamic response $F(4, 8) = 0.91$, $p =.504$; Wilks' $\Lambda = .688$.

At 6 hours post injection, there was a significant effect of stimulation frequency on haemodynamic response magnitude: ($F(20, 173.4) = 8.55$, $p <.001$; Wilks' $\Lambda = .103$) with significant effects for each haemodynamic response measure (Table 6.1). There was a marginally non-significant interaction effect between stimulation frequency and age at time of treatment ($F(20, 173.4) = 1.51$, $p =.082$; Wilks' $\Lambda = .587$) however univariate tests show that all measures have a significant interaction effect of stimulation frequency and age at time of treatment (Table 6.1). Age at time of treatment itself did not result in a significant change in the magnitude of the haemodynamic response $F(4, 8) = 0.35$, $p =.841$; Wilks' $\Lambda = .853$.

Post hoc analysis of individual stimulation frequencies using independent t-tests (Figure 6.1 A) indicate significant increases in response magnitude for HbO_2 at 20Hz (p=.045) and 40Hz (p=.014) and for HbT (p=.028) and CBF (p=.004) at 40Hz at +4 hours. Furthermore post hoc analysis indicate a significant decrease in HbR response magnitude at 20Hz (p=.030) and 40Hz (p=.005) at +4 hours. A representative haemodynamic response profile at a 10Hz stimulation frequency is plotted in Figure 6.1 B for each measure.

Table 6.1. Summary of univariate statistical analyses of haemodynamic responses to a mixed frequency 2s stimulation paradigm for LPS treated 12-month/ 3-month old animals. *Denotes a significant effect.

Time	Factor		*df*	*F*	*p*
+4 hours after injection	**Frequency**	HbO_2	5,55	32.23	<.001*
		HbR	5,55	33.34	<.001*
		HbT	5,55	27.79	<.001*
		CBF	5,55	27.00	<.001*
	Frequency x Age at time of treatment	HbO_2	5,55	6.12	<.001*
		HbR	5,55	7.18	<.001*
		HbT	5,55	4.94	=.001*
		CBF	5,55	2.64	=.033*
	Age at time of treatment	HbO_2	1,11	1.86	=.200
		HbR	1,11	2.62	=.134
		HbT	1,11	0.98	=.344
		CBF	1,11	2.96	=.113
+6 hours after injection	**Frequency**	HbO_2	5,55	21.45	<.001*
		HbR	5,55	23.86	<.001*
		HbT	5,55	15.25	<.001*
		CBF	5,55	19.13	<.001
	Frequency x Age at time of treatment	HbO	5,55	4.04	=.003*
		HbR	5,55	4.73	=.001*
		HbT	5,55	3.28	=.012*
		CBF	5,55	2.47	=.044*
	Age at time of treatment	HbO	1,11	0.01	=.935
		HbR	1,11	0.01	=.921
		HbT	1,11	0.05	=.836
		CBF	1,11	0.35	=.564

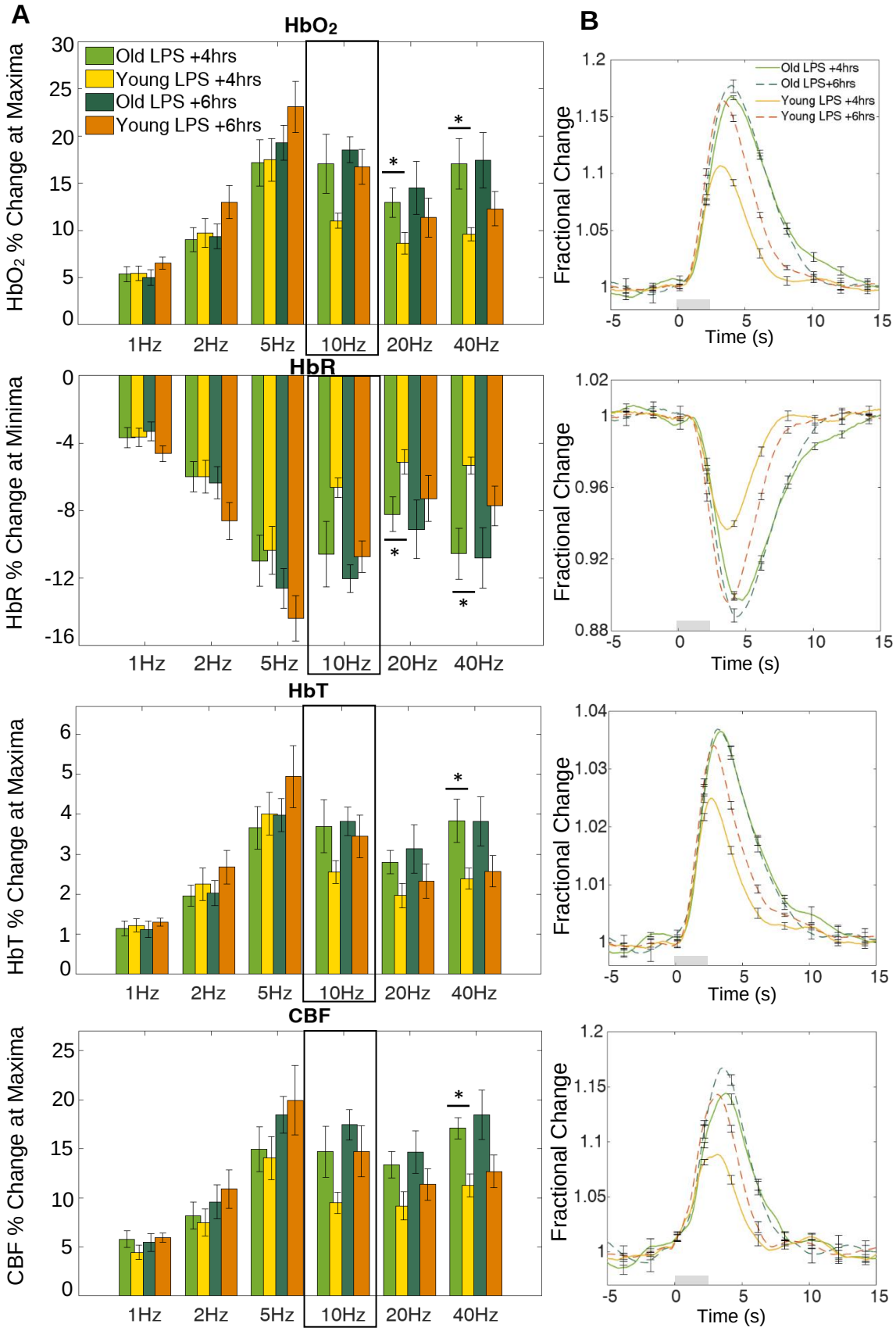

Figure 6.1. Haemodynamic response to 2s whisker stimulation at six frequencies at +4 and +6 hours for 12-month (old LPS) and 3-month (young LPS). (A) Bar charts show % change at maxima or minima (HbR). Post hoc analysis on stimulation frequencies reveal significant effects at 20 and 40Hz (*denotes significant differences at $p<0.04$) between groups. **(B)** Representative 10Hz time series showing mean fractional changes. Grey rectangle indicates stimulation onset/offset and error bars indicate standard error of the mean.

6.8.3 Haemodynamic responses to a long (16s) stimulation paradigm

MANOVAs were used to determine significant effects of age at time of treatment on the magnitude of the haemodynamic response (for HbO_2, HbR, HbT and CBF measures) to 16s whisker stimulation at +4 hours and at +6 hours post treatment. An AUC measure was used to quantify responses to 16s stimulation. Age at time of treatment had no effect on response magnitude at 4 hours post treatment ($F(4, 8) = .541$, $p = .711$; Wilks' $\Lambda = .787$). Effects for age at time of treatment for each measure were also not significant (HbO_2 [p=.272], HbR [p=.308], HbT [p=.281], CBF [p=.215]). At 6 hours age at time of treatment had no effect on overall response magnitude ($F(4, 8) = 1.04$, $p = .442$; Wilks' $\Lambda = .657$) (Figure 6.2) but did have a significant effect on increasing HbO_2 (p=.045) and HbR (p=.044) response magnitudes (Figure 6.2 B). HbT was marginally not significant (p=.063), CBF was not significant (p=.162) although both measures appear to be following the same trend (increases) as HbO_2 and HbR data.

6.8.4 Haemodynamic responses to hypercapnia

Analysis of variance (MANOVA) were used to determine significant effects of age at time of treatment on haemodynamic response magnitude (for HbO_2, HbR, HbT and CBF variables) to a 30s hypercapnia challenge at +4 hours and at +6 hours post treatment. Maxima (or minima) values were used to quantify the response. Age at time of treatment had no significant effect on response magnitude at 4 hours ($F(4,8)=1.24$, p=.366.; Wilks' Λ =.617) or at 6 hours ($F(4,8)=0.95$, p=.485; Wilks' $\Lambda = .679$) (Figure 6.3 A) and effects for each measure were also not significant (HbO_2 [+4hrs: p=.259; +6hrs: p=.333], HbR [+4hrs: p=.207; +6hrs: p=.419], HbT [+4hrs: p=.486; +6hrs: p=.396], CBF [+4hrs: p=.638; +6hrs: p=.344]) (Figure 6.3 B).

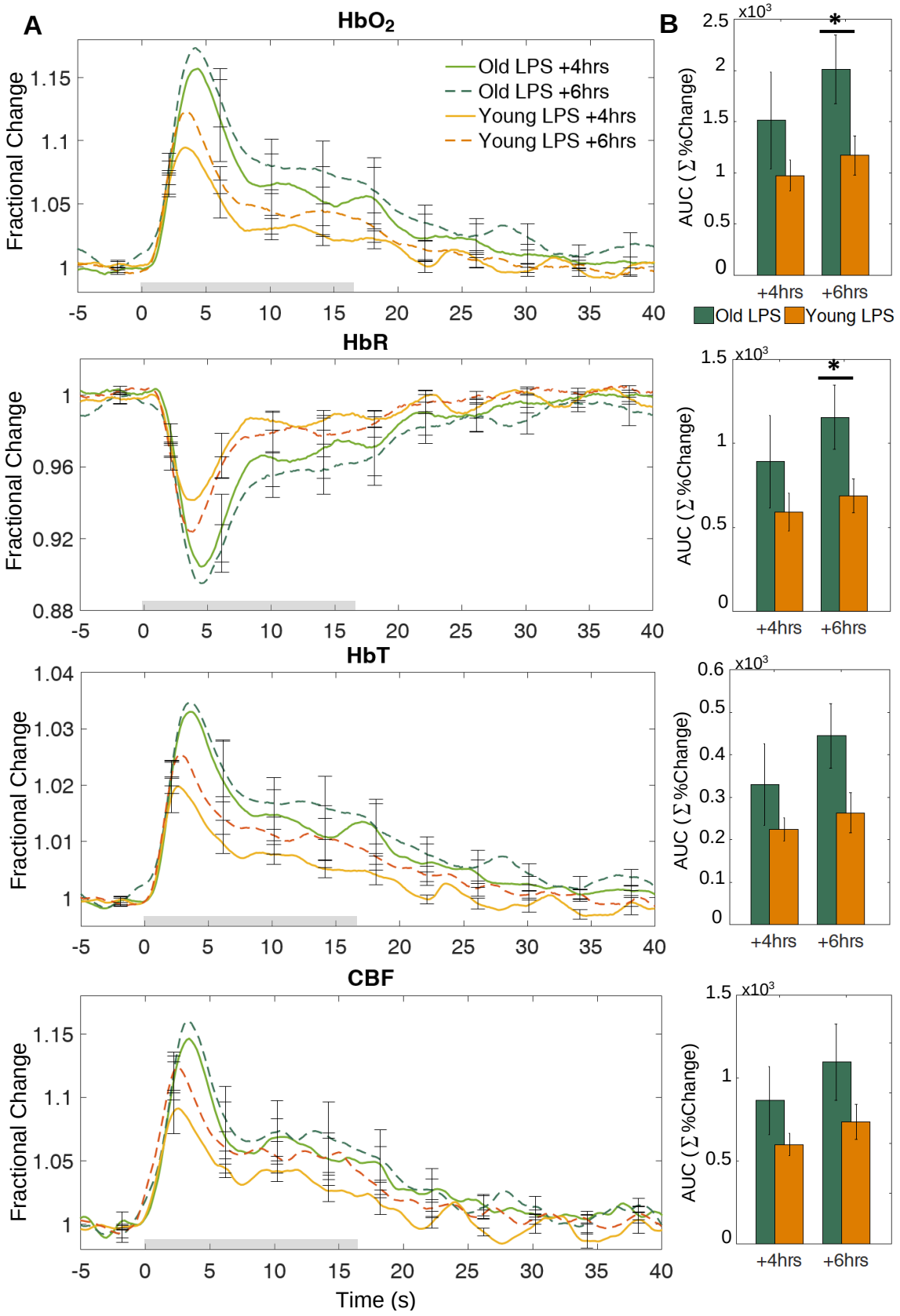

Figure 6.2. HbO_2, HbR, HbT and CBF responses to 16s whisker stimulation, at 10Hz, at +4hrs and +6hrs of LPS administration for 12-month (old LPS) and 3-month (young LPS) animals. (A) Time series show mean fractional changes and **(B)** Bar charts show change in area under the curve (AUC, units are summed percentage change). Grey rectangle indicates stimulation onset/offset. Error bars represents standard error of the mean. *Represents a significant difference at $p<0.05$ between groups.

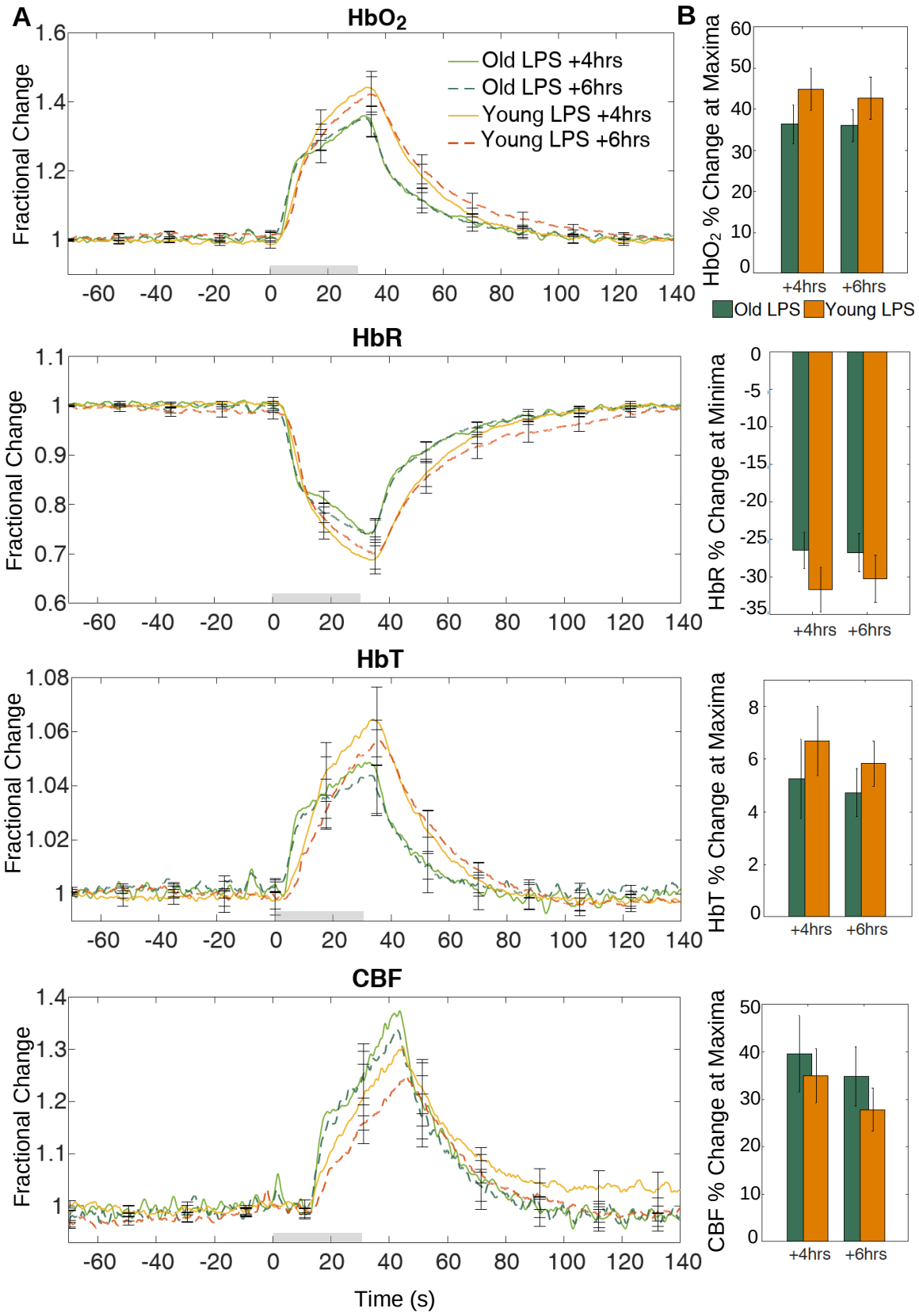

Figure 6.3. HbO_2, HbR, HbT and CBF responses to hypercapnia at +4hrs and +6hrs of LPS administration for 12-month (old LPS) and 3-month (young LPS) animals. (A) Time series show mean fractional changes and **(B)** Bar charts show change in area under the curve (AUC, units are summed percentage change). Grey rectangle indicates the 30s CO_2 challenge onset/offset. Error bars represents standard error of the mean.

6.8.5 $CMRO_2$ estimate

$CMRO_2$ changes were estimated (as described in Section 2.6.3) at both time points (+4 and +6 hours post injection) and for both 12-month and 3-month LPS treated animals (Figure 6.4). Response maxima was analysed with one-way ANOVA. Results reveal non-significant effects between groups at +4 hours ($F(1,12)=0.38$, $p=.550$) and at +6 hours ($F(1,12)=0.46$, $p=.513$) after treatment.

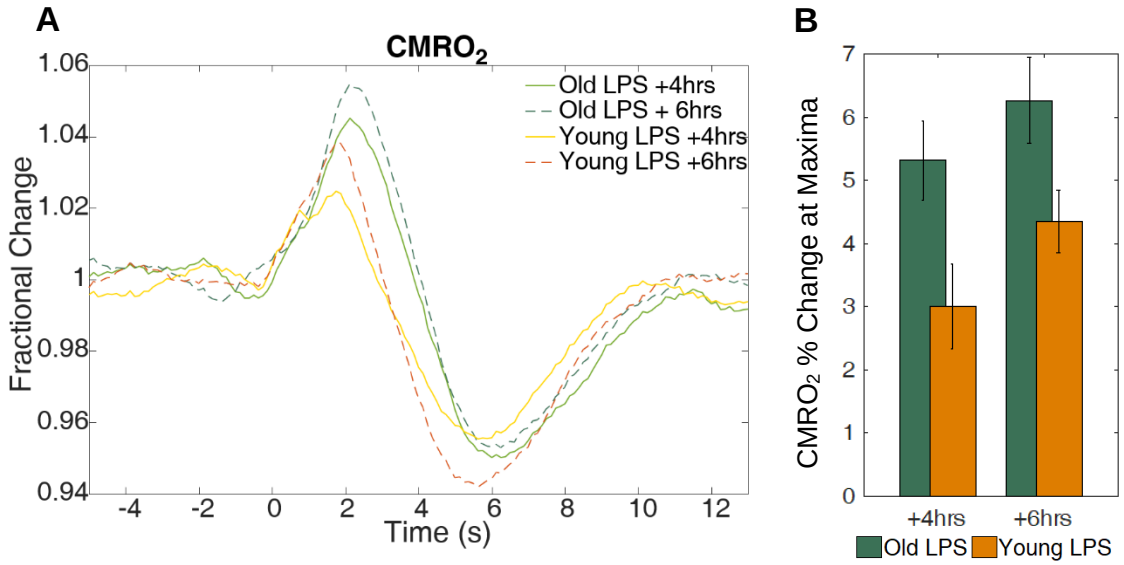

Figure 6.4. $CMRO_2$ estimation at +4hrs and +6hrs of 12-month and 3-month LPS treated animals. (A) Time series of $CMRO_2$ showing fractional change and **(B)** Bar chart showing percentage change at maxima.

6.9 Discussion

The main finding of this study was an interaction of age and stimulation frequency upon the magnitude of haemodynamic responses in animals acutely treated with LPS, such that the response profile across a range of stimulus inputs was modulated by age. This finding is in agreement with previous results (Section 4.9.1) but furthermore builds upon these findings suggesting that LPS mediated alterations in neurovascular function may occur more rapidly in a middle-aged cohort than in a young cohort. Furthermore long (16s) stimulation experiments suggest that inflammation in early ageing may impact upon long-latency changes in neurovascular coupling, although these findings require validation with an appropriate aged-matched (saline treated) control group. These results may thus have direct implications for human neuroimaging studies conducted in middle-aged individuals which utilise stimuli of such longer-durations. Lastly, CO_2-evoked changes in haemodynamic measures and $CMRO_2$ estimate results remain in line with those observed in young LPS treated animals. Again, both findings require further investigation with the addition of an aged matched (saline treated) control group to directly separate changes to neurovascular function which are mediated by early ageing alone from those evoked by an inflammation-ageing interaction.

6.9.1 Changes in baseline CBF

Baseline CBF analysis revealed a significant change (decrease) in baseline CBF for 12-month treated LPS animals (Section 6.8.1) when compared to 3-month treated LPS animals. This difference could be attributable to age as Chapter IV results (Section 4.8.1) show that LPS treatment does not cause a significant change in baseline CBF. An aged matched control group treated with saline is needed to correctly inform upon this finding and to clarify if this result is dependent on age alone or may be caused by an inflammation-age interaction. As the BOLD response utilises resting state as a baseline measure to infer changes in a given region of interest during activation (D'Esposito, Deouelle & Gazzaley, 2003) these results underline the need for caution when comparing differences in resting state CBF between aged populations.

It should, however, be noted that comparing CBF baseline changes across animals with LSCI methods is challenging. LSCI units are arbitrary and will vary across imaging sessions. Care was taken to implement a consistent experimental set up and set of imaging parameters across animal groups (see Section 2.3.1.1) therefore providing reassurance that this change in baseline CBF is a genuine effect. Furthermore changes in baseline CBF

as early as 8-12 months of age have been previously reported in mice (Balbi et al., 2015) and have also been observed in middle-aged humans (Schultz et al., 1999).

6.9.2 Alterations in neurovascular function occur earlier in 12-month aged LPS-treated animals

LPS treatment significantly alters haemodynamic response function and is in agreement with previous findings from this thesis (Chapter IV, Section 4.9.1). Altered response patterns can be qualitatively inspected from the bar charts (Figure 6.1) which display response magnitudes at each stimulation frequency. Interestingly this alteration in neurovascular function occurs at both 4 and 6 hours after LPS treatment (this effect was only significant at 6 hours in young LPS/saline treated animals). This suggests that age significantly accelerates neurovascular dysfunction, whereby age at time of treatment significantly impacts upon how stimulation inputs are converted to haemodynamic response functions as early as 4 hours following LPS administration. This effect furthermore remains present at the 6 hour time point. Many NVU cellular changes are known to occur in ageing. Astrocytes and microglia become primed, whereby their lowered activation threshold results in a heighted inflammatory response when triggered (Frank et al., 2010). Furthermore, ECs mediate the development of a chronic inflammatory response in the brain by losing contact with the BBB enabling infiltration of serum proteins (Sohrabji et al., 2013). It is possible that in early ageing these processes have already begun to develop and could therefore underlie the accelerated neurovascular response changes observed in 12-month LPS treated animals. Whereby neuroimmune actions, to the same level inflammatory challenge, are implemented by the NVU faster and more acutely, *speeding up* alterations in neurovascular function. With the addition of an aged-matched (saline) control group, a detailed IHC study, as conducted in Chapter V of this thesis, could be employed to investigate NVU cell morphology in early ageing and assess how underlying priming or morphological changes exacerbate the response to an acute inflammatory challenge.

By inspecting the haemodynamic profile (time series) of the short (2s) multifrequency data (Figure 6.1 B) it can be qualitatively noted that haemodynamic responses between 4 and 6 hours for middle-aged animals remain at the same peak level across time, whereas responses from young LPS-treated animals continue to increase. It would thus be interesting to measure *in vivo* haemodynamic changes for longer durations across aged groups to assess the temporal evolution and resolution of an acute inflammatory challenge and investigate if ageing has an effect upon its resolution.

Again in agreement with previous studies (Spain et al., 2015; Martin et al., 2006) and previous thesis results (Figure 4.1) multifrequency data shows frequency dependent effects, with significant difference between groups emerging at 20Hz (HbO_2, HbR) and 40Hz (all measures). These data may indicate that with ageing higher frequencies may be more suited to investigate neurovascular coupling, however these findings should be confirmed by including an appropriate aged-matched control group to ascertain that these results are due to ageing alone and are not instead mediated by an inflammation-ageing interaction.

6.9.3 Early ageing may impact upon longer-latency changes in neurovascular coupling

Age at time of treatment had a significant effect on HbO_2 and HbR response magnitudes, with a marginally not significant effect for HbT and a strong trend in CBF data in the long (16s) stimulation paradigm (Figure 6.2). This effect was not present in young saline/LPS treated animals. As such these results suggest that age at time of treatment significantly impacts upon longer-latency changes in neurovascular coupling which can't be assessed with short 2s stimulations. Again the addition of an aged matched control group will elucidate if these long-latency changes can be attributed to ageing alone or are mediated by an age-inflammation interaction. Examining changes in neurovascular coupling in long-latency stimulations may be particularly important for human neuroimaging studies investigating haemodynamic responses in middle-aged (and possible ageing) cohorts as these studies often employ stimulations paradigms of such longer durations.

6.9.4 Haemodynamic responses to hypercapnia are not significantly different between 12-month and 3-month old LPS treated animals

This study found no differences in the response to hypercapnia between 12-month and 3-month aged animals treated with LPS (Figure 6.3); suggesting that age at time of LPS treatment does not significantly change CO_2-mediated haemodynamic responses. Nevertheless, two important effects still require investigation. Firstly, how early ageing impacts upon CO_2-mediated changes in haemodynamic measures. From previous research, it can be hypothesised that by directly comparing between 12-month and 3-month control (saline treated) animals no effect of age will be present, as 12-month old mice show no changes in CBF responses following a CO_2 reactivity test (Balbi et al., 2015). CO_2 induced changes in CBF have only been shown to occur in late ageing (24 months) (Park et al., 2007) and have been attributed to the brain susceptibility to vascular insufficiency and ischemic injury (Farkas & Luiten, 2001) coupled with changes to the vasculature, including

narrowing and stiffening of vessels (Hajdu, Heistad, Siems, & Baumbach, 1990; Hutchins, Lynch, Cooney, & Curseen, 1996; Park et al., 2007). Secondly, if an acute systemic inflammatory challenge in middle age alters the 'baseline' response to hypercapnia by comparing 12-month aged saline/LPS treated rodents and determine how this effect may impact upon neurovascular function and neurovascular coupling.

6.9.5 $CMRO_2$ estimates in middle-aged LPS treated animals are in line with those observed in young LPS treated animals

12-month and 3-month treated animals showed no significant difference in $CMRO_2$ estimate maxima (Figure 6.4). Furthermore qualitative inspection of the shape of the curve reveals a very similar response profile between groups. This data therefore suggests that age at time of treatment does not appear to impact upon the $CMRO_2$ estimate. This provides reassurance that the change in metabolic demand observed between saline and LPS treated animals in Chapter IV (Section 4.8.6) is a treatment mediated effect. Without an appropriate aged-matched control group it is difficult to assess if an acute systemic inflammatory challenge administered to a middle-aged cohort will lead to an alteration in how oxygen delivery is matched to metabolic demand as ageing alone will undoubtedly impact upon this relationship. As such an appropriate aged-matched (saline treated) control group is need to assess any possible age-differences in the $CMRO_2$ estimate.

6.9.6 Future work

The addition of a control group. The addition of a control group would enable the characterisation of early-ageing changes in the brain, thereby quantifying baseline CBF, metabolism and cellular age-related changes which could then be directly compared to the already acquired measurements in young control animals (Chapter IV and V). Furthermore, the addition of a control group would enable interrogation of how an acute systemic inflammatory challenge in early-ageing impacts upon neurovascular function, clarifying its effects on long-latency changes in coupling, hypercapnia and $CMRO_2$.

IHC and gene expression investigation. A detailed investigation via IHC as employed in Chapter V would enable characterisation of NVU cellular change in early ageing and interrogate how morphological and priming exacerbates neuroimmune responses to an acute inflammatory challenge. This study would thereby help to clarify how early ageing *speeds up* the acute effects of a systemic inflammatory challenge on neurovascular response. Gene expression studies would offer an additional characterisation of early ageing-dependent brain changes and jointly with IHC data relate how cellular and gene expression results translate to haemodynamic changes measured *in vivo.*

Developing a longitudinal chronic model. Similarly to Chapter IV this study could be expanded into a chronic model in order to further increase its relevance to human ageing and ageing-related disease development. Furthermore, research has shown that repeated infections across the life span significantly increase the risk of developing AD (Dunn et al., 2011). Notwithstanding such evidence, there are currently no studies that have implemented longitudinal murine models of repeated infections across the life span. The development of this type of study design allows a more naturalistic way of modelling infections as they occur *in life* thereby increasing its translation to human disease processes and human ageing. This type of design could furthermore be developed to include older age cohorts (>18 months), which are known to present with functional cellular changes coupled with alterations in CBF and neurovascular function (as addressed in Section 6.2), to investigate how ageing-driven changes are affected and possibly exacerbated by inflammation. This design could then be finally extended into disease models, including AD to assess the impact of inflammation on an already challenged NVU and how this may exacerbate disease stage and development.

Assessing vascular fatigue. Balbi et al. (2015) reported that 12-month old mice displayed vascular fatigue, whereby they showed compromised maintenance of CBF responses over time. It may be interesting to assess if the same vascular fatigue effect is present in 12-month aged rats and investigate how an acute inflammatory challenge may exacerbate this difference. Furthermore investigation upon the mechanisms by which this vascular fatigue occurs is warranted, as this mechanism may be explained by structural damage to the NVU, impaired neuron-astrocyte-vasculature signalling, vascular wall dysfunction or by defective NO signalling (Balbi et al., 2015) and may change in disease-related processes.

6.9.7 Conclusion

In conclusion these results have demonstrated an alteration in neurovascular function, showing that age at time of LPS treatment significantly alters how stimulus inputs convert to haemodynamic response functions. Furthermore age appears to accelerate the acute response to LPS as neurovascular function alterations were already present at four hours after LPS treatment. Lastly these results demonstrate that age at time of treatment has a significant effect on measured HbO_2 and HbR variables during a long (16s) stimulation paradigm, suggesting a change in the neurovascular coupling relationship which underlies long-latency responses. These results require validation with the addition of an aged-matched (saline treated) control group to ascertain if these effects are mediated by ageing alone or by an inflammation-ageing interaction.

Chapter VII

General Discussion and Conclusions

7.1 Chapter summary

The previous chapters have described and discussed in detail the research background, methodology and experimental results of three manipulations to assess changes to neurovascular function and neurovascular coupling. This final chapter draws together the main research findings within each chapter and discusses their implications within the wider field of neurovascular research. It will furthermore discuss the link between cholinergic (dys)function and inflammation, proposing a final study combining cholinergic modulation and systemic inflammation into one model. Finally it will consider how the thesis findings may impact upon the interpretation of neuroimaging signals in human disease and help in the development of new imaging biomarkers.

7.2 Introduction

The **overarching aim** of this thesis was to utilise non-transgenic rodent models relevant to AD to assess *in vivo* neurovascular function and neurovascular coupling changes. The previous chapters have provided an overview of the research within the field of neurovascular function and coupling (Chapter I) as well as important elements of pathology associated with AD including cholinergic dysfunction, inflammation and ageing. It lastly gave an overview of the methodology (Chapter II) employed before presenting the relevant experimental results for each chapter. Each experimental chapter provides an in-depth discussion in relation to the research outcomes, therefore this final chapter will briefly review the thesis major findings and discuss their broader implications in neurovascular research. It will discuss the link between cholinergic (dys)function and inflammation, proposing the development of an additional rodent model and evaluate how the thesis findings may be relevant to the interpretation of neuroimaging signals in human disease and for the development of new imaging biomarkers.

7.3 Reduced cholinergic function leads to neurovascular uncoupling

The study conducted in Chapter III aimed at identifying the effects of pharmacological manipulations of ACh levels in the rat brain upon neuronal, haemodynamic and neurovascular coupling measures. This was motivated by research showing that disruption of the cholinergic system may lead to alterations in neurovascular coupling because of the known vasoactive properties of ACh (Bell et al., 2006; Farkas et al., 2001). Furthermore the study aimed to identify neurovascular coupling effects of donepezil (currently the only available treatment for AD) as its effects on neurovascular function have not been previously investigated. By identifying any possible neurovascular coupling effects *in vivo* this study aimed to inform upon the interpretation of imaging signals that use haemodynamics as proxy measures of neuronal activity (fMRI, PET) to acquired data from AD patients or other groups which present with cholinergic deficiencies. It is also important to consider the impact of acetylcholinesterase treatments upon functional imaging signals.

The study employed a repeated-measures design by concurrently imaging CBF changes and neuronal activity in the rat somatosensory cortex under either a cholinergic agonist (donepezil) or antagonist (scopolamine) treatment whilst investigating functional activation using a range of sensory stimuli. Results reveal haemodynamic and neuronal signal changes to scopolamine and donepezil administration. Altered response patterns for both pharmacological manipulations are qualitatively indicated by inspecting the bar

charts plotting CBF response magnitudes at each stimulation frequency (Figure 3.1) and similar effects are apparent for neuronal response data (Figure 3.3). Direct comparison across haemodynamic and neuronal data sets was challenging due to the range of sensory stimuli employed in this study, which is not routinely employed in neurovascular coupling research (see Sutherland et al., 2017; Lecrux et al. 2017; Sharp et al., 2015). The use of a multiple frequency stimulation approach is however a strength of this study as the frequency dependent effects observed for both scopolamine and donepezil treated groups highlight the underlying complexity of the neurovascular coupling relationship.

Furthermore upon plotting trial by trial haemodynamic and neuronal data together (Figure 3.5) a change in the neurovascular coupling relationship under scopolamine administration was revealed. The difference in the linear regression model before and after administration of scopolamine demonstrates an alteration of neurovascular coupling following pharmacological antagonism of brain acetylcholine by scopolamine, where stimulus evoked changes (increases or decreases) in neuronal demand are not accompanied by concomitant changes in CBF. This alteration was not apparent when analysing trial averaged haemodynamic and neuronal activity data independently, thereby suggesting that important effects of experimental manipulation upon relationships between neurophysiological parameters may be masked by trial averaging, where such features are discarded as noise.

These findings also reveal that donepezil treatment (at the current dose and modelled in a healthy animal) does affect the relationship between CBF and neuronal activity changes. Thereby this seems to suggest that changes in the magnitude of haemodynamic (including fMRI) signals in human or preclinical studies in response to cholinergic agonists do reflect changes in underlying neuronal activity, rather than effects on, for example, vascular reactivity.

Finally these findings support the notion that reduced cholinergic modulation of neurovascular function may be an important component of neurodegenerative diseases such as AD, highlighting a role for cholinergic drugs in normalising neurovascular function. An important extension of this research will be to determine if donepezil treatment is protective of neurovascular function under conditions of cholinergic loss (or blockade) either by pre-treatment with AChE antagonists or directly applied to an AD murine model.

7.4 An acute systemic inflammatory challenge is associated with *in vivo* haemodynamic changes and with significant underlying changes to the status of the NVU

The studies conducted in Chapter IV and V were aimed at identifying the effects of an acute systemic inflammatory challenge upon neurovascular function (Chapter IV) and NVU health (Chapter V) and relate how each approach (*in vivo* imagining and IHC) informs upon the understanding of the underlying changes from single cell to whole brain haemodynamics. Understanding the effects of a systemic inflammatory response, and subsequent neuroinflammatory processes upon NVU health and function *in vivo* is timely (and currently absent from the literature) as systemic inflammation has been strongly linked to the development of pathologies such as AD (Dunn et al., 2005) and has been shown to dramatically increase cognitive decline in AD patients (Holmes et al., 2009).

The *in vivo* component of the study measured haemodynamic changes (HbO_2, HbR, HbT and CBF,) in groups of LPS or saline challenged animals across two time points (+4 hours and +6 hours). *In vivo* results reveal an alteration in neurovascular function where LPS treatment significantly altered how stimulus inputs convert to haemodynamic response functions. This change is indicated by inspecting the bar charts plotting haemodynamic response magnitudes at each stimulation frequency (Figure 4.1). An estimate of $CMRO_2$ (Figure 4.4) suggested alterations in how oxygen delivery is matched to metabolic demand under an acute systemic inflammatory challenge. These results are relevant to fMRI research conducted in subjects or clinical cohorts with a systemic inflammatory response as they show changes in underlying fMRI signals ($CMRO_2$ and CBV) following a systemic inflammatory challenge.

Furthermore results indicate a trend of reduced vascular reactivity under LPS treatment as LPS-treated animals had decreased CO_2-evoked CBF responses compared to saline-treated animals. This may indicate an alteration (decrease) in COX-1, which has been shown to play a critical role in hypercapnia-evoked CBF increases *in vivo* (Niwa et al., 2001; Howarth et al., 2017). Possible changes to COX-1 expression could be assessed via IHC methods. This could furthermore elucidate the role of astrocytes in mediating CO_2-evoked CBF responses under a systemic inflammatory challenge as these cells have been recently implicated in mediating hypercapnic vasodilation in health (Howarth et al., 2017).

In vivo non-invasive electrophysiological measures are warranted as a limitation of this study is a lack of direct measurement of neuronal activity. Estimates of metabolic activity such as $CMRO_2$ offer some degree of assessment of neurovascular function but do not

enable a deeper characterisation of the neurovascular coupling relationships as evaluated in Chapter III (Figure 3.5). Direct measurement of neuronal activity will reveal if under an acute systemic inflammatory challenge stimulus evoked changes in neuronal demand are accompanied by concomitant changes in CBF and how an *oversupply* of oxygen, as measured in LPS-treated animals, may lead to a disruption in neurovascular coupling. Advances in methods enabling non-invasive electrophysiological recordings will also revolutionise the study of neurovascular coupling in awake preparations, thereby reducing the effects of anaesthesia upon neurovascular function.

The IHC component of the study, utilising brains from the same animals, characterised NVU cellular changes (astrocytes, endfeet, microglia, ECs and pericytes) by assessing morphological and expressional changes. IHC results reveal a change in both astrocyte and microglia cell morphology, whereby both cell types exhibit characteristics of a reactive phenotype (swollen, enlarged cell body) and significant increases in GFAP and IBA-1 immunoreactivity. ECs also show a marked change under LPS administration, dramatically increasing their expression of ICAM-1 on vessels and microglia. Although only qualitatively assessed (due to methodological difficulties) astrocyte endfeet and pericytes also show changes in LPS treated animals with increased APQ4 and PDGFRβ immunoreactivity. This study concluded that due to ECs location (at the interface between brain and blood), their known involvement in various phases of the inflammatory response (Pober & Sessa, 2007), the significant proportion of LPS binding (75%) which occurs on the luminal surface (Banks & Robinson, 2010) and the marked increase in ICAM-1 immunoreactivity observed in this study, ECs are initiators and mediators of the acute systemic inflammatory response. Where alterations in function, signalling and gene expression in these cells would then propagate and instigate changes in the remaining NVU members (astrocytes, endfeet, microglia, and pericytes).

Notwithstanding, this conclusion requires validation. Gene expression studies looking at EC-specific transcriptomic changes trigged by systemic inflammatory challenges are warranted. Further characterisation of EC gene expression would provide additional insights into the phenotype of ECs in diseases with an inflammatory component and potentially delineate the propagation of the inflammatory response among the cellular constituents of the NVU. Furthermore large scale gene expression studies in astrocytes and microglia would enable characterisation of transcriptomic changes in glia phenotype.

Immunohistochemical changes in ECs and AQP4 expression have been key to help explain the changes in haemodynamic signals measured *in vivo*. EC activation plays a critical role in increasing blood flow during systemic inflammation (Pober & Cotran, 1990) and in the

regulation of sensory (Chet et al., 2014) and CO_2-evoked haemodynamic changes (Uekawa et al., 2016). As such increased expression of ICAM-1 which indicates EC activation may underlie the observed increases in haemodynamic signals and changes in the response to hypercapnia in LPS-treated animals. Further investigation relating EC involvement in mediating haemodynamic changes and neurovascular coupling in health will be key in understanding EC roles in mediating systemic inflammation and their impact upon neurovascular function and neurovascular coupling.

Increases in AQP4 expression may underlie changes in the relationship between astrocytes and blood vessels thereby impacting upon the regulation of CBF and neurovascular function. Additional assessment via a fluorescent dual label of AQP4 and COLL IV and additional characterisation of the distribution of AQP4 will help elucidate the effects of an acute systemic inflammatory challenge on neurovascular function. Furthermore 2-photon microscopy measuring changes in function, structure and communication between NVU cells will reveal inflammation-driven changes in the regulation of CBF and the vasodilatory response to neuronal activity which may result in neurovascular uncoupling. This is of particular importance as inflammation-driven changes in these vasoactive pathways still requires investigation and may be key in understanding the neurovascular coupling changes observed in AD.

AD is characterised by a chronic low-grade inflammatory response, thereby the results of this study may not be directly applicable in understanding how inflammation impacts upon the pathophysiology of the disease. Furthermore ageing is a key factor in both AD pathology and in inflammation. It is, however, important to remember that, as chronic and acute inflammation are not completely separate processes and share some of the same mediators, including EC activation (Pober & Sessa, 2007) NVU changes measured in either acute or chronic inflammatory states can inform upon the other. Thereby the acute alterations in *in vivo* neurovascular function, which arise from NVU cellular changes may also underpin the neurovascular changes observed in a chronic low-grade inflammatory response. As such future work should aim to extend this model to include a low-dose chronically treated group with different aged animals to maximise its relevance to human pathology and human ageing.

7.5 Early ageing 'speeds up' the acute effects of a systemic inflammatory challenge on neurovascular response

The study conducted in Chapter VI aimed at identifying effects of age at time of systemic inflammatory treatment upon alterations in neurovascular function by comparing

additional data acquired in 12-month aged LPS treated animals with previously acquired (Chapter IV) 3-month old LPS treated cases. Understanding how ageing impacts upon neurovascular function is of particular importance as systemic inflammation and ageing have been shown to be intimately linked, dramatically increasing the risk of developing conditions such as AD and in exacerbating cognitive decline (Elahy et al., 2015; Fong et al., 2009). Furthermore changes to CBF have been shown to occur in midlife (Schultz et al., 1999; Balbi et al., 2015) therefore this may represent an optimal time to implement interventions aimed at halting age-related inflammatory changes.

The current lack of an aged-matched (saline) control group for 12-month LPS treated animals from which to distinguish between ageing-related and inflammation-ageing interaction effects makes interpretation of findings challenging. However, utilising the same methodological set up to acquire haemodynamic responses across two time points results reveal specific interaction effects between age and frequency. In agreement with previous findings from Chapter IV, short (2s) multifrequency stimulation data reveal a change in neurovascular function (Figure 6.1). Furthermore these data reveal that this effect occurs faster (significant at 4 hours) and remains present at the 6 hour time point. This may therefore be indicative of early ageing *speeding up* haemodynamic changes associated with an acute systemic inflammatory challenge. This effect may be mediated by NVU cellular changes that are known to occur in ageing, in particular astrocyte and microglia priming (Harris, Choi & Brooks, 2015; Erdő et al., 2017) and the role of ECs in the development of a chronic inflammatory brain response (Sohrabji et al., 2013) (as discussed in Section 6.2.1). To investigate this further, a detailed IHC study, as conducted in Chapter V of this thesis, should be employed to investigate changes in NVU cells. Large scale gene expression analysis could furthermore reveal changes in glia and EC phenotype which will be more able to relate functional changes to alterations in *in vivo* neurovascular responses.

Furthermore, long (16s) stimulation data reveal a significant effect of age on HbO_2 and HbR measures and strong trends of the same effect in HbT and CBF results (Figure 6.2). This may in turn suggest that ageing impacts upon long-latency coupling changes. This effect, however, requires validation with an aged-matched control group to ascertain if such effect is mediated by ageing alone or by an inflammation-ageing interaction. These results are particularly salient for human neuroimaging research testing middle-aged (and possibly late-ageing) cohorts as these findings demonstrate a possible change in the coupling relationship that underlies long stimulation paradigms, which are routinely used in fMRI research.

7.6 The importance of stimulation paradigm choice to assess neurovascular function and neurovascular coupling

The studies conducted in this thesis have clearly shown stimulation dependent effects upon assessment of neurovascular function under three different manipulations. It has been shown that cholinergic, inflammatory and ageing manipulations lead to an alteration in how stimulus inputs convert to haemodynamic response functions thereby indicating altered neurovascular responses. Utilising a range of sensory stimuli as employed in the multifrequency paradigms in the three experimental chapters of this thesis enables a deeper understanding of the neurovascular coupling relationships by better assessing how the neurovascular system is responding to different levels of input. Multifrequency designs provide unrivalled information relating to the *in vivo* function of neurovascular processes compared to experiments which utilise a single stimulation intensity or protocol. This would provide improved assurance that findings are robust beyond specific stimulation parameters and improve comparability between studies as a response pattern across a range of stimulation frequencies is likely to be more robust than comparing across response size from a single stimulation.

Effects of different stimulation inputs have been previously reported when comparing neurovascular coupling relationships between awake and anaesthetised animals (Martin et al., 2006; 2013) and during serotonergic manipulations (Spain et al., 2015). Notwithstanding such research, the use of a dynamic range of sensory stimuli is not routinely employed in neurovascular coupling research (see Sutherland et al., 2017; Lecrux et al. 2017; Sharp et al., 2015) despite the use of multi-modal methods of imaging, electrophysiology and IHC to assess neurovascular function. This most likely arises from the difficulty in directly comparing across haemodynamic and neuronal data that employ a range of stimulations (increasing the complexity of the study design), the subsequent challenges of interpreting the effects and interactions between different sensory inputs and measured variables and finally how to translate these findings to indicate possible changes to neurovascular health. Despite these challenges, multifrequency paradigms provide substantially more information on the *in vivo* function of neurovascular responses than single stimulation protocols. As such choice of stimulation paradigm is an important consideration to increase comparability between studies and is especially relevant for neurovascular coupling research where effects of pharmacological or disease-related manipulations could be dependent on the properties of the stimulus protocol utilised.

7.7 The link between cholinergic (dys)function and inflammation

As previously described (Section 3.2) ACh, primarily synthesised in interneurons, has been implicated in multiple roles within the CNS including memory, attention, decision making and arousal. ACh is further synthesised by other cells including ECs and immune cells (Kawashima, Yoshikawa, Fujii, Moriwaki, & Misawa, 2007; Rosas-Ballina & Tracey, 2009) and has been shown to attenuate production of TNF, IL-Iβ, IL-6 and IL-18 in human macrophages and to not impact upon IL-10 release (Borovikova, Ivanova, Zhang, & Yang, 2000). This anti-inflammatory property of ACh has been linked to a periphery-to-brain communication system which has since been termed the *cholinergic anti-inflammatory pathway* (Borovikova et al., 2000). This pathway involving the vagus nerve, ACh and the nicotinic acetylcholine receptor subunit alpha7 (α7) would communicate via the afferent component of the vagus nerve to the brain conveying information regarding peripheral inflammatory processes enabling suppression of pro-inflammatory cytokine release (Wang, Yu, Ochani, & Amella, 2003). Support for a cholinergic blockade of inflammation arises from evidence showing attenuation of pro-inflammatory cytokine levels and improved survival in experimental models of sepsis as well as a reduction of IL-Iβ in blood and brain via the administration of AChEIs (Hofer et al., 2008; Pollak et al., 2005). Furthermore cholinergic drugs which act through α7 have been shown to significantly modulate inflammation (Rosas-Ballina & Tracey, 2009) and enhancement of ACh release in the brain attenuates systemic TNF in endotoxaemic rats and increments vagus nerve activity (Pavlov et al., 2006). In microglia, activation of α7 attenuated pro-inflammatory cytokine release (De Simone, Ajmone-Cat, Carnevale, & Minghetti, 2005; Shytle et al., 2004) and more recently α7 activation promoted LPS-induced conversion of microglia phenotype from M1 to M2 whereas knockdown of α7 abolished ACh-mediated production of IL-4 and IL-10 and attenuation of IL-1β and IL-6 (Zhang, Lu, Bian, Guo, & Zhu, 2017). This evidence demonstrates a strong link between cholinergic function and inflammation and could thus be used to develop *in vivo* models to investigate if cholinergic treatment may attenuate and potentially reverse inflammation-derived changes to neurovascular function.

7.7.1 Developing a joint *in vivo* animal model of cholinergic dysfunction and inflammation

Galantamine, an AChEI currently used for the treatment of mild to moderate AD has been shown to attenuate serum TNF and IL-6 levels in a murine model of endotoxaemia (Pavlov et al., 2009) and the release of pro-inflammatory cytokines in cultured microglia (Giunta et al., 2004). It would therefore be interesting to validate if the same effects are observable

with other AD AChEIs (such as donepezil and rivastigmine) and to extend this research to an animal model to interrogate and define the mechanisms behind the anti-inflammatory role of AChEIs *in vivo*. A study design including both a cholinergic modulation and an inflammatory challenge in the same animal could provide further evidence supporting cholinergic mediation of inflammation as well as investigating the joint effects and interconnectivity between cholinergic (dys)function and inflammation on the NVU and upon neurovascular coupling. It would thus be interesting to establish if treatment with AChEIs following an LPS pre-treatment would ameliorate and/or attenuate an LPS induced inflammatory response and conversely if pre-treatment with an ACh antagonist such as scopolamine could exacerbate an LPS-induced inflammatory response thereby further impacting upon NVU health, function and neurovascular coupling. Findings from this research could additionally be compared to the individual effects of ACh and inflammation modulations, as investigated and reported in this thesis. Furthermore, the aforementioned studies reporting attenuation of pro-inflammatory cytokines only focus on severe models of inflammation such as sepsis and endotoxaemia in young animals or cultured microglia, thus validation of a cholinergic-based modulation on inflammation in a low-grade chronic model and in ageing requires validation. Such research will undoubtedly increase its translational value to human AD pathology and aetiology.

7.8 Translation of preclinical research to humans in health and disease

7.8.1 The challenge of BOLD fMRI in disease and ageing

BOLD fMRI and other imaging methods that rely on haemodynamic changes (including PET imaging applications) have a significant advantage of revealing changes in function within the human brain over preclinical research, which must overcome the challenges of translating *in vivo* animal findings to humans. This unique capability has unsurmountable potential to provide early diagnostic, treatment efficacy or basic research insights into a number of disease processes. However, its success relies on a sound understanding of what these measured imaging signals convey about health and disease-related processes within the CNS. This thesis reveals that in the context of three processes (cholinergic alterations, inflammation and ageing), which are known to be important components in the development or pathogenesis of AD, neurovascular function is altered. This has important implications for how functional neuroimaging is used in the future, as factors including age and disease which impact upon resting state CBF, haemodynamic responses, vascular structure and neurovascular coupling may hinder the ability to attribute changes in neuroimaging signals to changes in neuronal activity (D'Esposito, Deouelle & Gazzaley, 2003). This thesis results furthermore challenge overly simplistic interpretations of (e.g)

BOLD signals as indicating straightforward increases or decreases in neuronal activity in control compared to patient groups. Secondly, given that neurovascular disruption is an increasingly recognised and early component of many neurodegenerative diseases this thesis findings may provide an opportunity to develop new neurovascular biomarkers, aimed at improving specificity of clinical diagnosis, prediction of disease progression and potentially increase the sensitivity of fMRI and SPECT to measure neuronal dysfunction alongside haemodynamic changes. Finally, the findings of this thesis also suggest that assessment of neurovascular function using single readout approaches (e.g. just CBF or just BOLD) may be problematic, as the significant changes that occur are found in the relationships between neuronal and different vascular (e.g. CBF & CBV) elements.

7.8.2 Awake imaging – an anaesthetic-free animal preparation

Perhaps the most challenging aspect of relating studies from invasive *in vivo* animal models to human functional imaging studies is the predominant use of anaesthesia in animal preparations. Anaesthesia is widely used for invasive *in vivo* animal experiments (Vanzetta & Grinvald, 2008) even though it's known to affect cerebral haemodynamics, vascular reactivity, physiology, brain metabolism and neurovascular coupling (Masamoto & Kanno, 2012; Masamoto, Obata, & Kanno, 2010). Furthermore as different anaesthetics have different action sites, their effects on haemodynamics and neuronal excitability can differ dramatically (Chen, Friedman, Ramsden, LaMotte, & Roe, 2001a). Thus discrepancies in interpreting the mechanism/s of neurovascular coupling may result as a direct consequence of using different anaesthetic regimes. It has been shown that CBF responses are larger in un-anaesthetised animals (Nakao et al., 2001) and LFP neuronal responses do not attenuate in awake compared to anesthetised animals (Martin et al., 2013). Lastly, the role of NO in controlling stimulus-evoked CBF responses, thereby impacting upon neurovascular coupling, appears to play a dominant role in anesthetised preparations (urethane) (Gerrits, Stein, & Greene, 2001) but less so in awake experiments (Nakao et al., 2001). It is thus imperative to consider how anaesthesia may impact upon and modulate neurovascular coupling and take steps to minimise its effects.

When the use of anaesthesia is unavoidable, due to the application of invasive methods, such as the ones utilised in this thesis and/or to reduce movement artifacts, choice of aesthetic regime is vital. By choosing an anaesthetic which shows a high degree of concordance between evoked somatosensory responses in awake and anesthetised conditions, such as urethane, (Angel et al., 1982) will help to minimise anaesthetic effects and will more accurately inform and related findings to BOLD fMRI and BOLD phMRI data in both animal and human imaging studies.

The development of awake imaging preparations which are as stable and which can offer the same level of control as anaesthetised experiments will be key in understanding how anaesthesia impacts upon neurovascular measures. Efforts to overcome this limitation has seen a surge in the development of awake imaging preparations in neurovascular research both in mouse (Carandini et al., 2015; Haider, Häusser, & Carandini, 2013; Pisauro, Dhruv, Carandini, & Benucci, 2013; Sharp et al., 2015) and in rat (Chang et al., 2016; Martin et al., 2006; Martin et al., 2013; Urban et al., 2015). In time, the refinement of anaesthetic-free preparations in neurovascular research will not only inform and help to better interpret findings from studies utilising anaesthetised animals but ultimately increase translatability to awake human imaging studies.

7.9 Final conclusions

This thesis has given an insight into *in vivo* neurovascular changes that occur as a result of direct cholinergic or inflammatory challenges utilising a multimodal approach of imaging and electrophysiology measures. It has furthermore begun to characterise NVU cellular changes with immunohistological methods with the intention of relating how these alterations impact upon neurovascular function and neurovascular measures such as neurovascular coupling. It has also begun to investigate how ageing impacts upon neurovascular function changes that derive from underlying disease processes.

This thesis has demonstrated the importance of stimulus-protocol choice in neurovascular coupling research as all three investigated manipulations resulted in an alteration in how stimulus inputs convert to haemodynamic response functions. This finding underlines the complexity of the neurovascular coupling relationships which can't be assessed with the use of a single stimulus protocol, which is routinely used in neurovascular research. Choice of stimulation paradigm is therefore an important consideration as effects of pharmacological or disease-related manipulations could be dependent on the properties of the stimulus protocol utilised. Furthermore there is a pressing need to improve comparability between studies and assessment of changes in neurovascular function. As such a range of stimulation inputs will provide more robust effects than quantifying magnitude changes from a single stimulation. These results have furthermore highlighted important implications on how functional neuroimaging is used in the future, challenging simplistic interpretations of straightforward changes between haemodynamic responses and neuronal activity when comparing between control and patient cohorts. It finally outlines that single-readout approaches in both preclinical and human studies may be problematic as the findings of this thesis indicate that changes in neurovascular function relationships are found between neuronal and different vascular elements.

The importance of a multimodal approach in studying neurodegenerative disease processes is key and the results obtained in this thesis are an important first step in characterising changes associated with neurovascular function and neurovascular coupling under acute *disease processes*. Thus, an important next step is the development of these models into chronic preparations and ultimately in AD murine models, to maximise the translational value of preclinical neurovascular research to human pathology.

References

Abbott, N. J., Patabendige, A., Dolman, D., Yusof, S., & Begley, D. (2010). Structure and function of the blood–brain barrier. *Neurobiol Dis, 37*(1), 13-25.

Abbott, N. J., Rönnbäck, L., & Hansson, E. (2006). Astrocyte-endothelial interactions at the blood-brain barrier (Vol. 7, pp. 41-53): Nature Reviews Neuroscience.

Adlard, P. A., Tran, B. A., Finkelstein, D. I., Desmond, P. M., Johnston, L. A., Bush, A. I., & Egan, G. F. (2014). A review of β-amyloid neuroimaging in Alzheimer's disease. *Frontiers in neuroscience, 8*.

Agre, P., King, L. S., Yasui, M., Guggino, W. B., Ottersen, O. P., Fujiyoshi, Y., . . . Nielsen, S. (2002). Aquaporin water channels–from atomic structure to clinical medicine. *The Journal of physiology, 542*(1), 3-16.

Aguzzi, A., Barres, B. A., & Bennett, M. L. (2013). Microglia: scapegoat, saboteur, or something else? *Science, 339*(6116), 156-161.

Akiyama, H., Barger, S., Barnum, S., Bradt, B., Bauer, J., Cole, G. M., . . . Fiebich, B. L. (2000). Inflammation and Alzheimer's disease. *Neurobiol Aging, 21*(3), 383-421.

Amberg, G. C., & Navedo, M. F. (2013). Calcium dynamics in vascular smooth muscle. *Microcirculation, 20*(4), 281-289.

Angel, A., & Gratton, D., A (1982). The effect of anaesthetic agents on cerebral cortical responses in the rat. *British journal of pharmacology, 76*(4), 541-549.

Aoki-Yoshino, K., Uchihara, T., Duyckaerts, C., Nakamura, A., Hauw, J.-J., & Wakayama, Y. (2005). Enhanced expression of aquaporin 4 in human brain with inflammatory diseases. *Acta Neuropathol, 110*(3), 281-288.

Arendt, T., Bigl, V., Arendt, A., & Tennstedt, A. (1983). Loss of neurons in the nucleus basalis of Meynert in Alzheimer's disease, paralysis agitans and Korsakoff's Disease. *Acta Neuropathol, 61*(2), 101-108.

Arimura, K., Ago, T., Kamouchi, M., Nakamura, K., Ishitsuka, K., Kuroda, J., . . . Kitazono, T. (2012). PDGF receptor β signaling in pericytes following ischemic brain injury. *Current neurovascular research, 9*(1), 1-9.

Armulik, A., Abramsson, A., & Betsholtz, C. (2005). Endothelial/pericyte interactions. *Circulation research, 97*(6), 512-523.

Armulik, A., Genové, G., & Betsholtz, C. (2011). Pericytes: developmental, physiological, and pathological perspectives, problems, and promises. *Developmental cell, 21*(2), 193-215.

Armulik, A., Genové, G., Mäe, M., Nisancioglu, M. H., Wallgard, E., Niaudet, C., . . . Strittmatter, K. (2010). Pericytes regulate the blood-brain barrier. *Nature, 468*(7323), 557-561.

Aronoff, R., & Petersen, C. C. (2008). Layer, column and cell-type specific genetic manipulation in mouse barrel cortex. *Frontiers in neuroscience, 2*(1), 64.

Attwell, D., Buchan, A. M., Charpak, S., Lauritzen, M., Macvicar, B. A., & Newman, E. A. (2010). Glial and neuronal control of brain blood flow. *Nature, 468*(7321), 232-243. doi:10.1038/nature09613

Attwell, D., & Iadecola, C. (2002). The neural basis of functional brain imaging signals. *Trends Neurosci, 25*(12), 621-625.

Auguste, K. I., Jin, S., Uchida, K., Yan, D., Manley, G. T., Papadopoulos, M. C., & Verkman, A. (2007). Greatly impaired migration of implanted aquaporin-4-deficient astroglial cells in mouse brain toward a site of injury. *The FASEB Journal, 21*(1), 108-116.

Ayata, C., Dunn, A. K., Gursoy-Özdemir, Y., Huang, Z., Boas, D. A., & Moskowitz, M. A. (2004). Laser speckle flowmetry for the study of cerebrovascular physiology in normal and ischemic mouse cortex. *Journal of Cerebral Blood Flow & Metabolism, 24*(7), 744-755.

Ba, A. M., Guiou, M., Pouratian, N., Muthialu, A., Rex, D. E., Cannestra, A. F., . . . Toga, A. W. (2002). Multiwavelength optical intrinsic signal imaging of cortical spreading depression. *Journal of neurophysiology, 88*(5), 2726-2735.

Badaut, J., Fukuda, A. M., Jullienne, A., & Petry, K. G. (2014). Aquaporin and brain diseases. *Biochimica et Biophysica Acta (BBA)-General Subjects, 1840*(5), 1554-1565.

Badaut, J., Nehlig, A., Verbavatz, J. M., Stoeckel, M. E., Freund-Mercier, M. J., & Lasbennes, F. (2000). Hypervascularization in the Magnocellular Nuclei of the Rat Hypothalamus: Relationship with the Distribution of Aquaporin-4 and Markers of Energy Metabolism. *Journal of neuroendocrinology, 12*(10), 960-969.

Badea, A., Johnson, G. A., & Jankowsky, J. L. (2010). Remote sites of structural atrophy predict later amyloid formation in a mouse model of Alzheimer's disease. *Neuroimage, 50*(2), 416-427.

Bailey, T. L., Rivara, C. B., Rocher, A. B., & Hof, P. R. (2004). The nature and effects of cortical microvascular pathology in aging and Alzheimer's disease. *Neurological Research, 26*(5), 573-578. doi:10.1179/016164104225016272

Bajo, R., Pusil, S., López, M., Canuet, L., Pereda, E., Osipova, D., . . . Pekkonen, E. (2015). Scopolamine effects on functional brain connectivity: a pharmacological model of Alzheimer's disease. *Scientific reports, 5*.

Bakalova, R., Matsuura, T., & Kanno, I. (2002). The cyclooxygenase inhibitors indomethacin and Rofecoxib reduce regional cerebral blood flow evoked by somatosensory stimulation in rats. *Experimental Biology and Medicine, 227*(7), 465-473.

Balakrishnan, K., Verdile, G., Mehta, P. D., Beilby, J., Nolan, D., Galvão, D. A., . . . Martins, R. N. (2005). Plasma Aβ42 correlates positively with increased body fat in healthy individuals. *Journal of Alzheimer's Disease, 8*(3), 269-282.

Balasingam, V., & Yong, V. W. (1996). Attenuation of astroglial reactivity by interleukin-10. *Journal of Neuroscience, 16*(9), 2945-2955.

Balbi, M., Ghosh, M., Longden, T. A., Vega, M. J., Gesierich, B., Hellal, F., . . . Plesnila, N. (2015). Dysfunction of mouse cerebral arteries during early aging. *Journal of Cerebral Blood Flow & Metabolism, 35*(9), 1445-1453.

Ballabh, P., Braun, A., & Nedergaard, M. (2004). The blood–brain barrier: an overview: structure, regulation, and clinical implications. *Neurobiol Dis, 16*(1), 1-13.

Bandopadhyay, R., Orte, C., Lawrenson, J. G., Reid, A. R., De Silva, S., & Allt, G. (2001). Contractile proteins in pericytes at the blood-brain and blood-retinal barriers. *Journal of Neurocytology, 30*(1), 35-44. doi:10.1023/a:1011965307612

Banks, W. A., Gray, A. M., Erickson, M. A., Salameh, T. S., Damodarasamy, M., Sheibani, N., . . . Cook, D. G. (2015). Lipopolysaccharide-induced blood-brain barrier disruption: roles of cyclooxygenase, oxidative stress, neuroinflammation, and elements of the neurovascular unit. *Journal of neuroinflammation, 12*(1), 223.

Banks, W. A., & Robinson, S. M. (2010). Minimal penetration of lipopolysaccharide across the murine blood–brain barrier. *Brain, behavior, and immunity, 24*(1), 102-109.

Barger, S. W., & Harmon, A. D. (1997). Microglial activation by Alzheimer amyloid precursor protein and modulation by apolipoprotein E. *Nature, 388*(6645), 878-881.

Barres, B. A. (2008). The mystery and magic of glia: a perspective on their roles in health and disease. *Neuron, 60*(3), 430-440.

Bartus, R. T., Dean, R. r., Beer, B., & Lippa, A. S. (1982). The cholinergic hypothesis of geriatric memory dysfunction. *Science, 217*(4558), 408-414.

Bartzokis, G. (2004). Age-related myelin breakdown: a developmental model of cognitive decline and Alzheimer's disease. *Neurobiol Aging, 25*(1), 5-18.

Begley, D. (2003). Understanding and circumventing the blood-brain barrier. *Acta Paediatrica, 92*(s443), 83-91.

Bell, K., Ducatenzeiler, A., Ribeiro-da-Silva, A., Duff, K., Bennett, D., & Cuello, A. (2006). The amyloid pathology progresses in a neurotransmitter-specific manner. *Neurobiol Aging, 27*, 1644-1657.

Bell, R. D., Winkler, E. A., Sagare, A. P., Singh, I., LaRue, B., Deane, R., & Zlokovic, B. V. (2010). Pericytes control key neurovascular functions and neuronal phenotype in the adult brain and during brain aging. *Neuron, 68*(3), 409-427.

Belliveau, J., Kennedy, D., McKinstry, R., Buchbinder, B., Weisskoff, R., Cohen, M., . . . Rosen, B. (1991). Functional mapping of the human visual cortex by magnetic resonance imaging. *Science, 254*(5032), 716-719.

Ben-Menachem, E., Johansson, B. B., & Svensson, T. (1982). Increased vulnerability of the blood-brain barrier to acute hypertension following depletion of brain noradrenaline. *Journal of neural transmission, 53*(2-3), 159-167.

Berman, R. F., Goldman, H., & Altman, H. J. (1988). Age-related changes in regional cerebral blood flow and behavior in Sprague-Dawley rats. *Neurobiol Aging, 9*, 691-696.

Berwick, J., Johnston, D., Jones, M., Martindale, J., Martin, C., Kennerley, A., . . . Mayhew, J. (2008). Fine detail of neurovascular coupling revealed by spatiotemporal analysis of the hemodynamic response to single whisker stimulation in rat barrel cortex. *Journal of neurophysiology, 99*(2), 787-798.

Berwick, J., Johnston, D., Jones, M., Martindale, J., Redgrave, P., McLoughlin, N., . . . Mayhew, J. (2005). Neurovascular coupling investigated with two-dimensional optical imaging spectroscopy in rat whisker barrel cortex. *European Journal of Neuroscience, 22*(7), 1655-1666.

Billadeau, D. D., & Leibson, P. J. (2002). ITAMs versus ITIMs: striking a balance during cell regulation. *The Journal of clinical investigation, 109*(2), 161-168.

Blennow, K. (2010). Biomarkers in Alzheimer's disease drug development. *Nature Medicine, 16*(11), 1218-1222. doi:10.1038/nm.2221

Blennow, K., de Leon, M. J., & Zetterberg, H. (2006). Alzheimer's Disease. *Lancet, 368*(9533), 387-403. doi:10.1016/S0140-6736(06)69113-7

Block, M. L., & Hong, J.-S. (2005). Microglia and inflammation-mediated neurodegeneration: Multiple triggers with a common mechanism. *Progress in Neurobiology, 76*(2), 77-98. doi:10.1016/j.pneurobio.2005.06.004

Boas, D., Strangman, G., Culver, J., Hoge, R., Jasdzewski, G., Poldrack, R., . . . Mandeville, J. (2003). Can the cerebral metabolic rate of oxygen be estimated with near-infrared spectroscopy? *Physics in medicine and biology, 48*(15), 2405.

Boas, D. A., & Dunn, A. K. (2010). Laser speckle contrast imaging in biomedical optics. *Journal of biomedical optics, 15*(1), 011109-011109-011112.

Boche, D., Perry, V., & Nicoll, J. (2013). Review: activation patterns of microglia and their identification in the human brain. *Neuropathology and applied neurobiology, 39*(1), 3-18.

Böhrer, H., Qiu, F., Zimmermann, T., Zhang, Y., Jllmer, T., Männel, D., . . . Saeger, H.-D. (1997). Role of NFkappaB in the mortality of sepsis. *Journal of Clinical Investigation, 100*(5), 972.

Bokde, A. L., Ewers, M., & Hampel, H. (2009). Assessing neuronal networks: understanding Alzheimer's disease. *Progress in Neurobiology, 89*(2), 125-133.

Bookheimer, S. Y., Strojwas, M. H., Cohen, M. S., Saunders, A. M., Pericak-Vance, M. A., Mazziotta, J. C., & Small, G. W. (2000). Patterns of Brain Activation in People at Risk for Alzheimer's Disease. *New England Journal of Medicine, 343*(7), 450-456. doi:10.1056/nejm200008173430701

Boorman, L., Harris, S., Bruyns-Haylett, M., Kennerley, A., Zheng, Y., Martin, C., . . . Berwick, J. (2015). Long-latency reductions in gamma power predict hemodynamic changes that underlie the negative BOLD signal. *Journal of Neuroscience, 35*(11), 4641-4656.

Boorman, L., Kennerley, A. J., Johnston, D., Jones, M., Zheng, Y., Redgrave, P., & Berwick, J. (2010). Negative blood oxygen level dependence in the rat: a model for investigating the role of suppression in neurovascular coupling. *J Neurosci, 30*(12), 4285-4294. doi:10.1523/jneurosci.6063-09.2010

Borovikova, L. V., Ivanova, S., Zhang, M., & Yang, H. (2000). Vagus nerve stimulation attenuates the systemic inflammatory response to endotoxin. *Nature, 405*(6785), 458.

Bossù, P., Cutuli, D., Palladino, I., Caporali, P., Angelucci, F., Laricchiuta, D., . . . Petrosini, L. (2012). A single intraperitoneal injection of endotoxin in rats induces long-lasting modifications in behavior and brain protein levels of TNF-α and IL-18. *Journal of neuroinflammation, 9*(1), 1.

Brand, K., Page, S., Rogler, G., Bartsch, A., Brandl, R., Knuechel, R., . . . Neumeier, D. (1996). Activated transcription factor nuclear factor-kappa B is present in the atherosclerotic lesion. *Journal of Clinical Investigation, 97*(7), 1715.

Breteler, M. M. (2000). Vascular risk factors for Alzheimer's disease: An epidemiologic perspective. *Neurobiol Aging, 21*(2), 153-160.

Bridges, L. R., Andoh, J., Lawrence, A. J., Khoong, C. H., Poon, W. W., Esiri, M. M., . . . Hainsworth, A. H. (2014). Blood-brain barrier dysfunction and cerebral small vessel disease (arteriolosclerosis) in brains of older people. *Journal of Neuropathology & Experimental Neurology, 73*(11), 1026-1033.

Briers, J. D., & Webster, S. (1996). Laser speckle contrast analysis (LASCA): a nonscanning, full-field technique for monitoring capillary blood flow. *Journal of biomedical optics, 1*, 174-179.

Bundgaard, M., & Abbott, N. J. (2008). All vertebrates started out with a glial blood-brain barrier 4–500 million years ago. *Glia, 56*(7), 699-708.

Burke-Gaffney, A., & Hellewell, P. G. (1996). Tumour necrosis factor-α-induced ICAM-1 expression in human vascular endothelial and lung epithelial cells: modulation by tyrosine kinase inhibitors. *British journal of pharmacology, 119*(6), 1149-1158.

Bush, T. G., Puvanachandra, N., Horner, C. H., Polito, A., Ostenfeld, T., Svendsen, C. N., . . . Sofroniew, M. V. (1999). Leukocyte infiltration, neuronal degeneration, and neurite outgrowth after ablation of scar-forming, reactive astrocytes in adult transgenic mice. *Neuron, 23*(2), 297-308.

Bushong, E. A., Martone, M. E., Jones, Y. Z., & Ellisman, M. H. (2002). Protoplasmic astrocytes in CA1 stratum radiatum occupy separate anatomical domains. *Journal of Neuroscience, 22*(1), 183-192.

Busija, D. W., Bari, F., Domoki, F., & Louis, T. (2007). Mechanisms involved in the cerebrovascular dilator effects of N-methyl-d-aspartate in cerebral cortex. *Brain Research Reviews, 56*(1), 89-100.

Busse, R., & Fleming, I. (2006). Vascular endothelium and blood flow *The vascular endothelium II* (pp. 43-78): Springer.

Calamante, F., Thomas, D. L., Pell, G. S., Wiersma, J., & Turner, R. (1999). Measuring cerebral blood flow using magnetic resonance imaging techniques. *Journal of Cerebral Blood Flow & Metabolism, 19*(7), 701-735.

Campion, D., Dumanchin, C., Hannequin, D., Dubois, B., Belliard, S., Puel, M., . . . Charbonnier, F. (1999). Early-onset autosomal dominant Alzheimer disease: prevalence, genetic heterogeneity, and mutation spectrum. *The American Journal of Human Genetics, 65*(3), 664-670.

Carandini, M., Shimaoka, D., Rossi, L. F., Sato, T. K., Benucci, A., & Knöpfel, T. (2015). Imaging the awake visual cortex with a genetically encoded voltage indicator. *Journal of Neuroscience, 35*(1), 53-63.

Carvell, G. E., & Simons, D. (1990). Biometric analyses of vibrissal tactile discrimination in the rat. *The Journal of Neuroscience, 10*(8), 2638-2648.

Casserly, I., & Topol, E. J. (2004). Convergence of atherosclerosis and Alzheimer's disease: inflammation, cholesterol, and misfolded proteins. *The Lancet, 363*(9415), 1139-1146. doi:10.1016/s0140-6736(04)15900-x

Castro-Alamancos, M. A. (2002). Different temporal processing of sensory inputs in the rat thalamus during quiescent and information processing states in vivo. *The Journal of physiology, 539*(2), 567-578.

Cauli, B., & Hamel, E. (2010). Revisiting the role of neurons in neurovascular coupling. *Front Neuroenergetics, 2*, 9. doi:10.3389/fnene.2010.00009

Cevenini, E., Monti, D., & Franceschi, C. (2013). Inflamm-ageing. *Current Opinion in Clinical Nutrition & Metabolic Care, 16*(1), 14-20.

Chakrabarti, S., Zhang, M., & Alloway, K. D. (2008). MI neuronal responses to peripheral whisker stimulation: relationship to neuronal activity in SI barrels and septa. *Journal of neurophysiology, 100*(1), 50-63.

Chakravarty, S., & Herkenham, M. (2005). Toll-like receptor 4 on nonhematopoietic cells sustains CNS inflammation during endotoxemia, independent of systemic cytokines. *Journal of Neuroscience, 25*(7), 1788-1796.

Chang, P.-C., Procissi, D., Bao, Q., Centeno, M. V., Baria, A., & Apkarian, A. V. (2016). Novel method for functional brain imaging in awake minimally restrained rats. *Journal of neurophysiology, 116*(1), 61-80.

Chapin, J. K., & Lin, C.-S. (1984). Mapping the body representation in the SI cortex of anesthetized and awake rats. *The Journal of Comparative Neurology, 229*(2), 199-213. doi:10.1002/cne.902290206

Chelvarajan, R. L., Liu, Y., Popa, D., Getchell, M. L., Getchell, T. V., Stromberg, A. J., & Bondada, S. (2006). Molecular basis of age-associated cytokine dysregulation in LPS-stimulated macrophages. *Journal of leukocyte biology, 79*(6), 1314-1327.

Chen, B., Cheng, Q., Yang, K., & Lyden, P. D. (2010). Thrombin Mediates Severe Neurovascular Injury During Ischemia. *Stroke, 41*(10), 2348-2352. doi:10.1161/strokeaha.110.584920

Chen, B. R., Kozberg, M. G., Bouchard, M. B., Shaik, M. A., & Hillman, E. M. (2014). A critical role for the vascular endothelium in functional neurovascular coupling in the brain. *Journal of the American Heart Association, 3*(3), e000787.

Chen, L. M., Friedman, R. M., Ramsden, B. M., LaMotte, R. H., & Roe, A. W. (2001a). Fine-scale organization of SI (area 3b) in the squirrel monkey revealed with intrinsic optical imaging. *Journal of neurophysiology, 86*(6), 3011-3029.

Chen, X., Magnotta, V. A., Duff, K., Ponto, L. L. B., & Schultz, S. K. (2006). Donepezil effects on cerebral blood flow in older adults with mild cognitive deficits. *The Journal of neuropsychiatry and clinical neurosciences*.

Chen, Y., Vartiainen, N. E., Ying, W., Chan, P. H., Koistinaho, J., & Swanson, R. A. (2001b). Astrocytes protect neurons from nitric oxide toxicity by a glutathione-dependent mechanism. *Journal of Neurochemistry, 77*(6), 1601-1610.

Chisholm, N. C., & Sohrabji, F. (2016). Astrocytic response to cerebral ischemia is influenced by sex differences and impaired by aging. *Neurobiol Dis, 85*, 245-253.

Chodobski, A., Zink, B. J., & Szmydynger-Chodobska, J. (2011). Blood–brain barrier pathophysiology in traumatic brain injury. *Translational stroke research, 2*(4), 492-516.

Chung, H. Y., Cesari, M., Anton, S., Marzetti, E., Giovannini, S., Seo, A. Y., . . . Leeuwenburgh, C. (2009). Molecular inflammation: underpinnings of aging and age-related diseases. *Ageing research reviews, 8*(1), 18-30.

Cohen, L. (1973). Changes in neuron structure during action potential propagation and synaptic transmission. *Physiol. Rev, 53*(2), 373-418.

Coin, P. G., Lindroos, P. M., Bird, G., Osornio-Vargas, A. R., Roggli, V. L., & Bonner, J. C. (1996). Lipopolysaccharide up-regulates platelet-derived growth factor (PDGF) alpha-receptor expression in rat lung myofibroblasts and enhances response to all PDGF isoforms. *The Journal of Immunology, 156*(12), 4797-4806.

Colton, C. A., & Gilbert, D. L. (1987). Production of superoxide anions by a CNS macrophage, the microglia. *FEBS Letters, 223*(2), 284-288. doi:10.1016/0014-5793(87)80305-8

Cox, S. B., Woolsey, T. A., & Rovainen, C. M. (1993). Localized dynamic changes in cortical blood flow with whisker stimulation corresponds to matched vascular and neuronal architecture of rat barrels. *Journal of Cerebral Blood Flow & Metabolism, 13*(6), 899-913.

Cribbs, D. H., Berchtold, N. C., Perreau, V., Coleman, P. D., Rogers, J., Tenner, A. J., & Cotman, C. W. (2012). Extensive innate immune gene activation accompanies brain aging, increasing vulnerability to cognitive decline and neurodegeneration: a microarray study. *Journal of neuroinflammation, 9*(1), 179. doi:10.1186/1742-2094-9-179

Csiszar, A., Pacher, P., Kaley, G., & Ungvari, Z. (2005). Role of Oxidative and Nitrosative Stress, Longevity Genes and Poly (ADPribose) Polymerase in Cardiovascular Dysfunction Associated with Aging. *Current vascular pharmacology, 3*(3), 285-291.

Cummings, J. L. (2000). The role of cholinergic agents in the management of behavioural disturbances in Alzheimer's disease. *The International Journal of Neuropsychopharmacology, 3*(S2), S21-S29.

Cummings, J. L., & Back, C. (1998). The cholinergic hypothesis of neuropsychiatric symptoms in Alzheimer's disease. *The American Journal of Geriatric Psychiatry, 6*(2), S64-S78.

Cunningham, C. (2013). Microglia and neurodegeneration: the role of systemic inflammation. *Glia, 61*(1), 71-90.

D'Esposito, M., Deouell, L. Y., & Gazzaley, A. (2003). Alterations in the BOLD fMRI signal with ageing and disease: a challenge for neuroimaging. *Nat Rev Neurosci, 4*(11), 863.

da Fonseca, A. C. C., Matias, D., Garcia, C., Amaral, R., Geraldo, L. H., Freitas, C., & Lima, F. R. S. (2014). The impact of microglial activation on blood-brain barrier in brain diseases. *Frontiers in cellular neuroscience, 8*.

Dachet, F., Bagla, S., Keren-Aviram, G., Morton, A., Balan, K., Saadat, L., . . . Dratz, E. (2014). Predicting novel histopathological microlesions in human epileptic brain through transcriptional clustering. *Brain*, awu350.

Daëron, M. (1997). Fc receptor biology. *Annual review of immunology, 15*(1), 203-234.

Dalkara, T., & Alarcon-Martinez, L. (2015). Cerebral microvascular pericytes and neurogliovascular signaling in health and disease. *Brain Research, 1623*, 3-17.

Dalkara, T., Gursoy-Ozdemir, Y., & Yemisci, M. (2011). Brain microvascular pericytes in health and disease. *Acta Neuropathol, 122*(1), 1.

Daneman, R., Zhou, L., Kebede, A. A., & Barres, B. A. (2010). Pericytes are required for blood-brain barrier integrity during embryogenesis. *Nature, 468*(7323), 562-566.

Danton, G. H., & Dietrich, W. D. (2003). Inflammatory mechanisms after ischemia and stroke. *Journal of Neuropathology & Experimental Neurology, 62*(2), 127-136.

Das, A., Wallace, G., Holmes, C., McDowell, M. L., Smith, J. A., Marshall, J. D., . . . Ray, S. K. (2012). Hippocampal tissue of patients with refractory temporal lobe epilepsy is associated with astrocyte activation, inflammation, and altered expression of channels and receptors. *Neuroscience, 220*, 237-246.

De Simone, R., Ajmone-Cat, M. A., Carnevale, D., & Minghetti, L. (2005). Activation of α7 nicotinic acetylcholine receptor by nicotine selectively up-regulates cyclooxygenase-2 and prostaglandin E 2 in rat microglial cultures. *Journal of neuroinflammation, 2*(1), 4.

De Strooper, B., & Karran, E. (2016). The cellular phase of Alzheimer's disease. *Cell, 164*(4), 603-615.

Devor, A., Dunn, A. K., Andermann, M. L., Ulbert, I., Boas, D. A., & Dale, A. M. (2003). Coupling of total hemoglobin concentration, oxygenation, and neural activity in rat somatosensory cortex. *Neuron, 39*(2), 353-359.

Di Marco, L. Y., Farkas, E., Martin, C., Venneri, A., & Frangi, A. F. (2015). Is vasomotion in cerebral arteries impaired in Alzheimer's disease? *Journal of Alzheimer's Disease, 46*(1), 35-53.

Dickerson, B. C., & Sperling, R. A. (2009). Large-scale functional brain network abnormalities in Alzheimer's disease: insights from functional neuroimaging. *Behavioural neurology, 21*(1-2), 63-75.

Dirnagl, U., Kaplan, B., Jacewicz, M., & Pulsinelli, W. (1989). Continuous measurement of cerebral cortical blood flow by laser—Doppler flowmetry in a rat stroke model. *Journal of Cerebral Blood Flow & Metabolism, 9*(5), 589-596.

Do Carmo, S., & Cuello, A. C. (2013). Modeling Alzheimer's disease in transgenic rats. *Molecular neurodegeneration, 8*(1), 1.

Dohgu, S., Takata, F., Yamauchi, A., Nakagawa, S., Egawa, T., Naito, M., . . . Kataoka, Y. (2005). Brain pericytes contribute to the induction and up-regulation of blood–brain barrier functions through transforming growth factor-β production. *Brain Research, 1038*(2), 208-215.

Donath, M. Y., & Shoelson, S. E. (2011). Type 2 diabetes as an inflammatory disease. *Nature Reviews Immunology, 11*(2), 98-107.

Dore-Duffy, P., Owen, C., Balabanov, R., Murphy, S., Beaumont, T., & Rafols, J. A. (2000). Pericyte Migration from the Vascular Wall in Response to Traumatic Brain Injury. *Microvascular Research, 60*(1), 55-69. doi:10.1006/mvre.2000.2244

Dorshkind, K., Montecino-Rodriguez, E., & Signer, R. A. (2009). The ageing immune system: is it ever too old to become young again? *Nature Reviews Immunology, 9*(1), 57-62.

Drake, C., & Iadecola, C. (2007a). The role of neuronal signaling in controlling cerebral blood flow. *Brain and Language, 102*(2), 141-152. doi:10.1016/j.bandl.2006.08.002

Drake, C. T., & Iadecola, C. (2007b). The role of neuronal signaling in controlling cerebral blood flow. *Brain and Language, 102*(2), 141-152.

Du, P., Wood, K. M., Rosner, M. H., Cunningham, D., Tate, B., & Geoghegan, K. F. (2007). Dominance of amyloid precursor protein sequence over host cell secretases in determining β-amyloid profiles studies of interspecies variation and drug action by internally standardized immunoprecipitation/mass spectrometry. *Journal of Pharmacology and Experimental Therapeutics, 320*(3), 1144-1152.

Dunn, A. K., Bolay, H., Moskowitz, M. A., & Boas, D. A. (2001). Dynamic imaging of cerebral blood flow using laser speckle. *Journal of Cerebral Blood Flow & Metabolism, 21*(3), 195-201.

Dunn, N., Mullee, M., Perry, V. H., & Holmes, C. (2005). Association between dementia and infectious disease: evidence from a case-control study. *Alzheimer Disease & Associated Disorders, 19*(2), 91-94.

Durand, D. M., Park, E.-H., & Jensen, A. L. (2010). Potassium diffusive coupling in neural networks. *Philosophical Transactions of the Royal Society of London B: Biological Sciences, 365*(1551), 2347-2362.

Ebert, U., & Kirch, W. (1998). Scopolamine model of dementia: electroencephalogram findings and cognitive performance. *European journal of clinical investigation, 28*, 944-949.

Edelman, D. A., Jiang, Y., Tyburski, J., Wilson, R. F., & Steffes, C. (2006). Toll-like receptor-4 message is up-regulated in lipopolysaccharide-exposed rat lung pericytes. *Journal of Surgical Research, 134*(1), 22-27.

Edelman, D. A., Jiang, Y., Tyburski, J. G., Wilson, R. F., & Steffes, C. P. (2007a). Cytokine production in lipopolysaccharide-exposed rat lung pericytes. *Journal of Trauma and Acute Care Surgery, 62*(1), 89-93.

Edelman, D. A., Jiang, Y., Tyburski, J. G., Wilson, R. F., & Steffes, C. P. (2007b). Lipopolysaccharide activation of pericyte's Toll-like receptor-4 regulates co-culture permeability. *The American journal of surgery, 193*(6), 730-735.

Eikelenboom, P., Hoozemans, J. J., Veerhuis, R., van Exel, E., Rozemuller, A. J., & van Gool, W. A. (2012). Whether, when and how chronic inflammation increases the risk of developing late-onset Alzheimer's disease. *Alzheimer's research & therapy, 4*(3), 15.

Einevoll, G. T., Pettersen, K. H., Devor, A., Ulbert, I., Halgren, E., & Dale, A. M. (2007). Laminar population analysis: estimating firing rates and evoked synaptic activity from multielectrode recordings in rat barrel cortex. *Journal of neurophysiology, 97*(3), 2174-2190.

El Khoury, J., Hickman, S., Thomas, C., Loike, J., & Silverstein, S. (1998). Microglia, scavenger receptors, and the pathogenesis of Alzheimer's disease. *Neurobiol Aging, 19*(1), S81-S84.

Elahy, M., Jackaman, C., Mamo, J. C., Lam, V., Dhaliwal, S. S., Giles, C., . . . Takechi, R. (2015). Blood–brain barrier dysfunction developed during normal aging is associated with inflammation and loss of tight junctions but not with leukocyte recruitment. *Immunity & Ageing, 12*(1), 2.

Erchova, I. A., Lebedev, M. A., & Diamond, M. E. (2002). Somatosensory cortical neuronal population activity across states of anaesthesia. *European Journal of Neuroscience, 15*(4), 744-752.

Erdő, F., Denes, L., & de Lange, E. (2017). Age-associated physiological and pathological changes at the blood–brain barrier: A review. *Journal of Cerebral Blood Flow & Metabolism, 37*(1), 4-24.

Erinjeri, J. P., & Woolsey, T. A. (2002). Spatial integration of vascular changes with neural activity in mouse cortex. *Journal of Cerebral Blood Flow & Metabolism, 22*(3), 353-360.

Fabry, Z., Fitzsimmons, K. M., Herlein, J. A., Moninger, T. O., Dobbs, M. B., & Hart, M. N. (1993). Product ion of the cytokines interleukin 1 and 6 by murine brain microvessel endothelium and smooth muscle pericytes. *J Neuroimmunol, 47*(1), 23-34.

Fan, Y.-Y., Cai, Q.-L., Gao, Z.-Y., Lin, X., Huang, Q., Tang, W., & Liu, J.-H. (2017). APOE ε4 allele elevates the expressions of inflammatory factors and promotes Alzheimer's disease progression: A comparative study based on Han and She populations in the Wenzhou area. *Brain research bulletin, 132*, 39-43.

Faraci, F. M., & Heistad, D. D. (1998). Regulation of the cerebral circulation: role of endothelium and potassium channels. *Physiological reviews, 78*(1), 53-97.

Farkas, E., & Luiten, P. G. (2001). Cerebral microvascular pathology in aging and Alzheimer's disease. *Progress in neurobiology, 64*(6), 575-611.

Farrall, A. J., & Wardlaw, J. M. (2009). Blood–brain barrier: Ageing and microvascular disease – systematic review and meta-analysis. *Neurobiol Aging, 30*(3), 337-352. doi:10.1016/j.neurobiolaging.2007.07.015

Faulkner, J. R., Herrmann, J. E., Woo, M. J., Tansey, K. E., Doan, N. B., & Sofroniew, M. V. (2004). Reactive astrocytes protect tissue and preserve function after spinal cord injury. *The Journal of Neuroscience, 24*(9), 2143-2155.

Fercher, A., & Briers, J. D. (1981). Flow visualization by means of single-exposure speckle photography. *Optics communications, 37*(5), 326-330.

Fergus, A., & Lee, K. S. (1997). GABAergic Regulation of Cerebral Microvascular Tone in the Rat. *Journal of Cerebral Blood Flow & Metabolism*, 992-1003. doi:10.1097/00004647-199709000-00009

Ferreira, L. K., & Busatto, G. F. (2011). Neuroimaging in Alzheimer's disease: current role in clinical practice and potential future applications. *Clinics, 66*, 19-24.

Field, K. J., White, W. J., & Lang, C. M. (1993). Anaesthetic effects of chloral hydrate, pentobarbitone and urethane in adult male rats. *Laboratory Animals, 27*(3), 258-269. doi:10.1258/002367793780745471

Filippini, N., MacIntosh, B. J., Hough, M. G., Goodwin, G. M., Frisoni, G. B., Smith, S. M., . . . Mackay, C. E. (2009). Distinct patterns of brain activity in young carriers of the APOE-ε4 allele. *Proceedings of the National Academy of Sciences, 106*(17), 7209-7214.

Filosa, J. A., Bonev, A. D., Straub, S. V., Meredith, A. L., Wilkerson, M. K., Aldrich, R. W., & Nelson, M. T. (2006). Local potassium signaling couples neuronal activity to vasodilation in the brain. *Nature Neuroscience, 9*(11), 1397-1403. doi:10.1038/nn1779

Fong, T., Jones, R., Shi, P., Marcantonio, E., Yap, L., Rudolph, J., . . . Inouye, S. (2009). Delirium accelerates cognitive decline in Alzheimer disease. *Neurology, 72*(18), 1570-1575.

Ford, J. W., & McVicar, D. W. (2009). TREM and TREM-like receptors in inflammation and disease. *Current opinion in immunology, 21*(1), 38-46.

Franceschi, C., Capri, M., Monti, D., Giunta, S., Olivieri, F., Sevini, F., . . . Scurti, M. (2007). Inflammaging and anti-inflammaging: a systemic perspective on aging and longevity emerged from studies in humans. *Mechanisms of ageing and development, 128*(1), 92-105.

Frank-Cannon, T. C., Alto, L. T., McAlpine, F. E., & Tansey, M. G. (2009). Does neuroinflammation fan the flame in neurodegenerative diseases? *Molecular neurodegeneration, 4*(1), 1.

Frank, M. G., Barrientos, R. M., Watkins, L. R., & Maier, S. F. (2010). Aging sensitizes rapidly isolated hippocampal microglia to LPS ex vivo. *J Neuroimmunol, 226*(1), 181-184.

Fukuda, A. M., & Badaut, J. (2012). Aquaporin 4: a player in cerebral edema and neuroinflammation. *Journal of neuroinflammation, 9*(1), 1.

Gao, H.-M., Zhang, F., Zhou, H., Kam, W., Wilson, B., & Hong, J.-S. (2011). Neuroinflammation and [alpha]-Synuclein Dysfunction Potentiate Each Other, Driving Chronic Progression of Neurodegeneration in a Mouse Model of Parkinson's Disease. *Environmental health perspectives, 119*(6), 807.

Ge, Y., Zhang, Z., Lu, H., Tang, L., Jaggi, H., Herbert, J., . . . Grossman, R. I. (2012). Characterizing brain oxygen metabolism in patients with multiple sclerosis with T2-relaxation-under-spin-tagging MRI. *Journal of Cerebral Blood Flow & Metabolism, 32*(3), 403-412.

Gentet, L. J., Kremer, Y., Taniguchi, H., Huang, Z. J., Staiger, J. F., & Petersen, C. C. (2012). Unique functional properties of somatostatin-expressing GABAergic neurons in mouse barrel cortex. *Nature Neuroscience, 15*(4), 607-612.

Gerhardt, H., & Betsholtz, C. (2003). Endothelial-pericyte interactions in angiogenesis. *Cell and tissue research, 314*(1), 15-23.

Gerrits, R. J., Stein, E. A., & Greene, A. S. (2001). Anesthesia alters NO-mediated functional hyperemia. *Brain Research, 907*(1), 20-26.

Gibbs, R. A., Weinstock, G. M., Metzker, M. L., Muzny, D. M., Sodergren, E. J., Scherer, S., . . . Burch, P. E. (2004). Genome sequence of the Brown Norway rat yields insights into mammalian evolution. *Nature, 428*(6982), 493-521.

Girouard, H., & Iadecola, C. (2006). Neurovascular coupling in the normal brain and in hypertension, stroke, and Alzheimer disease. *J Appl Physiol (1985), 100*(1), 328-335. doi:10.1152/japplphysiol.00966.2005

Giunta, B., Ehrhart, J., Townsend, K., Sun, N., Vendrame, M., Shytle, D., . . . Fernandez, F. (2004). Galantamine and nicotine have a synergistic effect on inhibition of microglial activation induced by HIV-1 gp120. *Brain research bulletin, 64*(2), 165-170.

Glodzik, L., Randall, C., Rusinek, H., & de Leon, M. J. (2013). Cerebrovascular reactivity to carbon dioxide in Alzheimer's disease. *Journal of Alzheimer's Disease, 35*(3), 427-440.

Godbout, J., Chen, J., Abraham, J., Richwine, A., Berg, B., Kelley, K., & Johnson, R. (2005). Exaggerated neuroinflammation and sickness behavior in aged mice following activation of the peripheral innate immune system. *The FASEB Journal, 19*(10), 1329-1331.

Godbout, J. P., & Johnson, R. W. (2009). Age and neuroinflammation: a lifetime of psychoneuroimmune consequences. *Immunology and allergy clinics of North America, 29*(2), 321-337.

Goehler, L. E., Gaykema, R. P., Nguyen, K. T., Lee, J. E., Tilders, F. J., Maier, S. F., & Watkins, L. R. (1999). Interleukin-1β in immune cells of the abdominal vagus nerve: a link between the immune and nervous systems? *Journal of Neuroscience, 19*(7), 2799-2806.

Goehler, L. E., Relton, J. K., Dripps, D., Kiechle, R., Tartaglia, N., Maier, S. F., & Watkins, L. R. (1997). Vagal paraganglia bind biotinylated interleukin-1 receptor antagonist: a possible mechanism for immune-to-brain communication. *Brain research bulletin, 43*(3), 357-364.

Goense, J. B., & Logothetis, N. K. (2008). Neurophysiology of the BOLD fMRI signal in awake monkeys. *Current Biology, 18*(9), 631-640.

Golanov, E., Yamamoto, S., & Reis, D. (1994). Spontaneous waves of cerebral blood flow associated with a pattern of electrocortical activity. *American Journal of Physiology-Regulatory, Integrative and Comparative Physiology, 266*(1), R204-R214.

Gomi, H., Yokoyama, T., Fujimoto, K., Ikeda, T., Katoh, A., Itoh, T., & Itohara, S. (1995). Mice devoid of the glial fibrillary acidic protein develop normally and are susceptible to scrapie prions. *Neuron, 14*(1), 29-41.

Gonul, E., Duz, B., Kahraman, S., Kayali, H., Kubar, A., & Timurkaynak, E. (2002). Early Pericyte Response to Brain Hypoxia in Cats: An Ultrastructural Study. *Microvascular Research, 64*(1), 116-119. doi:10.1006/mvre.2002.2413

Gonzalo-Ruiz, A., Sanz, J., Arévalo, J., Geula, C., & Gonzalo, P. (2005). Amyloid beta peptide-induced cholinergic fibres loss in the cerebral cortex of the rat is modified by diet high in lipids and by age. *Journal of Chemical Neuroanatomy, 29*(1), 31-48.

Graeber, M. B., Li, W., & Rodriguez, M. L. (2011). Role of microglia in CNS inflammation. *FEBS Letters, 585*(23), 3798-3805. doi:10.1016/j.febslet.2011.08.033

Grammas, P. (2011). Neurovascular dysfunction, inflammation and endothelial activation: implications for the pathogenesis of Alzheimer's disease. *Journal of neuroinflammation, 8*(1), 1.

Griffin, W. S. T., Sheng, J. G., Roberts, G. W., & Mrak, R. E. (1995). Interleukin-1 expression in different plaque types in Alzheimer's disease: significance in plaque evolution. *Journal of Neuropathology & Experimental Neurology, 54*(2), 276-281.

Guerreiro, R., Wojtas, A., Bras, J., Carrasquillo, M., Rogaeva, E., Majounie, E., . . . Younkin, S. (2013). TREM2 variants in Alzheimer's disease. *New England Journal of Medicine, 368*(2), 117-127.

Haass, C. (2010). Initiation and propagation of neurodegeneration. *Nature Medicine, 16*(11), 1201-1204. doi:10.1038/nm.2223

Haider, B., Häusser, M., & Carandini, M. (2013). Inhibition dominates sensory responses in awake cortex. *Nature, 493*(7430), 97.

Hajdu, M. A., Heistad, D., Siems, J. E., & Baumbach, G. L. (1990). Effects of aging on mechanics and composition of cerebral arterioles in rats. *Circulation research, 66*(6), 1747-1754.

Hall, C. N., Reynell, C., Gesslein, B., Hamilton, N. B., Mishra, A., Sutherland, B. A., . . . Attwell, D. (2014). Capillary pericytes regulate cerebral blood flow in health and disease. *Nature, 508*(7494), 55-60.

Halliday, D., Little, H. J., & Paton, W. (1979). The effects of inert gases and other general anaesthetics on the release of acetylcholine from the guinea-pig ileum. *British journal of pharmacology, 67*(2), 229-237.

Hamel, E., Royea, J., Ongali, B., & Tong, X.-K. (2016). Neurovascular and cognitive failure in Alzheimer's disease: benefits of cardiovascular therapy. *Cellular and molecular neurobiology, 36*(2), 219-232.

Hamer, P., McGeachie, J., Davies, M., & Grounds, M. (2002). Evans Blue Dye as an in vivo marker of myofibre damage: optimising parameters for detecting initial myofibre membrane permeability. *Journal of anatomy, 200*(1), 69-79.

Hamilton, N. B., Attwell, D., & Hall, C. N. (2010). Pericyte-mediated regulation of capillary diameter: a component of neurovascular coupling in health and disease. *Frontiers in neuroenergetics, 2*, 5.

Handel, M. L., Mcmorrow, L. B., & Gravallese, E. M. (1995). Nuclear factor–kB in rheumatoid synovium. Localization of P50 and P65. *Arthritis & Rheumatism, 38*(12), 1762-1770.

Hansen, L., Armstrong, D., & Terry, R. (1987). An immunohistochemical quantification of fibrous astrocytes in the aging human cerebral cortex. *Neurobiol Aging, 8*(1), 1-6.

Hardy, J. (2006). Alzheimer's disease: the amyloid cascade hypothesis: an update and reappraisal. *Journal of Alzheimer's Disease, 9*(3 Supplement), 151-153.

Hardy, J., & Allsop, D. (1991). Amyloid deposition as the central event in the aetiology of Alzheimer's disease. *Trends in Pharmacological Sciences, 12*, 383-388.

Hardy, J., & Selkoe, D. J. (2002). The amyloid hypothesis of Alzheimer's disease: progress and problems on the road to therapeutics. *Science, 297*(5580), 353-356.

Hardy, J. A., & Higgins, G. A. (1992). Alzheimer's disease: the amyloid cascade hypothesis. *Science, 256*(5054), 184.

Harris, J. L., Choi, I.-Y., & Brooks, W. M. (2015). Probing astrocyte metabolism in vivo: proton magnetic resonance spectroscopy in the injured and aging brain. *Frontiers in aging neuroscience, 7*, 202.

Harry, G. J. (2013). Microglia during development and aging. *Pharmacology & Therapeutics, 139*(3), 313-326.

Hasselmo, M. E., & Sarter, M. (2011). Modes and models of forebrain cholinergic neuromodulation of cognition. *Neuropsychopharmacology, 36*(1), 52-73.

Hauss-Wegrzyniak, B., Dobrzanski, P., Stoehr, J. D., & Wenk, G. L. (1998). Chronic neuroinflammation in rats reproduces components of the neurobiology of Alzheimer's disease. *Brain Research, 780*(2), 294-303.

Hawkins, B. T., & Davis, T. P. (2005). The Blood-Brain Barrier/Neurovascular Unit in Health and Disease. *Pharmacol Rev, 57*(2), 173-185. doi:10.1124/pr.57.2.4

Haydon, P. G. (2001). GLIA: listening and talking to the synapse. *Nature Reviews Neuroscience, 2*(3), 185-193.

Heiss, W.-D., Graf, R., Wienhard, K., Löttgen, J., Saito, R., Fujita, T., . . . Wagner, R. (1994). Dynamic penumbra demonstrated by sequential multitracer PET after middle cerebral artery occlusion in cats. *Journal of Cerebral Blood Flow & Metabolism, 14*(6), 892-902.

Heppner, F. L., Ransohoff, R. M., & Becher, B. (2015). Immune attack: the role of inflammation in Alzheimer disease. *Nature Reviews Neuroscience, 16*(6), 358-372.

Herman, P., Sanganahalli, B. G., Blumenfeld, H., Rothman, D. L., & Hyder, F. (2013). Quantitative basis for neuroimaging of cortical laminae with calibrated functional MRI. *Proceedings of the National Academy of Sciences, 110*(37), 15115-15120.

Herron, P., & Schweitzer, J. B. (2000). Effects of cholinergic depletion on neural activity in different laminae of the rat barrel cortex. *Brain Research, 872*(1), 71-76.

Hill-Eubanks, D. C., Werner, M. E., Heppner, T. J., & Nelson, M. T. (2011). Calcium signaling in smooth muscle. *Cold Spring Harbor perspectives in biology, 3*(9), a004549.

Hillman, E. M. (2014). Coupling mechanism and significance of the BOLD signal: a status report. *Annual review of neuroscience, 37*, 161-181.

Himmelheber, A. M., Sarter, M., & Bruno, J. P. (2000). Increases in cortical acetylcholine release during sustained attention performance in rats. *Cognitive Brain Research, 9*(3), 313-325. doi:10.1016/s0926-6410(00)00012-4

Hirao, K., Ohnishi, T., Hirata, Y., Yamashita, F., Mori, T., Moriguchi, Y., . . . Asada, T. (2005). The prediction of rapid conversion to Alzheimer's disease in mild cognitive impairment using regional cerebral blood flow SPECT. *Neuroimage, 28*(1014-1021).

Hof, P. R., & Morrison, J. H. (2004). The aging brain: morphomolecular senescence of cortical circuits. *Trends Neurosci, 27*(10), 607-613. doi:10.1016/j.tins.2004.07.013

Hofer, S., Eisenbach, C., Lukic, I. K., Schneider, L., Bode, K., Brueckmann, M., . . . Werner, J. (2008). Pharmacologic cholinesterase inhibition improves survival in experimental sepsis. *Critical care medicine, 36*(2), 404-408.

Holland, P. R., Searcy, J. L., Salvadores, N., Scullion, G., Chen, G., Lawson, G., . . . Kalaria, R. (2015). Gliovascular disruption and cognitive deficits in a mouse model with features of small vessel disease. *Journal of Cerebral Blood Flow & Metabolism, 35*(6), 1005-1014.

Holmes, C. (2013). Review: systemic inflammation and Alzheimer's disease. *Neuropathology and applied neurobiology, 39*(1), 51-68.

Holmes, C., Cunningham, C., Zotova, E., Woolford, J., Dean, C., Kerr, S. u., . . . Perry, V. (2009). Systemic inflammation and disease progression in Alzheimer disease. *Neurology, 73*(10), 768-774.

Holthoff, K., & Witte, O. W. (1996). Intrinsic optical signals in rat neocortical slices measured with near-infrared dark-field microscopy reveal changes in extracellular space. *The Journal of Neuroscience, 16*(8), 2740-2749.

Holthoff, K., & Witte, O. W. (2000). Directed spatial potassium redistribution in rat neocortex. *Glia, 29*(3), 288-292.

Holtman, I. R., Raj, D. D., Miller, J. A., Schaafsma, W., Yin, Z., Brouwer, N., . . . Kamphuis, W. (2015). Induction of a common microglia gene expression signature by aging and neurodegenerative conditions: a co-expression meta-analysis. *Acta neuropathologica communications, 3*(1), 31.

Hossmann, K. A. (1994). Viability thresholds and the penumbra of focal ischemia. *Annals of Neurology, 36*(4), 557-565.

Howarth, C. (2014). The contribution of astrocytes to the regulation of cerebral blood flow. *Frontiers in neuroscience, 8*, 103.

Howarth, C., Sutherland, B., Choi, H. B., Martin, C., Lind, B. L., Khennouf, L., . . . Ellis-Davies, G. (2017). A critical role for astrocytes in hypercapnic vasodilation in brain. *Journal of Neuroscience, 37*(9), 2403-2414.

Huber, J. D., Campos, C. R., Mark, K. S., & Davis, T. P. (2006). Alterations in blood-brain barrier ICAM-1 expression and brain microglial activation after λ-carrageenan-induced inflammatory pain. *American Journal of Physiology-Heart and Circulatory Physiology, 290*(2), H732-H740.

Huber, L., Goense, J., Kennerley, A. J., Ivanov, D., Krieger, S. N., Lepsien, J., . . . Möller, H. E. (2014). Investigation of the neurovascular coupling in positive and negative BOLD responses in human brain at 7T. *Neuroimage, 97*, 349-362.

Hudetz, A. G., Roman, R. J., & Harder, D. R. (1992). Spontaneous Flow Oscillations in the Cerebral Cortex During Acute Changes in Mean Arterial Pressure. *Journal of Cerebral Blood Flow & Metabolism, 12*(3), 491-499. doi:10.1038/jcbfm.1992.67

Huo, B.-X., Smith, J. B., & Drew, P. J. (2014). Neurovascular coupling and decoupling in the cortex during voluntary locomotion. *Journal of Neuroscience, 34*(33), 10975-10981.

Hutchins, P. M., Lynch, C. D., Cooney, P. T., & Curseen, K. A. (1996). The microcirculation in experimental hypertension and aging. *Cardiovascular research, 32*(4), 772-780.

Hyder, F., Rothman, D. L., & Bennett, M. R. (2013). Cortical energy demands of signaling and nonsignaling components in brain are conserved across mammalian species and activity levels. *Proc Natl Acad Sci U S A, 110*(9), 3549-3554. doi:10.1073/pnas.1214912110

Iadecola, C. (1998). Neurogenic control of the cerebral microcirculation: is dopamine minding the store? *Nature Neuroscience, 1*(4).

Iadecola, C. (2004). Neurovascular regulation in the normal brain and in Alzheimer's disease. *Nat Rev Neurosci, 5*(5), 347-360. doi:10.1038/nrn1387

Iadecola, C. (2010). The overlap between neurodegenerative and vascular factors in the pathogenesis of dementia. *Acta Neuropathol, 120*(3), 287-296. doi:10.1007/s00401-010-0718-6

Iadecola, C., & Nedergaard, M. (2007). Glial regulation of the cerebral microvasculature. *Nature Neuroscience, 10*(11), 1369-1376.

Iadecola, C., Park, L., & Capone, C. (2009). Threats to the Mind: ageing, amyloid and hypertension. *Stroke, 40*(3 suppl 1), S40-S44.

Iadecola, C., Pelligrino, D. A., Moskowitz, M. A., & Lassen, N. A. (1994). Nitric oxide synthase inhibition and cerebrovascular regulation. *Journal of Cerebral Blood Flow & Metabolism, 14*(2), 175-192.

Iliff, J. J., Wang, M., Liao, Y., Plogg, B. A., Peng, W., Gundersen, G. A., . . . Goldman, S. A. (2012). A paravascular pathway facilitates CSF flow through the brain parenchyma and the

clearance of interstitial solutes, including amyloid β. *Science translational medicine, 4*(147), 147ra111-147ra111.

Iqbal, K., & Grundke-Iqbal, I. (2010). Alzheimer's disease, a multifactorial disorder seeking multitherapies: Elsevier.

Itagaki, S., McGeer, P., Akiyama, H., Zhu, S., & Selkoe, D. (1989). Relationship of microglia and astrocytes to amyloid deposits of Alzheimer disease. *J Neuroimmunol, 24*(3), 173-182.

Ito, D., Imai, Y., Ohsawa, K., Nakajima, K., Fukuuchi, Y., & Kohsaka, S. (1998). Microglia-specific localisation of a novel calcium binding protein, Iba1. *Molecular brain research, 57*(1), 1-9.

Jacob, H. J., & Kwitek, A. E. (2002). Rat genetics: attachign physiology and pharmacology to the genome. *Nature Reviews Genetics, 3*(1), 33-42.

Jennings, J. R., Heim, A. F., Kuan, D. C.-H., Gianaros, P. J., Muldoon, M. F., & Manuck, S. B. (2013). Use of total cerebral blood flow as an imaging biomarker of known cardiovascular risks. *Stroke, 44*(9), 2480-2485.

Johnson, K. A., Fox, N. C., Sperling, R. A., & Klunk, W. E. (2012). Brain imaging in Alzheimer disease. *Cold Spring Harbor perspectives in medicine, 2*(4), a006213.

Jones, B. E. (2005). From waking to sleeping: neuronal and chemical substrates. *Trends in Pharmacological Sciences, 26*(11), 578-586. doi:10.1016/j.tips.2005.09.009

Jones, L., Holmans, P. A., Hamshere, M. L., Harold, D., Moskvina, V., Ivanov, D., . . . Sims, R. (2010). Genetic evidence implicates the immune system and cholesterol metabolism in the aetiology of Alzheimer's disease. *PloS one, 5*(11), e13950.

Jones, M., Berwick, J., Johnston, D., & Mayhew, J. (2001). Concurrent optical imaging spectroscopy and laser-Doppler flowmetry: the relationship between blood flow, oxygenation, and volume in rodent barrel cortex. *Neuroimage, 13*(6 Pt 1), 1002-1015. doi:10.1006/nimg.2001.0808

Jonsson, T., Stefansson, H., Steinberg, S., Jonsdottir, I., Jonsson, P. V., Snaedal, J., . . . Lah, J. J. (2013). Variant of TREM2 associated with the risk of Alzheimer's disease. *New England Journal of Medicine, 368*(2), 107-116.

Jukkola, P., & Gu, C. (2015). Regulation of neurovascular coupling in autoimmunity to water and ion channels. *Autoimmunity reviews, 14*(3), 258-267.

Kahn, M. S., Kranjac, D., Alonzo, C. A., Haase, J. H., Cedillos, R. O., McLinden, K. A., . . . Chumley, M. J. (2012). Prolonged elevation in hippocampal Aβ and cognitive deficits following repeated endotoxin exposure in the mouse. *Behavioural Brain Research, 229*(1), 176-184.

Kassel, K. M., Sullivan, B. P., & Luyendyk, J. P. (2012). Lipopolysaccharide enhances transforming growth factor β1-induced PDGF-B expression in bile duct epithelial cells. *Journal of Gastroenterology and Hepatology, 27*(4), 714.

Kawashima, K., Yoshikawa, K., Fujii, Y. X., Moriwaki, Y., & Misawa, H. (2007). Expression and function of genes encoding cholinergic components in murine immune cells. *Life sciences, 80*(24), 2314-2319.

Kennerley, A. J., Berwick, J., Martindale, J., Johnston, D., Papadakis, N., & Mayhew, J. E. (2005). Concurrent fMRI and optical measures for the investigation of the hemodynamic response function. *Magnetic resonance in medicine, 54*(2), 354-365.

Kennerley, A. J., Mayhew, J. E., Boorman, L., Zheng, Y., & Berwick, J. (2012). Is optical imaging spectroscopy a viable measurement technique for the investigation of the negative BOLD phenomenon? A concurrent optical imaging spectroscopy and fMRI study at high field (7T). *Neuroimage, 61*(1), 10-20.

Kettenmann, H., Hanisch, U.-K., Noda, M., & Verkhratsky, A. (2011). Physiology of microglia. *Physiological reviews, 91*(2), 461-553.

Kettenmann, H., Kirchhoff, F., & Verkhratsky, A. (2013). Microglia: new roles for the synaptic stripper. *Neuron, 77*(1), 10-18.

Kim, H. J., Jung, K. J., Yu, B. P., Cho, C. G., Choi, J. S., & Chung, H. Y. (2002). Modulation of redox-sensitive transcription factors by calorie restriction during aging. *Mechanisms of ageing and development, 123*(12), 1589-1595.

Kisler, K., Nelson, A. R., Montagne, A., & Zlokovic, B. V. (2017). Cerebral blood flow regulation and neurovascular dysfunction in Alzheimer disease. *Nature Reviews Neuroscience*.

Kitazawa, M., Oddo, S., Yamasaki, T. R., Green, K. N., & LaFerla, F. M. (2005). Lipopolysaccharide-induced inflammation exacerbates tau pathology by a cyclin-dependent kinase 5-mediated pathway in a transgenic model of Alzheimer's disease. *The Journal of Neuroscience, 25*(39), 8843-8853.

Kiyota, T., Ingraham, K. L., Swan, R. J., Jacobsen, M. T., Andrews, S. J., & Ikezu, T. (2012). AAV serotype 2/1-mediated gene delivery of anti-inflammatory interleukin-10 enhances neurogenesis and cognitive function in APP+ PS1 mice. *Gene therapy, 19*(7), 724-733.

Klafki, H.-W., Staufenbiel, M., Kornhuber, J., & Wiltfang, J. (2006). Therapeutic approaches to Alzheimer's disease. *Brain, 129*(11), 2840-2855.

Knott, G. W., Quairiaux, C., Genoud, C., & Welker, E. (2002). Formation of dendritic spines with GABAergic synapses induced by whisker stimulation in adult mice. *Neuron, 34*(2), 265-273.

Ko, K. R., Ngai, A. C., & Winn, R. H. (1990). Role of adenosine in regulation of regional cerebral blood flow in sensory cortex. *American Journal of Physiology-Heart and Circulatory Physiology, 259*(6), H1703-H1708.

Kocsis, P., Gyertyán, I., Éles, J., Laszy, J., Hegedűs, N., Gajári, D., . . . Tihanyi, K. (2014). Vascular action as the primary mechanism of cognitive effects of cholinergic, CNS-acting drugs, a rat phMRI BOLD study. *Journal of Cerebral Blood Flow & Metabolism, 34*(6), 995-1000.

Koehler, R. C., Roman, R. J., & Harder, D. R. (2009). Astrocytes and the regulation of cerebral blood flow. *Trends Neurosci, 32*(3), 160-169. doi:10.1016/j.tins.2008.11.005

Kofler, J., & Wiley, C. A. (2011). Microglia Key Innate Immune Cells of the Brain. *Toxicologic pathology, 39*(1), 103-114.

Kontos, H. A., Raper, A. J., & Patterson, J. (1977). Analysis of vasoactivity of local pH, PCO2 and bicarbonate on pial vessels. *Stroke, 8*(3), 358-360.

Korhonen, P., Helenius, M., & Salminen, A. (1997). Age-related changes in the regulation of transcription factor NF-κB in rat brain. *Neurosci Lett, 225*(1), 61-64.

Kovac, A., Erickson, M. A., & Banks, W. A. (2011). Brain microvascular pericytes are immunoactive in culture: cytokine, chemokine, nitric oxide, and LRP-1 expression in response to lipopolysaccharide. *Journal of neuroinflammation, 8*(1), 1.

Kreutzberg, G. W. (1996). Microglia: a sensor for pathological events in the CNS. *Trends Neurosci, 19*(8), 312-318.

Krstic, D., Madhusudan, A., Doehner, J., Vogel, P., Notter, T., Imhof, C., . . . Schwerdel, C. (2012). Systemic immune challenges trigger and drive Alzheimer-like neuropathology in mice. *Journal of neuroinflammation, 9*(1), 1.

Kuchibhotla, K. V., Lattarulo, C. R., Hyman, B. T., & Bacskai, B. J. (2009). Synchronous Hyperactivity and Intercellular Calcium Waves in Astrocytes in Alzheimer Mice. *Science, 323*(5918), 1211-1215. doi:10.1126/science.1169096

Lassmann, H., Zimprich, F., Vass, K., & Hickey, W. (1991). Microglial cells are a component of the perivascular glia limitans. *J Neurosci Res, 28*(2), 236-243.

Lawrence, A. D., & Sahakian, B. J. (1995). Alzheimer disease, attention, and the cholinergic system. *Alzheimer Disease & Associated Disorders, 9*, 37-49.

Lazarides, E. (1982). Intermediate filaments: a chemically heterogeneous, developmentally regulated class of proteins. *Annual review of biochemistry, 51*(1), 219-250.

Lecrux, C., & Hamel, E. (2011). The neurovascular unit in brain function and disease. *Acta Physiol (Oxf), 203*(1), 47-59. doi:10.1111/j.1748-1716.2011.02256.x

Lecrux, C., & Hamel, E. (2016). Neuronal networks and mediators of cortical neurovascular coupling responses in normal and altered brain states. *Phil. Trans. R. Soc. B, 371*(1705), 20150350.

Lecrux, C., Sandoe, C. H., Neupane, S., Kropf, P., Toussay, X., Tong, X.-K., . . . Hamel, E. (2017). Impact of altered cholinergic tones on the neurovascular coupling response to whisker stimulation. *Journal of Neuroscience, 37*(6), 1518-1531.

Lecrux, C., Toussay, X., Kocharyan, A., Fernandes, P., Neupane, S., Lévesque, M., . . . Hamel, E. (2011). Pyramidal neurons are "neurogenic hubs" in the neurovascular coupling response to whisker stimulation. *Journal of Neuroscience, 31*(27), 9836-9847.

Ledeboer, A., Brevé, J. J., Wierinckx, A., Van Der Jagt, S., Bristow, A. F., Leysen, J. E., . . . Van Dam, A. M. (2002). Expression and regulation of interleukin-10 and interleukin-10 receptor in rat astroglial and microglial cells. *European Journal of Neuroscience, 16*(7), 1175-1185.

Lee, J. W., Lee, Y. K., Yuk, D. Y., Choi, D. Y., Ban, S. B., Oh, K. W., & Hong, J. T. (2008). Neuro-inflammation induced by lipopolysaccharide causes cognitive impairment through enhancement of beta-amyloid generation. *Journal of neuroinflammation, 5*(1), 37.

Lee, M., Schwab, C., & Mcgeer, P. L. (2011). Astrocytes are GABAergic cells that modulate microglial activity. *Glia, 59*(1), 152-165.

Lee, Y.-J., Choi, D.-Y., Choi, I. S., Kim, K. H., Kim, Y. H., Kim, H. M., . . . Han, S. B. (2012). Inhibitory effect of 4-O-methylhonokiol on lipopolysaccharide-induced neuroinflammation, amyloidogenesis and memory impairment via inhibition of nuclear factor-kappaB in vitro and in vivo models. *Journal of neuroinflammation, 9*(1), 1.

Lehnardt, S., Massillon, L., Follett, P., Jensen, F. E., Ratan, R., Rosenberg, P. A., . . . Vartanian, T. (2003). Activation of innate immunity in the CNS triggers neurodegeneration through a Toll-like receptor 4-dependent pathway. *Proceedings of the National Academy of Sciences, 100*(14), 8514-8519.

Leveen, P., Pekny, M., Gebre-Medhin, S., Swolin, B., Larsson, E., & Betsholtz, C. (1994). Mice deficient for PDGF B show renal, cardiovascular, and hematological abnormalities. *Genes & development, 8*(16), 1875-1887.

Ley, K., & Reutershan, J. (2006). Leucocyte-endothelial interactions in health and disease *The vascular endothelium II* (pp. 97-133): Springer.

Leybaert, L. (2005). Neurobarrier coupling in the brain: a partner of neurovascular and neurometabolic coupling? *Journal of Cerebral Blood Flow & Metabolism, 25*(1), 2-16.

Li, H. J., Hou, X. H., Liu, H. H., Yue, C. L., He, Y., & Zuo, X. N. (2015). Toward systems neuroscience in mild cognitive impairment and Alzheimer's disease: A meta-analysis of 75 fMRI studies. *Human brain mapping, 36*(3), 1217-1232.

Li, J., & Iadecola, C. (1994). Nitric oxide and adenosine mediate vasodilation during functional activation in cerebellar cortex. *Neuropharmacology, 33*(11), 1453-1461.

Li, J., Wang, Y., Zhang, M., Xu, Z., Gao, C., Fang, C., . . . Zhou, H. (2011). Vascular risk factors promote conversion from mild cognitive impairment to Alzheimer disease. *Neurology, 76*(17), 1485-1491.

Li, W., Antuono, P. G., Xie, C., Chen, G., Jones, J. L., Ward, B. D., . . . Li, S.-J. (2012). Changes in regional cerebral blood flow and functional connectivity in the cholinergic pathway associated with cognitive performance in subjects with mild Alzheimer's disease after 12-week donepezil treatment. *Neuroimage, 60*(2), 1083-1091.

Licastro, F., Carbone, I., Ianni, M., & Porcellini, E. (2011). Gene signature in Alzheimer's disease and environmental factors: the virus chronicle. *Journal of Alzheimer's Disease, 27*(4), 809-817.

Liddelow, S. A., & Barres, B. A. (2017). Reactive Astrocytes: Production, Function, and Therapeutic Potential. *Immunity, 46*(6), 957-967.

Lin, J. H.-C., Lou, N., Kang, N., Takano, T., Hu, F., Han, X., . . . Willecke, K. (2008). A central role of connexin 43 in hypoxic preconditioning. *The Journal of Neuroscience, 28*(3), 681-695.

Lin, J. H. (1995). Species similarities and differences in pharmacokinetics. *Drug Metabolism and Disposition, 23*(10), 1008-1021.

Lind, B. L., Brazhe, A. R., Jessen, S. B., Tan, F. C., & Lauritzen, M. J. (2013). Rapid stimulus-evoked astrocyte Ca2+ elevations and hemodynamic responses in mouse somatosensory cortex in vivo. *Proceedings of the National Academy of Sciences, 110*(48), E4678-E4687.

Lindblom, P., Gerhardt, H., Liebner, S., Abramsson, A., Enge, M., Hellström, M., . . . Nyström, H. C. (2003). Endothelial PDGF-B retention is required for proper investment of pericytes in the microvessel wall. *Genes & development, 17*(15), 1835-1840.

Liu, B., & Hong, J.-S. (2003). Role of microglia in inflammation-mediated neurodegenerative diseases: mechanisms and strategies for therapeutic intervention. *Journal of Pharmacology and Experimental Therapeutics, 304*(1), 1-7.

Liu, P., Huang, H., Rollins, N., Chalak, L. F., Jeon, T., Halovanic, C., & Lu, H. (2014). Quantitative assessment of global cerebral metabolic rate of oxygen (CMRO2) in neonates using MRI. *NMR in Biomedicine, 27*(3), 332-340.

Lobo-Silva, D., Carriche, G. M., Castro, A. G., Roque, S., & Saraiva, M. (2016). Balancing the immune response in the brain: IL-10 and its regulation. *Journal of neuroinflammation, 13*(1), 297.

Logothetis, N. K. (2008). What we can do and what we cannot do with fMRI. *Nature, 453*(7197), 869-878.

Logothetis, N. K., Pauls, J., Augath, M., Trinath, T., & Oeltermann, A. (2001). Neurophysiological investigation of the basis of the fMRI signal. *Nature, 412*(6843), 150-157.

Lok, J., Gupta, P., Guo, S., Kim, W. J., Whalen, M. J., van Leyen, K., & Lo, E. H. (2007). Cell–cell Signaling in the Neurovascular Unit. *Neurochem Res, 32*(12), 2032-2045. doi:10.1007/s11064-007-9342-9

Lübke, J., & Feldmeyer, D. (2007). Excitatory signal flow and connectivity in a cortical column: focus on barrel cortex. *Brain Structure and Function, 212*(1), 3-17.

Maggi, C., & Meli, A. (1986). Suitability of urethane anesthesia for physiopharmacological investigations in various systems Part 1: General considerations. *Experientia, 42*(2), 109-114.

Magistretti, P., & Pellerin, L. (1996). Cellular Mechanisms of Brain Energy Metabolism. Relevance to Functional Brain Imaging and to Neurodegenerative Disordersa. *Annals of the New York Academy of Sciences, 777*(1), 380-387.

Makarov, S. S. (2000). NF-κB as a therapeutic target in chronic inflammation: recent advances. *Molecular medicine today, 6*(11), 441-448.

Mandeville, J. B., Marota, J. J., Ayata, C., Zaharchuk, G., Moskowitz, M. A., Rosen, B. R., & Weisskoff, R. M. (1999). Evidence of a cerebrovascular postarteriole windkessel with delayed compliance. *Journal of Cerebral Blood Flow & Metabolism, 19*(6), 679-689.

Maragakis, N. J., Dietrich, J., Wong, V., Xue, H., Mayer-Proschel, M., Rao, M. S., & Rothstein, J. D. (2004a). Glutamate transporter expression and function in human glial progenitors. *Glia, 45*(2), 133-143.

Maragakis, N. J., Dykes-Hoberg, M., & Rothstein, J. D. (2004b). Altered expression of the glutamate transporter EAAT2b in neurological disease. *Annals of Neurology, 55*(4), 469-477.

Martin, C. (2014). Contributions and complexities from the use of in vivo animal models to improve understanding of human neuroimaging signals. *Frontiers in neuroscience, 8*, 211.

Martin, C., Berwick, J., Johnston, D., Zheng, Y., Martindale, J., Port, M., . . . Mayhew, J. (2002). Optical imaging spectroscopy in the unanaesthetised rat. *Journal of neuroscience methods, 120*(1), 25-34.

Martin, C., Martindale, J., Berwick, J., & Mayhew, J. (2006). Investigating neural–hemodynamic coupling and the hemodynamic response function in the awake rat. *Neuroimage, 32*(1), 33-48.

Martin, C., Zheng, Y., Sibson, N. R., Mayhew, J. E., & Berwick, J. (2013). Complex spatiotemporal haemodynamic response following sensory stimulation in the awake rat. *Neuroimage, 66*, 1-8.

Martindale, J., Mayhew, J., Berwick, J., Jones, M., Martin, C., Johnston, D., . . . Zheng, Y. (2003). The hemodynamic impulse response to a single neural event. *Journal of Cerebral Blood Flow & Metabolism, 23*(5), 546-555.

Marzolo, M. P., Von Bernhardi, R., Bu, G., & Inestrosa, N. C. (2000). Expression of α2-macroglobulin receptor/low density lipoprotein receptor-related protein (LRP) in rat microglial cells. *J Neurosci Res, 60*(3), 401-411.

Masamoto, K., & Kanno, I. (2012). Anesthesia and the quantitative evaluation of neurovascular coupling. *Journal of Cerebral Blood Flow & Metabolism, 32*(7), 1233-1247.

Masamoto, K., Obata, T., & Kanno, I. (2010). Intracortical microcirculatory change induced by anesthesia in rat somatosensory cortex *Oxygen Transport to Tissue XXXI* (pp. 57-61): Springer.

Massoud, F., & Gauthier, S. (2010). Update on the pharmacological treatment of Alzheimer's disease. *Current neuropharmacology, 8*(1), 69-80.

Matsuda, H. (2007). Role of neuroimaging in Alzheimer's disease, with emphasis on brain perfusion SPECT. *Journal of Nuclear Medicine, 48*(8), 1289-1300.

Matsuda, R., Nishikawa, A., & Tanaka, H. (1995). Visualization of dystrophic muscle fibers in mdx mouse by vital staining with Evans blue: evidence of apoptosis in dystrophin-deficient muscle. *The Journal of Biochemistry, 118*(5), 959-964.

Mayhew, J., Johnston, D., Berwick, J., Jones, M., Coffey, P., & Zheng, Y. (2000). Spectroscopic analysis of neural activity in brain: increased oxygen consumption following activation of barrel cortex. *Neuroimage, 12*(6), 664-675.

Mayhew, J., Johnston, D., Martindale, J., Jones, M., Berwick, J., & Zheng, Y. (2001). Increased oxygen consumption following activation of brain: theoretical footnotes using spectroscopic data from barrel cortex. *Neuroimage, 13*(6), 975-987.

Mayhew, J. E. W., Askew, S., Zheng, Y., Porrill, J., Westby, G. W. M., Redgrave, P., . . . Harper, R. M. (1996). Cerebral Vasomotion: A 0.1-Hz Oscillation in Reflected Light Imaging of Neural Activity. *Neuroimage, 4*(3), 183-193. doi:10.1006/nimg.1996.0069

Mcdonald, J. W., Althomsons, S. P., Hyrc, K. L., Choi, D. W., & Goldberg, M. P. (1998). Oligodendrocytes from forebrain are highly vulnerable to AMPA/kainate receptor-mediated excitotoxicity. *Nature Medicine, 4*(3), 291-297.

McGeer, P. L., Itagaki, S., Tago, H., & McGeer, E. G. (1987). Reactive microglia in patients with senile dementia of the Alzheimer type are positive for the histocompatibility glycoprotein HLA-DR. *Neurosci Lett, 79*(1), 195-200.

McGowan, E., Eriksen, J., & Hutton, M. (2006). A decade of modeling Alzheimer's disease in transgenic mice. *TRENDS in Genetics, 22*(5), 281-289.

Mehta, V., Pei, W., Yang, G., Li, S., Swamy, E., Boster, A., . . . Pitt, D. (2013). Iron is a sensitive biomarker for inflammation in multiple sclerosis lesions. *PloS one, 8*(3), e57573.

Metea, M. R., & Newman, E. A. (2006). Glial cells dilate and constrict blood vessels: a mechanism of neurovascular coupling. *Journal of Neuroscience, 26*(11), 2862-2870.

Meyer, J. S., Li, Y., Xu, G., Thornby, J., Chowdhury, M., & Quach, M. (2002). Feasibility of treating mild cognitive impairment withcholinesterase inhibitors. *International journal of geriatric psychiatry, 17*(6), 586-588.

Mhatre, M., Nguyen, A., Kashani, S., Pham, T., Adesina, A., & Grammas, P. (2004). Thrombin, a mediator of neurotoxicity and memory impairment. *Neurobiol Aging, 25*(6), 783-793.

Micheau, J., & Marighetto, A. (2011). Acetylcholine and memory: a long, complex and chaotic but still living relationship. *Behavioural Brain Research, 221*(2), 424-429.

Middeldorp, J., & Hol, E. (2011). GFAP in health and disease. *Progress in Neurobiology, 93*(3), 421-443.

Mitchell, G. F., van Buchem, M. A., Sigurdsson, S., Gotal, J. D., Jonsdottir, M. K., Kjartansson, Ó., . . . Gudnason, V. (2011). Arterial stiffness, pressure and flow pulsatility and brain structure and function: the Age, Gene/Environment Susceptibility–Reykjavik study. *Brain, 134*(11), 3398-3407.

Montacute, R., Foley, K., Forman, R., Else, K. J., Cruickshank, S. M., & Allan, S. M. (2017). Enhanced susceptibility of triple transgenic Alzheimer's disease (3xTg-AD) mice to acute infection. *Journal of neuroinflammation, 14*(1), 50. doi:10.1186/s12974-017-0826-5

Montagne, A., Barnes, S. R., Sweeney, M. D., Halliday, M. R., Sagare, A. P., Zhao, Z., . . . Amezcua, L. (2015). Blood-brain barrier breakdown in the aging human hippocampus. *Neuron, 85*(2), 296-302.

Moore, C. I., & Cao, R. (2008). The hemo-neural hypothesis: on the role of blood flow in information processing. *Journal of neurophysiology, 99*(5), 2035-2047.

Moretti, E. W., Morris, R. W., Podgoreanu, M., Schwinn, D. A., Newman, M. F., Bennett, E., . . . Laskowitz, D. T. (2005). APOE polymorphism is associated with risk of severe sepsis in surgical patients. *Critical care medicine, 33*(11), 2521-2526.

Morgan, S. C., Taylor, D. L., & Pocock, J. M. (2004). Microglia release activators of neuronal proliferation mediated by activation of mitogen-activated protein kinase, phosphatidylinositol-3-kinase/Akt and delta-Notch signalling cascades. *Journal of Neurochemistry, 90*(1), 89-101. doi:10.1111/j.1471-4159.2004.02461.x

Moskowitz, M. A., Lo, E. H., & Iadecola, C. (2010). The Science of Stroke: Mechanisms in Search of Treatments. *Neuron, 67*(2), 181-198. doi:10.1016/j.neuron.2010.07.002

Moss, D. W., & Bates, T. E. (2001). Activation of murine microglial cell lines by lipopolysaccharide and interferon-γ causes NO-mediated decreases in mitochondrial and cellular function. *European Journal of Neuroscience, 13*(3), 529-538. doi:10.1046/j.1460-9568.2001.01418.x

Mouton, P. R., Long, J. M., Lei, D.-L., Howard, V., Jucker, M., Calhoun, M. E., & Ingram, D. K. (2002). Age and gender effects on microglia and astrocyte numbers in brains of mice. *Brain Research, 956*(1), 30-35.

Nadeau, S., & Rivest, S. (2000). Role of microglial-derived tumor necrosis factor in mediating CD14 transcription and nuclear factor κ B activity in the brain during endotoxemia. *Journal of Neuroscience, 20*(9), 3456-3468.

Nakamura, K., Arimura, K., Nishimura, A., Tachibana, M., Yoshikawa, Y., Makihara, N., . . . Ooboshi, H. (2016). Possible involvement of basic FGF in the upregulation of PDGFRβ in pericytes after ischemic stroke. *Brain Research, 1630*, 98-108.

Nakano, S., Asada, T., Matsuda, H., Uno, M., & Takasaki, M. (2001). Donepezil hydrochloride preserves regional cerebral blood flow in patients with Alzheimer's disease. *Journal of Nuclear Medicine, 42*(10), 1441-1445.

Nakao, Y., Itoh, Y., Kuang, T.-Y., Cook, M., Jehle, J., & Sokoloff, L. (2001). Effects of anesthesia on functional activation of cerebral blood flow and metabolism. *Proceedings of the National Academy of Sciences, 98*(13), 7593-7598.

Nishioku, T., Dohgu, S., Takata, F., Eto, T., Ishikawa, N., Kodama, K. B., . . . Kataoka, Y. (2009). Detachment of brain pericytes from the basal lamina is involved in disruption of the blood–brain barrier caused by lipopolysaccharide-induced sepsis in mice. *Cellular and molecular neurobiology, 29*(3), 309-316.

Niwa, K., Araki, E., Morham, S. G., Ross, M. E., & Iadecola, C. (2000). Cyclooxygenase-2 contributes to functional hyperemia in whisker-barrel cortex. *The Journal of Neuroscience, 20*(2), 763-770.

Niwa, K., Haensel, C., Ross, M. E., & Iadecola, C. (2001). Cyclooxygenase-1 participates in selected vasodilator responses of the cerebral circulation. *Circulation research, 88*(6), 600-608.

Nizar, K., Uhlirova, H., Tian, P., Saisan, P. A., Cheng, Q., Reznichenko, L., . . . MacDonald, C. L. (2013). In vivo stimulus-induced vasodilation occurs without IP3 receptor activation and may precede astrocytic calcium increase. *Journal of Neuroscience, 33*(19), 8411-8422.

Noda, A., Ohba, H., Kakiuchi, T., Futatsubashi, M., Tsukada, H., & Nishimura, S. (2002). Age-related changes in cerebral blood flow and glucose metabolism in conscious rhesus monkeys. *Brain Research, 936*(1), 76-81.

Noda, M., Ifuku, M., Mori, Y., & Verkhratsky, A. (2013). Calcium influx through reversed NCX controls migration of microglia *Sodium Calcium Exchange: A Growing Spectrum of Pathophysiological Implications* (pp. 289-294): Springer.

Norden, D. M., Fenn, A. M., Dugan, A., & Godbout, J. P. (2014). TGFβ produced by IL-10 redirected astrocytes attenuates microglial activation. *Glia, 62*(6), 881-895.

Northrup, N. A., & Yamamoto, B. K. (2010). Neuroimmune Pharmacology from a Neuroscience Perspective. *Journal of Neuroimmune Pharmacology, 6*(1), 10-19. doi:10.1007/s11481-010-9239-2

O'shea, E., Urrutia, A., Green, A. R., & Colado, M. I. (2014). Current preclinical studies on neuroinflammation and changes in blood–brain barrier integrity by MDMA and methamphetamine. *Neuropharmacology, 87*, 125-134.

O'Donnell, J., Ding, F., & Nedergaard, M. (2015). Distinct functional states of astrocytes during sleep and wakefulness: Is norepinephrine the master regulator? *Current sleep medicine reports, 1*(1), 1-8.

Ohata, M., Sundaram, U., Fredericks, W., London, E., & Rapoport, S. (1981). Regional cerebral blood flow during development and ageing of the rat brain. *Brain: a journal of neurology, 104*(2), 319-332.

Onos, K. D., Rizzo, S. J. S., Howell, G. R., & Sasner, M. (2016). Toward more predictive genetic mouse models of Alzheimer's disease. *Brain research bulletin, 122*, 1-11.

Palop, J. J., & Mucke, L. (2010). Amyloid-[beta]-induced neuronal dysfunction in Alzheimer's disease: from synapses toward neural networks. *Nature Neuroscience, 13*(7), 812-818.

Park, L., Anrather, J., Girouard, H., Zhou, P., & Iadecola, C. (2007). Nox2-derived reactive oxygen species mediate neurovascular dysregulation in the aging mouse brain. *Journal of Cerebral Blood Flow & Metabolism, 27*(12), 1908-1918.

Paul, J., Strickland, S., & Melchor, J. P. (2007). Fibrin deposition accelerates neurovascular damage and neuroinflammation in mouse models of Alzheimer's disease. *The Journal of Experimental Medicine, 204*(8), 1999-2008. doi:10.1084/jem.20070304

Pavlov, V. A., Ochani, M., Gallowitsch-Puerta, M., Ochani, K., Huston, J. M., Czura, C. J., . . . Tracey, K. J. (2006). Central muscarinic cholinergic regulation of the systemic inflammatory response during endotoxemia. *Proc Natl Acad Sci U S A, 103*(13), 5219-5223.

Pavlov, V. A., Parrish, W. R., Rosas-Ballina, M., Ochani, M., Puerta, M., Ochani, K., . . . Tracey, K. J. (2009). Brain acetylcholinesterase activity controls systemic cytokine levels through the cholinergic anti-inflammatory pathway. *Brain, behavior, and immunity, 23*(1), 41-45.

Paxinos, G., & Watson, C. (1998). *The Rat Brain in Stereotaxic Coordinates*: Academic Press.

Peinado, M. A., Quesada, A., Pedrosa, J. A., Torres, M. I., Martinez, M., Esteban, F. J., . . . Peinado, J. M. (1998). Quantitative and ultrastructural changes in glia and pericytes in the parietal cortex of the aging rat. *Microscopy research and technique, 43*(1), 34-42.

Pekny, M., Leveen, P., Pekna, M., Eliasson, C., Berthold, C.-H., Westermark, B., & Betsholtz, C. (1995). Mice lacking glial fibrillary acidic protein display astrocytes devoid of intermediate filaments but develop and reproduce normally. *The EMBO Journal, 14*(8), 1590.

Pellerin, L., Pellegri, G., Bittar, P. G., Charnay, Y., Bouras, C., Martin, J.-L., . . . Magistretti, P. J. (1998). Evidence supporting the existence of an activity-dependent astrocyte-neuron lactate shuttle. *Developmental neuroscience, 20*(4-5), 291-299.

Perez-Asensio, F. J., Perpiñá, U., Planas, A. M., & Pozas, E. (2013). Interleukin-10 regulates progenitor differentiation and modulates neurogenesis in adult brain. *J Cell Sci, 126*(18), 4208-4219.

Perlmutter, L. S., Barron, E., & Chui, H. C. (1990). Morphologic association between microglia and senile plaque amyloid in Alzheimer's disease. *Neurosci Lett, 119*(1), 32-36.

Perry, V. H., Cunningham, C., & Holmes, C. (2007). Systemic infections and inflammation affect chronic neurodegeneration. *Nature Reviews Immunology, 7*(2), 161-167.

Perry, V. H., Newman, T. A., & Cunningham, C. (2003). The impact of systemic infection on the progression of neurodegenerative disease. *Nature Reviews Neuroscience, 4*(2), 103-112.

Perry, V. H., & Teeling, J. (2013). *Microglia and macrophages of the central nervous system: the contribution of microglia priming and systemic inflammation to chronic neurodegeneration.* Paper presented at the Seminars in immunopathology.

Peters, A., Josephson, K., & Vincent, S. L. (1991). Effects of aging on the neuroglial cells and pericytes within area 17 of the rhesus monkey cerebral cortex. *The Anatomical Record, 229*(3), 384-398.

Petzold, G. C., & Murthy, V. N. (2011). Role of astrocytes in neurovascular coupling. *Neuron, 71*(5), 782-797. doi:10.1016/j.neuron.2011.08.009

Pintado, C., Gavilán, M. P., Gavilán, E., García-Cuervo, L., Gutiérrez, A., Vitorica, J., . . . Ruano, D. (2012). Lipopolysaccharide-induced neuroinflammation leads to the accumulation of ubiquitinated proteins and increases susceptibility to neurodegeneration induced by proteasome inhibition in rat hippocampus. *Journal of neuroinflammation, 9*(1), 1.

Pisauro, M. A., Dhruv, N. T., Carandini, M., & Benucci, A. (2013). Fast hemodynamic responses in the visual cortex of the awake mouse. *Journal of Neuroscience, 33*(46), 18343-18351.

Pober, J. S., & Cotran, R. S. (1990). The role of endothelial cells in inflammation. *Transplantation, 50*(4), 537-544.

Pober, J. S., & Sessa, W. C. (2007). Evolving functions of endothelial cells in inflammation. *Nature Reviews Immunology, 7*(10), 803-815.

Pocock, J. M., & Kettenmann, H. (2007). Neurotransmitter receptors on microglia. *Trends Neurosci, 30*(10), 527-535.

Polazzi, E., Gianni, T., & Contestabile, A. (2001). Microglial cells protect cerebellar granule neurons from apoptosis: Evidence for reciprocal signaling. *Glia, 36*(3), 271-280. doi:10.1002/glia.1115

Pollak, Y., Gilboa, A., Ben-Menachem, O., Ben-Hur, T., Soreq, H., & Yirmiya, R. (2005). Acetylcholinesterase inhibitors reduce brain and blood interleukin-1β production. *Annals of Neurology, 57*(5), 741-745.

Qin, L., Wu, X., Block, M. L., Liu, Y., Breese, G. R., Hong, J. S., . . . Crews, F. T. (2007). Systemic LPS causes chronic neuroinflammation and progressive neurodegeneration. *Glia, 55*(5), 453-462.

Qiu, C., Kivipelto, M., & von Strauss, E. (2009). Epidemiology of Alzheimer's disease: occurrence, determinants, and strategies toward intervention. *Dialogues Clin Neurosci, 11*(2), 111-128.

Quan, N., He, L., & Lai, W. (2003). Endothelial activation is an intermediate step for peripheral lipopolysaccharide induced activation of paraventricular nucleus. *Brain research bulletin, 59*(6), 447-452.

Ramos Reis, P. M., Eckhardt, H., Denise, P., Bodem, F., & Lochmann, M. (2013). Localization of scopolamine induced electrocortical brain activity changes, in healthy humans at rest. *The Journal of Clinical Pharmacology, 53*(6), 619-625.

Ramsauer, M., Krause, D., & Dermietzel, R. (2002). Angiogenesis of the blood-brain barrier in vitro and the function of cerebral pericytes. *The FASEB Journal*. doi:10.1096/fj.01-0814fje

Readnower, R. D., Chavko, M., Adeeb, S., Conroy, M. D., Pauly, J. R., McCarron, R. M., & Sullivan, P. G. (2010). Increase in blood–brain barrier permeability, oxidative stress, and activated microglia in a rat model of blast-induced traumatic brain injury. *J Neurosci Res, 88*(16), 3530-3539.

Recasens, M., Ricart, W., & Fernández-Real, J. (2003). Obesity and inflammation. *Revista de medicina de la Universidad de Navarra, 48*(2), 49-54.

Rodriguez, J., Olabarria, M., Chvatal, A., & Verkhratsky, A. (2009). Astroglia in dementia and Alzheimer's disease. *Cell Death & Differentiation, 16*(3), 378-385.

Rombouts, S., Goekoop, R., Stam, C., Barkhof, F., & Scheltens, P. (2005). Delayed rather than decreased BOLD response as a marker for early Alzheimer's disease. *Neuroimage, 26*, 1078-1085.

Rosas-Ballina, M., & Tracey, K. (2009). Cholinergic control of inflammation. *Journal of internal medicine, 265*(6), 663-679.

Rosengarten, B., Paulsen, S., Burr, O., & Kaps, M. (2009). Neurovascular coupling in Alzheimer patients: effect of acetylcholine-esterase inhibitors. *Neurobiol Aging, 30*(12), 1918-1923. doi:10.1016/j.neurobiolaging.2008.02.017

Rosengarten, B., Paulsen, S., Molnar, S., Kaschel, R., & Gallhofer, B. (2006). Acetylcholine esterase inhibitor donepezil improves dynamic cerebrovascular regulation in Alzheimer patients. *Journal of neurology, 253*(1), 58-64.

Rosi, S., Ramirez-Amaya, V., Hauss-Wegrzyniak, B., & Wenk, G. L. (2004). Chronic brain inflammation leads to a decline in hippocampal NMDA-R1 receptors. *Journal of neuroinflammation, 1*(1), 12.

Rothstein, J. D., Dykes-Hoberg, M., Pardo, C. A., Bristol, L. A., Jin, L., Kuncl, R. W., . . . Schielke, J. P. (1996). Knockout of glutamate transporters reveals a major role for astroglial transport in excitotoxicity and clearance of glutamate. *Neuron, 16*(3), 675-686.

Rovelet-Lecrux, A., Hannequin, D., Raux, G., Le Meur, N., Laquerrière, A., Vital, A., . . . Vercelletto, M. (2006). APP locus duplication causes autosomal dominant early-onset Alzheimer disease with cerebral amyloid angiopathy. *Nature genetics, 38*(1), 24-26.

Ruitenberg, A., den Heijer, T., Bakker, S. L. M., van Swieten, J. C., Koudstaal, P. J., Hofman, A., & Breteler, M. M. B. (2005). Cerebral hypoperfusion and clinical onset of dementia: The Rotterdam study. *Annals of Neurology, 57*(6), 789-794. doi:10.1002/ana.20493

Salehi, A., Dubelaar, E. J. G., Mulder, M., & Swaab, D. F. (1998). Aggravated decrease in the activity of nucleus basalis neurons in Alzheimer's disease is apolipoprotein E-type dependent. *Proceedings of the National Academy of Sciences, 95*(19), 11445-11449. doi:10.1073/pnas.95.19.11445

Sanganahalli, B. G., Herman, P., Behar, K. L., Blumenfeld, H., Rothman, D. L., & Hyder, F. (2013). Functional MRI and neural responses in a rat model of Alzheimer's disease. *Neuroimage, 79*, 404-411. doi:10.1016/j.neuroimage.2013.04.099

Sankowski, R., Mader, S., & Valdés-Ferrer, S. I. (2015). Systemic inflammation and the brain: novel roles of genetic, molecular, and environmental cues as drivers of neurodegeneration. *Frontiers in cellular neuroscience, 9*, 28.

Sannita, W. G., Maggi, L., & Rosadini, G. (1987). Effects of scopolamine (0.25–0.75 mg im) on the quantitative EEG and the neuropsychological status of healthy volunteers. *Neuropsychobiology, 17*(4), 199-205.

Sarasa, M., & Pesini, P. (2009). Natural non-trasgenic animal models for research in Alzheimer's disease. *Current Alzheimer Research, 6*(2), 171-178.

Saunders, N. R., Dziegielewska, K. M., Møllgård, K., & Habgood, M. D. (2015). Markers for blood-brain barrier integrity: how appropriate is Evans blue in the twenty-first century and what are the alternatives? *Frontiers in neuroscience, 9*.

Sawada, M., Kondo, N., Suzumura, A., & Marunouchi, T. (1989). Production of tumor necrosis factor-alpha by microglia and astrocytes in culture. *Brain Research, 491*(2), 394-397. doi:10.1016/0006-8993(89)90078-4

Sawada, M., Sawada, H., & Nagatsu, T. (2008). Effects of aging on neuroprotective and neurotoxic properties of microglia in neurodegenerative diseases. *Neurodegenerative Diseases, 5*(3-4), 254-256.

Scheibel, A., Fried, I., Alger, S., Gershon, A., Grimm, S., & Toffano, V. (1983). Age-related changes in the peri-capillary environment of the brain. *Aging of the brain, 22*.

Schmidt, R., Schmidt, H., Curb, J. D., Masaki, K., White, L. R., & Launer, L. J. (2002). Early inflammation and dementia: A 25-year follow-up of the Honolulu-Asia aging study. *Annals of Neurology, 52*(2), 168-174. doi:10.1002/ana.10265

Schultz, S. K., O'leary, D. S., Ponto, L. L. B., Watkins, G. L., Hichwa, R. D., & Andreasen, N. C. (1999). Age-related changes in regional cerebral blood flow among young to midlife adults. *Neuroreport, 10*(12), 2493-2496.

Selkoe, D. J., & Podlisny, M. B. (2002). Deciphering the genetic basis of Alzheimer's disease. *Annual review of genomics and human genetics, 3*(1), 67-99.

Semple, B. D., Blomgren, K., Gimlin, K., Ferriero, D. M., & Noble-Haeusslein, L. J. (2013). Brain development in rodents and humans: Identifying benchmarks of maturation and vulnerability to injury across species. *Progress in Neurobiology, 106*, 1-16.

Sengillo, J. D., Winkler, E. A., Walker, C. T., Sullivan, J. S., Johnson, M., & Zlokovic, B. V. (2013). Deficiency in mural vascular cells coincides with blood–brain barrier disruption in Alzheimer's disease. *Brain Pathology, 23*(3), 303-310.

Sengupta, P. (2013). The laboratory rat: relating its age with human's. *International journal of preventive medicine, 4*(6).

Sharp, P. S., Shaw, K., Boorman, L., Harris, S., Kennerley, A. J., Azzouz, M., & Berwick, J. (2015). Comparison of stimulus-evoked cerebral hemodynamics in the awake mouse and under a novel anesthetic regime. *Scientific reports, 5*, 12621.

Sheng, J. G., Bora, S. H., Xu, G., Borchelt, D. R., Price, D. L., & Koliatsos, V. E. (2003). Lipopolysaccharide-induced-neuroinflammation increases intracellular accumulation of amyloid precursor protein and amyloid β peptide in APPswe transgenic mice. *Neurobiol Dis, 14*(1), 133-145.

Shibuki, K., Gomi, H., Chen, L., Bao, S., Kim, J. J., Wakatsuki, H., . . . Ikeda, T. (1996). Deficient cerebellar long-term depression, impaired eyeblink conditioning, and normal motor coordination in GFAP mutant mice. *Neuron, 16*(3), 587-599.

Shin, J.-W., Nguyen, K. T., Pow, D. V., Knight, T., Buljan, V., Bennett, M. R., & Balcar, V. J. (2009). Distribution of glutamate transporter GLAST in membranes of cultured astrocytes in the presence of glutamate transport substrates and ATP. *Neurochemical research, 34*(10), 1758-1766.

Shin, W. H., Lee, D. Y., Park, K. W., Kim, S. U., Yang, M. S., Joe, E. H., & Jin, B. K. (2004). Microglia expressing interleukin-13 undergo cell death and contribute to neuronal survival in vivo. *Glia, 46*(2), 142-152.

Shytle, R. D., Mori, T., Townsend, K., Vendrame, M., Sun, N., Zeng, J., . . . Tan, J. (2004). Cholinergic modulation of microglial activation by α7 nicotinic receptors. *Journal of Neurochemistry, 89*(2), 337-343.

Sierra, A., Gottfried-Blackmore, A. C., McEwen, B. S., & Bulloch, K. (2007). Microglia derived from aging mice exhibit an altered inflammatory profile. *Glia, 55*(4), 412-424.

Simard, A. R., Soulet, D., Gowing, G., Julien, J.-P., & Rivest, S. (2006). Bone marrow-derived microglia play a critical role in restricting senile plaque formation in Alzheimer's disease. *Neuron, 49*(4), 489-502.

Simard, M., & Nedergaard, M. (2004). The neurobiology of glia in the context of water and ion homeostasis. *Neuroscience, 129*(4), 877-896.

Sofroniew, M. V. (2009). Molecular dissection of reactive astrogliosis and glial scar formation. *Trends Neurosci, 32*(12), 638-647.

Sofroniew, M. V., & Vinters, H. V. (2010). Astrocytes: biology and pathology. *Acta Neuropathol, 119*(1), 7-35.

Sokoya, E. M., Burns, A. R., Setiawan, C. T., Coleman, H. A., Parkington, H. C., & Tare, M. (2006). Evidence for the involvement of myoendothelial gap junctions in EDHF-mediated relaxation in the rat middle cerebral artery. *American Journal of Physiology-Heart and Circulatory Physiology, 291*(1), H385-H393.

Spain, A., Howarth, C., Khrapitchev, A. A., Sharp, T., Sibson, N. R., & Martin, C. (2015). Neurovascular and neuroimaging effects of the hallucinogenic serotonin receptor agonist psilocin in the rat brain. *Neuropharmacology, 99*, 210-220.

Sperling, R. (2011). The potential of functional MRI as a biomarker in early Alzheimer's disease. *Neurobiol Aging, 32*, S37-S43.

St Hillaire, C., Vargas, D., Pardo, C. A., Gincel, D., Mann, J., Rothstein, J. D., . . . Conant, K. (2005). Aquaporin 4 is increased in association with human immunodeficiency virus dementia: implications for disease pathogenesis. *Journal of neurovirology, 11*(6), 535-543.

Staiger, J., Bisler, S., Schleicher, A., Gass, P., Stehle, J., & Zilles, K. (2000). Exploration of a novel environment leads to the expression of inducible transcription factors in barrel-related columns. *Neuroscience, 99*(1), 7-16.

Staiger, J. F. (2006). Immediate-early gene expression in the barrel cortex. *Somatosensory & motor research, 23*(3-4), 135-146.

Stanimirovic, D. B., & Friedman, A. (2012). Pathophysiology of the neurovascular unit: disease cause or consequence? *J Cereb Blood Flow Metab, 32*(7), 1207-1221. doi:10.1038/jcbfm.2012.25

Stark, K., Eckart, A., Haidari, S., Tirniceriu, A., Lorenz, M., von Brühl, M.-L., . . . Pless, R. (2013). Capillary and arteriolar pericytes attract innate leukocytes exiting through venules and'instruct'them with pattern-recognition and motility programs. *Nature immunology, 14*(1), 41-51.

Stolp, H., & Dziegielewska, K. (2009). Review: role of developmental inflammation and blood–brain barrier dysfunction in neurodevelopmental and neurodegenerative diseases. *Neuropathology and applied neurobiology, 35*(2), 132-146.

Strandberg, T. E., Pitkala, K. H., Linnavuori, K. H., & Tilvis, R. S. (2003). Impact of viral and bacterial burden on cognitive impairment in elderly persons with cardiovascular diseases. *Stroke, 34*(9), 2126-2131.

Streit, W. J. (2004). Microglia and Alzheimer's disease pathogenesis. *J Neurosci Res, 77*(1), 1-8. doi:10.1002/jnr.20093

Streit, W. J. (2005). Microglia and neuroprotection: implications for Alzheimer's disease. *Brain Research Reviews, 48*(2), 234-239.

Streit, W. J., Sammons, N. W., Kuhns, A. J., & Sparks, D. L. (2004). Dystrophic microglia in the aging human brain. *Glia, 45*(2), 208-212.

Strosznajder, J., Chalimoniuk, M., Strosznajder, R. P., Albanese, V., & Alberghina, M. (1996). Arachidonate transport through the blood-retina and blood-brain barrier of the rat during aging. *Neurosci Lett, 209*(3), 145-148.

Sugimoto, N., Nishimura, N., Ohnishi, N., Matsumoto, T., Kitaura, T., Shido, O., & Yachie, A. (2017). Lipopolysaccharide increases the expression level of the aquaporin-4 water channel. *The FASEB Journal, 31*(1 Supplement), lb686-lb686.

Sumi, N., Nishioku, T., Takata, F., Matsumoto, J., Watanabe, T., Shuto, H., . . . Kataoka, Y. (2010). Lipopolysaccharide-activated microglia induce dysfunction of the blood–brain barrier in rat microvascular endothelial cells co-cultured with microglia. *Cellular and molecular neurobiology, 30*(2), 247-253.

Sun, J., Zheng, J. H., Zhao, M., Lee, S., & Goldstein, H. (2008). Increased in vivo activation of microglia and astrocytes in the brains of mice transgenic for an infectious R5 human immunodeficiency virus type 1 provirus and for CD4-specific expression of human cyclin T1 in response to stimulation by lipopolysaccharides. *Journal of virology, 82*(11), 5562-5572.

Sun, W., McConnell, E., Pare, J.-F., Xu, Q., Chen, M., Peng, W., . . . Nedergaard, M. (2013). Glutamate-dependent neuroglial calcium signaling differs between young and adult brain. *Science, 339*(6116), 197-200.

Suri, S., Mackay, C. E., Kelly, M. E., Germuska, M., Tunbridge, E. M., Frisoni, G. B., . . . Filippini, N. (2015). Reduced cerebrovascular reactivity in young adults carrying the APOE ε4 allele. *Alzheimer's & Dementia, 11*(6), 648-657. e641.

Sutherland, B. A., Fordsmann, J. C., Martin, C., Neuhaus, A. A., Witgen, B. M., Piilgaard, H., . . . Lauritzen, M. (2017). Multi-modal assessment of neurovascular coupling during cerebral ischaemia and reperfusion using remote middle cerebral artery occlusion. *Journal of Cerebral Blood Flow & Metabolism, 37*(7), 2494-2508.

Suzuki, R., Watanabe, J., Arata, S., Funahashi, H., Kikuyama, S., & Shioda, S. (2003). A transgenic mouse model for the detailed morphological study of astrocytes. *Neuroscience research, 47*(4), 451-454.

Svoboda, K., & Yasuda, R. (2006). Principles of two-photon excitation microscopy and its applications to neuroscience. *Neuron, 50*(6), 823-839.

Sweeney, M. D., Sagare, A. P., & Zlokovic, B. V. (2015). Cerebrospinal fluid biomarkers of neurovascular dysfunction in mild dementia and Alzheimer's disease. *Journal of Cerebral Blood Flow & Metabolism, 35*(7), 1055-1068.

Szymanski, F. D., Rabinowitz, N. C., Magri, C., Panzeri, S., & Schnupp, J. W. (2011). The laminar and temporal structure of stimulus information in the phase of field potentials of auditory cortex. *Journal of Neuroscience, 31*(44), 15787-15801.

Takada, Y., Yonezawa, A., Kume, T., Katsuki, H., Kaneko, S., Sugimoto, H., & Akaike, A. (2003). Nicotinic acetylcholine receptor-mediated neuroprotection by donepezil against glutamate neurotoxicity in rat cortical neurons. *J Pharmacol Exp Ther, 306*(2), 772-777. doi:10.1124/jpet.103.050104

Takano, T., Han, X., Deane, R., Zlokovic, B., & Nedergaard, M. (2007). Two-Photon Imaging of Astrocytic Ca2+ Signaling and the Microvasculature in Experimental Mice

Models of Alzheimer's Disease. *Annals of the New York Academy of Sciences, 1097*(1), 40-50. doi:10.1196/annals.1379.004

Takano, T., Tian, G.-F., Peng, W., Lou, N., Libionka, W., Han, X., & Nedergaard, M. (2006). Astrocyte-mediated control of cerebral blood flow. *Nature Neuroscience, 9*(2), 260-267.

Tanzi, R., Moir, R., & Wagner, S. (2004). Clearance of Alzheimer's Aβ PeptideThe Many Roads to Perdition. *Neuron, 43*(5), 605-608. doi:10.1016/s0896-6273(04)00533-1

Tateno, M., Kobayashi, S., Utsumi, K., Morii, H., & Fujii, K. (2008). Quantitative analysis of the effects of donepezil on regional cerebral blood flow in Alzheimer's disease by using an automated program, 3DSRT. *Neuroradiology, 50*(8), 723-727. doi:10.1007/s00234-008-0401-y

The FIL Methods Group, U. (2016, 23/06/2016). Statistical Parametric Mapping (SPM). Retrieved from http://www.fil.ion.ucl.ac.uk/spm/

Thrane, A. S., Rappold, P. M., Fujita, T., Torres, A., Bekar, L. K., Takano, T., . . . Enger, R. (2011). Critical role of aquaporin-4 (AQP4) in astrocytic Ca2+ signaling events elicited by cerebral edema. *Proceedings of the National Academy of Sciences, 108*(2), 846-851.

Tian, P., Teng, I. C., May, L. D., Kurz, R., Lu, K., Scadeng, M., . . . Mandeville, J. B. (2010a). Cortical depth-specific microvascular dilation underlies laminar differences in blood oxygenation level-dependent functional MRI signal. *Proceedings of the National Academy of Sciences, 107*(34), 15246-15251.

Tian, P., Teng, I. C., May, L. D., Kurz, R., Lu, K., Scadeng, M., . . . Devor, A. (2010b). Cortical depth-specific microvascular dilation underlies laminar differences in blood oxygenation level-dependent functional MRI signal. *Proceedings of the National Academy of Sciences, 107*(34), 15246-15251. doi:10.1073/pnas.1006735107

Tigges, J., Herndon, J., & Rosene, D. (1995). Mild age-related changes in the dentate gyrus of adult rhesus monkeys. *Cells Tissues Organs, 153*(1), 39-48.

Tomás-Camardiel, M., Venero, J. L., De Pablos, R., Rite, I., Machado, A., & Cano, J. (2004). In vivo expression of aquaporin-4 by reactive microglia. *Journal of neurochemistry, 91*(4), 891-899.

Toth, P., Tarantini, S., Ashpole, N. M., Tucsek, Z., Milne, G. L., Valcarcel-Ares, N. M., . . . Csiszar, A. (2015). IGF-1 deficiency impairs neurovascular coupling in mice: implications for cerebromicrovascular aging. *Aging cell, 14*(6), 1034-1044.

Toth, P., Tucsek, Z., Tarantini, S., Sosnowska, D., Gautam, T., Mitschelen, M., . . . Ungvari, Z. (2014). IGF-1 deficiency impairs cerebral myogenic autoregulation in hypertensive mice. *Journal of Cerebral Blood Flow & Metabolism, 34*(12), 1887-1897.

Turner, R. (2002). How much cortex can a vein drain? Downstream dilution of activation-related cerebral blood oxygenation changes. *Neuroimage, 16*(4), 1062-1067.

Uekawa, K., Koizumi, K., Hwang, J., Brunier, N., Hattori, Y., Zhou, P., & Park, L. (2016). Obligatory Role of EP1 Receptors in the Increase in Cerebral Blood Flow Produced by Hypercapnia in the Mice. *PloS one, 11*(9), e0163329.

Urban, A., Dussaux, C., Martel, G., Brunner, C., Mace, E., & Montaldo, G. (2015). Real-time imaging of brain activity in freely moving rats using functional ultrasound. *Nature methods, 12*(9), 873-878.

van de Haar, H. J., Jansen, J. F., van Osch, M. J., van Buchem, M. A., Muller, M., Wong, S. M., . . . Backes, W. H. (2016). Neurovascular unit impairment in early Alzheimer's disease measured with magnetic resonance imaging. *Neurobiol Aging, 45*, 190-196.

Vanzetta, I., & Grinvald, A. (2008). Coupling between neuronal activity and microcirculation: implications for functional brain imaging. *HFSP journal, 2*(2), 79-98.

Varatharaj, A., & Galea, I. (2017). The blood-brain barrier in systemic inflammation. *Brain, behavior, and immunity, 60*, 1-12.

Vaughan, D. W., & Peters, A. (1974). Neuroglial cells in the cerebral cortex of rats from young adulthood to old age: an electron microscope study. *Journal of Neurocytology, 3*(4), 405-429.

Verma, S., Nakaoke, R., Dohgu, S., & Banks, W. A. (2006). Release of cytokines by brain endothelial cells: a polarized response to lipopolysaccharide. *Brain, behavior, and immunity, 20*(5), 449-455.

Vermeer, S. E., Prins, N. D., den Heijer, T., Hofman, A., Koudstaal, P. J., & Breteler, M. M. B. (2003). Silent Brain Infarcts and the Risk of Dementia and Cognitive Decline. *New England Journal of Medicine, 348*(13), 1215-1222. doi:10.1056/nejmoa022066

von Tell, D., Armulik, A., & Betsholtz, C. (2006). Pericytes and vascular stability. *Experimental Cell Research, 312*(5), 623-629.

Voskuhl, R. R., Peterson, R. S., Song, B., Ao, Y., Morales, L. B. J., Tiwari-Woodruff, S., & Sofroniew, M. V. (2009). Reactive astrocytes form scar-like perivascular barriers to leukocytes during adaptive immune inflammation of the CNS. *The Journal of Neuroscience, 29*(37), 11511-11522.

Walsh, D. M., Klyubin, I., Fadeeva, J. V., Cullen, W. K., Anwyl, R., Wolfe, M. S., . . . Selkoe, D. J. (2002). Naturally secreted oligomers of amyloid β protein potently inhibit hippocampal long-term potentiation in vivo. *Nature, 416*(6880), 535-539. doi:10.1038/416535a

Wang, H., Yu, M., Ochani, M., & Amella, C. A. (2003). Nicotinic acetylcholine receptor alpha7 subunit is an essential regulator of inflammation. *Nature, 421*(6921), 384.

Wang, S., Cao, C., Chen, Z., Bankaitis, V., Tzima, E., Sheibani, N., & Burridge, K. (2012). Pericytes regulate vascular basement membrane remodeling and govern neutrophil extravasation during inflammation. *PloS one, 7*(9), e45499.

Wang, X., Lou, N., Xu, Q., Tian, G.-F., Peng, W. G., Han, X., . . . Nedergaard, M. (2006). Astrocytic Ca2+ signaling evoked by sensory stimulation in vivo. *Nature Neuroscience, 9*(6), 816-823.

Wang, X., & Michaelis, E. K. (2010). Selective neuronal vulnerability to oxidative stress in the brain. *Frontiers in aging neuroscience, 2*, 12.

Waring, S. C., & Rosenberg, R. N. (2008). Genome-wide association studies in Alzheimer disease. *Archives of neurology, 65*(3), 329-334.

Wertheimer, S. J., Myers, C. L., Wallace, R. W., & Parks, T. P. (1992). Intercellular adhesion molecule-1 gene expression in human endothelial cells. Differential regulation by tumor necrosis factor-alpha and phorbol myristate acetate. *Journal of Biological Chemistry, 267*(17), 12030-12035.

Whitehouse, P. J., Price, D. L., Clark, A. W., Coyle, J. T., & DeLong, M. R. (1981). Alzheimer disease: Evidence for selective loss of cholinergic neurons in the nucleus basalis. *Annals of Neurology, 10*(2), 122-126. doi:10.1002/ana.410100203

Wildt, D., Hillen, F., Rauws, A., & Sangster, B. (1983). Etomidate-anaesthesia, with and without fentanyl, compared with urethane-anaesthesia in the rat. *British journal of pharmacology, 79*(2), 461-469.

Winkler, E. A., Bell, R. D., & Zlokovic, B. V. (2010). Pericyte-specific expression of PDGF beta receptor in mouse models with normal and deficient PDGF beta receptor signaling. *Molecular neurodegeneration, 5*(1), 1.

Winship, I. R. (2014). Laser Speckle Contrast Imaging to Measure Changes in Cerebral Blood Flow. In R. Milner (Ed.), *Cerebral Angiogenesis: Methods and Protocols* (pp. 223-235). New York, NY: Springer New York.

Witthoft, A., & Karniadakis, G. E. (2012). A bidirectional model for communication in the neurovascular unit. *Journal of theoretical biology, 311*, 80-93.

Wu, Z., Guo, H., Chow, N., Sallstrom, J., Bell, R. D., Deane, R., . . . Zlokovic, B. V. (2005). Role of the MEOX2 homeobox gene in neurovascular dysfunction in Alzheimer disease. *Nature Medicine*. doi:10.1038/nm1287

Wyss-Coray, T., & Mucke, L. (2002). Inflammation in neurodegenerative disease—a double-edged sword. *Neuron, 35*(3), 419-432.

Xaio, H., Banks, W. A., Niehoff, M. L., & Morley, J. (2001). Effect of LPS on the permeability of the blood–brain barrier to insulin. *Brain Research, 896*(1), 36-42.

Xie, L., Kang, H., Xu, Q., Chen, M. J., Liao, Y., Thiyagarajan, M., . . . Iliff, J. J. (2013). Sleep drives metabolite clearance from the adult brain. *Science, 342*(6156), 373-377.

Xie, Z., Morgan, T. E., Rozovsky, I., & Finch, C. E. (2003). Aging and glial responses to lipopolysaccharide in vitro: greater induction of IL-1 and IL-6, but smaller induction of neurotoxicity. *Experimental Neurology, 182*(1), 135-141.

Xing, D., Yeh, C.-I., Burns, S., & Shapley, R. M. (2012). Laminar analysis of visually evoked activity in the primary visual cortex. *Proceedings of the National Academy of Sciences, 109*(34), 13871-13876.

Ye, S.-M., & Johnson, R. W. (1999). Increased interleukin-6 expression by microglia from brain of aged mice. *J Neuroimmunol, 93*(1), 139-148.

Zhang, Q., Lu, Y., Bian, H., Guo, L., & Zhu, H. (2017). Activation of the α7 nicotinic receptor promotes lipopolysaccharide-induced conversion of M1 microglia to M2. *American journal of translational research, 9*(3), 971.

Zhong, Z., Ilieva, H., Hallagan, L., Bell, R., Singh, I., Paquette, N., . . . Zlokovic, B. V. (2009). Activated protein C therapy slows ALS-like disease in mice by transcriptionally inhibiting SOD1 in motor neurons and microglia cells. *Journal of Clinical Investigation*. doi:10.1172/jci38476

Zhou, Z., Peng, X., Insolera, R., Fink, D. J., & Mata, M. (2009a). IL-10 promotes neuronal survival following spinal cord injury. *Experimental Neurology, 220*(1), 183-190.

Zhou, Z., Peng, X., Insolera, R., Fink, D. J., & Mata, M. (2009b). Interleukin-10 provides direct trophic support to neurons. *Journal of Neurochemistry, 110*(5), 1617-1627.

Zipser, B. D., Johanson, C. E., Gonzalez, L., Berzin, T. M., Tavares, R., Hulette, C. M., . . . Stopa, E. G. (2007). Microvascular injury and blood–brain barrier leakage in Alzheimer's disease. *Neurobiol Aging, 28*(7), 977-986. doi:10.1016/j.neurobiolaging.2006.05.016

Zlokovic, B. V. (2005). Neurovascular mechanisms of Alzheimer's neurodegeneration. *Trends Neurosci, 28*(4), 202-208. doi:10.1016/j.tins.2005.02.001

Zlokovic, B. V. (2008). The blood-brain barrier in health and chronic neurodegenerative disorders. *Neuron, 57*(2), 178-201. doi:10.1016/j.neuron.2008.01.003

Zlokovic, B. V. (2011). Neurovascular pathways to neurodegeneration in Alzheimer's disease and other disorders. *Nat Rev Neurosci, 12*(12), 723-738. doi:10.1038/nrn3114

Zonta, M., Angulo, M. C., Gobbo, S., Rosengarten, B., Hossmann, K.-A., Pozzan, T., & Carmignoto, G. (2003). Neuron-to-astrocyte signaling is central to the dynamic control of brain microcirculation. *Nature Neuroscience, 6*(1), 43-50.

Zou, Y., Jung, K. J., Kim, J. W., Yu, B. P., & Chung, H. Y. (2004). Alteration of soluble adhesion molecules during aging and their modulation by calorie restriction. *The FASEB Journal, 18*(2), 320-322.

Appendix A

Brain slicing preparation of rat brain prior to wax embedding.
The olfactory bulbs were removed (a) followed by the brain stem (b). The brain was then divided through the junction of the cerebellum (c) and further sectioned in three: posterior to the olfactory bulbs (prefrontal cortex) (d) frontal cortex to middle cortex (e) and middle cortex to posterior cortex. Sections a to d, d to e and e to c were embedded in one paraffin block as these contained the two regions of interest in Study 2. Section c to b was embedded in a separate paraffin block. A small incision (grey triangle) was made on the left side of the most posterior of the three sections to facilitate orientation during analysis. Olfactory bulbs and brain stem were discarded. Figure adapted from University of Wilsconsin-Madison Brain Collection.

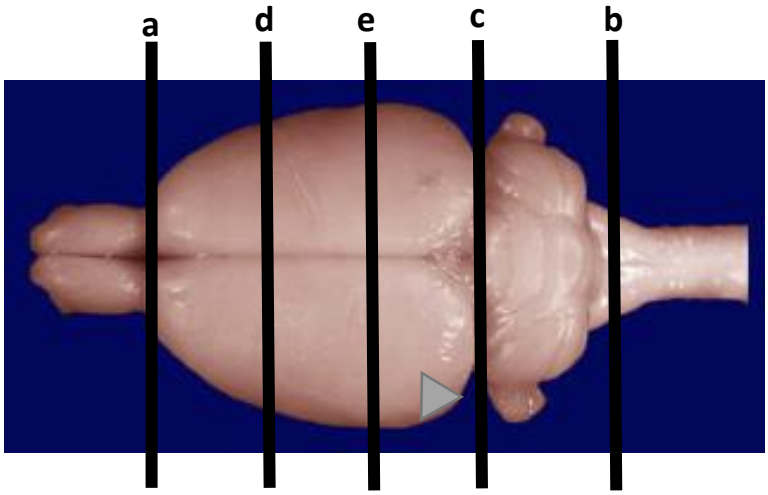

Appendix B

Antibody optimisation procedure.

Initial optimisation of PDGFRβ antibody at three different concentrations 1:50, 1:100 and 1:200. Antigen retrieval was carried out using pH9 pressure cooker. Staining intensity can be seen to degrade as the concentration of the primary antibody is halved, thus a concentration of 1:50 was chosen as the final dilution. Images in black border are at higher magnification. Scale bar represent 50µm.

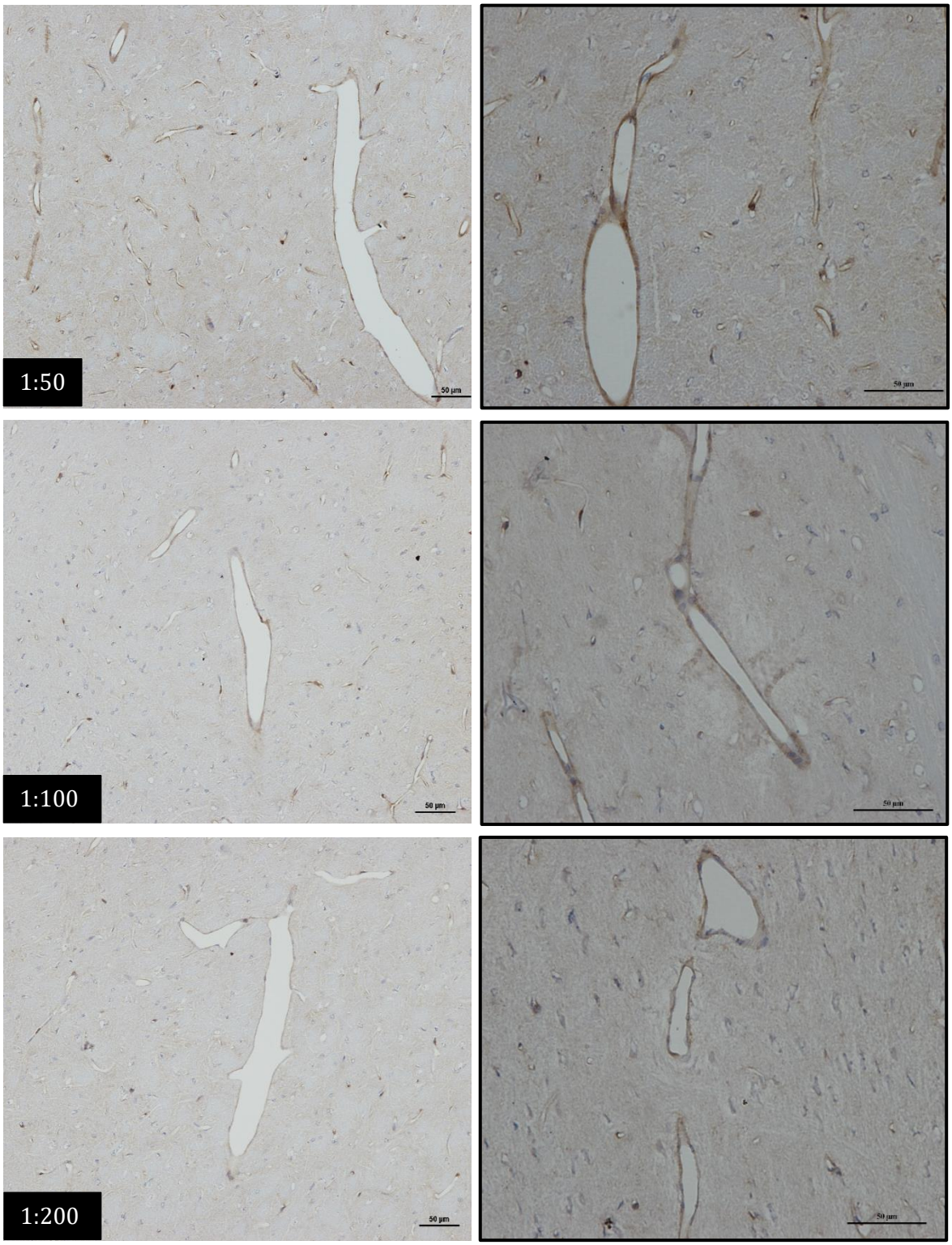

Appendix C

AnalySIS^{D} software customised macro for immunoreactivity detection for ICAM-1 image in somatosensory cortex. Displayed is the image before (A) and after (B) overlaid with macro to quantify level of immunoreactivity within this image area. Overlay shows a good coverage of vessel lining. Programme is not able to detect any immunoreactivity that is less than one megapixel or fainter immunoreactivity.

A

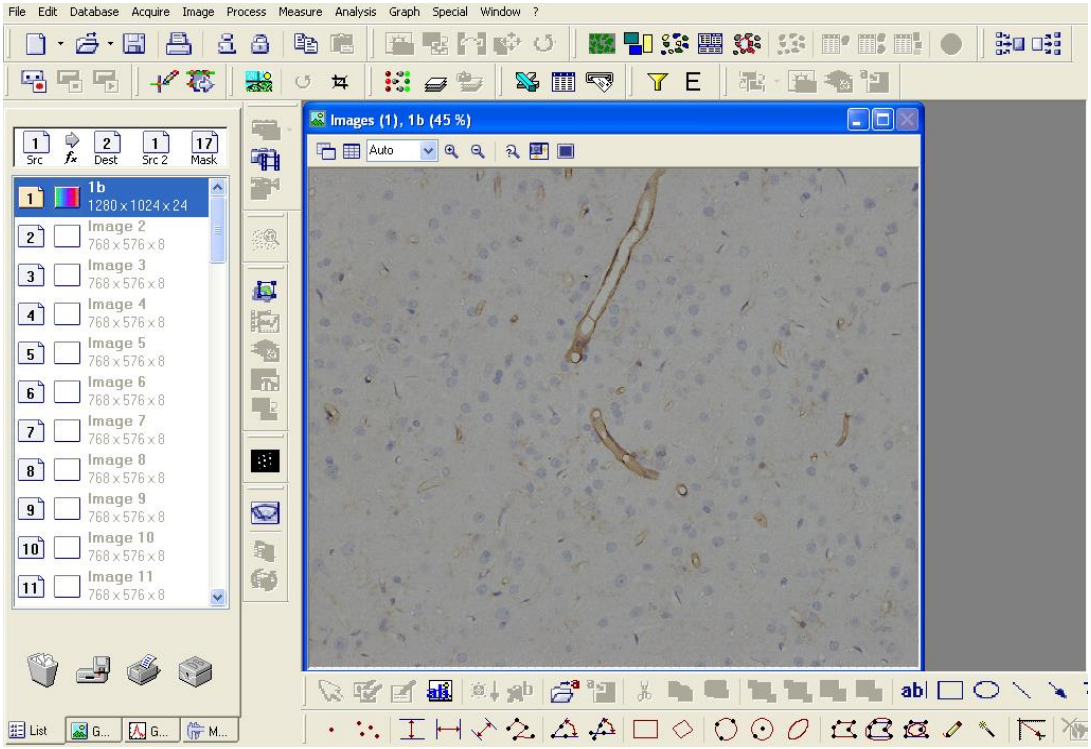

B

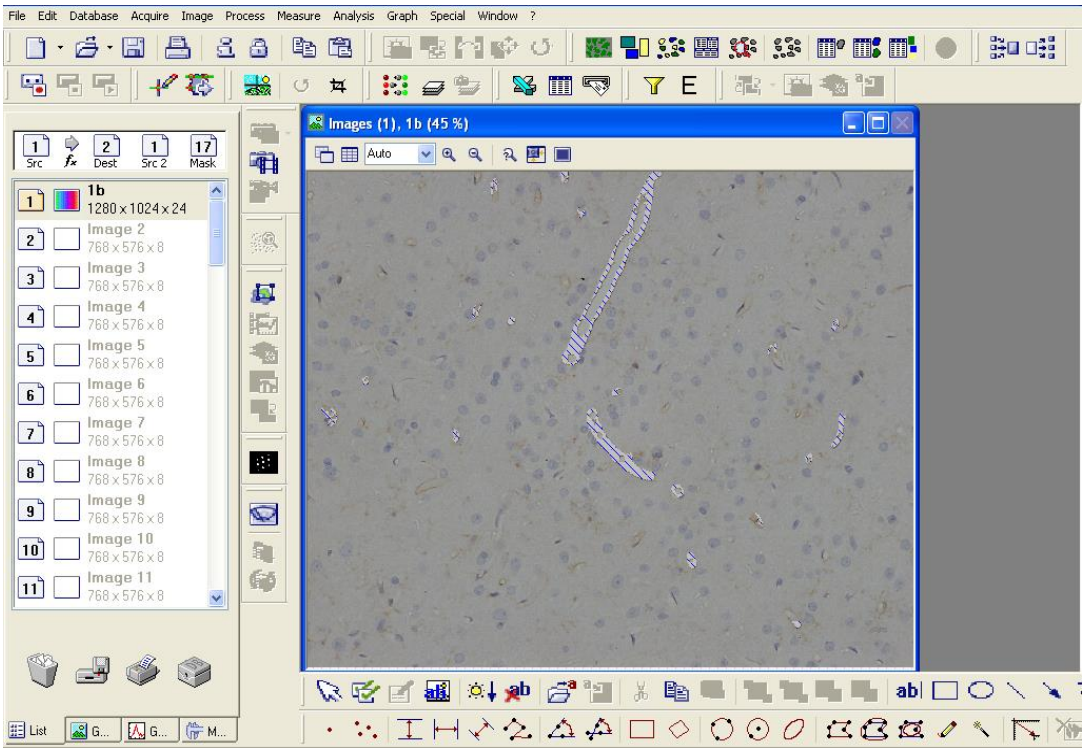

Appendix D

Laboratory recipes

Histology solutions and reagents

TBS
6.05g of Tris buffer (Fisher Scientific, Loughborough, UK) and
8.76g Sodium Chloride (Merck) made up to 1L in dH_2O, pH to 7.6

Acid Alcohol (H&E)
20ml concentrate hydrochloric acid diluted in 1780ml of 70% ethanol.

Scott's Tap Water (Counterstain & H&E)
8.75g of sodium bicarbonate and
50g magnesium sulphate dissolved in 2.5L of water

TSC (antigen retrieval)
1.5g of tri-sodium citrate diluted in 500ml of dH_2O pH 6.5

1% Periodic Acid solution
1g of Periodic acid
100ml of dH_2O